To the Graduate Council:

I am submitting herewith a dissertation written by John Raymond Haines entitled "Optimal Wall Heat Flux Distributions For Natural Convection Flows In Rectangular Enclosures." I have examined the final copy of this dissertation for form and content and recommend that it be accepted in partial fulfillment of the requirements for the degree of Doctor of Philosophy, with a major in Mechanical Engineering.

Robert J. Krane, Major Professor

We have read this dissertation
and recommend its acceptance:

Accepted for the Council:

Vice Provost
and Dean of The Graduate School

OPTIMAL WALL HEAT FLUX DISTRIBUTIONS FOR NATURAL CONVECTION FLOWS IN RECTANGULAR ENCLOSURES

A Dissertation

Presented for the

Doctor of Philosophy

Degree

The University of Tennessee, Knoxville

John Raymond Haines

May, 1991

DEDICATION

I dedicate this work to my wife, Rebecca. Her support and encouragement were lovingly given in large doses and were absolutely essential to the successful completion of this effort. I also wish to express my appreciation to my three daughters, Leslie, Elizabeth, and Sara, who patiently accepted the fact that considerable time had to be devoted to the preparation of this dissertation, and to my parents, who taught me, by their example, the value of hard work and perseverance.

ACKNOWLEDGEMENTS

I am greatly indebted to Professor Robert J. Krane, who served as the chairman of my graduate committee, for the guidance and encouragement he provided throughout the course of my dissertation research. With his consultation, criticism, and support, I was able to achieve results otherwise impossible. I also wish to acknowledge the generous support and guidance of the other members of my committee, including Professors J. W. Hodgson, J. R. Parsons, M. Parang, and J. J. Perona.

In addition, I am thankful for the support of my employer McDonnell Douglas Missile Systems Company and for the encouragement given by my supervisor, Mr. John W. Davis, and other colleagues at McDonnell Douglas.

ABSTRACT

An analytical study was performed to determine optimal heat flux distributions along one vertical wall of a two-dimensional rectangular enclosure cooled by natural convection. Two different optimization problems were investigated. The primary problem of interest, referred to as "optimization problem number 1", was to determine the local heat flux distribution along the heated vertical wall of the rectangular enclosure such that either the average or peak temperature of the heated wall is minimized with the constraint that the total heating rate along the wall is a specified constant. The alternative problem, referred to as "optimization problem number 2," was to determine the local heat flux distribution along the heated vertical wall of the rectangular enclosure such that the total heating rate is maximized subject to the constraints that the average temperature of the heated wall is a specified constant and the peak temperature of the heated wall is less than a specified constant.

To perform these studies a numerical model of the steady state, laminar, natural convection process that occurs in the enclosure was constructed using the finite volume approach as embodied in the SIMPLER algorithm. The natural convection model was coupled with a numerical optimization code which is based on the generalized reduced gradient (GRG) method.

Preliminary studies were performed for a reference set of parameters to define appropriate grid sizes and to fix the methods to be used for a parametric study. The reference parameters included a modified Rayleigh number (based on average heat flux on the heated vertical wall) of 10^5, a Prandtl number and enclosure aspect ratio of unity, and boundary conditions with adiabatic top and bottom walls and an isothermal vertical wall opposite the heated vertical wall.

Results of grid refinement studies show that a 13 x 13 nonuniformly spaced grid is adequate to accurately predict the behavior of the natural

convection process and is compatible with performing optimization studies which require many repeated solutions of the natural convection problem. Solutions to optimization problems number 1 and number 2 are identical for corresponding constraints. However, because optimization problem number 2 has constraints that are nonlinear functions of the heat flux, considerably more computing time was required for its solution. Two alternative methods for representing the local nonuniform heat flux distribution on the heated vertical wall were also evaluated. Approximating the continuous heat flux distribution as the set of heat fluxes at each discrete grid point along the heated wall was shown to achieve more optimal results and required only slightly more computing time than using the coefficients of polynomial heat flux distributions as the independent variables.

Parametric studies were performed to determine the sensitivity of the optimal solutions to the nondimensional parameters and type of thermal boundary conditions. Based on the results of the preliminary studies, these parametric studies were performed using a 13 x 13 nonuniform grid with the heat flux at the grid points treated as the independent variables and the total heating rate along the heated vertical wall fixed (optimization problem number 1). Rayleigh numbers from 10^3 to 10^6, Prandtl numbers from 0.1 to 100, enclosure aspect ratios from 0.5 to 2, and three sets of thermal boundary conditions on the remaining walls of the enclosure were considered in the parametric sudies.

Optimization study results demonstrated that compared to a uniform heat flux distribution significant reductions in either average or peak temperature of the heated wall are possible for optimal heat flux distributions. For example, at reference parameters, the minimal average nondimensional temperature of the heated vertical wall is 17% lower than the average nondimensional temperature achieved for a uniform heat flux distribution with the same total heating rate.

TABLE OF CONTENTS

CHAPTER		PAGE
1.	INTRODUCTION	1
	1.1 Motivation For The Present Research	1
	1.2 Selection Of The Configurations To Be Investigated	2
	1.3 The Governing Equations And Boundary Conditions For The Natural Convection Flows In The Enclosures	4
	1.4 Formal Statements Of The Optimization Problems	10
	1.5 Literature Review	13
	1.5.1 General References On Natural Convection	13
	1.5.2 Natural Convection Flows In Enclosures	13
	1.5.3 Numerical Techniques For Solving The Natural Convection Flows	19
	1.5.4 Optimization Techniques	20
	1.6 Objectives Of The Research	21
2.	FORMULATION AND IMPLEMENTATION OF THE NUMERICAL MODEL	23
	2.1 Introduction	23
	2.2 Formulation Of The Numerical Model For Solving The Natural Convection Flows In The Enclosures	23
	2.2.1 General Specifications For The Natural Convection Code	23
	2.2.2 Implementation Of The SIMPLER Algorithm In The Natural Convection Code	25
	2.2.3 Convergence Tolerances Used In The Natural Convection Code	26
	2.2.4 Computation Of The Streamlines And Heatlines	27
	2.2.5 Physical Interpretations Of The Streamlines And Heatlines	32
	2.2.6 Evaluation Of The Nusselt Number	33
	2.3 The GRG2 Optimization Code	34
	2.3.1 A General Description Of The GRG2 Program	34

2.4 Alternative Methods For Representing The Nonuniform Local Heat Flux Distribution On The Left-Hand Vertical Wall 40
2.5 Coupling Of The Natural Convection And GRG2 Optimization Codes 42
2.6 Computational Facilities 43

3. PRESENTATION AND INTERPRETATION OF RESULTS 46

3.1 Introduction 46
3.2 Preliminary Studies 46
3.2.1 Validation Of The Natural Convection Code 46
3.2.2 Grid Refinement Study 50
3.2.3 Sensitivity To The Definitions Of The Constraint And Objective Functions 62
3.2.4 Study Of Alternate Ways Of Representing The Heat Flux 83
3.2.5 Summary Of Conclusions Based On Preliminary Studies 90
3.3 Results Of Parametric Studies 91
3.3.1 Computational Matrix 91
3.3.2 Sensitivity To The Modified Rayleigh Number 91
3.3.2 Sensitivity To The Prandtl Number 101
3.3.4 Sensitivity To The Enclosure Aspect Ratio 105
3.3.5 Sensitivity To The Thermal Boundary Conditions 111

4. SUMMARY AND CONCLUSIONS 115

4.1 Numerical Model Validation And Grid Size Selection 115
4.2 Optimal Heat Flux Distribution For Various Approaches And Constraints 116
4.3 Parametric Studies 118
4.4 Design Guidance For Optimum Placement Of Electronic Components On Circuit Boards Cooled By Natural Convection 120

LIST OF REFERENCES 124

APPENDIXES 129

APPENDIX A - DESCRIPTION OF THE ALGORITHM USED FOR THE NUMERICAL SOLUTION OF THE NATURAL CONVECTION FLOWS 130
APPENDIX B - FORTRAN PROGRAM LISTINGS 145
APPENDIX C - CONTOUR PLOTS 197

VITA 279

LIST OF TABLES

TABLE		PAGE
2-1.	Roles of functions calculated by the natural convection model for each of the optimization cases	44
3-1.	Comparison of results obtained with the natural convection code developed in this study with results from the "benchmark" solution by de Vahl Davis (1983) for $Ra=10^5$, Pr=.71, A=1	48
3-2.	Comparison of results obtained using the SIMPLER algorithm with results of Kimura and Bejan (1984)	51
3-3.	Computational matrix for optimization constraint and objective function sensitivity studies	64
3-4.	Minimal average temperature on the LHVW obtained using the polynomial heat flux distribution approach	84
3-5.	Computational matrix for parametric studies	92
3-6.	Summary of results for Rayleigh number sensitivity studies (Pr=1, A=1)	95
3-7.	Summary of results for Prandtl number sensitivity studies	104
3-8.	Summary of results for aspect ratio sensitivity studies	108

LIST OF FIGURES

FIGURE		PAGE
1-1.	Use of a liquid-filled rectangular enclosure to cool a component board by natural convection	3
1-2.	Idealized enclosure geometries and thermal boundary conditions	5
2-1.	Schematic representation of the required computations	24
3-1.	Comparison of SIMPLER algorithm results with the benchmark solution of de Vahl Davis (1983)	49
3-2.	Effect of grid size on dimensionless temperature on the LHVW	53
3-3.	Streamlines for various grid sizes with uniform heat flux distribution along the LHVW	54
3-4.	Heatlines for various grid sizes with uniform heat flux distribution along the LHVW	55
3-5.	Isothermal contour lines for various grid sizes with uniform heat flux distribution along the LHVW	56
3-6.	Effect of grid spacing on predicted temperatures on the LHVW	58
3-7.	The nonuniform 13 x 13 grid used for optimization studies	59
3-8.	Effect of grid size on the computer CPU time required for solution of the natural convection problem	60
3-9.	Effect of grid size on temperatures obtained from optimal heat flux distribution studies	61
3-10.	Effect of grid size on computer CPU time required for solution of the optimal heat flux distribution problem	63

3-11. Optimal heat flux distribution for minimizing the average temperature of the LHVW (Case 1 of optimization problem number 1) 66

3-12. Summary of results for Case 1 of optimization problem number 1 68

3-13. Optimal heat flux distribution for minimizing the peak temperature of the LHVW (Case 2 of optimization problem number 1) 70

3-14. Summary of results for Case 2 of optimization problem number 1 71

3-15. Optimal heat flux distribution for minimizing the average temperature on the LHVW with $\theta_{max} \leq 0.6$ and fixed total heating rate 73

3-16. Optimal heat flux distribution for minimizing the average temperature on the LHVW with $\theta_{max} \leq 0.4$ and fixed total heating rate 74

3-17. Minimum average nondimensional temperature on the LHVW versus upperbound on peak nondimensional temperature on the LHVW 75

3-18. Summary of results for Case 3 of optimization problem number 1 with $\theta_{max} \leq 0.6$ 76

3-19. Summary of results for Case 3 of optimization problem number 1 with $\theta_{max} \leq 0.4$ 77

3-20. Comparison of heat flux distributions for Case 3 of optimization problem number 1 and the corresponding case for optimization problem number 2 82

3-21. Optimal polynomial heat flux distribution for Case 1 of optimization problem number 1 86

3-22. Optimal polynomial heat flux distribution for Case 2 of optimization problem number 1 88

3-23. Optimal polynomial heat flux distribution for Case 3 of optimization problem number 1 with $\theta_{max} \leq 0.4$ 89

3-24. Sensitivity of the optimal average nondimensional temperature on the LHVW to modified Rayleigh number 93

3-25. Optimal nondimensional temperatures on the LHVW for modified Rayleigh numbers from 10^3 to 10^6 94

3-26. Comparison of numerically predicted values of Nusselt number with approximate relationship for isothermal vertical walls 99

3-27. Sensitivity of the optimal average nondimensional temperatures on the LHVW to Prandtl number 102

3-28. Optimal nondimensional temperatures on the LHVW for Prandtl numbers from .1 to 100 103

3-29. Sensitivity of the optimal average nondimensional temperatures on the LHVW to enclosure aspect ratio 106

3-30. Optimal nondimensional temperatures on the LHVW for enclosure aspect ratios from .2 to 5 107

3-31. Comparison of numerically predicted Nusselt number dependence on enclosure aspect ratio with relationship derived by Berkovsky and Polevikov (1976) 110

3-32. Sensitivity of the optimal temperatures on the LHVW to Rayleigh number for thermal boundary condition Type 2 112

3-33. Sensitivity of the optimal temperatures on the LHVW to Rayleigh number for thermal boundary condition Type 3 113

A-1. Nomenclature for the computational grid 134

A-2. Boundary control volume geometry 135

A-3. Staggered grid for velocities 140

C-1. Summary of results from modified Rayleigh number sensitivity studies for uniform heat flux distribution with $Ra^*=10^3$ 200

C-2. Summary of results from modified Rayleigh number sensitivity studies for Case 1 type optimization with $Ra^*=10^3$ 201

C-3. Summary of results from modified Rayleigh number sensitivity studies for Case 2 type optimization with $Ra^*=10^3$ 202

C-4. Summary of results from modified Rayleigh number sensitivity studies for Case 3 type optimization with $Ra^*=10^3$ 203

C-5. Summary of results from modified Rayleigh number sensitivity studies for uniform heat flux distribution with $Ra^*=10^4$ 204

C-6. Summary of results from modified Rayleigh number sensitivity studies for Case 1 type optimization with $Ra^*=10^4$ 205

C-7. Summary of results from modified Rayleigh number sensitivity studies for Case 2 type optimization with $Ra^*=10^4$ 206

C-8. Summary of results from modified Rayleigh number sensitivity studies for Case 3 type optimization with $Ra^*=10^4$ 207

C-9. Summary of results from modified Rayleigh number sensitivity studies for uniform heat flux distribution with $Ra^*=10^5$ 208

C-10. Summary of results from modified Rayleigh number sensitivity studies for Case 1 type optimization with $Ra^*=10^5$ 209

C-11. Summary of results from modified Rayleigh number sensitivity studies for Case 2 type optimization with $Ra^*=10^5$ 210

C-12. Summary of results from modified Rayleigh number sensitivity studies for Case 3 type optimization with $Ra^*=10^5$ 211

C-13. Summary of results from modified Rayleigh number sensitivity studies for uniform heat flux distribution with $Ra^*=10^6$ 212

C-14. Summary of results from modified Rayleigh number sensitivity studies for Case 1 type optimization with $Ra^*=10^6$ 213

C-15. Summary of results from modified Rayleigh number sensitivity studies for Case 2 type optimization with $Ra^*=10^6$ 214

C-16. Summary of results from modified Rayleigh number sensitivity studies for Case 3 type optimization with $Ra^*=10^6$ 215

C-17. Summary of results from Prandtl number sensitivity studies for uniform heat flux distribution with Pr = 0.1 217

C-18. Summary of results from Prandtl number sensitivity studies for Case 1 type optimization with Pr = 0.1 218

C-19. Summary of results from Prandtl number sensitivity studies for Case 2 type optimization with Pr = 0.1 219

C-20. Summary of results from Prandtl number sensitivity studies for Case 3 type optimization with Pr = 0.1 220

C-21. Summary of results from Prandtl number sensitivity studies for uniform heat flux distribution with Pr = 6 221

C-22. Summary of results from Prandtl number sensitivity studies for Case 1 type optimization with Pr = 6 222

C-23. Summary of results from Prandtl number sensitivity studies for Case 2 type optimization with Pr = 6 223

C-24. Summary of results from Prandtl number sensitivity studies for Case 3 type optimization with Pr = 6 224

C-25. Summary of results from Prandtl number sensitivity studies for uniform heat flux distribution with Pr = 100 225

C-26. Summary of results from Prandtl number sensitivity studies for Case 1 type optimization with Pr = 100 226

C-27. Summary of results from Prandtl number sensitivity studies for Case 2 type optimization with Pr = 100 227

C-28. Summary of results from Prandtl number sensitivity studies for Case 3 type optimization with Pr = 100 228

C-29. Summary of results from aspect ratio sensitivity studies for uniform heat flux distribution with A = 0.2 230

C-30. Summary of results from aspect ratio sensitivity studies for Case 1 type optimization with A = 0.2 231

C-31. Summary of results from aspect ratio sensitivity studies for Case 2 type optimization with A = 0.2 232

C-32. Summary of results from aspect ratio sensitivity studies for Case 3 type optimization with A = 0.2 233

C-33. Summary of results from aspect ratio sensitivity studies for uniform heat flux distribution with A = 0.5 234

C-34. Summary of results from aspect ratio sensitivity studies for Case 1 type optimization with A = 0.5 235

C-35. Summary of results from aspect ratio sensitivity studies for Case 2 type optimization with A = 0.5 236

C-36. Summary of results from aspect ratio sensitivity studies for Case 3 type optimization with A = 0.5 237

C-37. Summary of results from aspect ratio sensitivity studies for uniform heat flux distribution with A = 2 238

C-38. Summary of results from aspect ratio sensitivity studies for Case 1 type optimization with A = 2 239

C-39. Summary of results from aspect ratio sensitivity studies for Case 2 type optimization with A = 2 240

C-40. Summary of results from aspect ratio sensitivity studies for Case 3 type optimization with A = 2 241

C-41. Summary of results from aspect ratio sensitivity studies for uniform heat flux distribution with A = 5 242

C-42. Summary of results from aspect ratio sensitivity studies for Case 1 type optimization with A = 5 243

C-43. Summary of results from aspect ratio sensitivity studies for Case 2 type optimization with A = 5 244

C-44. Summary of results from aspect ratio sensitivity studies for Case 3 type optimization with A = 5 245

C-45. Summary of results from thermal boundary condition sensitivity studies for uniform heat flux distribution with thermal boundary condition Type 2 and $Ra^*=10^3$ 247

C-46. Summary of results from thermal boundary condition sensitivity studies for Case 1 type optimization with thermal boundary condition Type 2 and $Ra^*=10^3$ 248

C-47. Summary of results from thermal boundary condition sensitivity studies for Case 2 type optimization with thermal boundary condition Type 2 and $Ra^*=10^3$ 249

C-48. Summary of results from thermal boundary condition sensitivity studies for Case 3 type optimization with thermal boundary condition Type 2 and $Ra^*=10^3$ 250

C-49. Summary of results from thermal boundary condition sensitivity studies for uniform heat flux distribution with thermal boundary condition Type 2 and $Ra^*=10^4$ 251

C-50. Summary of results from thermal boundary condition sensitivity studies for Case 1 type optimization with thermal boundary condition Type 2 and $Ra^*=10^4$ 252

C-51. Summary of results from thermal boundary condition sensitivity studies for Case 2 type optimization with thermal boundary condition Type 2 and $Ra^*=10^4$ 253

C-52. Summary of results from thermal boundary condition sensitivity studies for Case 3 type optimization with thermal boundary condition Type 2 and $Ra^*=10^4$ 254

C-53. Summary of results from thermal boundary condition sensitivity studies for uniform heat flux distribution with thermal boundary condition Type 2 and $Ra^*=10^5$ 255

C-54. Summary of results from thermal boundary condition sensitivity studies for Case 1 type optimization with thermal boundary condition Type 2 and $Ra^*=10^5$ 256

C-55. Summary of results from thermal boundary condition sensitivity studies for Case 2 type optimization with thermal boundary condition Type 2 and $Ra^*=10^5$ 257

C-56. Summary of results from thermal boundary condition sensitivity studies for Case 3 type optimization with thermal boundary condition Type 2 and $Ra^*=10^5$ 258

C-57. Summary of results from thermal boundary condition sensitivity studies for uniform heat flux distribution with thermal boundary condition Type 2 and $Ra^*=10^6$ 259

C-58. Summary of results from thermal boundary condition sensitivity studies for Case 1 type optimization with thermal boundary condition Type 2 and $Ra^*=10^6$ 260

C-59. Summary of results from thermal boundary condition sensitivity studies for Case 2 type optimization with thermal boundary condition Type 2 and $Ra^*=10^6$ 261

C-60. Summary of results from thermal boundary condition sensitivity studies for Case 3 type optimization with thermal boundary condition Type 2 and $Ra^*=10^6$ 262

C-61. Summary of results from thermal boundary condition sensitivity studies for uniform heat flux distribution with thermal boundary condition Type 3 and $Ra^*=10^3$ 263

C-62. Summary of results from thermal boundary condition sensitivity studies for Case 1 type optimization with thermal boundary condition Type 3 and $Ra^*=10^3$ 264

C-63. Summary of results from thermal boundary condition sensitivity studies for Case 2 type optimization with thermal boundary condition Type 3 and $Ra^*=10^3$ 265

C-64. Summary of results from thermal boundary condition sensitivity studies for Case 3 type optimization with thermal boundary condition Type 3 and $Ra^*=10^3$ 266

C-65. Summary of results from thermal boundary condition sensitivity studies for uniform heat flux distribution with thermal boundary condition Type 3 and $Ra^*=10^4$ 267

C-66. Summary of results from thermal boundary condition sensitivity studies for Case 1 type optimization with thermal boundary condition Type 3 and $Ra^*=10^4$ 268

C-67. Summary of results from thermal boundary condition sensitivity studies for Case 2 type optimization with thermal boundary condition Type 3 and $Ra^*=10^4$ 269

C-68. Summary of results from thermal boundary condition sensitivity studies for Case 3 type optimization with thermal boundary condition Type 3 and $Ra^*=10^4$ 270

C-69. Summary of results from thermal boundary condition sensitivity studies for uniform heat flux distribution with thermal boundary condition Type 3 and $Ra^*=10^5$ 271

C-70. Summary of results from thermal boundary condition sensitivity studies for Case 1 type optimization with thermal boundary condition Type 3 and $Ra^*=10^5$ 272

C-71. Summary of results from thermal boundary condition sensitivity studies for Case 2 type optimization with thermal boundary condition Type 3 and $Ra^*=10^5$ 273

C-72. Summary of results from thermal boundary condition sensitivity studies for Case 3 type optimization with thermal boundary condition Type 3 and $Ra^*=10^5$ 274

C-73. Summary of results from thermal boundary condition sensitivity studies for uniform heat flux distribution with thermal boundary condition Type 3 and $Ra^*=10^6$ 275

C-74. Summary of results from thermal boundary condition sensitivity studies for Case 1 type optimization with thermal boundary condition Type 3 and $Ra^*=10^6$ 276

C-75. Summary of results from thermal boundary condition sensitivity studies for Case 2 type optimization with thermal boundary condition Type 3 and $Ra^*=10^6$ 277

C-76. Summary of results from thermal boundary condition sensitivity studies for Case 3 type optimization with thermal boundary condition Type 3 and $Ra^*=10^6$ 278

LIST OF SYMBOLS

A = aspect ratio of the rectangular enclosure = W/H

c_p = constant pressure specific heat of fluid

g = gravitational acceleration

h = heatfunction

$\overline{h}_H$ = heat transfer coefficient averaged over the height of the enclosure

H = height of the rectangular enclosure

k = thermal conductivity of fluid

$\overline{Nu}_H$ = average Nusselt number based on enclosure height = $h_H H / k$

p_d = "motion pressure" in the fluid - defined as the difference between the actual pressure in the fluid and the pressure in the fluid at rest at the (uniform) reference temperature

P = nondimensional pressure = $\dfrac{p_d}{\rho(\alpha^2/H^2)}$

Pr = Prandtl number = $\dfrac{c_p\ \mu}{k} = \dfrac{\nu}{\alpha}$

Q_o = total rate of heat transfer from the heated vertical wall of the enclosure to the fluid

$$= \int_0^H q_o(y)\ dy$$

Q = dimensionless total rate of heat transfer from the heated vertical wall of the enclosure to the fluid, based on the (specified) total rate of heat transfer

$$= \int_0^1 q(Y)\ dY = 1$$

Q' = dimensionless total rate of heat transfer from the heated vertical wall of the enclosure to the fluid, based on the (specified) average temperature of the heated vertical wall

$$= \frac{Q_o}{k\ (T_{ave} - T_o)} = \int_0^1 q'(Y)\ dY$$

$q_o(y)$ = local heat flux on the heated vertical wall of the enclosure

q_{ave} = average heat flux along the heated vertical wall of the enclosure

$$= Q_o/H = \frac{1}{H} \int_0^H q_o(y)\ dy$$

$q(Y)$ = local nondimensional heat flux on the heated vertical wall of the enclosure, based on the (specified) total rate of heat transfer from the heated vertical wall

$$= \frac{q_o(y)}{(Q_o/H)} = \frac{q_o(y)}{q_{ave}}$$

$q'(Y)$ = local nondimensional heat flux on the heated vertical wall of the enclosure based on the (specified) average temperature of the heated vertical wall

$$= \frac{q_o(y)}{k\ (T_{ave} - T_o)\ /\ H}$$

Ra^* = modified Rayleigh number based on the average heat flux along the heated vertical wall

$$= \frac{g\ \beta\ q_{ave}\ H^4}{k\ \nu\ \alpha}$$

Ra = Rayleigh number based on the (specified) average temperature of the heated vertical wall

$$= \frac{g\ \beta\ H^3\ (T_{ave} - T_o)}{\nu\ \alpha}$$

$T(x,y)$ = temperature of the fluid

T_{ave} = average temperature of the heated vertical wall

$$= \frac{1}{H} \int_0^H T(0,y)\, dy$$

T_{max} = maximum temperature of the heated vertical wall

T_o = temperature of the isothermal wall(s) of the enclosure

u = fluid velocity in the x-direction

U = nondimensional fluid velocity in the x-direction = $\frac{u}{(\alpha/H)}$

v = fluid velocity in the y-direction

V = nondimensional fluid velocity in the y-direction = $\frac{v}{(\alpha/H)}$

x = horizontal spatial coordinate

X = nondimensional horizontal spatial coordinate = x / H

y = vertical spatial coordinate

Y = nondimensional vertical spatial coordinate = y / H

α = thermal diffusivity of the fluid

β = thermal expansion coefficient of the fluid

Φ = nondimensional heatfunction = h/Q_o

μ = dynamic viscosity of the fluid

ν = kinematic viscosity of the fluid

θ = nondimensional temperature based on the (specified) average heat flux along the heated vertical wall

$$= \frac{k\,(T(x,y) - T_o)}{H\, q_{ave}}$$

θ' = nondimensional temperature based on the (specified) average temperature of the heated vertical wall

$$= \frac{(T(x,y) - T_o)}{(T_{ave} - T_o)}$$

θ_{ave} = average nondimensional temperature along the left-hand vertical wall of the enclosure

$$= \int_0^1 \theta(0,Y)\, dY$$

θ_{max} = maximum nondimensional temperature along the left-hand vertical wall of the enclosure

ρ = density of the fluid

ψ = streamfunction

Ψ = nondimensional streamfunction = ψ/α

CHAPTER 1

INTRODUCTION

1.1 Motivation For The Present Research

Current trends in electronic design are resulting in increasingly smaller devices being mounted on component boards in ever denser arrays. The net result has been a rapid rise in the average heat flux on a typical component board. Simultaneously, performance and reliability requirements have been dictating lower and lower operating temperatures (Oktay, et al, 1986). Clearly, these trends cannot continue without the adoption of new approaches to the electronics cooling problem. This dissertation addresses one such approach, a possible modification of the design process itself, which may help alleviate cooling problems in electronic equipment.

Traditionally, the thermal aspects of design have not been fully incorporated in the initial phases of the design process for electronic equipment. Instead, the heat transfer engineer is presented with a "completed" design and then asked to devise some suitable scheme for satisfying the cooling requirements. This is obviously an undesireable situation and in light of the trends alluded to above, it would seem that the time to integrate thermal considerations into the initial phase of the design process has arrived. This realization served as the motivation for the present research.

Of specific interest in this work is the optimum placement of electronic components on a circuit board. The placement of components on a circuit board is typically based on considerations such as functional requirements and the ease of design and manufacture. Little or no thought has been given to the possibility of requiring that the location of each component on a board must depend on its ultimate impact on the cooling requirements for that board. Thus, the purpose of the present work is to assess the alleviation of

component board cooling problems that might occur if designers were given the freedom to specify the location of every component based on thermal considerations alone. The examination of this limiting case will establish an upper bound on the possible benefits to be derived from incorporating thermal considerations in the initial phase of the design process.

In order to proceed, it is necessary to focus attention on a specific electronics cooling application that will serve as a "model problem" in this initial investigation.

1.2 Selection Of The Configurations To Be Investigated

For reasons of economy and reliability, design engineers consider natural convection as the most desirable mode of cooling for electronic equipment whenever conditions permit its use. Thus, one newly important class of electronic cooling problems involves the use of natural convection flows in a liquid-filled rectangular enclosure to cool a component board that forms one vertical wall of the enclosure. This technique is illustrated in Figure 1-1. Either the top horizontal surface, or the vertical surface directly opposite the component board, or both of these surfaces, are actively cooled, isothermal surfaces. The bottom horizontal surface of the enclosure and the vertical walls that are perpendicular to the component board are all heavily insulated surfaces.

In an actual application, the natural convection flows in the enclosure are fully three-dimensional and the components serve as discrete heat sources that protrude from the surface of the component board into the dielectric liquid coolant in the enclosure. Since the fluid in this case is a liquid, radiation heat transfer can be assumed to be negligible. Three simplifications of the conditions encountered in an actual enclosure have been adopted for the purposes of this study. First, the natural convection flows are assumed to be two-dimensional. The two-dimensional enclosure geometries and the three

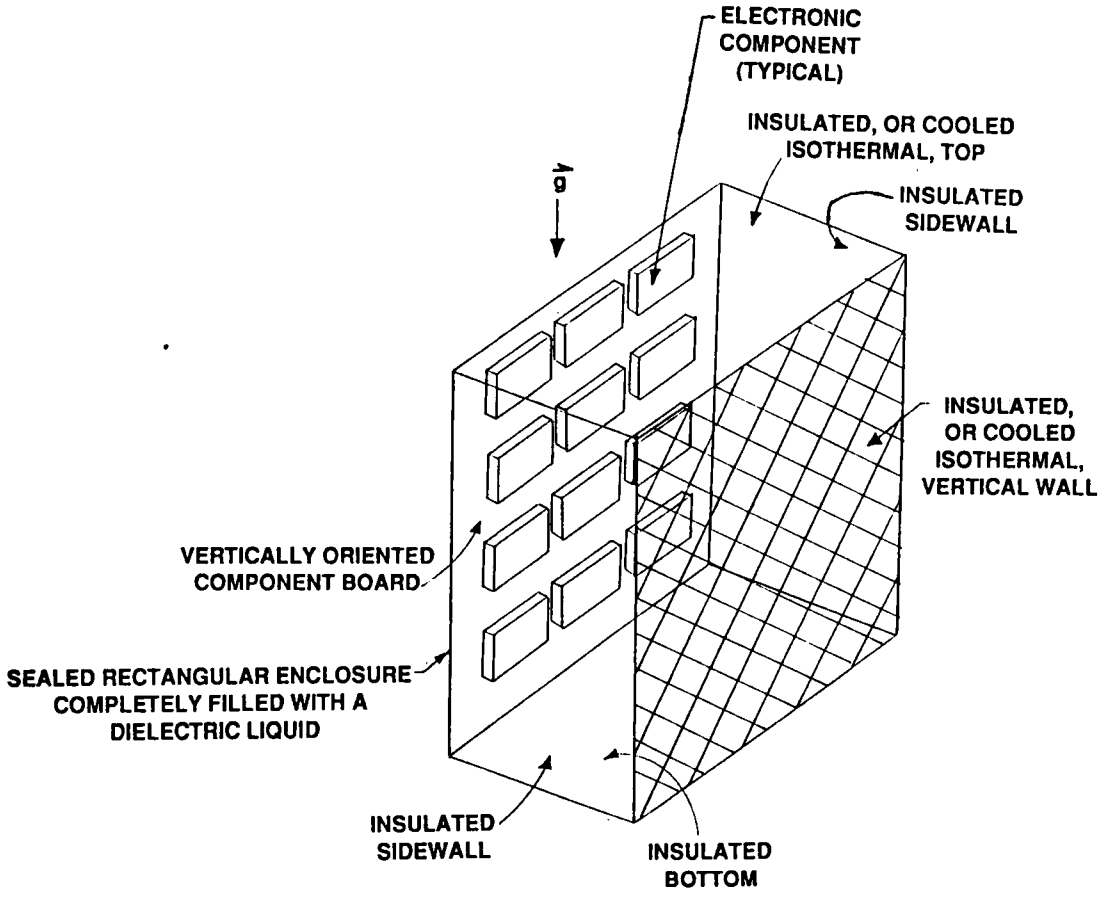


Figure 1-1. Use of a liquid-filled rectangular enclosure to cool a component board by natural convection

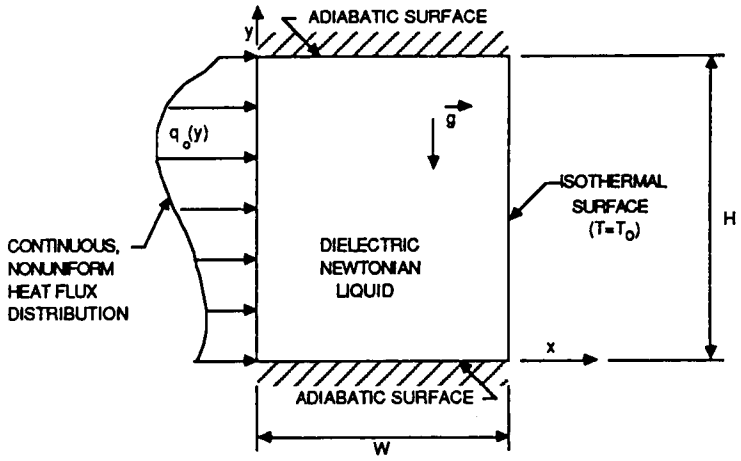
types of thermal boundary conditions examined are shown in Figure 1-2. In addition to the arbitrary heat flux distribution on the left-hand vertical wall (LHVW), the thermal boundary conditions for the enclosure shown in Figure 1-2 include various combinations of adiabatic and isothermal surfaces. "Type 1 boundary conditions", which include adiabatic horizontal walls and a cold, isothermal right-hand vertical wall, are considered extensively in this study and are therefore referred to as the "reference set" of boundary conditions. "Type 2 boundary conditions", which consist of adiabatic lower horizontal and right-hand vertical walls and a cold, isothermal upper horizontal wall, and "Type 3 boundary conditions", which consist of an adiabatic lower horizontal wall and cold, isothermal upper horizontal and right-hand vertical walls, are considered only for a limited number of cases.

The second simplification of the conditions found in an actual enclosure involves modeling the discrete local heat flux distribution on a real component board as a continuous distribution, which is also shown in Figure 1-2. Finally, the third simplification involves modeling the rough surface of a component board as a smooth surface.

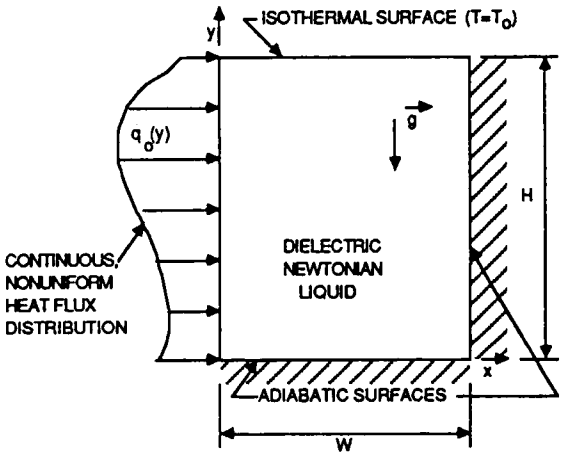
Before presenting a formal statement of the problem, the governing equations and boundary conditions for the natural convection flows in the enclosure will be discussed.

1.3 The Governing Equations And Boundary Conditions For The Natural Convection Flows In The Enclosures

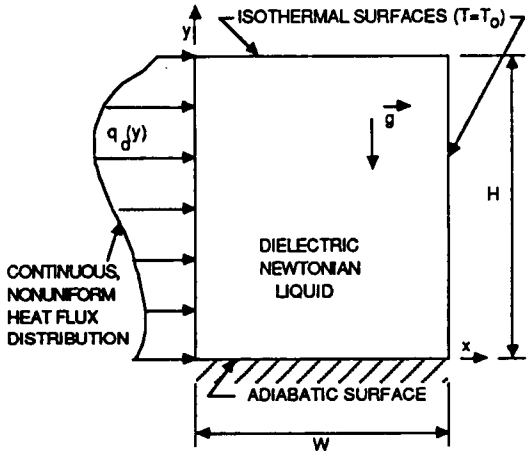
Examination of the dimensionless forms of the governing equations and boundary conditions for the natural convection flows in the enclosures will reveal the functional dependence of the objective functions in the optimization problems on the dimensionless parameters that govern these flows. Thus, these equations and their boundary conditions will first be stated in terms of



(1-2a) Type 1 (Reference) Boundary Conditions



(1-2b) Type 2 Boundary Conditions



(1-2c) Type 3 Boundary Conditions

Figure 1-2. Idealized enclosure geometries and thermal boundary conditions

physical variables and then recast in nondimensional form by introducing an appropriate set of dimensionless variables.

The governing equations are the equations for conservation of mass, Newton's second law in the x- and y-directions and the conservation of energy. If the well-known Boussinesq approximation (Gebhart, et al, 1988) is employed, the laminar, two-dimensional, steady-state forms of these equations may be written in physical variables as:

$$\frac{\partial u}{\partial x} + \frac{\partial v}{\partial y} = 0, \tag{1-1}$$

$$u\frac{\partial u}{\partial x} + v\frac{\partial u}{\partial y} = -\frac{1}{\rho}\frac{\partial p_d}{\partial x} + \nu\left(\frac{\partial^2 u}{\partial x^2} + \frac{\partial^2 u}{\partial y^2}\right), \tag{1-2}$$

$$u\frac{\partial v}{\partial x} + v\frac{\partial v}{\partial y} = -\frac{1}{\rho}\frac{\partial p_d}{\partial y} + \nu\left(\frac{\partial^2 v}{\partial x^2} + \frac{\partial^2 v}{\partial y^2}\right) + g\beta(T - T_o), \tag{1-3}$$

and,

$$u\frac{\partial T}{\partial x} + v\frac{\partial T}{\partial y} = \alpha\left(\frac{\partial^2 T}{\partial x^2} + \frac{\partial^2 T}{\partial y^2}\right), \tag{1-4}$$

where u is the horizontal (x-direction) component of the velocity, v is the vertical (y-direction) component of the velocity, p_d is the so-called motion pressure, which is the difference between the actual pressure in the fluid and the pressure in the fluid at rest in the (uniform) reference condition, T is the local fluid temperature, T_o is the temperature of the isothermal wall(s), g is the magnitude of the acceleration due to gravity, ρ is the fluid density, ν is the kinematic viscosity of the fluid, α is the thermal diffusivity of the fluid, and β is the thermal expansion coefficient of the fluid. Next, the boundary conditions will be stated in physical variables.

The boundary conditions that remain valid for all three of the cases considered are given by:

$$u(0,y) = v(0,y) = 0 \qquad \text{for } 0 \le y \le H, \qquad (1\text{-}5)$$

$$-k\frac{\partial T}{\partial x}\Big|_{x=0} = q_o(y) \qquad \text{for } 0 \le y \le H, \qquad (1\text{-}6)$$

$$u(W,y) = v(W,y) = 0 \qquad \text{for } 0 \le y \le H, \qquad (1\text{-}7)$$

$$u(x,0) = v(x,0) = 0 \qquad \text{for } 0 \le x \le W, \qquad (1\text{-}8)$$

$$\frac{\partial T}{\partial y}\Big|_{y=0} = 0 \qquad \text{for } 0 \le x \le W, \qquad (1\text{-}9)$$

and,

$$u(x,H) = v(x,H) = 0 \qquad \text{for } 0 \le x \le W \qquad (1\text{-}10)$$

where k is the thermal conductivity of the fluid and W and H are the width and height, respectively, of the rectangular enclosure.

The "Type 1 Boundary Conditions" shown in Figure 1-2(a) are given by:

$$T(W,y) = T_o \qquad \text{for } 0 \le y \le H, \qquad (1\text{-}11)$$

on the cold, isothermal, right-hand vertical wall, and

$$\frac{\partial T}{\partial y}\Big|_{y=H} = 0 \qquad \text{for } 0 \le x \le W, \qquad (1\text{-}12)$$

on the adiabatic, top horizontal surface.

Similarly, the "Type 2 Boundary Conditions" shown in Figure 1-2(b) are given by:

$$T(x,H) = T_o \qquad \text{for } 0 \le x \le W, \qquad (1\text{-}13)$$

on the cold, isothermal, top horizontal surface, and

$$\frac{\partial T}{\partial x}\Big|_{x=W} = 0 \qquad \text{for } 0 \le y \le H, \qquad (1\text{-}14)$$

on the adiabatic, right-hand vertical wall.

Finally, the "Type 3 Boundary Conditions" shown in figure 1-2(c) are given by:

$$T(W,y) = T_o \qquad \text{for } 0 \le y \le H, \qquad (1\text{-}15)$$

and,

$$T(x,H) = T_o \qquad \text{for } 0 < x < W, \tag{1-16}$$

on the cold, isothermal, top horizontal and right-hand vertical surfaces.

The governing equations and their boundary conditions will now be recast in an appropriate nondimensional form. This process is begun by defining the following nondimensional variables:

$$X \equiv x/H = \text{nondimensional horizontal spatial coordinate,} \tag{1-17}$$

$$Y \equiv y/H = \text{nondimensional vertical spatial coordinate,} \tag{1-18}$$

$$U(X,Y) \equiv \frac{u(x,y)}{(\alpha/H)} = \text{nondimensional velocity component in the horizontal direction,} \tag{1-19}$$

$$V(X,Y) \equiv \frac{v(x,y)}{(\alpha/H)} = \text{nondimensional velocity component in the vertical direction,} \tag{1-20}$$

$$P(X,Y) \equiv \frac{p_d(x,y)}{\rho(\alpha^2/H^2)} = \text{nondimensional motion pressure,} \tag{1-21}$$

and,

$$\theta(X,Y) \equiv \frac{k\,(T(x,y) - T_o)}{H\,q_{ave}} = \text{nondimensional temperature,} \tag{1-22}$$

where

$$q_{ave} = \frac{1}{H}\int_0^H q_o(y)\,dy \tag{1-23}$$

is the average heat flux along the heated (left-hand) vertical wall.

Substituting these nondimensional forms of the variables into the governing equations yields

$$\frac{\partial U}{\partial X} + \frac{\partial V}{\partial Y} = 0, \tag{1-24}$$

$$U\frac{\partial U}{\partial X} + V\frac{\partial U}{\partial Y} = -\frac{\partial P}{\partial X} + Pr\left(\frac{\partial^2 U}{\partial X^2} + \frac{\partial^2 U}{\partial Y^2}\right), \tag{1-25}$$

$$U\frac{\partial V}{\partial X} + V\frac{\partial V}{\partial Y} = -\frac{\partial P}{\partial Y} + Pr\left(\frac{\partial^2 V}{\partial X^2} + \frac{\partial^2 V}{\partial Y^2}\right) + Ra^*\,Pr\,\theta, \tag{1-26}$$

and,

$$U\frac{\partial\theta}{\partial X} + V\frac{\partial\theta}{\partial Y} = \left(\frac{\partial^2\theta}{\partial X^2} + \frac{\partial^2\theta}{\partial Y^2}\right), \tag{1-27}$$

where: $Pr = \frac{c_p \mu}{k} = \frac{\nu}{\alpha}$ = Prandtl number, (1-28)

and,

$Ra^* = \frac{\beta g q_{ave} H^4}{k \nu \alpha}$ = modified Rayleigh number (based on the average heat flux, q_{ave}, along the LHVW). (1-29)

The nondimensional forms of the boundary conditions that hold for all of the cases considered are given by:

$$\left.\begin{aligned} U(0,Y) = V(0,Y) = 0 \quad &(1\text{-}30)\\ -\frac{\partial\theta}{\partial X}\Big|_{X=0} = q(Y) \quad &(1\text{-}31)\end{aligned}\right\} \quad \text{for } 0 \le Y \le 1,$$

$$U(A,Y) = V(A,Y) = 0 \qquad \text{for } 0 \le Y \le 1, \tag{1-32}$$

$$\left.\begin{aligned} U(X,0) = V(X,0) = 0 \quad &(1\text{-}33)\\ \frac{\partial\theta}{\partial Y}\Big|_{Y=0} = 0 \quad &(1\text{-}34)\end{aligned}\right\} \quad \text{for } 0 \le X \le A,$$

and,

$$U(X,1) = V(X,1) = 0 \qquad \text{for } 0 \le X \le A, \tag{1-35}$$

where: $A = (W/H)$ = aspect ratio of the enclosure, (1-36)

$$q(Y) = \frac{q_o(y)}{(Q_o/H)} = \frac{q_o(y)}{q_{ave}}, \tag{1-37}$$

and,

$Q_o = \int_0^H q_o(y)\, dy$ = total rate of heat transfer from the heated vertical wall (the LHVW) to the fluid. (1-38)

The nondimensional forms of the Type 1 boundary conditions (Figure 1-2a) are given by:

$$\theta(A,Y) = 0 \qquad \text{for } 0 \le Y \le 1\,, \tag{1-39}$$

and,

$$\left.\frac{\partial\theta}{\partial Y}\right|_{Y=1} = 0 \qquad \text{for } 0 \le X \le A. \tag{1-40}$$

Similarly, the nondimensional forms of the Type 2 boundary conditions (Figure 1-2b) are given by:

$$\theta(X,1) = 0 \qquad \text{for } 0 \le X \le A\,, \tag{1-41}$$

and,

$$\left.\frac{\partial\theta}{\partial X}\right|_{X=A} = 0 \qquad \text{for } 0 \le Y \le 1\,. \tag{1-42}$$

Finally, the nondimensional forms of the Type 3 boundary conditions (Figure 1-2c) are given by:

$$\theta(A,Y) = 0 \qquad \text{for } 0 \le Y \le 1\,, \tag{1-43}$$

and,

$$\theta(X,1) = 0 \qquad \text{for } 0 \le X \le A\,. \tag{1-44}$$

As shown above, the natural convection flows in the enclosures depend on the values of three dimensionless parameters: the modified Rayleigh number (Ra^*), the Prandtl number (Pr), and the aspect ratio of the enclosure (A). The details of a given natural convection flow in an enclosure will also depend upon the specific form of the local heat flux distribution on the LHVW and the type of thermal boundary conditions (1,2, or 3) imposed on the top horizontal and right-hand vertical walls.

1.4 Formal Statements Of The Optimization Problems

Consider the two-dimensional, steady-state, laminar, natural convection flows in a vertically-oriented, rectangular enclosure that is completely filled

with a Newtonian fluid. The unknown local heat flux distribution along the actively heated LHVW is denoted by $q_o(y)$. The thermal boundary conditions on the top horizontal and right-hand vertical walls are either "Type 1", "Type 2", or "Type 3" boundary conditions as designated in Figure 1-2, and the bottom horizontal wall is assumed to be an adiabatic surface. As shown above, a given natural convection flow is completely determined by specifying: (1) the dimensionless local heat flux distribution, q(Y), on the LHVW; (2) the values of the modified Rayleigh number, Ra*, the Prandtl number, Pr, and the aspect ratio of the enclosure, A; and (3) the type of thermal boundary conditions for the top horizontal and right-hand vertical walls.

Two different optimization problems were investigated in this work. The primary problem of interest here, to be referred to as "optimization problem number one", is to determine the dimensionless local heat flux distribution, q(Y), on the heated vertical wall such that either (1) the average nondimensional temperature of this wall is minimized (referred to as Case 1), (2) the maximum nondimensional temperature on this wall is minimized (referred to as Case 2), or (3) the average nondimensional temperature of this wall is minimized subject to the constraint that the maximum nondimensional temperature on the wall remains below a specified upper bound (referred to as Case 3). For all three of these cases, which are subsets of optimization problem number 1, the optimization is performed subject to the integral constraint that the dimensionless total rate of heat transfer from the LHVW, Q, is specified to be equal to unity. The dimensionless total rate of heat transfer from the LHVW, Q, is given by:

$$Q = \frac{Q_o}{q_{ave} H} = \int_0^1 q(Y)\, dY = 1 \quad . \tag{1-45}$$

The solutions of this problem will provide electronic designers with the

information required to properly distribute a total thermal load, Q, along the LHVW of the enclosure through optimal placement of electronic components along this surface.

A second class of optimization problems was also investigated to determine the dimensionless local heat flux distribution on the heated vertical wall such that the dimensionless total rate of heat transfer from the LHVW is maximized subject to the constraints that (1) the average temperature of the LHVW is a specified constant, and (2) the peak temperature of the LHVW remains below an upper bound. This problem will be referred to as "optimization problem number 2". The purpose of examining this second class of problems is to compare this alternate optimization approach with the reference approach discussed above to determine whether it has any advantages (eg. less computer run time). Since the average temperature of the LHVW is a specified constant and the total rate of heat transfer is the objective function for this alternate class of problems, it is convenient to nondimensionalize the heat flux, total rate of heat transfer, and temperature in terms of the specified average temperature instead of the unknown (i.e., to be determined) total rate of heat transfer. The dimensionless forms of the local heat flux , q'(Y), total heat transfer from the LHVW , Q', and temperature, θ', for this class of problems are given by:

$$q'(Y) = \frac{q_o(y)}{(k\,(T_{ave} - T_o)/H)} \quad , \tag{1-46}$$

$$Q' = \frac{\int_0^H q_o(y)\,dy}{[k\,(T_{ave} - T_o)]} \tag{1-47}$$

$$\theta' = \frac{(T(x,y) - T_o)}{(T_{ave} - T_o)} \tag{1-48}$$

where T_{ave} is the (specified) average temperature along the LHVW, given by:

$$T_{ave} = \frac{1}{H} \int_0^H T(0,y)\, dy \quad \text{for } 0 \le y \le H \qquad (1\text{-}49)$$

The nondimensional variables X, Y, U, V, and P are defined as stated previously in equations 1-17 through 1-21. Substituting this set of nondimensional variables into the dimensional forms of the governing equations (equations 1-1 through 1-4) yields a set of nondimensional equations that are identical to those listed as equations 1-24 through 1-27 except that the modified Rayleigh number based on the total heating rate, Ra*, is replaced by the Rayleigh number, Ra, which is based on a (specified) average wall temperature, and the nondimensional temperature based on average wall temperature, θ', which is defined above, replaces the nondimensional temperature based on total heating rate, θ. The Rayleigh number based on average temperature is given by

$$Ra = \frac{\beta g (T_{ave} - T_o) H^3}{\nu \alpha} \quad . \qquad (1\text{-}50)$$

1.5 Literature Review

1.5.1 General References On Natural Convection. Natural convection flows in various configurations and geometries have been studied experimentally and analytically. Many of the results of greatest engineering interest have been included in the textbooks by Jaluria (1980) and Gebhart et al (1988).

1.5.2 Natural Convection Flows In Enclosures. Much of the previous research in natural convection has concentrated on external flows that form on bodies which are placed in a quiescent ambient environment at a temperature different from these bodies. When such flows are parabolic in nature, they can be understood and analyzed by use of the boundary layer approximation.

The boundary layer flow near the solid body is "weakly coupled" to the ambient surroundings; that is, to lowest order, the flow in the boundary layer may be computed by assuming that the flow outside the boundary layer region is known. Natural convection flows in enclosures, however, are quite different from external flows. These enclosure flows are elliptic in nature. Thus, the flows in any boundary layers that form on the solid surfaces of an enclosure are "strongly coupled" to the flows in the so-called "core" regions outside of these boundary layers, such that the motion at any point in the enclosure depends on the conditions at all other points in the flow field. Therefore, the flows immediately adjacent to the solid surfaces cannot be computed by assuming that the flow in the core region is known. Instead, simultaneous solution of the flows in all regions of the enclosure must be performed.

Survey papers by Ostrach (1972 and 1982), Catton (1978), Churchill (1983), and Hoogendorn (1986) on natural convection in enclosures summarize the experimental and analytical progress on this subject. Kimura and Bejan (1984) analyzed the natural convection in a rectangular enclosure with uniform heat fluxes on opposite vertical walls. This paper along with the works by de Vahl Davis and Jones (1983) and de Vahl Davis (1983) provide excellent test cases for verification of the numerical model of the two-dimensional natural convection flows of interest in the present study.

The effects of nonuniform boundary conditions (temperature or heat flux distributions) on natural convection in enclosures have been studied in several previous investigations, including those of Torrance and Rockett (1969), Torrance et al (1969), Berkovsky et al (1971), Chu et al (1976), Turner and Flack (1980), Chao et al (1981), Kelleher et al (1987), Lee et al (1987), Liu et al (1987), and Ozoe et al (1987). The geometries and boundary conditions investigated in each of these references are discussed below.

Torrance and Rockett (1969) performed numerical studies of the natural

convection flows induced in a vertically-oriented circular cylinder with a small heated spot centrally located on the bottom surface. The height of the cylinder was set equal to its radius. The radius of the isothermal hot spot was one-tenth of the radius of the cylinder. All other surfaces were assumed to be maintained at a cooler, uniform temperature. Results of their calculations, for a Prandtl number of 0.7 and Rayleigh numbers (based on hot spot temperature and enclosure height) ranging from 10^4 to 10^{10}, compared favorably with flow patterns and heat transfer rates determined in the companion experiments by Torrance et al (1969). The velocities and heat transfer rates were shown to scale with the square-root of the Rayleigh number. The experiments also included results for a rectangular enclosure with a centrally located hot spot on its bottom surface.

Berkovsky et al (1971) performed both experiments and numerical calculations of natural convection in rectangular enclosures. Their experiments considered a very small aspect ratio (aspect ratio = height/width = .015) enclosure with an imposed temperature distribution on the upper horizontal surface and a uniform cooler temperature on the bottom horizontal wall. Their numerical studies considered the natural convection in a two-dimensional, square enclosure with nonuniform temperature distributions of various types, including sinusoidal and linear variations. The other walls were considered to be isothermal. Streamfunction and isothermal contour plots and mean Nusselt numbers for various temperature distributions along the upper horizontal wall were presented for a Prandtl number of .707 (air) and Rayleigh numbers up to about 10^6. Their results showed that the circulation patterns and the dependence of the Nusselt number on Rayleigh number is very sensitive to the type of temperature distribution on the top wall.

Chu et al (1976) examined the effect of heater size and location on the natural convection in a two-dimensional rectangular enclosure. In their numerical simulation, the heater was modeled as an isothermal strip located

on an otherwise adiabatic vertical wall. The other vertical wall was assumed to be isothermal. The horizontal walls were assumed to be either both isothermal or both adiabatic. Calculations were performed for a Prandtl number of .7, Rayleigh numbers based on hot spot temperature up to 10^5, and aspect ratios of the rectangular enclosure ranging from .4 to 5. Their results showed that for the case with adiabatic horizontal walls the minimum peak wall temperature and maximum flow circulation occurs if the center of the discrete heat source is located below the midpoint of the vertical wall.

Turner and Flack (1980) performed experiments with natural convection of air in a rectangular enclosure that extended the numerical results of Chu et al to Rayleigh numbers up to about 10^7. Their experimental apparatus was configured to simulate the case with adiabatic horizontal walls. Their results confirmed that the optimal heater location for minimizing the peak wall temperature of the discrete heat source is at a position slightly less than half of the way up the vertical wall.

Chao et al (1981) performed numerical analyses to predict the natural convection flows in a three-dimensional rectangular enclosure with nonuniform temperature distributions on the bottom surface. Triangular wave-shaped temperature profiles were used to simulate the effect of having rows of cooling channels spaced at intervals along a cooled surface. The top surface was held at a cool isothermal temperature and the sides were adiabatic. The effect of inclination of the enclosure was studied for angles of inclination up to 180°. Computations were performed for a single set of parameters with a Rayleigh number of 6,000 and Prandtl number of 10. The general nature of the flow patterns was not significantly affected by the nonuniform temperature distributions. However, the transition from two roll cells to a single roll cell occured at a slightly higher angle of inclination for the nonuniform profiles compared with an isothermal profile. The variation of the mean Nusselt number with inclination was not changed significantly but the

magnitude increased with the amplitude of the surface temperature variations for angles up to 90°.

Kelleher et al (1987) performed an experimental study of natural convection in a water-filled rectangular enclosure with a small heater protruding from one vertical wall. The remainder of the vertical walls were insulated and the top and bottom walls were isothermal heat sinks. The enclosure had a depth of 203 mm, a horizontal width of 12.8 mm, and a vertical height of 152 mm. Three heater elevations were examined for Rayleigh numbers based on hot spot temperature ranging from $1x10^6$ to $8x10^6$. The Nusselt number was found to decrease as the heater position along the vertical wall was raised, which is consistent with the results by Chu et al and Turner and Flack.

Lee et al (1987) performed numerical studies of the same geometry and boundary conditions investigated experimentally by Kelleher et al in a companion paper. Nusselt numbers predicted from their three-dimensional model agree well with those obtained experimentally by Kelleher et al, especially at the higher end of the Rayleigh number range ($8x10^6$). It is interesting to note that Lee et al found that the flow velocity and heat transfer can be accurately predicted with a two-dimensional model in regions near the midplane in the direction of the enclosure depth.

Liu et al (1987) numerically modeled an array of discrete heat sources (power dissipating electronic chips) placed uniformly along one vertical wall of a three-dimensional rectangular enclosure filled with a dielectric fluid. The remaining vertical surfaces were adabatic and the top and bottom horizontal surfaces were isothermal. The Prandtl number and the Rayleigh number (based on chip height and surface heat flux at the chip) were 26 and 8.7 x 10^6, respectively, at a reference temperature of 21.1 °C. The temperature dependence of the fluid properties was accounted for in the analysis. Thus, the Boussinesq approximation was not invoked. The height and depth of the

enclosure were fixed at 120 mm and 140 mm, respectively. Widths of 9 mm, 18 mm and 30 mm were investigated. An array of nine chips, each with a length of 8 mm, height of 24 mm, and protruding 6 mm into the enclosure were placed along the 120 mm deep by 140 mm high vertical wall. Results for the two larger widths were shown to be qualitatively the same. That is, the temperature distribution in the enclosure is characterized by a boundary layer region surrounding each chip with stably stratified fluid elsewhere. For the smallest width (9 mm) the gap between the chips and the opposite vertical wall is only 3 mm. The increased internal flow resistance and relatively small heat sink area on the top and bottom walls lead to much higher chip temperatures for this narrow width case.

Ozoe et al (1987) performed two-dimensional numerical calculations for natural convection in a square enclosure with nine sources of uniform heat flux uniformly spaced within the enclosure. Either the top horizontal surface or a vertical sidewall surface was cooled uniformly or kept isothermal with all other surfaces adiabatic. The Prandtl number of the fluid was 0.7 and Rayleigh numbers from 10^4 to 10^6 were investigated. At a Rayleigh number of 10^4, velocities were found to be roughly 50% higher and peak heat source temperatures were shown to be roughly a factor of three lower for top surface cooling compared to side wall cooling.

There are a number of papers in the recent literature on the cooling of electronic systems that investigate natural convection flows in enclosures with discrete heat sources on the walls. The references by Kelleher et al (1987), Lee et al (1987), Liu et al (1987), and Ozoe et al (1987) that were discussed above are some of the more notable works in this category. However, for the sake of brevity, all such references will not be listed here.

The purpose for undertaking the present research is to determine the wall heat flux distribution that minimizes the average, or peak, temperature along the heated vertical wall of a rectangular enclosure with natural convection for

the case in which the total rate of heat transfer from this wall is specified. As cited above, several previous studies have addressed the optimal location of discrete heat sources. However, no previous work on the determination of optimal wall heat flux distributions for natural convection flows in enclosures, such as those shown in Figure 1-2, could be found in the open literature.

1.5.3 Numerical Techniques For Solving The Natural Convection Flows. The solution to this problem must combine a method to solve the fully-coupled equations that govern the natural convection flow in the enclosure, which are subject to an arbitrary heat flux distribution on one vertical wall of a rectangular enclosure, with a nonlinear optimization method. The impossibility of achieving a closed form, analytical solution of such a complex problem is beyond question. Thus, a numerical model will be constructed and used to solve the governing equations. Numerous textbooks (e.g. Patankar 1980, Baker 1983, Anderson et al 1984, and Jaluria and Torrance 1986) describe the numerical methods available for solving nonlinear, partial differential equations of the type of interest in this study.

A finite volume scheme employing the SIMPLER ("Semi-Implicit Pressure Linked Equation - Revised") algorithm developed by Patankar (1980) and (1981) was selected for use in this study. With this algorithm, the pressure and temperature values are determined at a set of grid points that are staggered with respect to the grid points where the velocity components are determined. This feature ensures that terms including a first derivative with respect to x or y (such as the pressure gradient term in the momentum equations or the terms in the continuity equation) are correctly modeled throughout the entire flow field. The main advantages of the SIMPLER algorithm over other techniques are that it: (1) insures that physically realistic solutions are obtained for all choices of grid size; (2) uses the so-called primitive variables, namely the velocity components, pressure, and

temperature instead of variables such as stream function and vorticity, which are defined in terms of the primitive variables; and (3) can easily be extended to the calculation of three-dimensional flows. Further discussions of the SIMPLER algorithm are presented in Chapter 2 and Appendix A.

1.5.4 Optimization Techniques. The optimal heat flux distribution will be determined by driving the algorithms used to solve the governing equations for the natural convection flow with a numerical optimization program that is capable of finding the optimal value of an objective function, which in this case is either the average or peak temperature on the heated wall of the enclosure. Optimization methods which have been applied to a wide variety of engineering problems are described in references by Lasdon et al (1978), Siddall (1982), Reklaitis et al (1983), and Vanderplaats (1984).

The generalized reduced gradient (GRG) algorithm as embodied in the GRG2 computer code, which is described by Lasdon et al (1978) and Lasdon and Waren (1986), is used in this study. This method is capable of determining the extremal value of a user-defined objective function subject to multiple, nonlinear equality and/or inequality constraints on either the dependent or independent variables. The GRG algorithm solves a set of nonlinear equations to obtain the minimal value of an objective function, $g_{m+1}(x)$, subject to the constraints:

$$0 < g_j(X) < b_j \; ; \; j = 1, m \qquad (1\text{-}51)$$

$$lb_i < X_i < ub_i \; ; \; i = 1, n \qquad (1\text{-}52)$$

where X is a vector of n variables, the g_j's are functions of X which may be linear or nonlinear, b_j is the upper bound on the function g_j, and lb and ub are the lower bounds and upper bounds, respectively, for each component of the vector X.

The GRG method converts this general (i.e. nonlinear) system of equations consisting of the equation to be minimized and the set of constraint equations into a single reduced objective function, which is minimized subject to no constraints. The gradient method uses the well-known property that a function f undergoes its maximum change in magnitude along the direction defined by the gradient vector $-\nabla f$. To minimize the function, the GRG algorithm calculates the gradient by numerically evaluating the derivatives of the reduced objective function with respect to each variable and proceeds in a stepwise fashion along the $-\nabla f$ direction. The gradient is updated periodically until one of several criteria for terminating the calculations is satisfied. Further discussions of the GRG method and the GRG2 computer code are given in Chapter 2.

1.6 Objectives Of The Research

The four objectives of this research may now be formally stated as follows:

(1) Develop a numerical model of the two-dimensional, steady state, laminar, natural convection flows that occur in the enclosures shown in Figure 1-2 (this model must accomodate a specified nonuniform heat flux on the heated vertical wall and all of the various boundary conditions shown in Figure 1-2).

(2) Couple this numerical natural convection model with the GRG2 optimization code to determine the solution of optimization problem number 1; that is, to find the local heat flux distribution on the heated vertical wall of the enclosure that either (1) minimizes the average temperature on this wall (Case 1), (2) minimizes the peak temperature on this wall (Case 2), or (3) minimizes the average temperature on this wall subject to the constraint that the peak temperature on this wall remains below a specified upper bound

(Case 3). For all three of these variations, or cases, of optimization problem number 1, the minimization is carried out subject to the constraint that the total rate of heat transfer from the wall is a specified constant. The solution of the alternative problem; that is, optimization problem number 2, which is to find the local heat flux distribution that maximizes the total rate of heat transfer from the LHVW, Q_o, subject to the constraints that the average temperature of this wall is a specified constant and that the peak temperature of the LHVW remains below a specified upper bound is also to be determined.

(3) Perform a parametric study with the coupled natural convection and optimization codes.

(4) Compare the differences between the wall temperatures obtained with the extremal heat flux distribution and those obtained with a uniform heat flux distribution to quantify the effect of choosing an optimal arrangement of heat sources along the wall on the wall temperatures.

CHAPTER 2

FORMULATION AND IMPLEMENTATION OF THE NUMERICAL MODEL

2.1 Introduction

This chapter discusses the development and implementation of the numerical model used to solve the two optimization problems defined in Chapter 1. The numerical model consists of two major parts: (1) the natural convection code, which is used to compute the objective functions for the two optimization problems, and (2) the optimization code, which manipulates the natural convection code to minimize or maximize the appropriate objective function. Both of these codes, as well as their theoretical foundations, are discussed below in detail.

2.2 Formulation Of The Numerical Model For Solving The Natural Convection Flows In The Enclosures

2.2.1 General Specifications For The Natural Convection Code. The various options that the natural convection code must accomodate are shown schematically in Figure 2-1. The analyst begins the solution of a specific case by designating which of the two optimization problems described in Section 1.4 is to be solved. This is followed by a choice of Type 1, Type 2, or Type 3 thermal boundary conditions. Next, the analyst must specify the method for representing the nonuniform heat flux distribution, $q_o(y)$, on the left-hand vertical wall of the enclosure. (As will be discussed below, $q_o(y)$ may be represented by either a polynomial, or by a set of discrete values.) Finally, the analyst must specify the values of the Rayleigh number, Prandtl number, and enclosure aspect ratio that define the particular system of interest.

After the case of interest has been defined by making the decisions outlined above, the computations are initiated. These computations involve

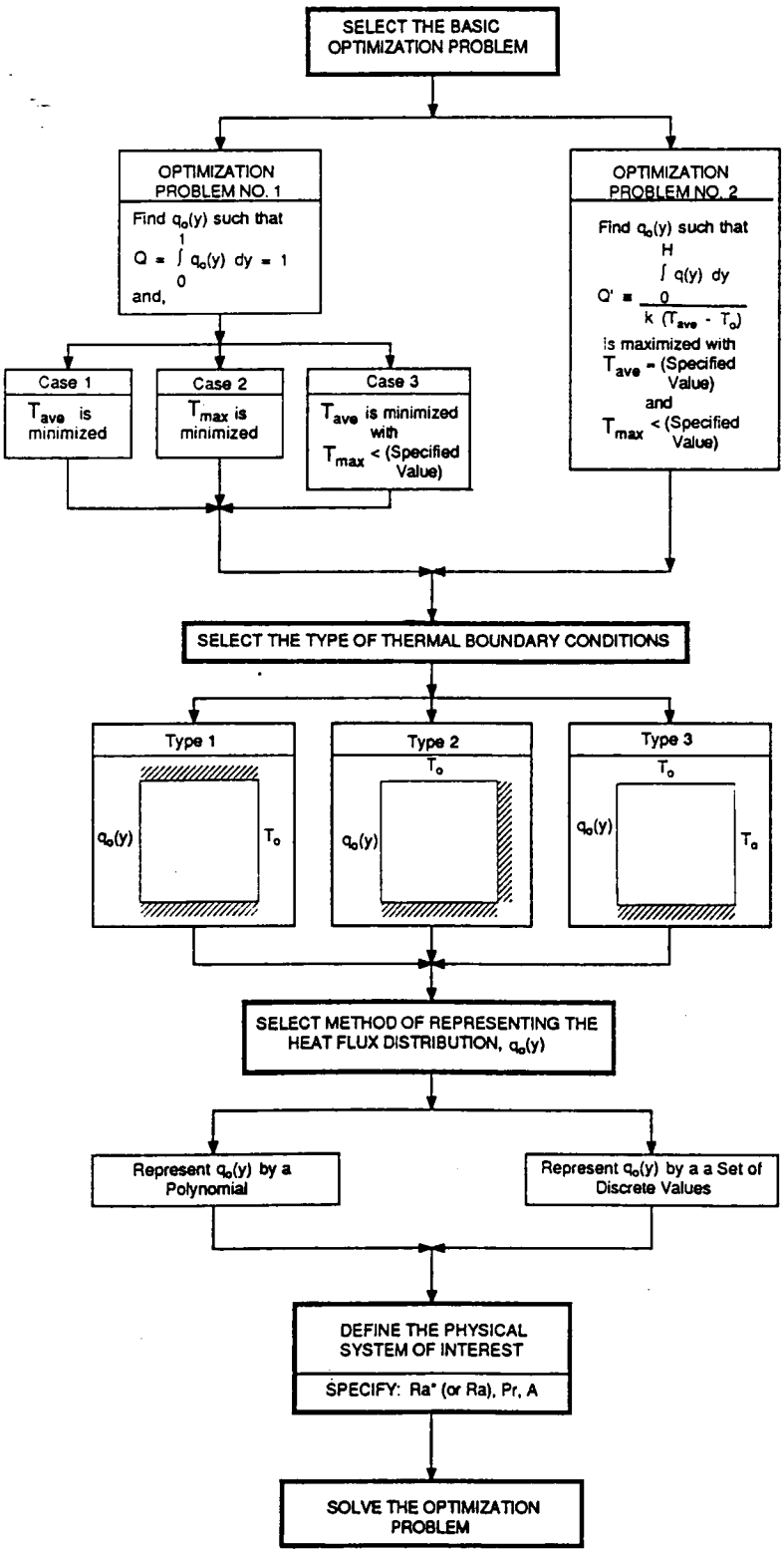


Figure 2-1. Schematic representation of the required computations

the manipulation of the natural convection code by the optimization program, GRG2, to achieve the minimization, or maximization, of the desired objective function. Specifically, these computations entail the repeated evaluation of the objective function that takes place when the optimization program systematically varies the nonuniform heat flux distribution on the left-hand vertical wall of the enclosure to obtain an extremal value of the objective function. Depending on which of the optimization problems is being solved, the objective function is one of the following quantities: (1) the average temperature, T_{ave}, on the left-hand vertical wall of the enclosure, (2) the maximum temperature, T_{max}, on the left-hand vertical wall, or (3) the total rate of heat transfer, Q_o, from the left-hand vertical wall. In order to compute any of these objective functions, the code must first solve the equations that govern the natural convection flow in the enclosure corresponding to the given local heat flux distribution on the heated vertical wall, $q_o(y)$, the specified values of the Rayleigh number, the Prandtl number, and enclosure aspect ratio, and the type of thermal boundary conditions that have been selected.

Finally, once the objective function has been minimized, or maximized, the code must perform additional calculations to determine the spatial distributions of the streamfunction, ψ, and the heat function, h. These distributions, along with that of the temperature, allow contour plots showing the streamlines, isotherms, and heatlines to be constructed, which facilitate the physical interpretation of the natural convection flows in the enclosures.

2.2.2 Implementation Of The SIMPLER Algorithm In The Natural Convection Code. The numerical model of natural convection used in this study is based on the SIMPLER algorithm as described by Patankar (1980, 1981). This algorithm employs a finite volume approach to solve the equations governing the fluid flow and heat transfer. The use of SIMPLER ensures physically

realistic solutions in terms of the so-called "primitive variables"; that is, the velocity, pressure, and temperature distributions in the enclosure flows. An extremely attractive feature of the finite volume formulation of SIMPLER is that the resulting solutions exactly satisfy the integral conservation of mass, momentum, and energy over any group of control volumes, including the entire calculational domain. Since this conservation property is an inherent characteristic of the algorithm, it is independent of grid size. Thus, coarse-grid solutions can be used to debug a code in the most efficient manner. The finite volume approach and the SIMPLER algorithm as applied to the problems of interest in this study are discussed in more detail in Appendix A. The natural convection calculations are carried out in a FORTRAN subroutine, GCOMP. A self-documented listing of subroutine GCOMP, along with listings of its supporting subroutines (TAB, TDMA2D, MAXMIN, and FCA) are presented in Appendix B.

2.2.3 Convergence Tolerances Used In The Natural Convection Code. Early computational experience with the natural convetion code revealed that unusually tight tolerances are required in the present implementation of the SIMPLER algorithm. These tight tolerances are dictated by the accuracy needed for the numerical approximation of certain derivatives required by the optimization code. Since the values of these tolerances should be "optimized" to achieve the desired accuracy and to permit the most efficient possible operation of the code, they are discussed here in detail.

The velocity and temperature fields are updated during each iteration in the SIMPLER procedure. This process is repeated until convergence is achieved. The basis for the convergence of the solution is the annihilation, to within some tolerance, of the mass source term, "b" in equation A-22. The convergence tolerance, ε_b, defined by

$$\varepsilon_b = |b| \qquad (2\text{-}1)$$

was set at less than 10^{-7} for nominal parameters ($Ra^*=10^5$, A=1, Pr=1), but was varied in the range between 10^{-4} to 10^{-8}, depending on the specific values of the parameters.

This tight tolerance on the mass source, in turn led to rather tight convergence tolerances for the line-by-line iterative solution method used to calculate the velocity, pressure, and temperature at each grid point. The tolerances on the maximum change of any variable from one iteration to the next (relative to the maximum minus minimum value of the same variable) were nominally set at 2×10^{-11} for the velocities, 2×10^{-9} for the pressure, and 5×10^{-9} for the temperature. The line-by-line iterative method employed the tridiagonal matrix algorithm to solve for the variables by alternatively sweeping across the entire two-dimensional calculation grid in one direction and then in the other.

Underrelaxation of the velocity and temperature were required to obtain convergent solutions. Since using a relaxation coefficient that is smaller than necessary could lead to prohibitively long computer run times, considerable effort was devoted during initial computations to establish reasonable relaxation factors. Relaxation factors of 0.55 for velocities and 0.45 for temperature were acceptable for the nominal parameters ($Ra^*=10^5$, A=1, Pr=1). For extreme values of the parameters, such as $Ra^*=10^6$, relaxation factors of about 0.3 and 0.2 for the velocity and temperature, respectively, were required to obtain convergent solutions.

2.2.4 Computation Of The Streamlines And Heatlines. To aid in the visualization of results, contour plots showing the isotherms, streamlines, and heatlines are presented in Chapter 3 for selected cases and are also provided in Appendix C as back-up data for all of the other cases in the parametric study.

The plots of the isotherms were obtained by simply passing the values of the dimensionless temperature computed at each grid point by the natural convection code (subroutine GCOMP) to a contour plotting package. A similar approach was employed to plot the streamlines and heatlines, except that the values of the dimensionless streamfunction and dimensionless heatfunction had to first be calculated by a separate subroutine (REPORT) as part of a "postprocessing operation" performed after the successful solution of an optimization problem. The governing equations and the boundary conditions for the dimensionless streamfunction and the dimensionless heatfunction and the algorithms used for their solutions are discussed below.

The streamfunction, ψ, is defined by the relations

$$u = \frac{\partial \psi}{\partial y} , \quad v = - \frac{\partial \psi}{\partial x} \tag{2-2}$$

such that ψ satisfies equation (1-1) for conservation of mass identically. The governing equation for the streamfunction is obtained from the definition of the vorticity vector, $\vec{\omega}$, given by

$$\vec{\omega} = \nabla \times \vec{V} \tag{2-3}$$

where $\vec{V}$ is the fluid velocity vector. For the two-dimensional flows of interest here, equations (2-2) and (2-3) give

$$\frac{\partial^2 \psi}{\partial x^2} + \frac{\partial^2 \psi}{\partial y^2} = - \omega_z = \left(\frac{\partial u}{\partial y} - \frac{\partial v}{\partial x} \right) . \tag{2-4}$$

The boundary conditions for this equation are obtained by (arbitrarily) assigning the value of zero to the streamfunction along the streamline represented by the walls of the enclosure. This gives:

$$\psi(0,y) = 0 \qquad (0 \le y \le H) , \tag{2-5a}$$

$$\psi(W,y) = 0 \qquad (0 \le y \le H) , \tag{2-5b}$$

$$\psi(x,0) = 0 \qquad (0 \le x \le W) , \tag{2-5c}$$

and

$$\psi(x,H) = 0 \qquad (0 \le x \le W). \tag{2-5d}$$

Defining the nondimensional streamfunction as

$$\Psi = \frac{\Psi}{\alpha}, \tag{2-6}$$

and rewriting the above equations and boundary conditions in terms of the nondimensionsl variables gives

$$U = \frac{\partial \Psi}{\partial Y}, \quad V = -\frac{\partial \Psi}{\partial X} \tag{2-7}$$

and,

$$\frac{\partial^2 \Psi}{\partial X^2} + \frac{\partial^2 \Psi}{\partial Y^2} = \left(\frac{\partial U}{\partial Y} - \frac{\partial V}{\partial X} \right) \tag{2-8}$$

with

$$\Psi(0,Y) = 0 \qquad (0 \le Y \le 1), \tag{2-9a}$$

$$\Psi(A,Y) = 0 \qquad (0 \le Y \le 1), \tag{2-9b}$$

$$\Psi(X,0) = 0 \qquad (0 \le X \le A), \tag{2-9c}$$

and

$$\Psi(X,1) = 0 \qquad (0 \le X \le A). \tag{2-9d}$$

For the thermal boundary conditions used in this study; that is, a heated left-hand vertical wall and cooled right-hand vertical and/or top horizontal walls; the natural convection flows in the enclosure are predominantly in a clockwise direction. This results in negative values of the streamfunction.

The heatfunction, h, was devised by Kimura and Bejan (1983); however, their original formulation contained an error that is corrected in the present work. The heatfunction is defined by the relations

$$\frac{\partial h}{\partial y} = \rho c_p u (T - T_{REF}) - k \frac{\partial T}{\partial x} = \left[\begin{array}{c} \text{total transport of} \\ \text{energy by convection} \\ \text{and conduction in the} \\ \text{x-direction} \end{array} \right] \tag{2-10a}$$

and,

$$\frac{\partial h}{\partial x} = \rho c_p v (T - T_{REF}) - k \frac{\partial T}{\partial y} = \left[\begin{array}{c} \text{total transport of} \\ \text{energy by convection} \\ \text{and conduction in the} \\ \text{y-direction} \end{array} \right] \quad (2\text{-}10b)$$

such that h satisfies equation (1-4) for conservation of energy identically. In their formulation Kimura and Bejan (1983) did not include the reference temperature, T_{REF}, in the first terms on the right-hand sides of equations (2-10). This omission yields heatlines that do not exhibit the required property of "centrosymmetry" that is characteristic of many natural convection flows in enclosures. Inclusion of this term ensures that the calculated heatlines are centrosymmetric in the appropriate flows. The bulk temperature of the fluid in the enclosure; that is, the volume averaged temperature, is used as the reference temperature for the flows considered in this study.

Differentiating equation (2-10a) with respect to y and equation (2-10b) with respect to x and subtracting the second result from the first yields the following governing equation for h in physical variables

$$\frac{\partial^2 h}{\partial x^2} + \frac{\partial^2 h}{\partial y^2} = (\rho c_p) \left\{ \frac{\partial}{\partial y} [u (T - T_{REF})] - \frac{\partial}{\partial x} [v (T - T_{REF})] \right\} . \quad (2\text{-}11)$$

The right-hand side of equation (2-11) is evaluated using the velocity and temperature distributions obtained from the solution of the governing equations for the natural convection flow in the enclosure.

The boundary conditions for equation (2-11) will now be written in their most general forms. First, along the bottom horizontal wall

$$h (x,0) = 0 . \qquad (0 \le x \le W) \qquad (2\text{-}12)$$

Next, along the left-hand vertical wall

$$h (0,y) = \int_0^y -k \left. \frac{\partial T}{\partial x} \right|_{x=0} dy , \quad (0 \le y \le H) \qquad (2\text{-}13)$$

while along the top horizontal surface of the enclosure

$$h (x,H) = h (0,H) + \int_0^x -k \left. \frac{\partial T}{\partial y} \right|_{y=H} dx . \qquad (0 \le x \le W) \qquad (2\text{-}14)$$

Similarly, along the right-hand vertical wall of the enclosure

$$h(W,y) = h(W,H) + \int_{H}^{y} -k \left.\frac{\partial T}{\partial x}\right|_{x=W} dy \quad . \qquad (0 \le y \le H) \qquad (2\text{-}15)$$

These boundary conditions for the heatfunction, h, are evaluated by using the temperature distribution obtained from the solution of the natural convection flow in the enclosure.

Independent of the type of thermal boundary conditions being employed, equation (2-12) always holds on the bottom horzontal wall and equation (2-13) always yields

$$h(0,H) = \int_{0}^{H} -k \left.\frac{\partial T}{\partial x}\right|_{x=0} dy = \int_{0}^{H} q_o(y)\, dy$$

$$= Q_o = \left[\begin{array}{c} \text{total rate of heat transfer} \\ \text{from the left-hand vertical} \\ \text{wall to the fluid} \end{array} \right] . \qquad (2\text{-}16)$$

For Type 1 thermal boundary conditions, however, the top surface of the enclosure is insulated and equations (2-14) and (2-16) give

$$h(x,H) = Q_o \qquad (0 \le x \le W) \quad . \qquad (2\text{-}17)$$

Similarly, for Type 2 thermal boundary conditions the right-hand vertical wall is insulated and equations (2-14) and (2-15) give

$$h(W,y) = 0 \qquad (0 \le y \le H) \qquad (2\text{-}18)$$

along this wall.

Defining the nondimensional heat function as

$$\Phi = \frac{h}{Q_o} \qquad (2\text{-}19)$$

and rewriting equation (2-11) and its boundary conditions given by equations (2-12) - (2-15) in terms of the nondimensional variables gives

$$\frac{\partial^2 \Phi}{\partial X^2} + \frac{\partial^2 \Phi}{\partial Y^2} = \left\{ \frac{\partial}{\partial Y}[U(\theta - \theta_{REF})] - \frac{\partial}{\partial X}[V(\theta - \theta_{REF})] \right\} , \qquad (2\text{-}20)$$

$$\Phi(X,0) = 0 , \qquad (0 \le x \le A) \qquad (2\text{-}21a)$$

$$\Phi(0,Y) = \int_0^Y - \left.\frac{\partial\theta}{\partial X}\right|_{X=0} dY \quad , (0 \le Y \le 1) \qquad (2\text{-}21b)$$

$$\Phi(X,1) = \Phi(0,1) + \int_0^X - \left.\frac{\partial\theta}{\partial Y}\right|_{Y=1} dX \quad , \qquad (0 \le X \le A) \qquad (2\text{-}21c)$$

and

$$\Phi(A,Y) = \Phi(A,1) + \int_1^Y - \left.\frac{\partial\theta}{\partial X}\right|_{X=A} dY \quad . \qquad (0 \le Y \le 1) \qquad (2\text{-}21d)$$

Equations (2-4) and (2-20) that govern the distributions of the nondimensional streamfunction and the nondimensional heatfunction, respectively, can be treated as special cases of equation A-1, which is the general differential equation used to develop the SIMPLER algorithm. This entails treating the right-hand sides of these equations as source terms. Thus, the governing equations for $\Psi(X,Y)$ and $\Phi(X,Y)$ are solved by using the same procdeure as that used for computing the solutions of the equations that govern the natural convection flows in the enclosure. (Coefficients are computed and subroutine TDMA2D, which incorporates a line-by-line iteration method, is used to determine Ψ and Φ at all grid points.) the numerical calculations for Ψ and Φ are carried out by a FORTRAN subroutine, REPORT. A self-documented listing of subroutine REPORT is given in Appendix B.

2.2.5 Physical Interpretations Of The Streamlines And Heatlines. The physical interpretation of the heatfunction, Φ, is easily made by analogy with the more familiar streamfunction, Ψ. As is well-known: (1) the streamfunction is defined such that it satisfies the equation for conservation of mass exactly, (2) lines of constant Ψ, called "streamlines", are everywhere tangent to the velocity vector so that there is no mass flowrate across a streamline, and (3) the mass flowrate between two neighboring streamlines is a constant. Thus, a contour plot of the streamfunction shows the streamlines, which provide a

"picture" of the flowfield. By analogy: (1) the heatfunction , Φ, is defined such that it satisfies the equation for conservation of energy exactly, (2) lines of constant Φ, called "heatlines", are everywhere tangent to the total energy flux vector, which accounts for the <u>total</u> transport of thermal energy by the combined action of conduction and convection, and (3) the total rate of thermal energy transport between any two neighboring heatlines is a constant. Thus, for the heatfunction a contour plot shows the heatlines, which provide a "picture" of the energy transport paths by the combined effects of convection and conduction through the flowfield.

2.2.6 <u>Evaluation Of The Nusselt Number.</u> The average nusselt number for the natural convection flow in the enclosure is defined as

$$\overline{Nu}_H = \overline{h}_H H / k \quad . \tag{2-22}$$

The total rate of heat transfer from the heated, left-hand vertical wall to the fluid is given by

$$Q_o = \int_0^H - k \frac{\partial T}{\partial x}\Big|_{x=0} dy = \overline{h}_H H (T_{ave} - T_o) \quad . \tag{2-23}$$

Rewriting this equation in terms of the nondimensional variables for optimization problem number 1 and rearranging yields:

$$\overline{Nu}_H = \left(\frac{\overline{h}_H H}{k}\right) = \left(\frac{Q_o}{q_{ave} H \theta_{ave}}\right) = \frac{\int_0^1 - \frac{\partial \theta}{\partial X}\Big|_{X=0} dY}{\theta_{ave}} \quad . \tag{2-24}$$

But, by definition

$$\frac{Q_o}{q_{ave} H} = \int_0^1 - \frac{\partial \theta}{\partial X}\Big|_{X=0} dY = 1 \quad . \tag{2-25}$$

Therefore,

$$\overline{Nu}_H = 1 / \theta_{ave} \quad . \tag{2-26}$$

Thus, the average Nusselt number for optimization problem number 1 is simply equal to the reciprocal of the average nondimensional temperature on the left-hand vertical wall of the enclosure. The Nusselt number is also computed in the FORTRAN subroutine REPORT, a listing of which is presented in Appendix B.

For optimization problem number 2, equations (2-22) and (2-23) are valid representations of the Nusselt number and total rate of heat transfer across the enclosure, respectively. In terms of the nondimensional variables which apply to optimization number 2, the Nusselt number is given by:

$$\overline{Nu}_H = \left(\frac{\bar{h}_H H}{k}\right) = \left(\frac{Q_o}{k\,(T_{ave} - T_o)}\right) = Q' \quad . \qquad (2\text{-}27)$$

Therefore, the Nusselt number for optimization problem number 2 is identically equal to the objective function (Q').

2.3 The GRG2 Optimization Code

2.3.1 A General Description Of The GRG2 Program. The GRG2 optimization code employed in the present work is a very large FORTRAN program (approximately 5,000 lines of code) written by Leon S. Lasdon and Allen D. Waren (Lasdon, et al, 1978). Each user receives a complete source listing of the code; however, since the program is sold on a commercial basis, this listing is considered proprietary. Thus, only an outline of the generalized reduced gradient optimization technique and its implementation in the GRG2 program will be presented here.

The generalized reduced gradient (GRG) method (Lasdon, et al, 1978) is used to solve a set of nonlinear equations to obtain the minimum value of an objective function, $g_{m+1}(X)$, subject to the constraints that

$$0 \le g_j(X) \le b_j \qquad \text{for } j = 1, \ldots, m \quad , \qquad (2\text{-}28a)$$

and,

$$lb_i \leq X_i \leq ub_i \qquad \text{for } i = 1, ..., n \quad , \qquad (2\text{-}28b)$$

where X is a vector of n "design variables", the g_j's are functions of X which may be linear or nonlinear, b_j is the upper bound on the function g_j, and lb and ub are the lower bounds and upper bounds, respectively, for each component of the vector X. As will be discussed below, the variables X_i in the present study are either the values of the heat fluxes at the grid-points along the LHVW or the values of the coefficients of a family of functions used to express the heat flux distribution along the LHVW. Depending on which of the two optimization problems described in Section 1.4 is being worked, the functions, g_j, may be either one or two of the possible constraints. These constraints include (1) a fixed total heating rate along the LHVW, (2) an upper bound on the average temperature of the LHVW, and (3) an upper bound on the peak temperature of the LHVW. The objective function, g_{m+1}, is one of the remaining functions (or, the only remaining function if two of the above constraints are used); that is, g_{m+1} is either the total heating rate, the average temperature, or the peak temperature of the LHVW.

Thus, the m constraint equations may be equality, or inequality, constraints, such as a fixed total heating rate along the LHVW, or an upper bound on peak or average temperature of the LHVW, respectively. For inequality constraints, a set of slack variables X_k, where k = n+1, ..., n+m are defined so that the inequality constraints are converted to equality constraints at the expense of adding one new variable for each constraint. These slack variables are defined by the relations

$$g_j(X) - X_{n+j} = 0 \qquad \text{for } j = 1, ..., m \quad , \qquad (2\text{-}29a)$$

and,

$$0 \leq X_{n+j} \leq bj \qquad \text{for } j = 1, ..., m \quad . \qquad (2\text{-}29b)$$

The n variables, X_i, for i = 1, ..., n are called "natural variables" to distinguish them from the m artificial slack variables.

The first step in the GRG method is to convert the nonlinear, or general, system of equations consisting of the function to be minimized (the objective function) and the set of constraint equations into a single reduced objective function, which has no constraints. The reduced objective function is then minimized using a steepest descent, or gradient, method. The GRG method, as implemented in the GRG2 computer code described by Lasdon and Warren (1986) , is outlined below.

We define X_o to be a specific value for the vector X of n variables that satisfies the constraints of equations (2-29a) and (2-29b). The number of g_j constraints that are binding; that is, that hold as equalities (either equality constraints or inequality constraints with the function g_j at its upper bound of b_j or lower bound of zero), at X_o is assumed to be n_b. A constraint is assumed to be binding if:

$$| g_j - b_j | < \varepsilon \quad , \quad \text{or} \quad | g_j | < \varepsilon \quad . \qquad (2\text{-}30)$$

The tolerance ε is a key parameter in the GRG2 code. Values ranging from 10^{-4} to 10^{-6} were found to be appropriate for this study. An excessively small (tight) tolerance can overly restrict the search for improved, i.e. smaller, values of the objective function and leads to increased computing time being spent on calculations at intermediate (i.e. nonoptimal) points. A value of ε that is too large, however, can stop the search prematurely; that is, before the "true" minimum is reached. It was found that a large value of ε, say 10^{-4}, is desirable for initial steps in the calculation, but a smaller value, say 10^{-6}, is desirable after approaching near to the optimal point. The GRG2 code

incorporates this flexibility, by allowing a large value of ε to be used until the improvement in the objective function ceases, and then using a smaller value to search for the final optimal point.

GRG2 uses the n_b binding constraint equations to determine n_b of the variables, called "basic variables", in terms of the remaining n - n_b natural variables and n_b slack variables associated with the binding constraints. These remaining n variables are referred to as "nonbasic variables". Defining the vector of n_b basic variables as y and the vector of n nonbasic variables as x, the functions $g_j(X)$ can be written as $g_j(y,x)$. In the neighborhood of X_o, the values of y depend only on x, so that these functions, including the objective function, are reduced to functions of x only. The corresponding reduced objective function, called F(x), is given by:

$$F(x) = g_{m+1}(y(x), x) \quad . \qquad (2\text{-}31)$$

Therefore, in the neighborhood of X_o, the original problem, which was to minimize the objective function $g_{m+1}(X)$ subject to the m constraints on the functions and the n constriants on the variables X_i, is reduced to minimizing F(x) subject only to the n constraints on the nonbasic variables (x).

The direction used for searching for a lower value of the reduced objective function is obtained by forming the gradient of the function F(x). This gradient, ∇F, is called the "reduced gradient". The search direction, d_o, is simply $-\nabla F$ evaluated at x_o. The search is performed by evaluating the function $F(x_o + \alpha d_o)$ where α is a sequence of positive values that define the step size along the gradient direction for each iteration. Evaluating this function is, of course, equivalent to evaluating

$$g_{m+1}(y(x_o + \alpha d_o), x_o + \alpha d_o). \qquad (2\text{-}32)$$

To evaluate g_{m+1}, the function $y(x_o + \alpha d_o)$ must be determined first. This calculation is performed using Newton's method. The values of α are adjusted on the initial iterations, if necessary, to achieve a convergent solution. Once an initial convergent solution is achieved, the values of α are adjusted until either:

(1) Newton's method no longer converges;

(2) some g_j constraint that was previously nonbinding or a basic variable exceeds a bound;

(3) an objective function value is reached which is larger than the previous value.

If condition (1) occurs, the search terminates and a new value of X_o is determined. This new value is given by:

$$X_o = (y(x_o + \alpha_1 d_o), x_o + \alpha_1 d_o) \qquad (2\text{-}33)$$

where α_1 is the last value of α that had a convergent solution. A new value of the reduced gradient is determined and a new search is initiated.

If condition (2) occurs, a new value of α is determined, say α_2, such that all constraints are satisfied and at least one of the previously nonbinding constraints or variables is at its bounds. If the value of the objective function is lower at this new point compared to all previous feasible points, the new constraint is considered binding, thus allowing further reduction of the objective function. This new reduced objective function is now used to initiate a new search from an updated value of X_o.

If the third condition occurs, an attempt is made to determine the value of α that minimizes F. Using the designations of i-1, i, and i+1 to refer to the sequence of iterations, the relationships that exist in this third condition are

$$F(x_o + \alpha_i d_o) < F(x_o + \alpha_{i-1} d_o) \qquad (2\text{-}34a)$$

and,

$$F(x_o + \alpha_i d_o) < F(x_o + \alpha_{i+1} d_o) \; . \qquad (2\text{-}34b)$$

Therefore, the value of α that minimizes F is betweeen α_{i-1} and α_{i+1}. A quadratic is fit to the three values of α (α_{i-1}, α_i, and α_{i+1}) and the value of F is evaluated at the minimum of this quadratic (α_{min}). The value of α, either α_i or α_{min}, which has the minimum value of F is selected to define the new point X_o. The reduced gradient is evaluated at this new point , and the process continues.

The current set of values of the vector of unknown variables, X_o, is considered optimal if either of two tests are met. The first test, which gives the highest level of confidence that at least a local optimum has been found, employs the Kuhn-Tucker optimality conditions (Reklaitis, et al, 1983). The Kuhn-Tucker conditions are simply the first order optimality conditions for the general nonlinear problem with both equality and inequality constraints. In terms of the variable names used here, the Kuhn-Tucker conditions are given by:

$$\nabla g_{m+1} - \sum_{j=1}^{m} \beta_j \nabla g_j = 0 \qquad (2\text{-}35a)$$

and,

$$\beta_j (g_j - X_{n+j}) = 0 \quad \text{for } j = 1, \ldots, m \qquad (2\text{-}35b)$$

with $\beta_j = 0$ for nonbinding constraints. The values of β are simply the Lagrange multipliers for each constraint and are calculated in the GRG method as part of the process of forming the reduced gradient. If the left-hand-sides of equations (2-35a) and (2-35b) are less than a specified

tolerance, ε_s, then the Kuhn-Tucker conditions are assumed to be satisfied. A value of $\varepsilon_s = 10^{-5}$ was typically used in the present studies.

The second test for optimality terminates the process if the fractional change in the value of the objective function is less than ε_s for a specified number, N_s, of consecutive iterations. The value of N_s was set at five for these studies.

A third type of termination occurs if an improved point was not found along the last search direction despite further attempts such as changing the basic variables or releasing a single variable from its bound.

It should be noted that many of the optimal points reported in this study were initially obtained with this third type of termination. In these cases, the variables were rescaled, calculation tolerances in the natural convection model were tightened, and/or the tolerances in the GRG2 code were adjusted and the run was restarted. The usual result was that either of the first two types of terminations were obtained, but the values of the objective function and variables were not significantly changed.

A self-documented FORTRAN listing of a typical GRG2 input file is presented in Appendix B. No listing of the GRG2 code itself is included in this work since the code is proprietary.

2.4 Alternative Methods For Representing The Nonuniform Local Heat Flux Distribution On The Left-Hand Vertical Wall

As mentioned in Section 2.2.1, this investigation employs two alternative methods for approximating the nondimensional local heat flux distribution, q(Y), along the left-hand vertical wall of the enclosure. These two methods will now be discussed in detail.

The first method involves approximating the continuous local heat flux distribution, q(Y), by a finite set of discrete values. Thus, the n = N unknown

"design variables" (X_i's) are defined as the N discrete values of the nondimensional heat flux, q(Y), at the N grid points along the left-hand vertical wall in the natural convection model. For example, consider a solution of optimization problem number 1 in which the average nondimensional temperature on the LHVW, θ_{ave}, given by

$$\theta_{ave} = \int_0^1 \theta(0,Y)\, dY \qquad (2\text{-}36)$$

is to be minimized subject to the equality constraint on the total nondimensional rate of heat transfer across the enclosure, Q, given by

$$Q = \left(\frac{Q_o}{q_{ave}\, H}\right) = \int_0^1 q(Y)\, dY = 1 \quad . \qquad (2\text{-}37)$$

In this case, the N design variables to be manipulated by GRG2 to minimize θ_{ave} subject to the above equality constraint on Q are given by:

$$X_i = q_i(Y) \geq 0 \quad , \quad (1 \leq i \leq N) \quad . \qquad (2\text{-}38)$$

Note that the design variables (the N discrete values of q(Y)) are themselves subject to an inequality constraint given by equation (2-38). The integrals in equations (2-36) and (2-37) are evaluated numerically in subroutine GCOMP using the discrete values of the nondimensional temperature, $\theta_i(0,Y)$, and nondimensional heat flux, $q_i(Y)$, at the N grid points on the heated vertical wall of the enclosure.

The second method for approximating the nondimensional local heat flux distribution, q(Y), will now be discussed in terms of solving the same optimization problem used to illustrate the first method. the second method employs an expansion of the (initially unknown) function, q(Y), in terms of a family of trial functions, $\omega_i(Y)$, as follows

$$q(Y) = \sum_{i=1}^{N} a_i\ \omega_i(Y) \quad . \qquad (2\text{-}39)$$

The (unknown) coefficients (a_i's) in this expansion are taken to be the n = N design variables to be manipulated by GRG2 to minimize θ_{ave} subject to the constraint given by equation (2-37); that is,

$$X_i = a_i \quad , \quad (1 \leq i \leq N) \quad . \tag{2-40}$$

The a_i's are also determined subject to the inequality constraint that the local heat flux, q(Y), must always be greater than, or equal to, zero. As with the first method, all required integrals are evaluated numerically in subroutine GCOMP.

2.5 Coupling Of The Natural Convection And GRG2 Optimization Codes

The numerical model of natural convection, which is embodied in the FORTRAN subroutine GCOMP, computes the objective function that is being minimized, or maximized, by the GRG2 optimization code. GRG2 acts as a "driver". which manipulates the natural convection model and iteratively updates the solution for the vector of design variables given by either

$$X_i = q_i(Y) \quad , \qquad (1 \leq i \leq N) \tag{2-41a}$$

or,

$$X_i = a_i \quad , \qquad (1 \leq i \leq N) \tag{2-41b}$$

depending on which method is being used to approximate the local heat flux distribution on the left-hand vertical wall of the enclosure. This process continues until either the optimum set of X_i's (the set that extremalize the objective function) are determined, or a maximum allowable number of iterations is exceeded.

Four functions are calculated in subroutine GCOMP:

Q = total nondimensional heating rate along the LHVW = g(1)

θ_{ave} = average nondimensional temperature along the LHVW = g(2)

θ_{max} = peak nondimensional temperature along the LHVW = g(3)

q_{min} = minimum nondimensional heat flux along LHVW = g(4)

The status of these functions is listed in Table 2-1 for each of the three cases that constitute optimization problem number 1 as well as for optimization problem number 2. For all cases, g(4) is constrained to be greater than or equal to zero. This constraint is redundant when the local heat flux distribution on the left-hand vertical wall is being represented by a finite set of discrete values which are themselves constrained to be greater than or equal to zero. However, this constraint was required for the polynomial type heat flux distributions to ensure that the heat flux was greater than zero at all locations along the LHVW. For Case 1, g(1) is fixed, g(2) is the objective function, and g(3) has no upper bound. For Case 2, g(1) is fixed, g(2) has no upper bound, and g(3) is the objective function. For Case3, g(1) is fixed, g(2) is the objective function, and g(3) is constrained to remain below an upper bound. For optimization problem number 2, g(1) is the objective function, and g(2) and g(3) are constrained to remain below upper bounds.

Each time that the objective function is evaluated, the subroutine GCOMP, containing the natural convection model, is called. The reduced gradient is determined by calling the subroutine GCOMP n times to form the numerical forward difference derivative of the objective function with respect to each of the n variables or 2n times to calculate the numerical derivatives by central difference.

2.6 Computational Facilities

All calculations were performed on the CRAY-2 supercomputers located at the National Magnetic Fusion Energy Computer Center (NMFECC) in Livermore, California. The use of a supercomputer was essential to the successful completion of this work in a reasonable period of time because each evaluation of an objective function requires a separate solution of the natural convection flow in the enclosure and the optimum value of an

Table 2.1 Roles of functions calculated by the natural convection model for each of the optimization cases

FUNCTION	PHYSICAL MEANING	DESIGNATION IN GRG2	OPTIMIZATION PROBLEM NUMBER 1			OPTIMIZATION PROBLEM NUMBER 2
			CASE1	CASE 2	CASE 3	
Q	total nondimensional heating rate along the LHVW	g(1)	FIXED	FIXED	FIXED	OBJECTIVE FUNCTION
θ_{ave}	average nondimensional temperature along the LHVW	g(2)	OBJECTIVE FUNCTION	-	OBJECTIVE FUNCTION	< UPPER BOUND
θ_{max}	peak nondimensional temperature along the LHVW	g(3)	-	OBJECTIVE FUNCTION	<UPPER BOUND	< UPPER BOUND
q_{min}	minimum nondimensional heat flux along the LHVW	g(4)	> 0	> 0	> 0	> 0

objective function is found by an iterative procedure which requires a large number of iterations. Typical runs involved solution of the natural convection problem several hundred, and in some extreme cases over a thousand, times.

CHAPTER 3

PRESENTATION AND INTERPRETATION OF RESULTS

3.1 Introduction

Results of the studies designed to determine the optimal heat flux distribution along a vertical wall of a two-dimensional enclosure with natural convection are presented and discussed in the sections that compose this chapter. Results of preliminary studies which were designed to: (1) validate the natural convection code, (2) verify that the mesh used in the optimization studies was adequately fine to yield meaningful results, (3) demonstrate the sensitivity of the optimization results to the use of different constraints or objection functions, and (4) compare results obtained using two different methods of specifying the heat flux distribution, are presented in the next section of this chapter. The final section of this chapter discusses the results of parametric studies that were designed to examine the sensitvity of the optimal heat flux distribution to the parameters of the problem. These parameters are the modified Rayleigh number (Ra*), the Prandtl number (Pr), the aspect ratio of the rectangular enclosure (A), and the thermal boundary conditions along the walls of the enclosure.

3.2 Preliminary Studies

3.2.1 Validation Of The Natural Convection Code. The natural convection code was validated by comparing results with the results given in two previously published numerical studies. Specifically, results were compared with: (1) the "benchmark solution" of de Vahl Davis (1983) for natural convection in a square enclosure in which the two vertical walls are isothermal surfaces maintained at different temperatures and the horizontal walls are adiabatic surfaces, and (2) the solution of Kimura and Bejan (1984)

for natural convection in a rectangular enclosure with the same uniform heat flux on each vertical wall and adiabatic horizontal walls.

In the benchmark solution study, de Vahl Davis performed a series of calculations using a streamfunction-vorticity formulation which he solved by a finite difference method. The desired results were obtained by extrapolating from the results for several grid sizes to the "exact", or "benchmark", solution that corresponds to "zero" mesh size. Some of his results for $Ra = 10^5$, $Pr = 0.71$, and $A = 1$ are listed in Table 3-1. For this problem, the Rayleigh number is defined in terms of the temperature difference, ΔT, between the vertical walls and is given by:

$$Ra = \frac{g\ b\ H^3\ \Delta T}{\alpha\ \nu} \quad . \qquad (3\text{-}1)$$

Results obtained with the finite volume model based on the SIMPLER algorithm constructed for the present investigation are also included in Table 3-1 for comparison. Streamlines and isotherms for the same set of dimensionless parameters are shown in Figure 3-1. The results obtained using the SIMPLER model with a uniformly-spaced 21 x 21 grid compare favorably with the benchmark solution and the results obtained by de Vahl Davis with the streamfunction-vorticity model for the same 21 x 21 grid size. Results for a 13 x 13 nonuniform grid (SIMPLER algorithm) are also in reasonably good agreement. For example, comparing the solution obtained with the 13 x 13 nonuniform grid to the benchmark solution the following observations can be made: (1) the maximum x-direction and y-direction velocities are within 4.0% and 10%, respectively, of the benchmark solution results, (2) the maximum value of the streamfunction is within 0.6%, and (3) the maximum and average values of the Nusselt number on the left-hand vertical wall (LHVW) are within 13%and 8.4%, respectively. The details of this 13 x 13 nonuniform grid are described later in this chapter.

A comparison of results from the uniform wall heat flux studies of Kimura and Bejan (1984) with those results obtained using the model developed for

Table 3-1. Comparison of results obtained with the natural convection code developed in this study with results from the "benchmark" solution by de Vahl Davis (1983) for Ra = 10^5, Pr = .71, A = 1.

	de Vahl Davis (1983)		Present Study	
Parameter	Uniform 21 x 21 Grid	Benchmark Solution	Uniform 21 x 21 Grid	Nonuniform 13 x 13 Grid
$\|\Psi\|_{mid}$	9.70	9.11	8.84	9.46
$\|\Psi\|_{max}$	10.24	9.61	9.11	9.55
x,y location for $\|\Psi\|_{max}$	0.29,0.60	0.28,0.60	0.28,0.56	0.37,0.5
u_{max}	36.5	34.7	34.1	36.1
y location for u_{max}	0.85	0.86	0.83	0.83
v_{max}	62.8	68.6	70.6	61.5
x location for v_{max}	0.075	0.066	0.056	0.029
Nu_o	4.72	4.51	4.67	4.89
Nu_{max}	7.90	7.72	8.16	8.75
y location for Nu_{max}	0.13	0.081	0.055	0.092
Nu_{min}	0.80	0.73	0.87	0.90
y location for Nu_{min}	0.973	1	0.97	0.97

$|\Psi|_{mid}$ = the streamfunction at the mid-point of the enclosure

$|\Psi|_{max}$ = the maximum absolute value of the streamfunction

Nu_o = the average Nusselt number on the LHVW (x=0)

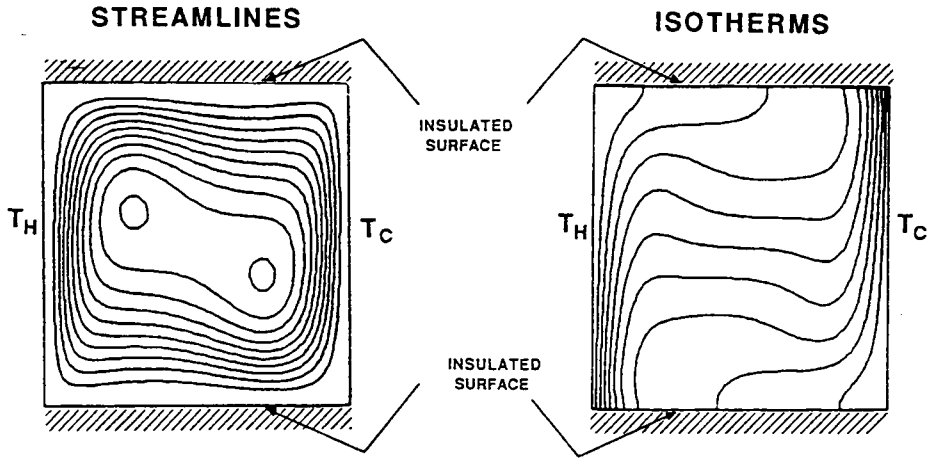
Nu_{max} = the the maximum value of the local Nusselt number on the LHVW

Nu_{min} = the minimum value of the local Nusselt number on the LHVW

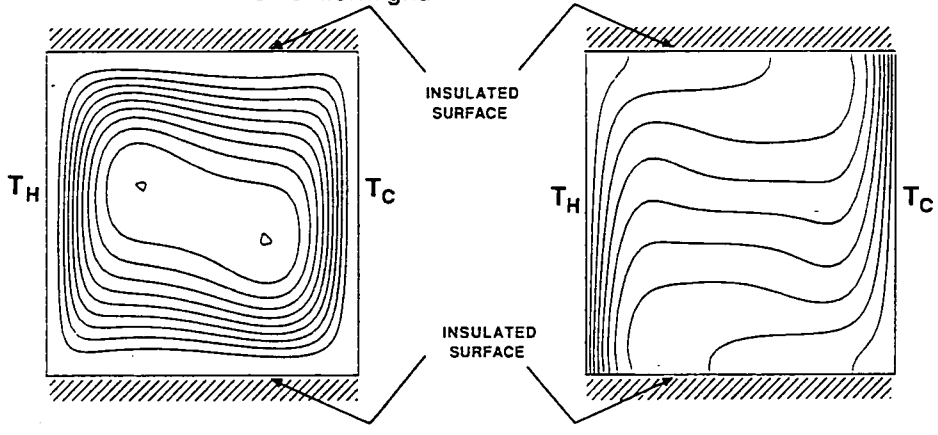
u_{max} = the maximum horizontal velocity on the vertical mid-plane of the enclosure

v_{max} = the maximum vertical velocity on the horizontal mid-plane of the enclosure

(3-1a) Results of de Vahl Davis (1983) "benchmark" solution (extrapolated to a mesh size of zero)



(3-1b) Results computed with the SIMPLER model of this work using a 31 x 31 uniform grid



(3-1c) Results computed with the SIMPLER model of this work using a 13 x 13 nonuniform grid

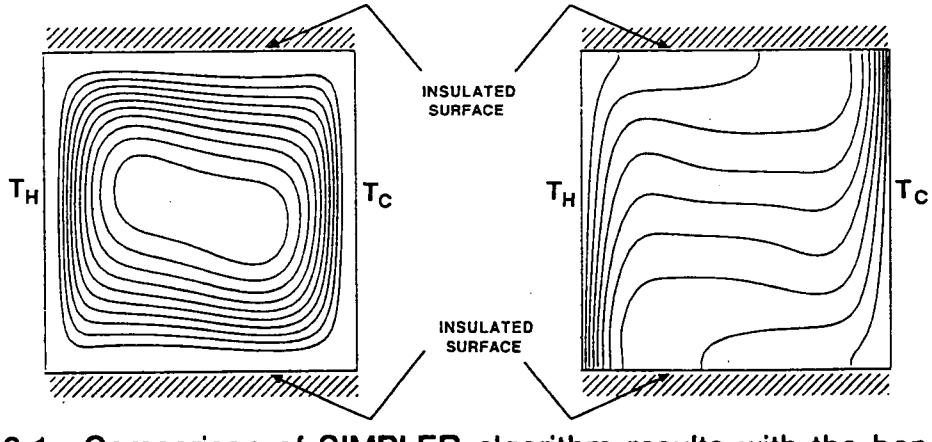


Figure 3-1. Comparison of SIMPLER algorithm results with the benchmark solution of de Vahl Davis (1983)

the present work is shown in Table 3-2. Kimura and Bejan used a streamfunction-vorticity formulation with a finite difference method to obtain their numerical results. They aslo developed an analytical expression for the Nusselt number in the vertical wall boundary layer regions (regions along the vertical walls not close to the horizontal walls. As shown in Table 3-2, the results obtained using the natural convection model constructed for this study with Pr = 7.0, A = 1, and $Ra^* = 3.5 \times 10^5$ and 3.5×10^6 (Ra^* is based on the uniform heat flux on the vertical walls) show reasonably good agreement with Kimura and Bejan's numerical calculations and analytical predictions. For example, the results obtained using the SIMPLER algorithm with a 13 x 13 nonuniform grid show that the Nusselt number at the midpoint of the vertical wall, which is the location furthest from the horizontal walls, is within 2.1% of the analytical result for the $Ra^* = 3.5 \times 10^5$ case and within 3.4% for the $Ra^* = 3.5 \times 10^6$ case.

The agreement shown above between the results obtained using the present natural convection code and the results of de Vahl Davis and Kimura and Bejan is assumed to be good enough to validate this code.

3.2.2 Grid Refinement Study. Prior to performing the computer resource intensive numerical computations required to obtain the optimal heat flux distributions, it was of critical importance to determine the appropriate grid size to be used in the two-dimensional natural convection model. Although the use of the SIMPLER algorithm ensures that the results will be physically realistic (i.e. conservation principles are satisfied) for all grid sizes, a grid which is too coarse will not give adequately detailed definition of the natural convection flow and heat transfer. A grid size which is too large (fine mesh) will result in impractically long run times, and is therefore, inappropriate for the parametric analyses performed in this study.

To determine an appropriate grid, studies were performed to examine the

Table 3-2. Comparison of results obtained using the SIMPLER algorithm with results of Kimura and Bejan (1984)

- 2-D Enclosure with Natural Convection
- Uniform Heat Fluxes Along Vertical Walls
- Adiabatic Horizontal Walls
- Pr = 7, A = 1

	Ra*	Grid	Nu		
			Overall	at y=H/2	Analytical
Kimura and Bejan (1984)	350,000	21 x 21 Uniform	4.61	5.66	5.80
SIMPLER	350,000	21 x 21 Uniform	5.14	6.26	5.80
SIMPLER	350,000	13 x 13 Nonuniform	5.14	5.92	5.80
Kimura and Bejan (1984)	3,500,000	31 x 31 Uniform	7.94	9.19	9.68
SIMPLER	3,500,000	31 x 31 Uniform	9.16	10.57	9.68
SIMPLER	3,500,000	13 x 13 Nonuniform	9.32	10.01	9.68

effects of grid size on the solution of the natural convection problem of interest. Studies were also carried out to examine the effect of grid size on the solution of the optimal heat flux distribution problem.

To examine the effects on the natural convection predictions, results were obtained for various grid sizes with a uniform heat flux distribution along the LHVW. The number of grid points at which the temperature, velocity components, and pressure were calculated was varied from 49 (7 x 7 grid) to 961 (31 x 31 grid). For purposes of this discussion, the results for the 31 x 31 grid are referred to as the "exact" results. A modified Rayleigh number of 10^5, Prandtl number and aspect ratio of unity, and Type 1 thermal boundary conditions (adiabatic top and bottom horizontal walls and isothermal right-hand vertical wall) were used for these initial grid size studies.

Predicted average and peak temperatures for the LHVW are plotted in Figure 3-2 for the full range of grid sizes considered. The temperatures approach the exact results (31 x 31 grid) for a relatively modest number of grid points. The peak and average nondimensional temperatures for the 13 x 13 grid are within 4.4% and 4.0%, respectively, of the exact results.

Streamline, heatline, and isothermal contour plots are shown in Figures 3-3 through 3-5 for grid sizes from 7 x 7 to 31 x 31. As expected when using the SIMPLER algorithm, the general nature of the contour plots for the 7 x 7 grid is the same as that for the exact solution. However, rather significant differences in the detailed structure of these contours can be found. As shown in the streamline patterns (Figure 3-3), the flow near the walls is underestimated with the 7 x 7 grid, which therefore underestimates the effectiveness of the natural convection heat transfer. This can be seen in the heatline profiles (Figure 3-4), by noting that the heatlines continue in a near normal direction from the vertical walls (indicating conduction) for a further distance in the 7 x 7 grid compared to the results for finer meshes.

The streamline, heatline, and isothermal contours continue to improve,

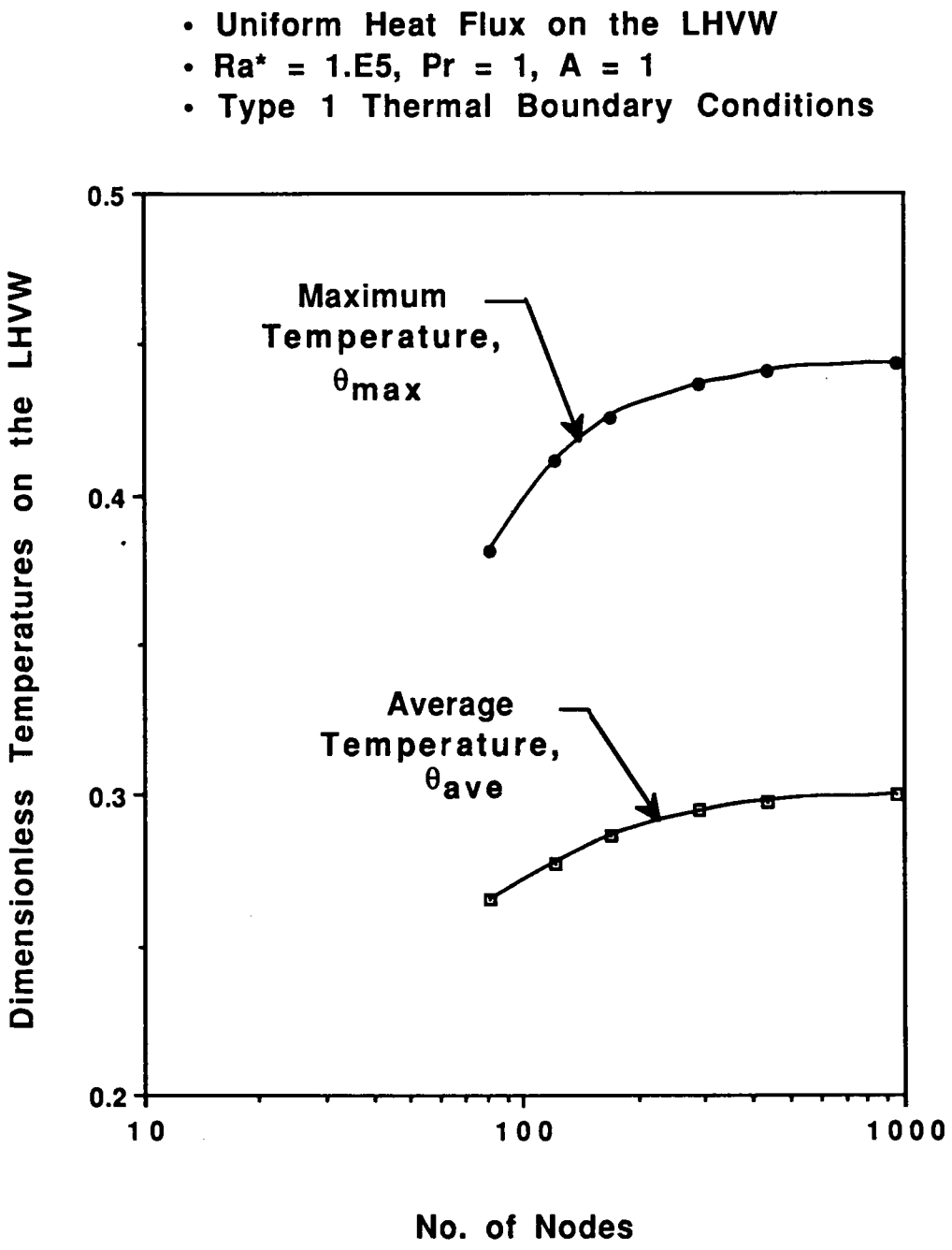


Figure 3-2. Effect of grid size on dimensionless temperature on the LHVW

- **Uniform Heat Flux On LHVW**
- **Ra* = 10^5, Pr = 1, A =1**
- **Type 1 Thermal Boundary Condtions**

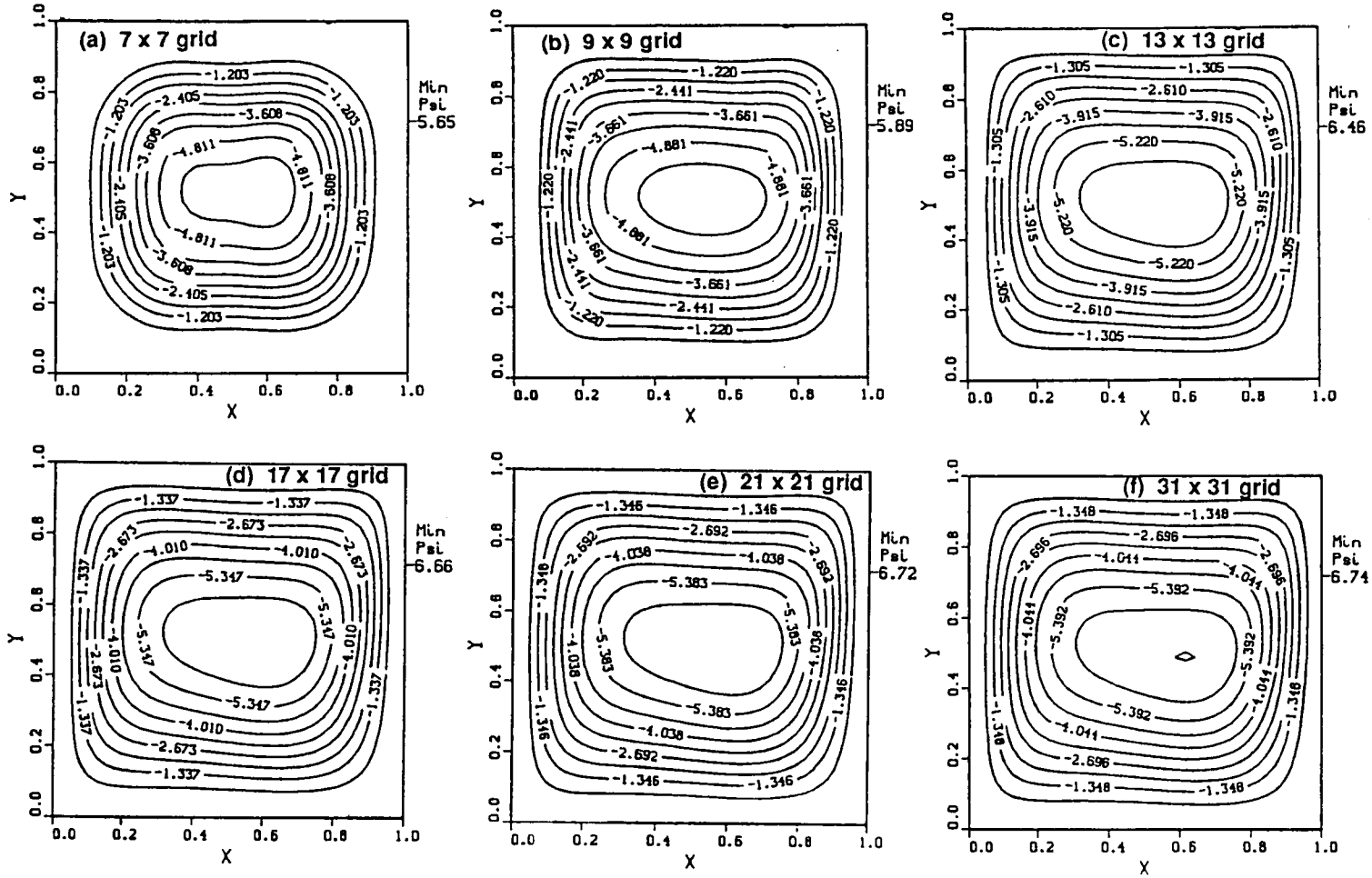


Figure 3-3. Streamlines for various grid sizes with uniform heat flux distribution along the LHVW

- Uniform Heat Flux On LHVW
- $Ra^* = 10^5$, Pr = 1, A =1
- Type 1 Thermal Boundary Condtions

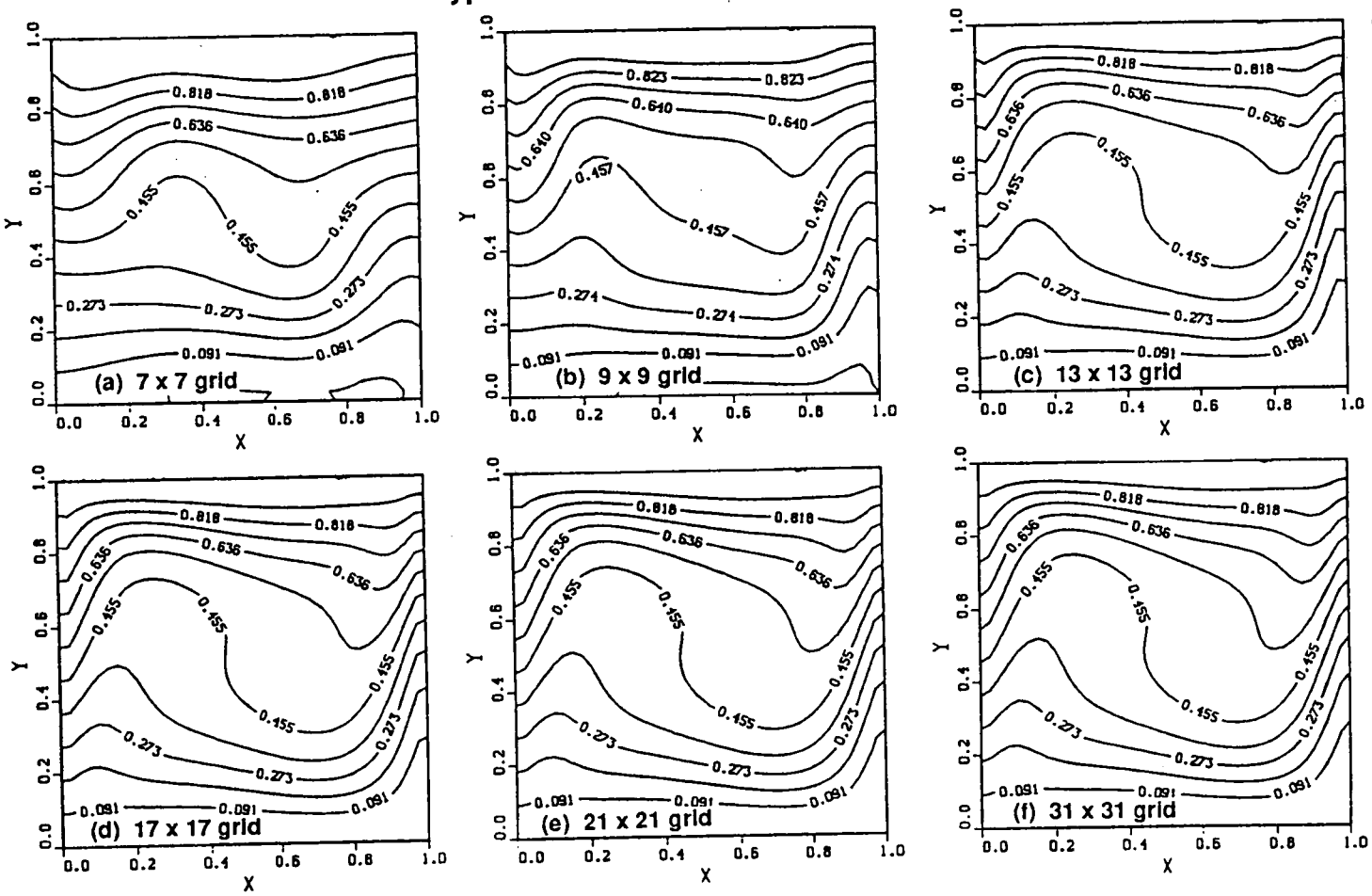


Figure 3-4. Heatlines for various grid sizes with uniform heat flux distribution along the LHVW

- Uniform Heat Flux On LHVW
- $Ra^* = 10^5$, Pr = 1, A =1
- Type 1 Thermal Boundary Condtions

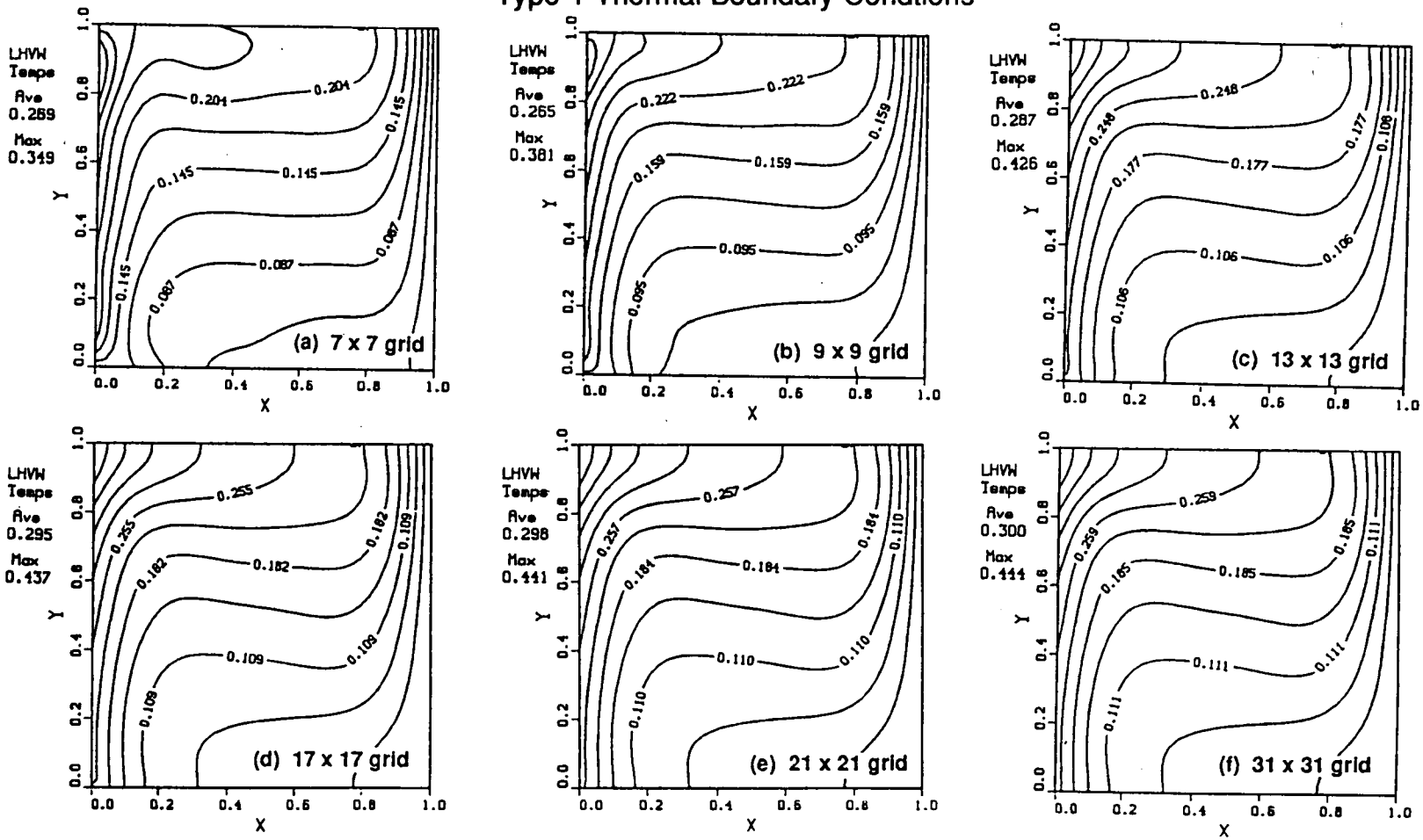


Figure 3-5. Isothermal contour lines for various grid sizes with uniform heat flux distribution along the LHVW

i.e., appear to converge to the exact results, as the number of grid points increases. However, it is evident from these results that the contours for grids as coarse as 13 x 13 are quite close to those for the exact solution.

The above results were obtained using a variable (nonuniform) grid size formed by increasing the linear dimension of each grid volume by a factor of 1.2 as the distance from the wall is increased. The center grid volume is therefore the largest and the mesh size decreases in any direction away from this element. This variable grid improves the resolution in the regions near the walls which is where the largest gradients occur (except of course for the temperature near the adiabatic horizontal walls).

Several nonuniform grid sizes were examined. As indicated in the results plotted in Figure 3-6, the selected variable grid size improves the accuracy in predicting the peak and average temperatures of the LHVW compared to a uniform grid with the same number of grid points. This same nonuniform grid was used for the optimization studies. An example of this nonuniform grid for a 13 x 13 mesh is shown in Figure 3-7.

The effect of grid size on computer resource requirements, expressed as normalized central processing unit (CPU) time, is shown in Figure 3-8. For reference purposes, the actual CPU time for the 13 x 13 grid was 74 seconds on the CRAY-2 supercomputer used in these studies. Using a logarithmic curve fit to this data, the CPU time is shown to vary as the total number of grid points, N, raised to the 1.7 power ($N^{1.7}$). Therefore, if the number of grid points is increased from say 13 x 13 to 21 x 21 the individual grid elements are decreased in linear dimension by about a factor of 1.7 but the computer "cost" is increased by a factor of 5.1.

The effect of number of grid points on the results of optimization calculations is shown in Figure 3-9 for the optimization method that employs the discrete values of the heat flux at each node along the LHVW as the independent variable. The average and peak temperatures for the LHVW are

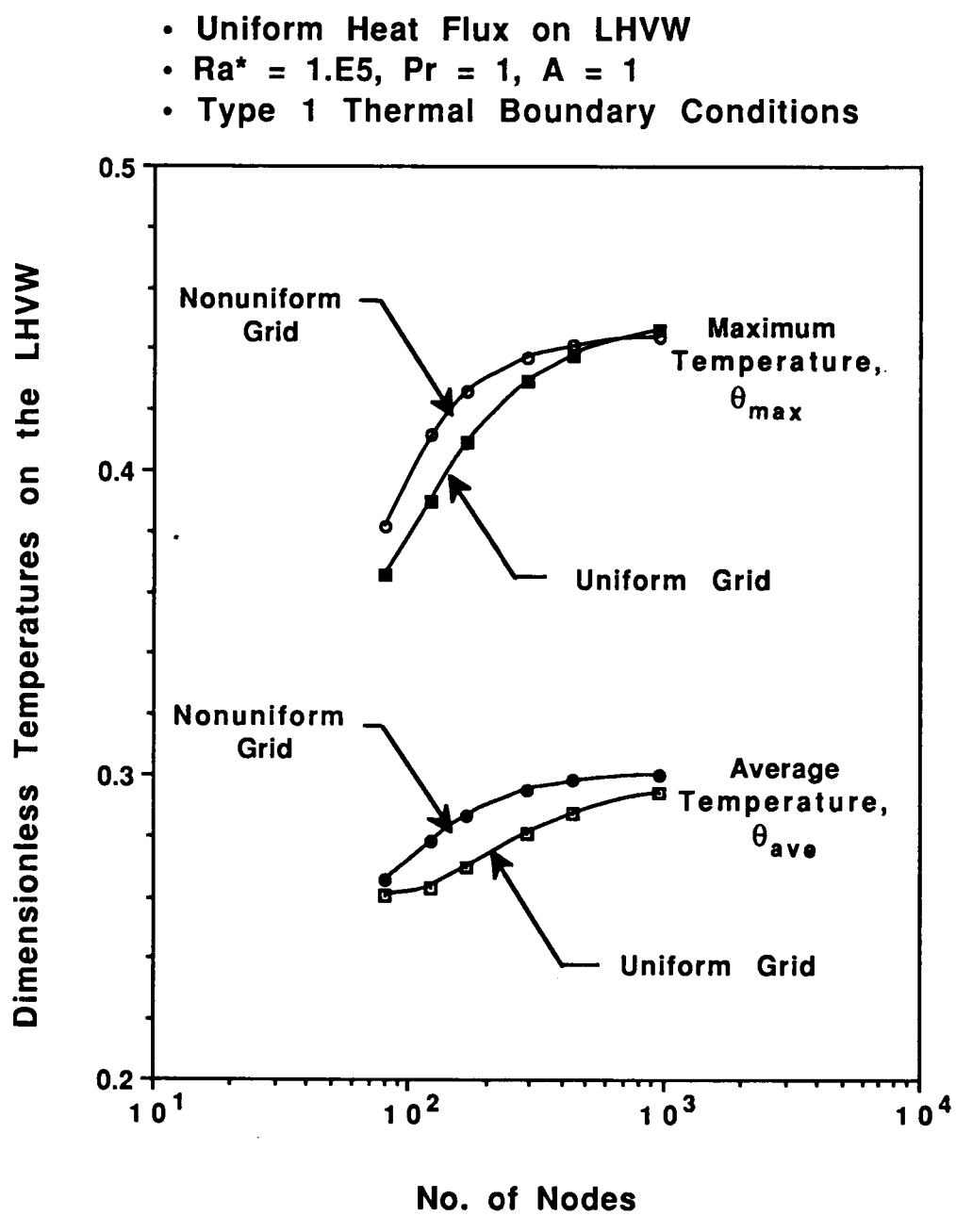


Figure 3-6. Effect of grid spacing on predicted temperatures on the LHVW

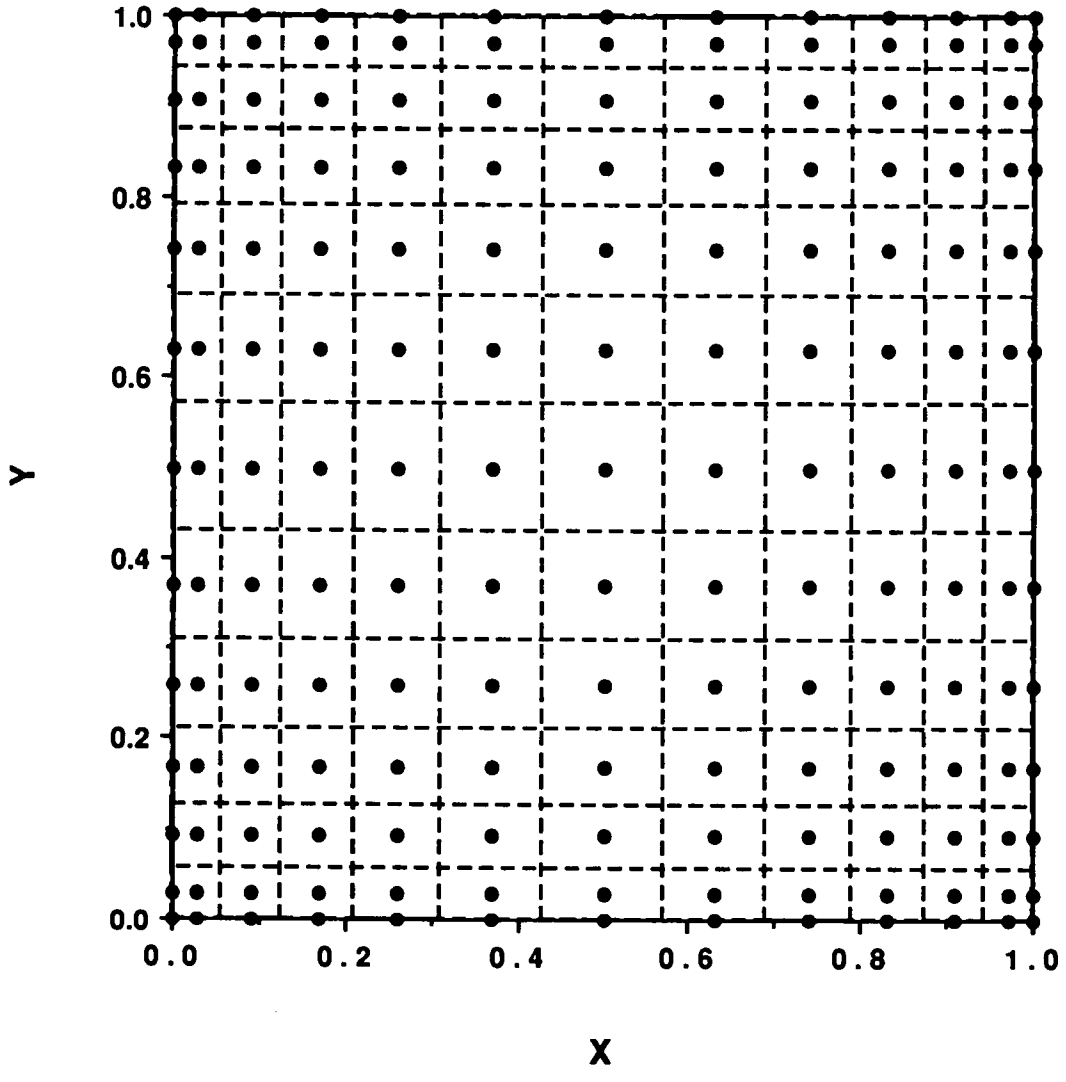


Figure 3-7. The nonuniform 13 x 13 grid used for optimization studies

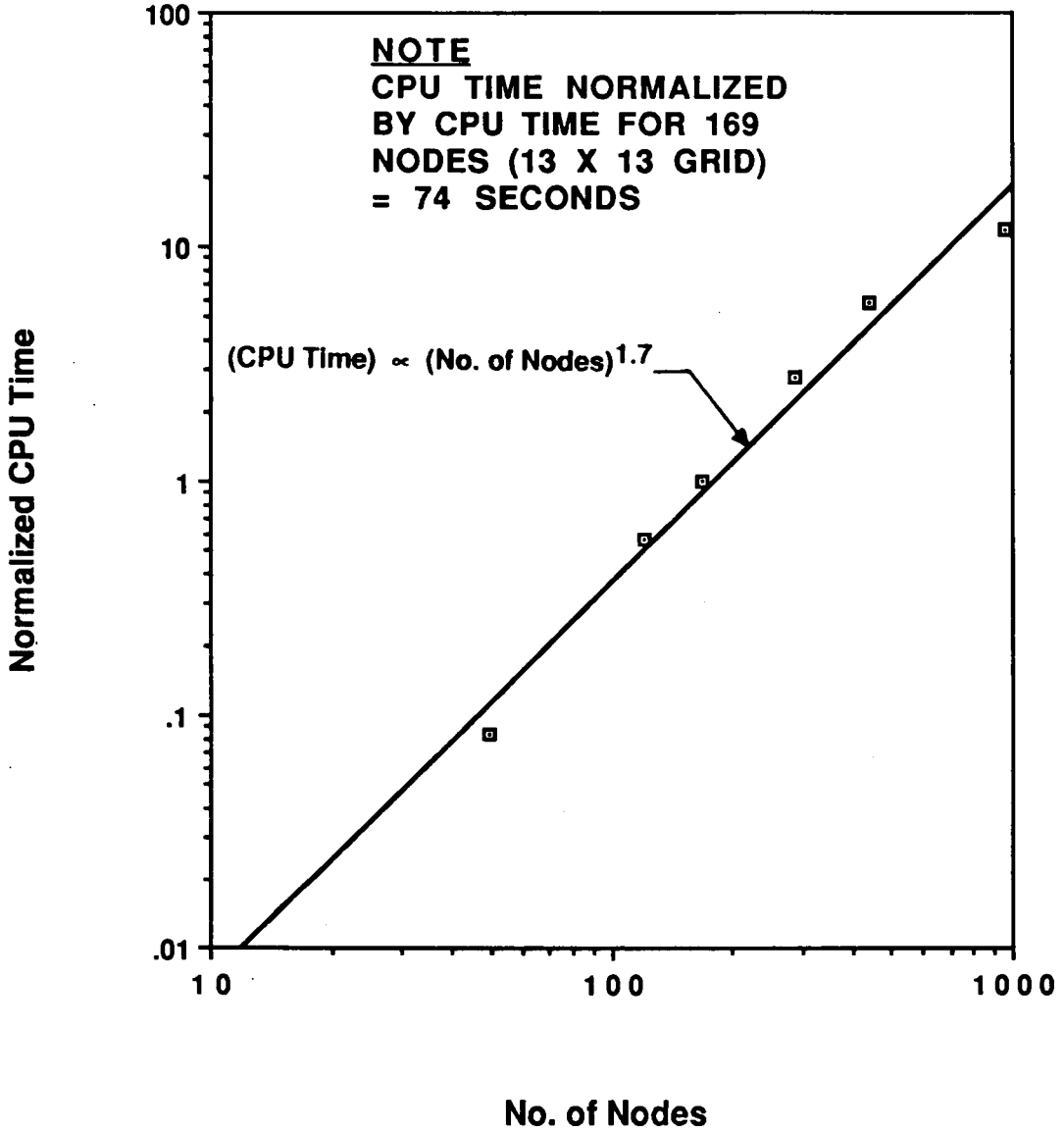


Figure 3-8. Effect of grid size on the computer CPU time required for solution of the natural convection problem

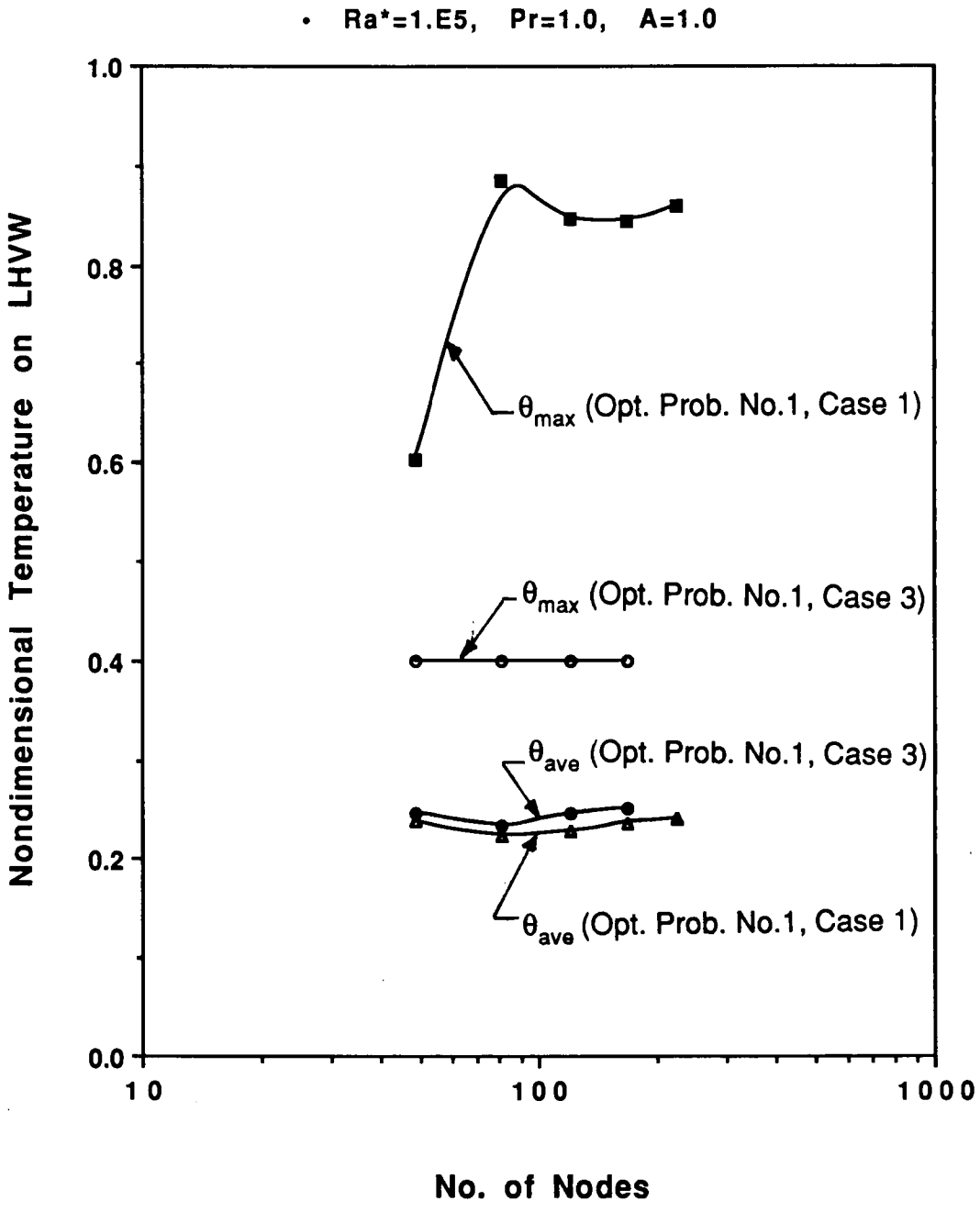


Figure 3-9. Effect of grid size on temperatures obtained from optimal heat flux distribution studies

shown in this figure for Case 1 of optimization problem number 1 (minimum average temperature of the LHVW with fixed total heating rate) and Case 3 of optimization problem number 1 (same as Case 1 but with the peak temperature of the LHVW constrained to remain below an upper limit). With the exception of the peak temperature for Case 1 with the coarsest (7 x 7) grid, these results are relatively insensitive to grid size. The nature of the optimal heat flux distribution profiles will be discussed in subsequent sections of this chapter.

The computer resources required for Case 1 type optimization studies using the heat flux at each grid point along the LHVW to define the heat flux distribution are plotted in Figure 3-10. These results indicate that the CPU time for optimization runs scales as $N^{2.86}$. The CPU time required to run this simplest type of optimization for a 13 x 13 grid is almost one hour (3360 seconds) on a CRAY-2 supercomputer.

Based on the results of these grid size studies, it is clear that the use of meshes finer than about 13 x 13 for performing optimal heat flux distribution studies is impractical. For example, increasing the number of grid points to only 15 x 15 more than doubles the run time! Fortunately, as pointed out above, the 13 x 13 nonuniform grid appears to be quite adequate for predicting the overall nature of the natural convection flow and is expected to yield heat flux distributions of sufficient definition to insure that minimum LHVW temperatures are accurately predicted.

3.2.3 Sensitivity To The Definitions Of The Constraint And Objective Functions.

As shown in Table 3-3, four types of optimization problems were solved. The first three problems are designated as Cases 1, 2, and 3 of optimization problem number 1. For all cases of optimization problem number 1, the total heating rate along the LHVW is fixed and either the average or peak temperature on the LHVW is minimized. For Case 1 of optimization

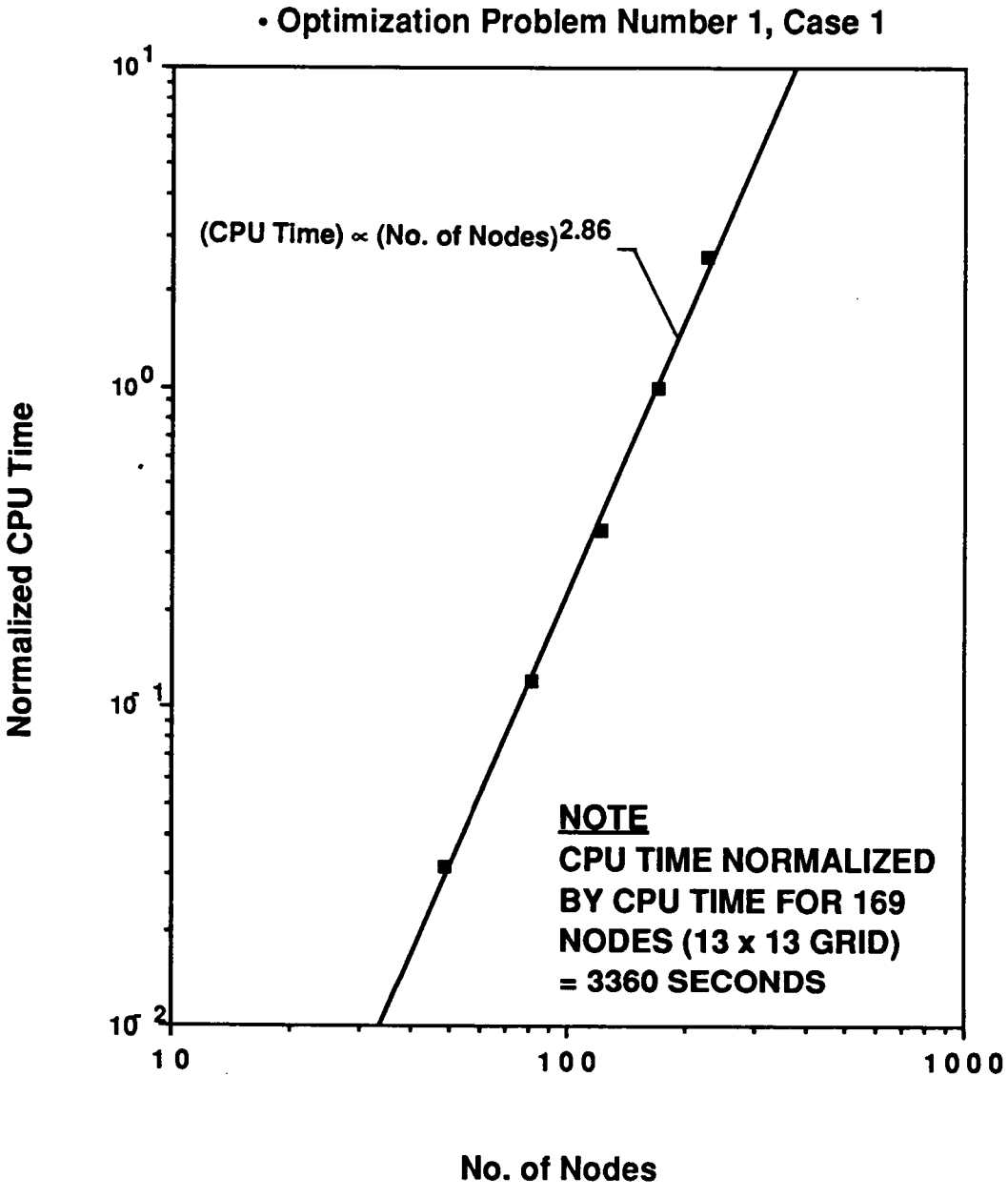


Figure 3-10. Effect of grid size on computer CPU time required for solution of the optimal heat flux distribution problem

Table 3-3. Computational matrix for optimization constraint and objective function sensitivity studies

- $Ra^* = 10^5$, Pr = 1.0, A = 1.0, Type 1 thermal boundary conditions

Optimization Problem No.	Case	Constraints	Objective Function
		CONSTRAINTS AND OBJECTIVE FUNCTIONS IN TERMS OF PHYSICAL VARIABLES	
1	1	Q_o = constant	Minimum T_{ave}
1	2	Q_o = constant	Minimum T_{max}
1	3	Q_o = constant T_{max} < upper limit	Minimum T_{ave}
2	-	T_{ave} = constant, T_{max} < upper limit	Maximum Q_o
		CONSTRAINTS AND OBJECTIVE FUNCTIONS IN TERMS OF NONDIMENSIONAL VARIABLES	
1	1	Ra^* = constant	Minimum θ_{ave}
1	2	Ra^* = constant	Minimum θ_{max}
1	3	Ra^* = constant θ_{max} < upper limit	Minimum θ_{ave}
2	-	Ra = constant (θ'_{ave} = constant = 1) θ'_{max} < upper limit	Maximum Q'

problem number 1, the peak temperature of the LHVW is unconstrained, while the average temperature of the LHVW is mimimized. For Case 2 of optimization problem number 1, the average temperature is unconstrained, and the peak temperature is minimized. For Case 3 of optimization problem number 1, the peak temperature is constrained to be below an upper limit, and the average temperature is minimized. The total heating rate along the LHVW is the objective function to be maximized for optimization problem number 2 with the average temperatures on the LHVW constrained to be equal to a specified constant and the peak temperature on the LHVW constrained to be less than a specified value.

The parameters and thermal boundary conditions on the walls of the enclosure were held fixed at $Ra^* = 10^5$, Pr = 1, A = 1, and thermal boundary condition Type 1 (see Figure 1-2) for these constraint and objective function sensitivity studies. The effects of varying each of these parameters and of alternate boundary conditions are discussed in the final sections of this chapter.

Optimization problem number 1, Case1. The heat flux distribution that minimizes the average temperature of the LHVW subject to a fixed total heating rate on the LHVW is shown in Figure 3-11 for the grid point heat flux optimization approach. As shown in this figure, the total heating is deposited on a single boundary grid surface, which is located approximately 75% of the way up the left-hand vertical wall.

The value of the average nondimensional temperature for this optimal heat flux distribution is 0.2367 which is about 17% lower than the average temperature for a corresponding uniform heat flux distribution case, and, as will be shown later, 21% lower than the isothermal LHVW case with the same total heating rate. The value of the maximum nondimensional temperature (unconstrained) of the LHVW is 0.8454 for this case, which is almost twice as high as the value for a uniform heat flux distribution.

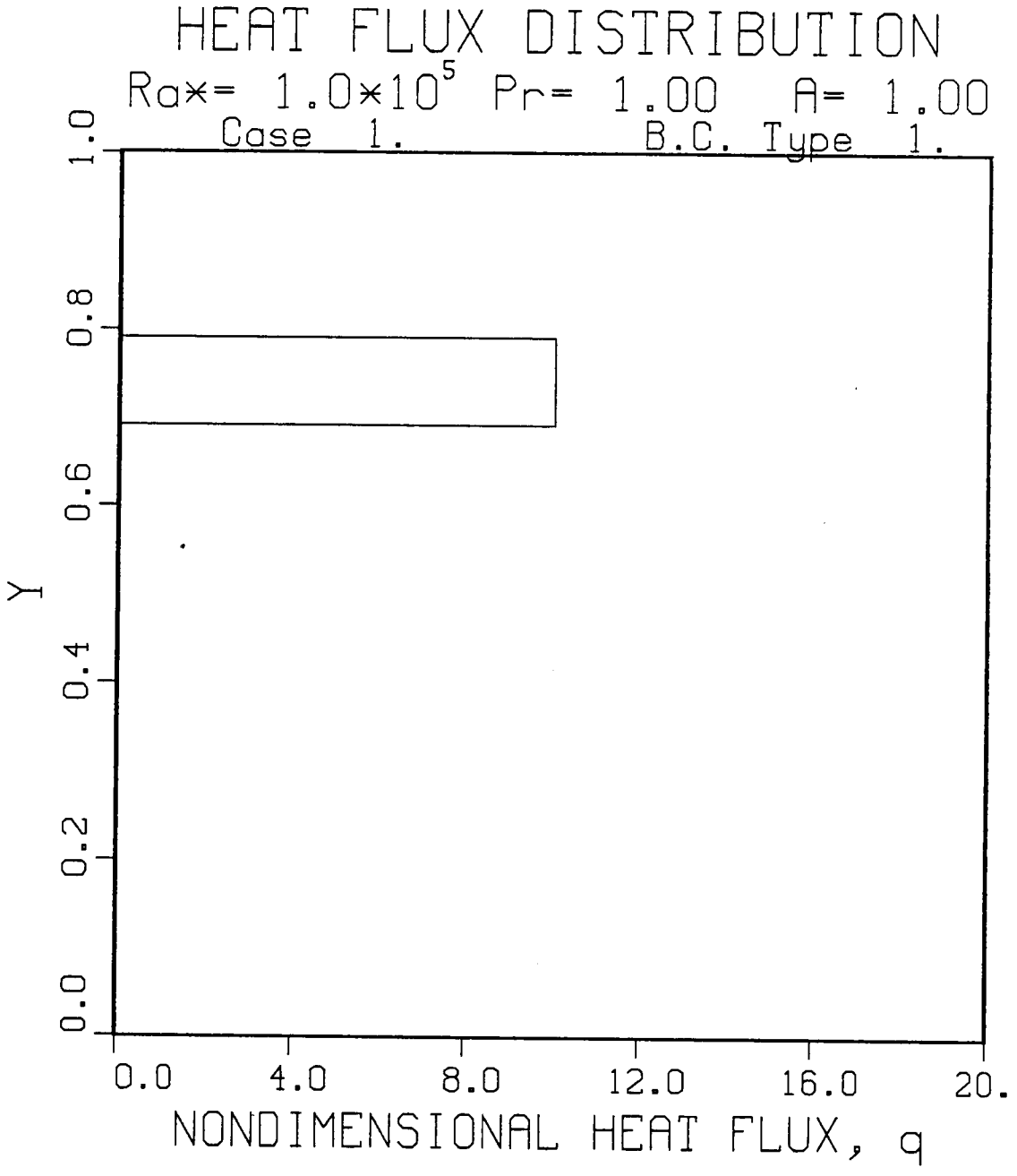


Figure 3-11. Optimal heat flux distribution for minimizing the average temperature of the LHVW (Case 1 of optimization problem number 1)

Streamline, heatline, and isothermal contour and heat flux distribution plots for this case are shown in Figure 3-12. Relative to the streamline contour plots for the uniform heat flux distribution which were presented in Figure 3-3, it can be seen that the region near the bottom of the enclosure has very little flow for the Case 1 type optimization. The maximum absolute value of the streamfunction ($|\Psi|_{max}$) is 4.6 for Case 1 and 6.5 for the uniform heat flux distribution case. As discussed later, the circulation rate for Case 1 was also found to be less than that for the Case 2 type optimization which had more heat deposited in the lower regions of the LHVW. These results are qualitatively consistent with the results of Chu et al (1976). In their experimental and numerical analysis studies of natural convection with discrete heat sources placed at various locations along the LHVW of a rectangular enclosure with natural convection, they showed that maximum circulation occurs with the heater located at positions lower than .5H. However, maximum circulation does not necessarily imply minimum average temperature (although as discussed in the results for Case 2 high circulation rates seem to be consistent with minimum peak temperature).

The heatlines for Case 1 (Figure 3-12) emanate from the heated region of the LHVW and are very closely spaced in this region. Note that the heatlines leaving the LHVW are spread over a slightly broader region of the wall than is indicated by the heat flux distribution shown in Figure 3-11. This is caused by the data smoothing process which is carried out by the contour plotting program in constructing the continuous heatlines from the values of the heatfunction at discrete grid points. Most of the heat flows in the upper regions of the enclosure. The isotherms shown in Figure 3-11 are closely spaced near the heat source. The bottom half of the enclosure is nearly isothermal. Although the temperature in the heated region of the wall is relatively high and remains high for the region above the heated location, the temperature of the remainder of the wall (approximately $Y < 0.6$) is very low.

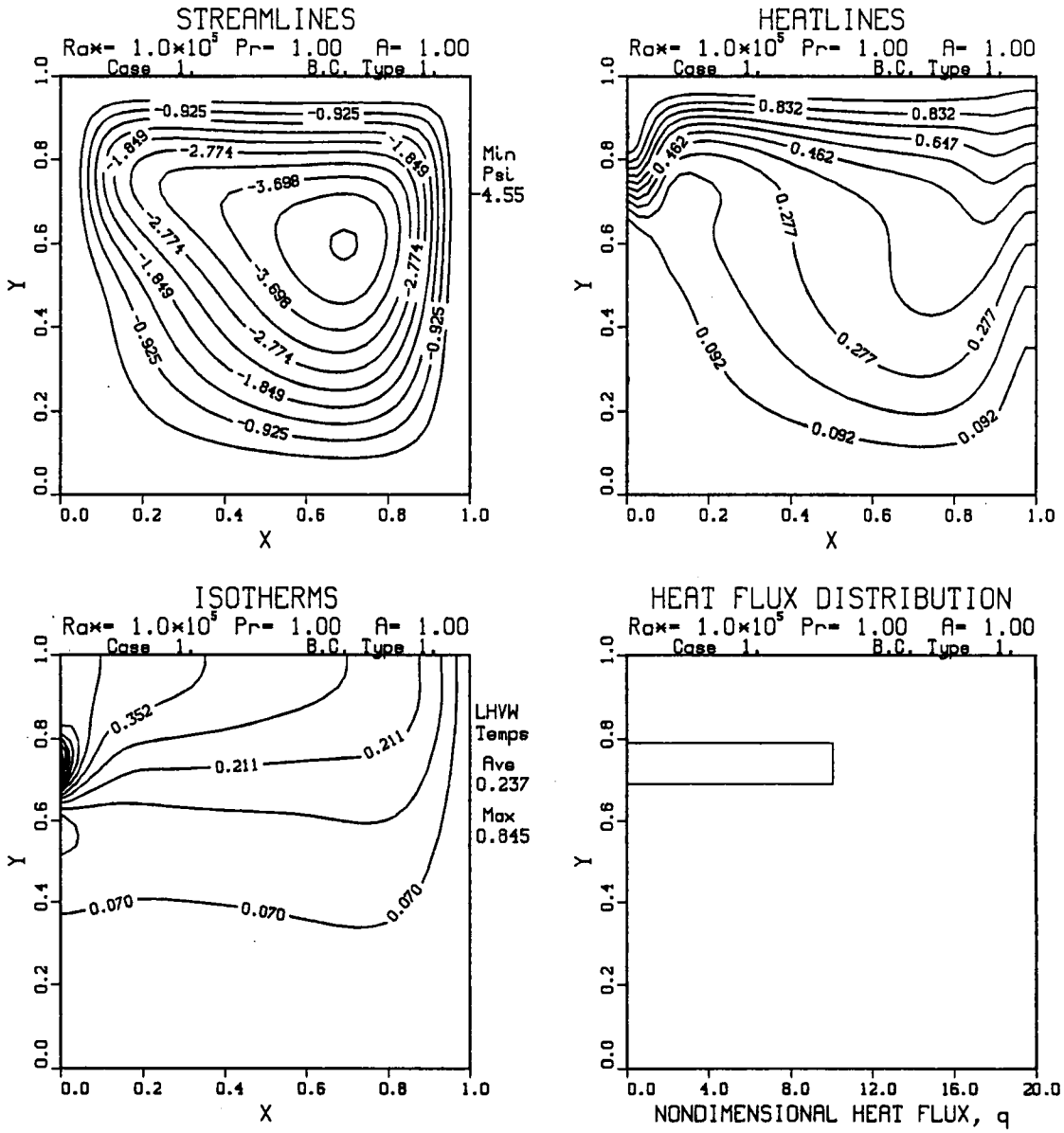


Figure 3-12. Summary of results for Case 1 of optimization problem number 1

The nondimensional temperature varies from 0.06 at Y=0 to 0.14 at Y=0.63. The highly peaked optimal heat flux distribution leads to very low temperatures in the lower portion of the LHVW and very high temperatures in the upper portion of the LHVW. Averaging the temperature over the entire LHVW, the net result is a minimal average temperature. Depositing the heat further up the wall is not optimal because of the poor circulation in the upper left-hand corner of the enclosure.

Optimization problem number 1, Case 2. For Case 2 of optimization problem number 1, the heat flux distribution that minimizes the peak temperature of the LHVW with a fixed total heating rate is sought. The optimization process for this combination of constraint and objective functions leads to an isothermal temperature profile along the LHVW with a value of nondimensional temperature equal to 0.3000. The optimal heat flux profile, which is identical to the isothermal wall heat flux profile, is shown in Figure 3-13. This result is intuitively obvious, since any peaking in the temperature profile can be relieved by redistributing the heat flux from the region of peak temperature, thus lowering the peak value until all temperatures are at the same/peak value.

The streamline, heatline, and isothermal contour plots for Case 2 are shown in Figure 3-14. By comparison to the heatline profiles for Case 1 shown in Figure 3-12, the heat flux for Case 2 is distributed over a much broader region of the LHVW. Since for Case 2 both vertical walls are isothermal and both horizontal walls are adiabatic, the contours are centrosymmetric.

Relative to the Case 1 results (see Figure 3-12), the circulation for Case 2 is much greater and fills the entire enclosure. The value of $|\Psi|_{max}$ is 7.4 for Case 2 compared to only 4.6 for Case 1. The heatlines for Case 2 are closely spaced along the lower region of the enclosure indicating that the heat flux is peaked in this region. Due to the upward motion along the boundary layer of

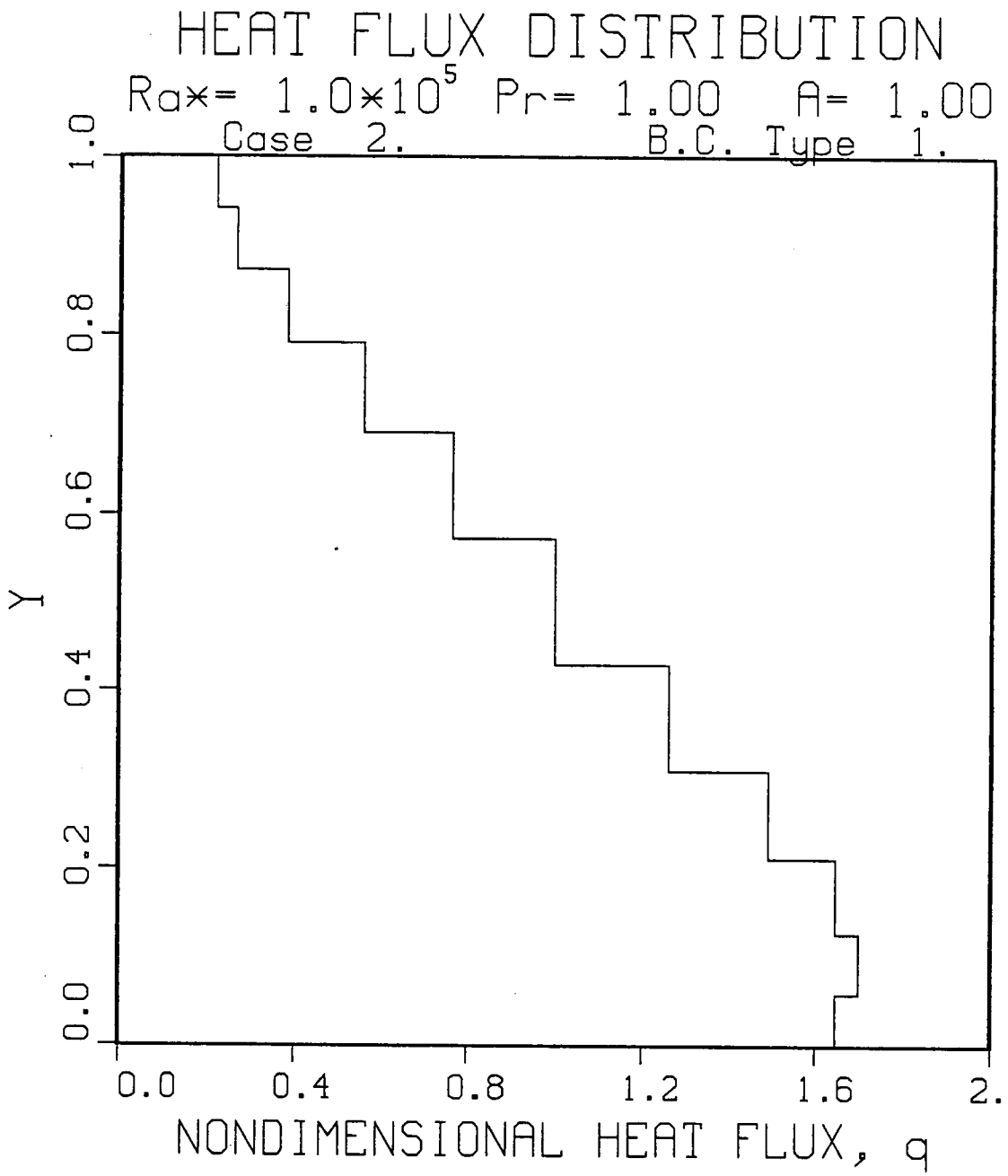


Figure 3-13. Optimal heat flux distribution for minimizing the peak temperature of the LHVW (Case 2 of optimization problem number 1)

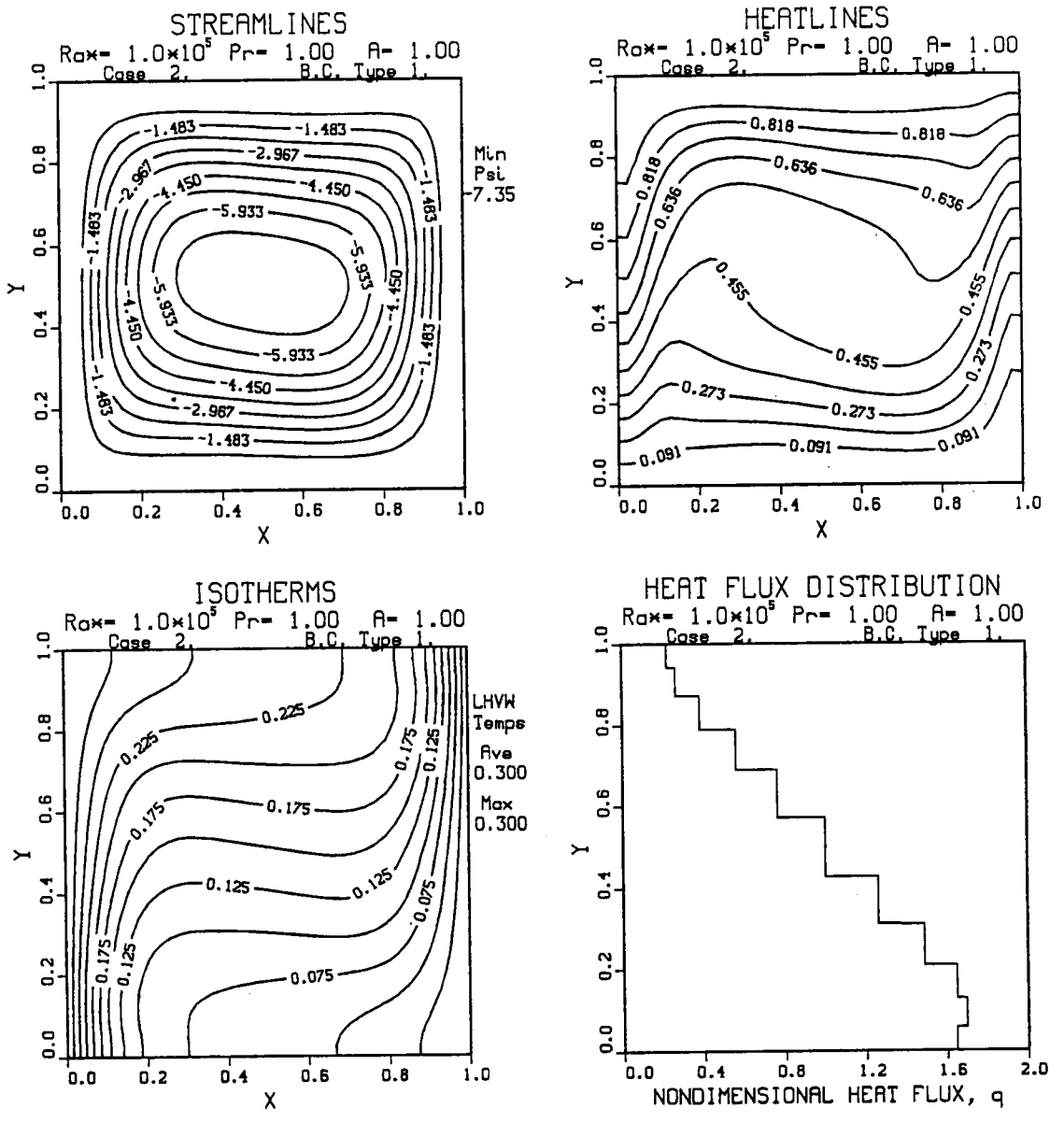


Figure 3-14. Summary of results for Case 2 of optimization problem number 1

the LHVW a significant portion of the heat flows by natural convection through the upper portion of the enclosure.

Because of the uniform temperature distribution along both vertical walls the isothermal contours are nearly vertical in the fluid near the walls. If heat was transferred by conduction only, the isothermal contours would remain vertical throughout the enclosure. However, isothermal contours in the central region of the enclosure are nearly horizontal for this case ($Ra^* = 10^5$), thus demonstrating the effectiveness of the natural convection heat transfer.

Comparing the results for Case 2 with those for the uniform heat flux distribution, the grid point heat flux optimization approach leads to a 30% decrease in the peak temperature (0.3000 for Case 2 and 0.4258 for uniform heating). It should be further noted that the average nondimensional temperature of 0.3000 for Case 2 is only 5% higher than the value of 0.2866 for the uniform heating case.

Optimization problem number 1, Case 3. For Case 3 of optimization problem number 1, the heat flux distribution along the LHVW that minimizes the average temperature of the LHVW, subject to the constraints that the total heating rate is fixed and the peak temperature of the LHVW remains below a specified upper limit, must be determined. Solutions to this problem are summarized in Figures 3-15 to 3-19 for upper limits on peak nondimensional temperature of 0.6 and 0.4 These two values of the upper limit on peak temperature were chosen because they are intermediate values between the minimum peak nondimensional temperature of 0.3000 obtained for Case 2 of optimization problem number 1 and the unconstrained value of 0.8454 obtained for Case1 of optimization problem number 1.

The heat flux distribution presented in Figure 3-15 for $\theta_{max} \leq 0.6$ shows a less peaked profile than that for the unbounded case (see Figure 3-10 for Case 1), but the peak value of the heat flux remains at the same location, that is, approximately 75% of the total height of the vertical wall. Imposing the

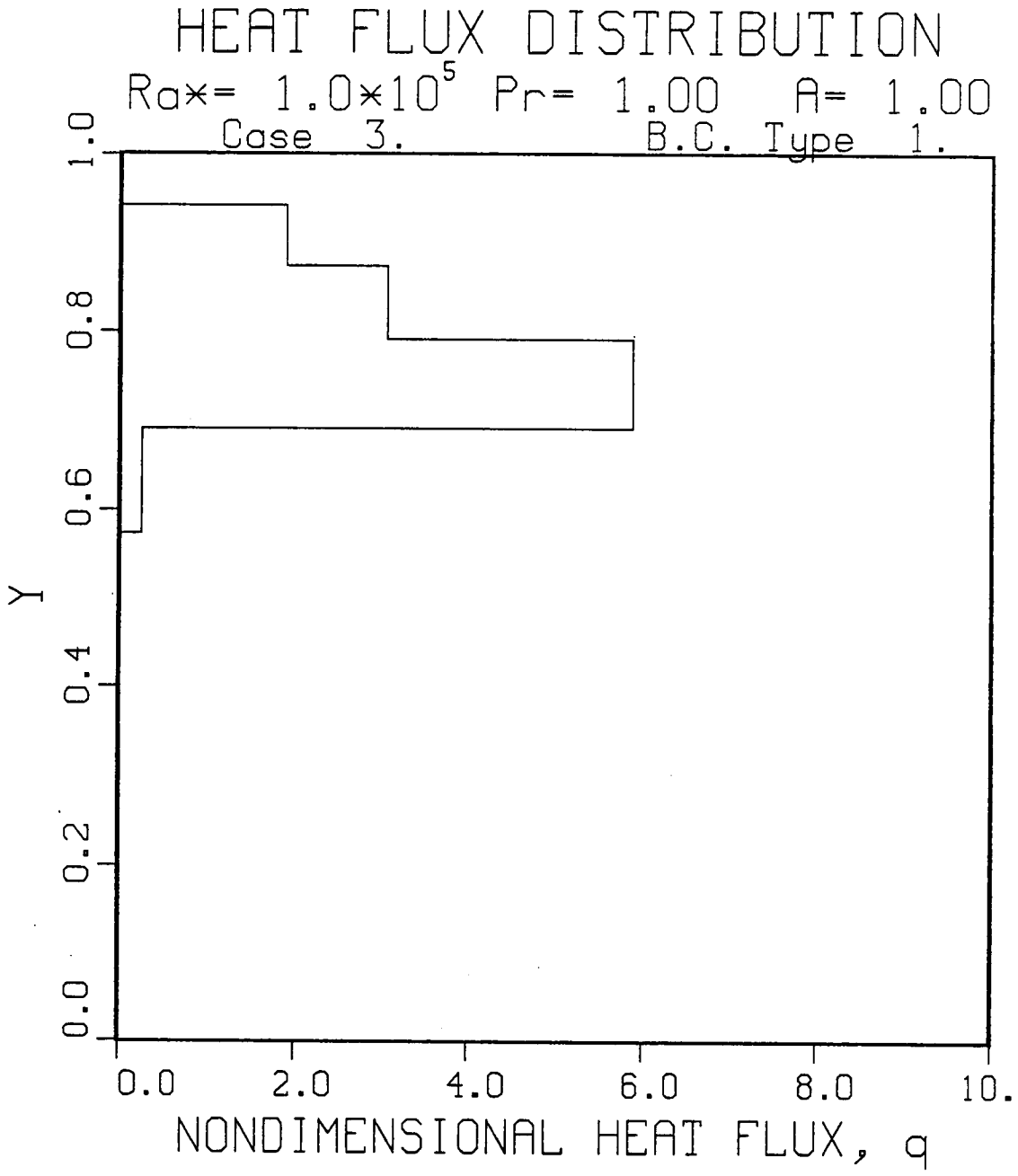


Figure 3-15. Optimal heat flux distribution for minimizing the average temperature on the LHVW with $\theta_{max} \leq 0.6$ and fixed total heating rate

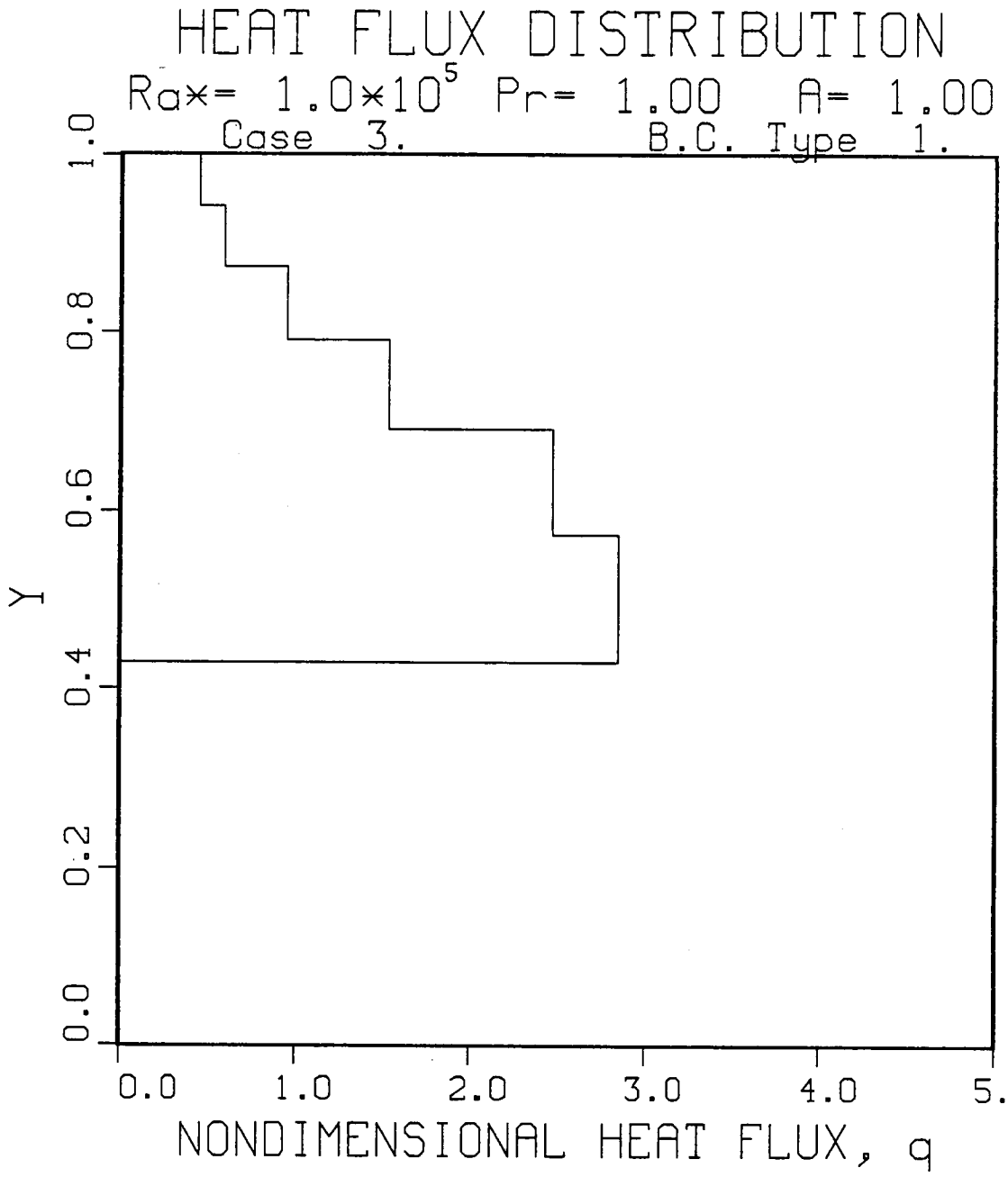


Figure 3-16. Optimal heat flux distribution for minimizing the average temperature on the LHVW with $\theta_{max} \leq 0.4$ and fixed total heating rate

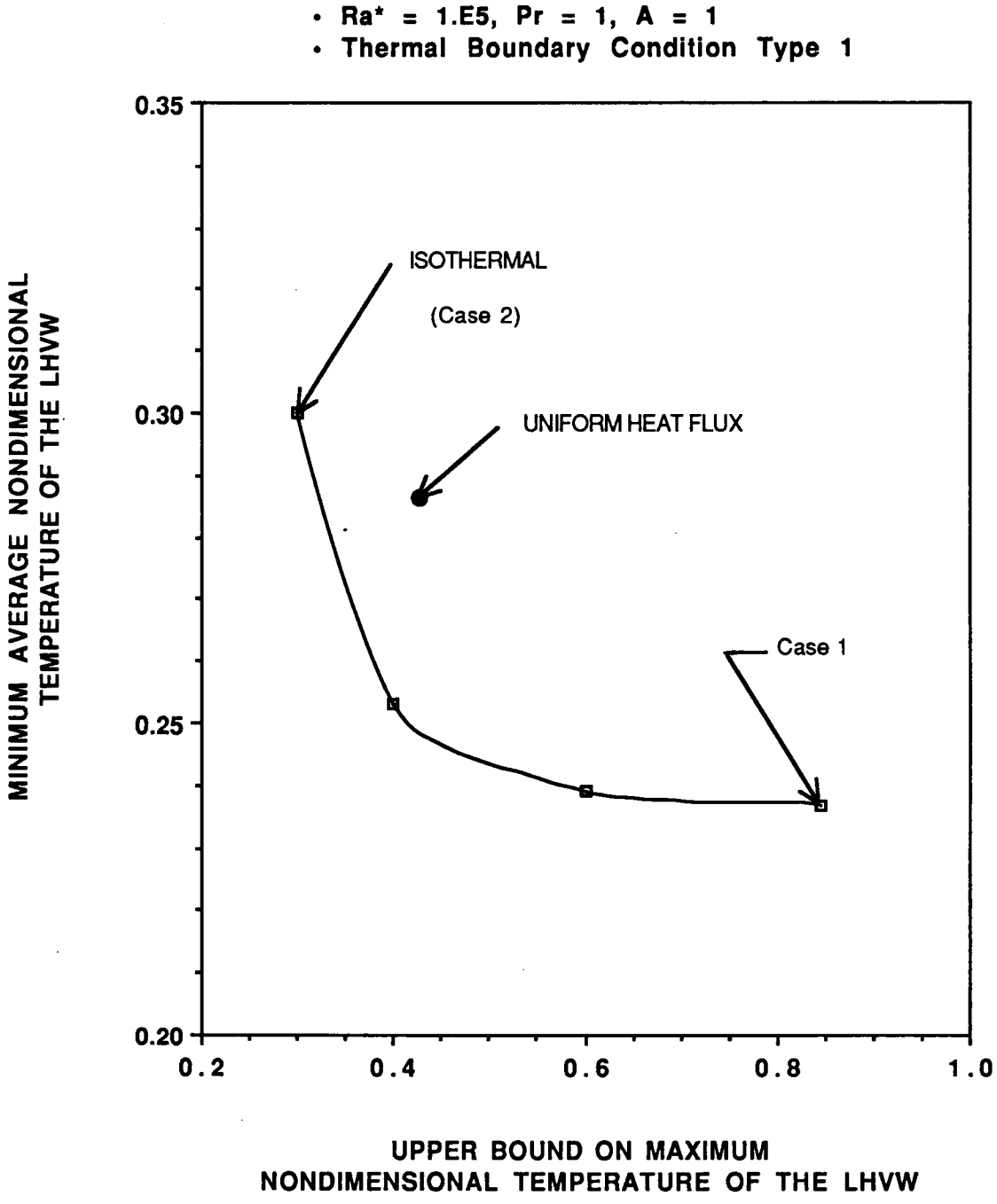


Figure 3-17. Minimum average nondimensional temperature on the LHVW versus upper bound on peak nondimensional temperature on the LHVW

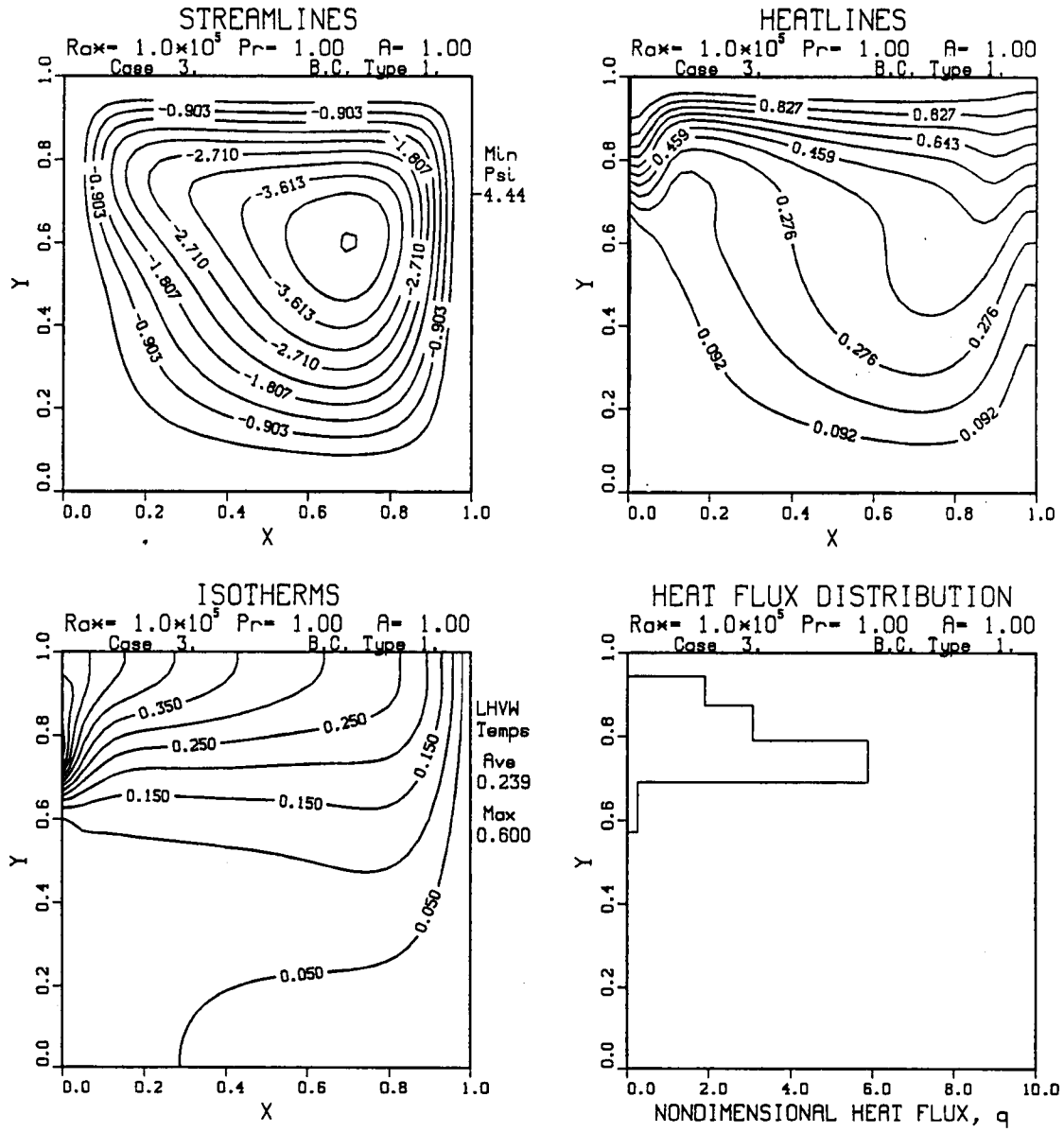


Figure 3-18. Summary of results for Case 3 of optimization problem number 1 with $\theta_{max} \leq 0.6$

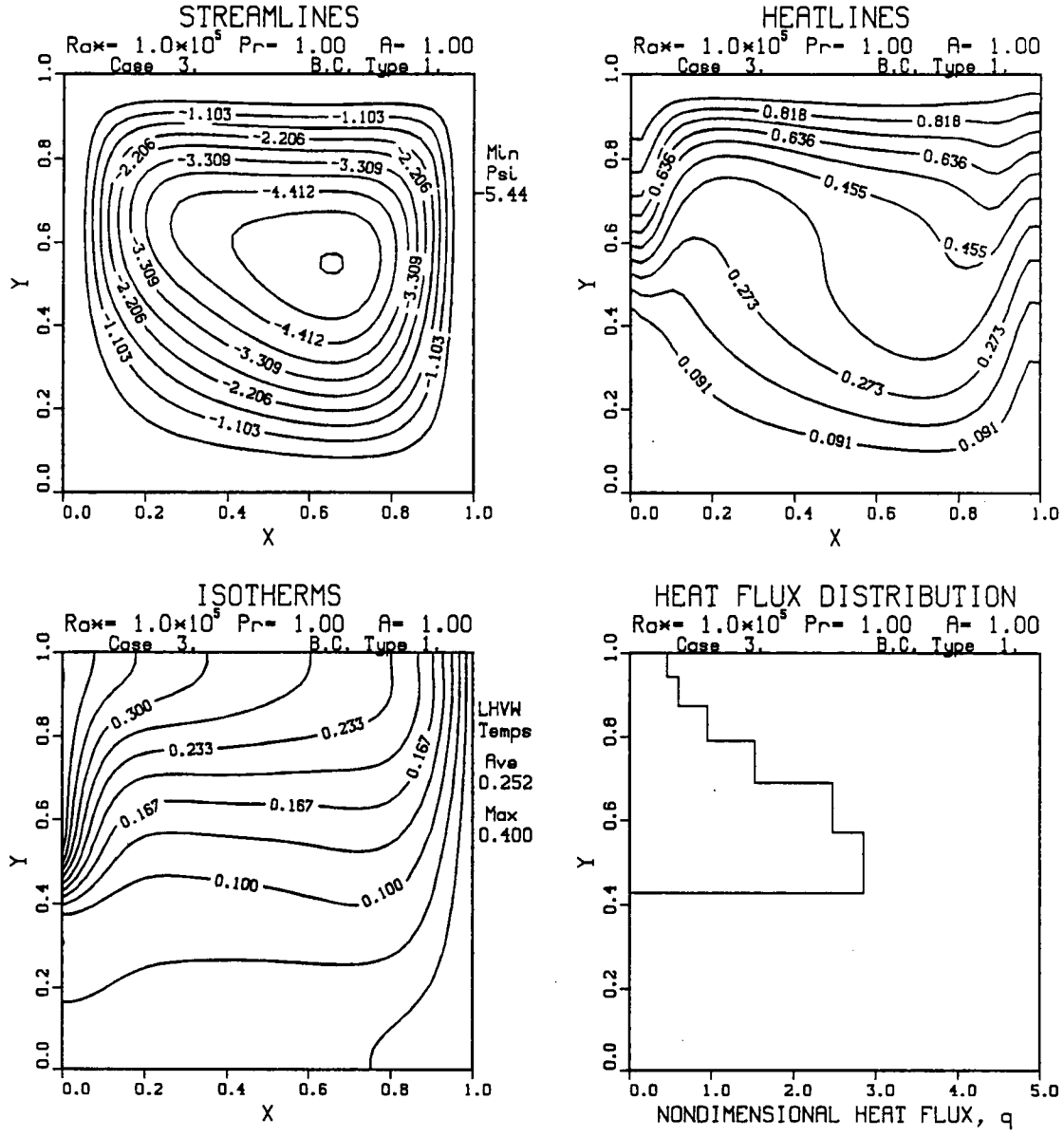


Figure 3-19. Summary of results for Case 3 of optimization problem number 1 with $\theta_{max} \leq 0.4$

constraint that the peak nondimensional temperature be less than or equal to a value that is 29% lower than the unbounded peak temperature case (0.6 for this case compared with 0.8454 for Case 1), results in less than a 1% increase in the average temperature, thus demonstrating that constraining the peak nondimensional temperature to remain less than 0.6 does not severely impact the resulting minimum average temperature.

Constraining the peak nondimensional temperature to be less than or equal to 0.4, leads to the optimal heat flux distribution shown in Figure 3-16. The heat flux for this case becomes more spread out along the LHVW and the peak heat flux shifts to a lower position (Y = 0.5). The 53% reduction in peak temperature, compared to the unconstrained Case 1 results, leads to a 6.5% increase in the minimal average temperature.

The optimization problem number 1 results for Case 1, Case 3 with $\theta_{max} \leq 0.6$, Case 3 with $\theta_{max} \leq 0.4$, and Case 2 can be thought of as representing a "family" of optimal solutions leading from a case of unconstrained peak temperature ($\theta_{max} = 0.8454$), to lower and lower values of the constraint on θ_{max} until the minimal value of θ_{max} (0.3000 for Case 2) is reached. If the upper limit on peak temperature for a Case 3 type optimization is set at a value above that obtained for Case 1, the Case 3 results will be identical with the Case 1 results. If the upper limit on peak temperature is set at the value found in the Case 2 results (isothermal wall), the Case 2 results will be obtained. If the upper limit on peak temperature is set lower than the Case 2 result, a solution cannot be obtained. Thus, Cases 1 and 2 of optimization problem number 1 can be thought of as special cases which define the extremes of the family of optimization problem number 1 solutions.

The minimum average nondimensional temperatures are plotted in Figure 3-17 as a function of the constraint on θ_{max} for the entire range of optimal

solutions. The point representing the average and peak nondimensional temperatures for a uniform heat flux profile is shown in this figure for comparison. Displaying the results in this fashion graphically demonstrates the sensitivity of the minimum average temperature to the upper temperature limit. It is easy to envision that this type of information would be very useful to a designer of electronic components who is considering the potential benefits of using this technique for positioning a set of heat producing components along a vertical wall of an enclosure with natural convection.

The streamline, heatline, and isothermal contour and heat flux distribution plots for both peak temperature limits are shown in Figures 3-18 and 3-19. By comparison of these plots with those for Case 1 (Figure 3-12) and Case 2 (Figure 3-14), it is further demonstrated that these cases represent a transition between Case 1 with its highly localized heat flux profile and Case 2 with its uniform temperature and much broader heat flux profile.

The isothermal contour plots shown in Figures 3-18 and 3-19 illustrate that for the optimal heat flux distribution the LHVW becomes nearly isothermal beyond a certain point up the LHVW. For the $\theta_{max} \leq 0.4$ case, the optimal heat flux distribution results in an isothermal region of the wall ($\theta(Y) = 0.4$) for $Y > 0.55$, whereas for the $\theta_{max} \leq 0.6$ case, this occurs for $Y > 0.75$.

Optimization problem number 2. For optimization problem number 2, the total heating rate is maximized subject to the constraint that the average temperature of the LHVW is a specified constant and the peak temperature on the LHVW is constrained to be less than a specified value. By selecting the constraints for optimization problem number 2 to be equal to the average and peak temperatures of the LHVW obtained from Case 1 of optimization problem number 1 (discussed above) a comparison of the two optimization approaches can be made. The average nondimensional temperature of the LHVW, θ_{ave}, for Case 1 of optimization problem number 1 with nominal

parameters was found to be 0.2367. As discussed in Chapter 1, the alternate nondimensional temperature, θ', Rayleigh number, Ra, and total nondimensional heating rate from the LHVW, Q', used for studies of optimization problem number 2 (i.e. for cases which seek a maximum total heating rate with specified average temperature) are given by:

$$\theta' = \frac{(T(x,y) - T_o)}{(T_{ave} - T_o)} \tag{3-2}$$

$$Ra = \frac{\beta g (T_{ave} - T_o) H^3}{\nu \alpha} \tag{3-3}$$

$$Q' = \frac{\int_0^H q_o(y)\, dy}{[k (T_{ave} - T_o)]} \tag{3-4}$$

By examining equations (3-4) and (1-22), the alternate nondimensional heat flux, Q', can be seen to be simply the inverse of the average nondimensional temperature, θ_{ave}. The alternate nondimensional parameters corresponding to the Case 1 conditions of $Ra^* = 10^5$ and $\theta_{ave} = 0.2367$ are $Ra = 2.367 \times 10^4$ and $\theta'_{ave} = 1$.

The value of the alternate dimensionless total heating rate (Q') from the LHVW resulting from the solution of optimization problem number 2 (i.e., the objective function for optimization problem number 2) was found to be 4.2249, which is the expected value. The heat flux profile obtained for this case is the same as that shown in Figure 3-11. These results demonstrate that using the total heating rate as the objective function is a valid approach and may be a useful technique in practical applications of this methodology. However, it was found that the solution of optimization problem number 2 required approximately 30% more computing time compared with the equivalent optimization problem number 1 case. This is due to the additional iterations

(i.e., solutions of the natural convection problem) required to satisfy the nonlinear constraint on the average LHVW temperature for the solution of optimization problem number 2 compared with the minimal number of iterations required to satisy the linear constraint imposed by the fixed total heating rate on the LHVW for the solution of optimization problem number 1.

The effect of decreasing the upper limit on the peak temperature of the LHVW was also examined for optimization problem number 2. To facilitate a further comparison between the optimization approaches, average and peak temperatures of the LHVW corresponding to the optimization problem number 1, Case 3 results discussed above were used for the optimization problem number 2 studies. The nondimensional temperatures of $\theta_{ave} = 0.2522$ and $\theta_{max} = 0.4000$ for optimization problem number 1 (Case 3) with $Ra^* = 10^5$ correspond to alternate nondimensional temperatures of $\theta'_{ave} = 1.0000$ and $\theta'_{max} = 1.5861$ for optimization problem number 2 with $Ra = 2.522 \times 10^4$.

Results indicate that, for equivalent tolerances on convergence of the natural convection model and on convergence of the optimization calculations, about 90% more computing time is required for the solution of optimization problem number 2. The maximum alternate dimensionless total heating rate, Q', for the solution of optimization problem number 2 was found to be 3.870, which is slightly less than the expected value of 3.965 ($1/\theta_{ave}$). As shown in Figure 3-20, the optimal heat flux distribution is roughly the same for the solutions to the two optimization problems except near the midpoint of the LHVW. Agreement between these two distributions was achieved, that is, the optimization problem number 2 solution converged to the optimization problem number 1 (Case 3) solution (Q' = 3.965), after reducing the convergence tolerances and restarting the optimization problem number 2 run. However, it should be noted that almost a factor of two additional

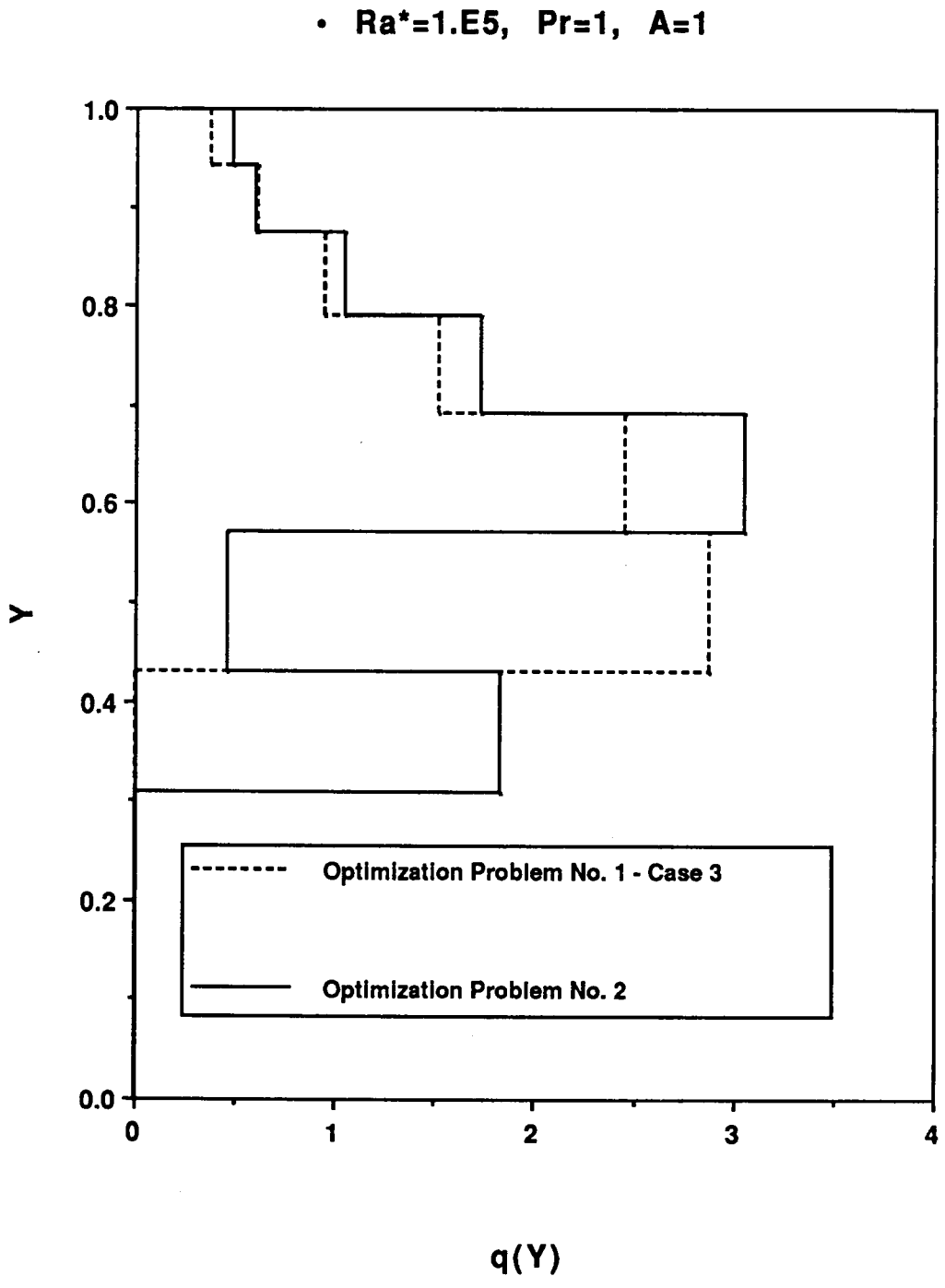


Figure 3-20. Comparison of heat flux distributions for Case 3 of optimization problem number 1 and the corresponding case for optimization problem number 2

computing time was required for optimization problem number 2 to achieve this agreement.

The increased difficulty in achieving the optimal heat flux distribution for the solution of optimization problem number 2 with a specified upper bound on the peak temperature of the LHVW is not surprising. Under these circumstances, the intermediate steps taken during the optimization process required many iterations to determine a feasible solution which satisfied both nonlinear constraints (fixed average temperature on the LHVW and a specified upper bound on the peak temperature of the LHVW).

3.2.4 Study Of Alternate Ways Of Representing The Heat Flux. The optimal heat flux distribution along the LHVW was determined using two approaches. These two approaches considered either: (1) the values of the heat flux at each grid point along the LHVW, or (2) the coefficients of a polynomial distribution defining the heat flux along the LHVW, as the independent parameters to be varied in determining the extremal heat flux distribution.

Results obtained using the first method are described in the previous sections. Results obtained by solving Case 1 of optimization problem number 1 using the second method, that is, employing the coefficients of a polynomial distribution of heat flux along the LHVW as the independent variables, are summarized in Table 3-4 for various grid sizes. These results demonstrate that the values of the coefficients that define the optimal heat flux distribution are relatively insensitive to the calculation mesh for grids ranging in size from 7 x 7 to 13 x 13.

The computer resource requirements for the optimization approach which uses the coefficients of a polynomial heat flux distribution were examined to determine whether there is any potential benefit to be gained by using this alternate approach. A fourth order polynomial heat flux distribution with a 13 x 13 grid requires about 2600 seconds of CPU time on the CRAY-2

Table 3-4. Minimal average temperature on the LHVW obtained using the polynomial heat flux distribution approach

- Case 1 of optimization problem number 1 (minimum average temperature with fixed total heating rate)
- Polynomial Heat Flux Distribution Along LHVW
- $q(Y) = C_0 + C_1 Y + C_2 Y^2 + \ldots$
- $Ra^* = 10^5$, $Pr = 1.0$, $A = 1.0$

Order of Polynomial	Grid Size	C_0	C_1	C_2	C_3	C_4	θ_{ave}
First	7 x 7	0.000	2.000	-	-	-	0.2539
	9 x 9	0.000	2.000	-	-	-	0.2455
	11 x 11	0.000	2.000	-	-	-	0.2556
	13 x 13	0.000	2.000	-	-	-	0.2640
	15 x 15	0.000	2.000	-	-	-	0.2694
Second	7 x 7	0.112	-1.482	4.886	-	-	0.2447
	9 x 9	0.114	-1.496	4.902	-	-	0.2333
	11 x 11	0.118	-1.522	4.931	-	-	0.2422
	13 x 13	0.115	-1.501	4.903	-	-	0.2508
Third	7 x 7	0.000	0.224	-2.477	6.855	-	0.2419
	9 x 9	0.000	0.223	-2.476	6.855	-	0.2297
	11 x 11	0.000	0.223	-2.477	6.856	-	0.2383
	13 x 13	0.000	0.224	-2.477	6.855	-	0.2471
Fourth	7 x 7	0.000	0.631	-4.530	7.797	1.227	0.2414
	9 x 9	0.000	0.608	-4.433	7.372	1.173	0.2291
	11 x 11	0.000	0.621	-4.489	7.780	1.203	0.2377
	13 x 13	0.000	0.624	-4.502	7.786	1.211	0.2465

supercomputer to perform a Case 1 type optimization. This is roughly 80% of the CPU time required for the grid point heat flux distribution with the same 13 x 13 grid. This was somewhat surprising, since there were only five variables (5 coefficients for a fourth order polynomial) in the polynomial optimization approach compared to eleven (the top and bottom nodes along the LHVW are boundary control volumes with zero thickness in the x- and y-directions and therefore, do not enter into the definition of the heat flux along the LHVW) in the grid point heat flux approach. The long computing time for the polynomial approach is caused by the difficulty in constraining the polynomial heat flux distribution to remain greater than zero for all values $0 \leq Y \leq H$. This constraint is trivial to apply for the grid point heat flux approach, but leads to a nonlinear relationship between the variables (i.e. coefficients of the polynomial) for the higher order polynomial heat flux distributions.

As shown in Figure 3-21, most of the heating is deposited along the upper portion of the LHVW for the first through fourth order optimal polynomial heat flux distributions for Case 1 of optimization problem number 1. This is qualitatively consistent with the results obtained using the grid point heat flux optimization approach. The heat flux profiles plotted in Figure 3-21 appear to converge as higher order polynomials are used with only a slight change in the heat flux profile realized in going from a third to a fourth order polynomial. Although these polynomial profiles do not accurately fit the "singularity-like" heat deposition profile obtained for the grid point heat flux optimization approach, the resulting minimum LHVW temperature for higher order polynomials is reasonably well approximated. For example, the minimum average nondimensional temperature is 0.2465 for polynomial distributions of fourth order, whereas it is 0.2367 for the grid point heat flux approach. Relative to the average temperature of 0.2866 for a uniform heat flux distribution, the optimal fourth order polynomial distribution reduces the average temperature by 14%, compared to a 17% reduction for the grid point

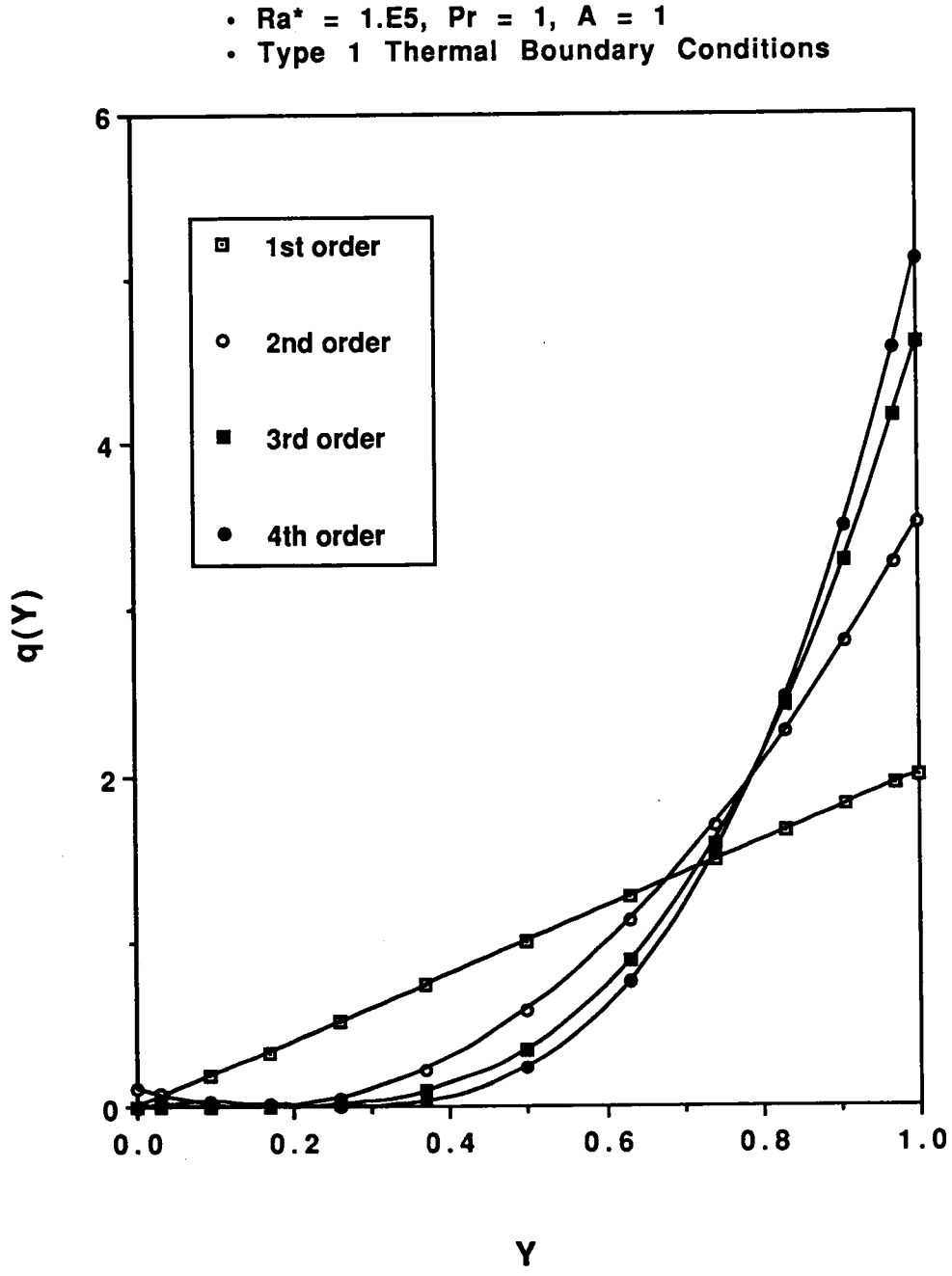


Figure 3-21. Optimal polynomial heat flux distribution for Case 1 of optimization problem number 1

heat flux optimization approach. The peak temperature for the fourth order polynomial distribution is 0.8862 compared with 0.8454 for the grid point heat flux optimization approach.

The highly peaked heat flux distributions obtained using the grid point heat flux optimization approach for Case 1 of optimization problem number 1 may be difficult to achieve in many applications to real situations such as the arrangement of electronic components. However, the polynomial heat flux distribution approach eliminates the "singularity" in heat flux deposition. Although the peak temperature for the polynomial distribution is relatively high, the apparent convergence of the optimal distribution for polynomials of third order and above, the practicality of locating heat sources in a distribution that simulates this type of distribution in an actual application, and the relatively minor difference between the minimal average temperature for this profile compared to the more optimal but less realistic single grid point deposition profiles are features that make the use of the polynomial distribution approach attractive for applications where minimal average temperature is important and peak temperature is a secondary consideration.

Results for Case 2 of optimization problem number 1 obtained using the polynomial heat flux distribution approach are shown in Figures 3-22. Near isothermal temperatures are achieved for all polynomial distributions above first order and very marginal benefit is obtained by going beyond a second order polynomial distribution. For example, the peak temperature for the optimal first order polynomial is 0.3090, whereas for a second order polynomial it is 0.3049.

The optimal heat flux profiles for polynomial heat flux distributions from first through fourth order are shown in Figure 3-23 for Case 3 with the upper limit on the peak nondimensional temperature set at 0.4. The fourth order polynomial solution is essentially identical to the third order solution. The minimum average nondimensional temperature for the fourth order

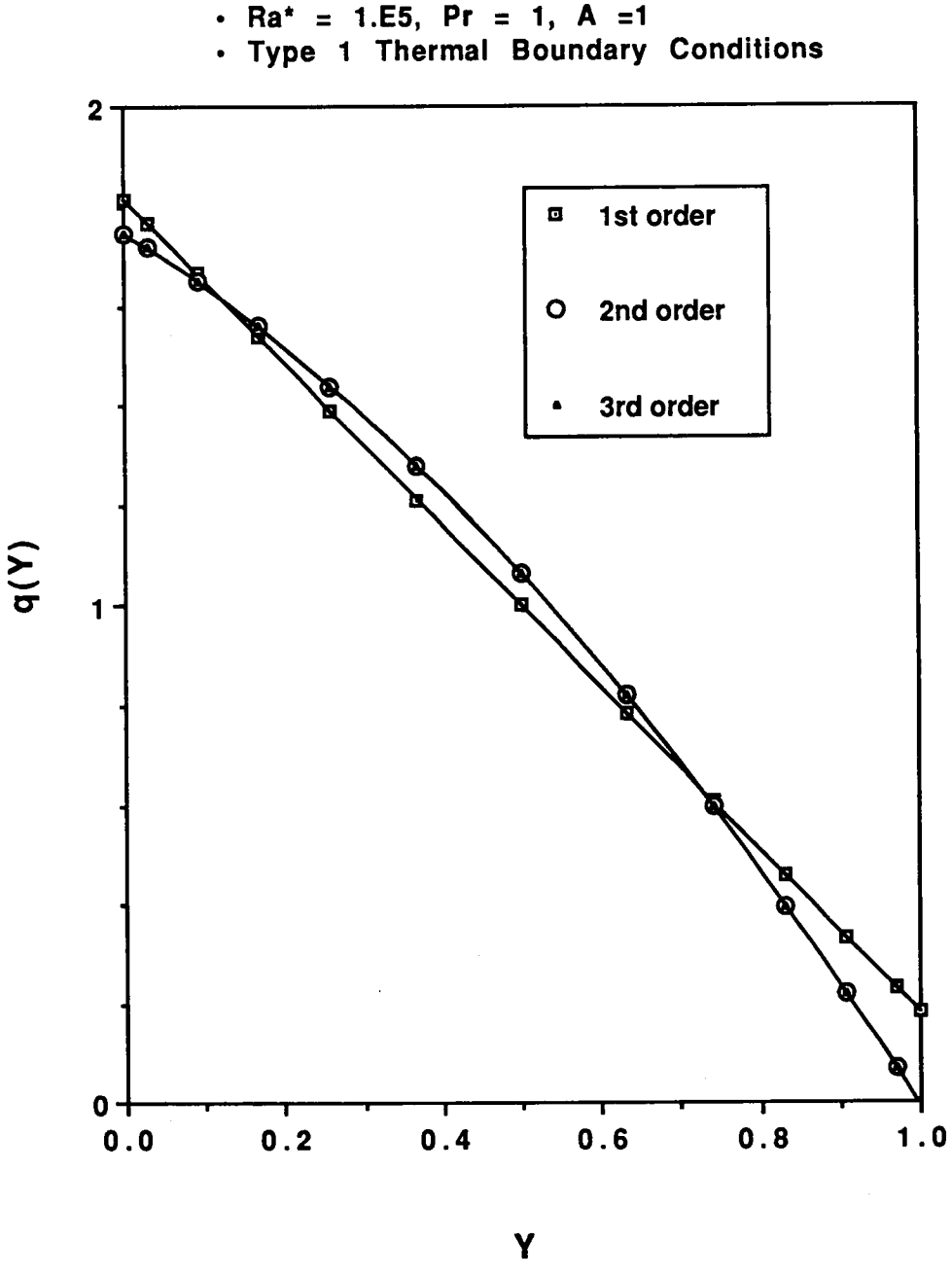


Figure 3-22. Optimal polynomial heat flux distribution for Case 2 of optimization problem number 1

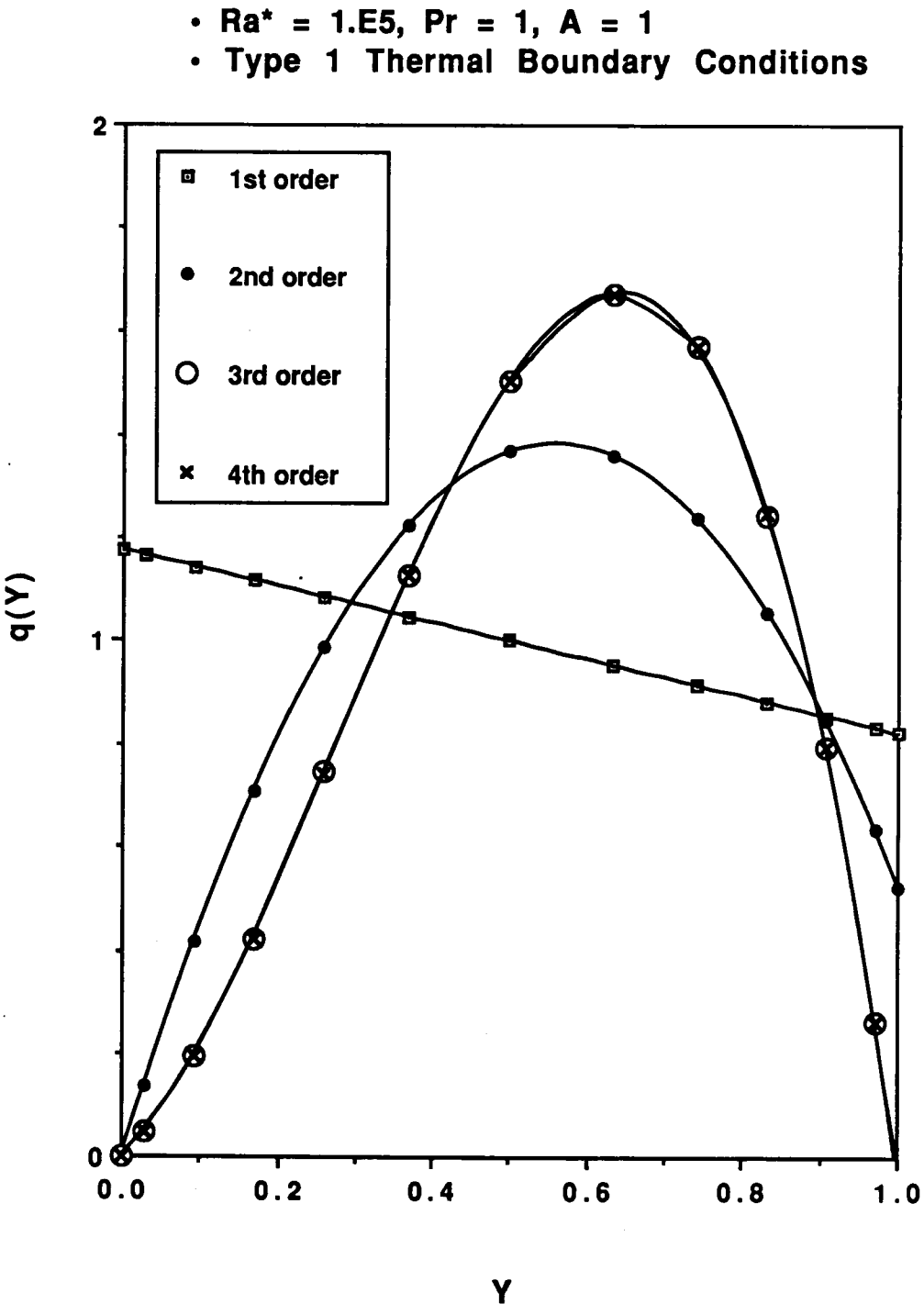


Figure 3-23. Optimal polynomial heat flux distribution for Case 3 of optimization problem number 1 with $\theta_{max} \leq 0.4$

polynomial solution is 0.2677 compared with 0.2522 for the grid point heat flux optimization approach.

3.2.5 Summary Of Conclusions Based On Preliminary Studies. Based on the results discussed above, several conclusions were drawn before proceeding with the parametric studies. Results of the natural convection code validation and grid size studies demonstrated that a 13 x 13 nonuniform grid was adequate to define the natural convection flow and resulting temperatures on the heated vertical wall. Optimization studies for various grid sizes showed that results were relatively insensitive to grid size for meshes finer than 9 x 9. These results also illustrated that the 13 x 13 nonuniform grid represented a practical upper limit on the number of grid points, from a computing time viewpoint, that could be used to carry out the parametric studies.

The optimization problem number 2 approach of seeking the heat flux distribution that maximizes the total heating rate on the LHVW subject to constraints on the peak and average temperatures on the LHVW was shown to lead to the same optimal heat flux distribution as obtained in solving a corresponding optimization problem number 1 (fixed total heating rate) case. However, because of the nonlinear nature of the temperature constraints, considerably more computing time is required for solution of optimization problem number 2.

Results obtained using the coefficients of fourth order polynomial heat flux distributions as the independent variables to be manipulated in optimizing the heat flux profile were shown to reasonably well approximate the results obtained using the discrete heat flux at each grid point along the LHVW as the independent variables. However, despite the smaller number of independent variables (five instead of eleven) there was only a relatively minor savings in computing time for the less optimal, polynomial heat flux approach.

For the reasons given above, the parametric studies discussed in the

following section were performed using a 13 x 13 nonuniform grid with the heat flux at the grid points treated as the independent variables and the total heating rate along the heated vertical wall fixed (i.e., optimization problem number 1).

3.3 Results Of Parametric Studies

3.3.1 Computational Matrix. Studies were performed to evaluate the sensitivity of the optimal heat flux distribution to variations in each of the significant parameters for this problem. The values of parameters included in the computational matrix are listed in Table 3-5. As shown in this table, modified Rayleigh numbers from 10^3 to 10^6, Prandtl numbers from 0.1 to 100, and aspect ratios from 0.2 to 5 were considered. Optimal heat flux distributions were also examined for two alternate sets of thermal boundary conditions (see Figure 1-2) at modified Rayleigh numbers from 10^3 to 10^6.

As discussed above, the grid point heat flux optimization approach, as opposed to the polynomial heat flux distribution approach, was used for these parametric studies. The entire range of optimal temperatures for each parameter variation were examined by determining solutions to optimization problem number 1 for Case 1 (minimum θ_{ave}), Case 2 (minimum θ_{max}), and an intermediate Case 3 (minimum θ_{ave} with an upper limit on θ_{max}) type optimizations. The upper bound on the peak nondimensional temperature of the LHVW for Case 3 of optimization number 1 was selected to be the value of the peak temperature for an equivalent set of parameters with a uniform heat flux distribution along the LHVW.

3.3.2 Sensitivity To The Modified Rayleigh Number. Results from optimal heat flux distribution studies for modified Rayleigh numbers ranging from 10^3 to 10^6 are shown in Figures 3-24 and 3-25 and are summarized in Table 3-6.

Table 3-5. Computational matrix for parametric studies

BOUNDARY CONDITION TYPE	Ra^*	Pr	A
1	10^3	1.0	1.0
1	10^4	1.0	1.0
1	10^5	1.0	1.0
1	10^6	1.0	1.0
1	10^5	0.1	1.0
1	10^5	6.0	1.0
1	10^5	100.	1.0
1	10^5	1.0	0.2
1	10^5	1.0	0.5
1	10^5	1.0	2.0
1	10^5	1.0	5.0
2	10^3	1.0	1.0
2	10^4	1.0	1.0
2	10^5	1.0	1.0
2	10^6	1.0	1.0
3	10^3	1.0	1.0
3	10^4	1.0	1.0
3	10^5	1.0	1.0
3	10^6	1.0	1.0

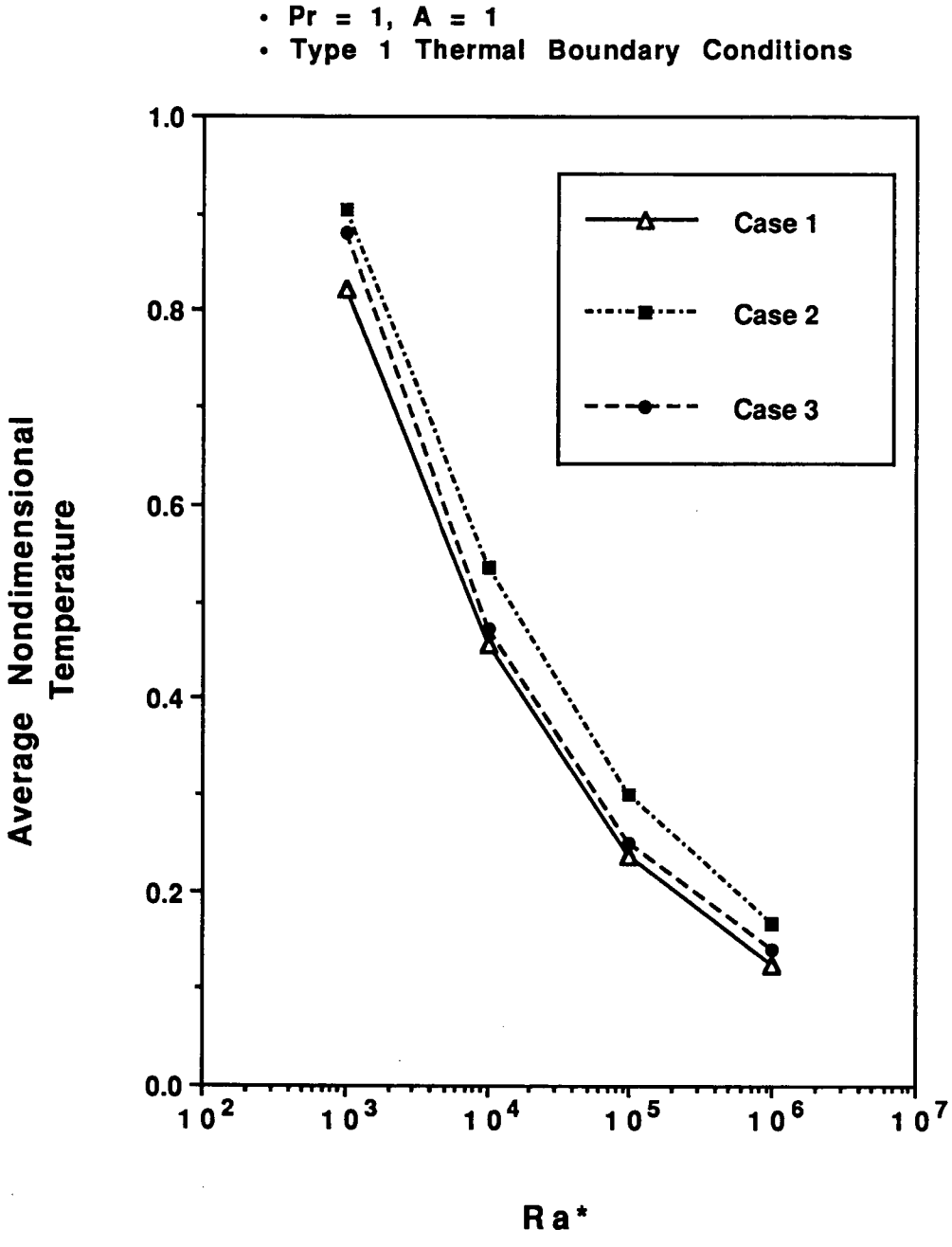


Figure 3-24. Sensitivity of the optimal average nondimensional temperatures on the LHVW to modified Rayleigh number

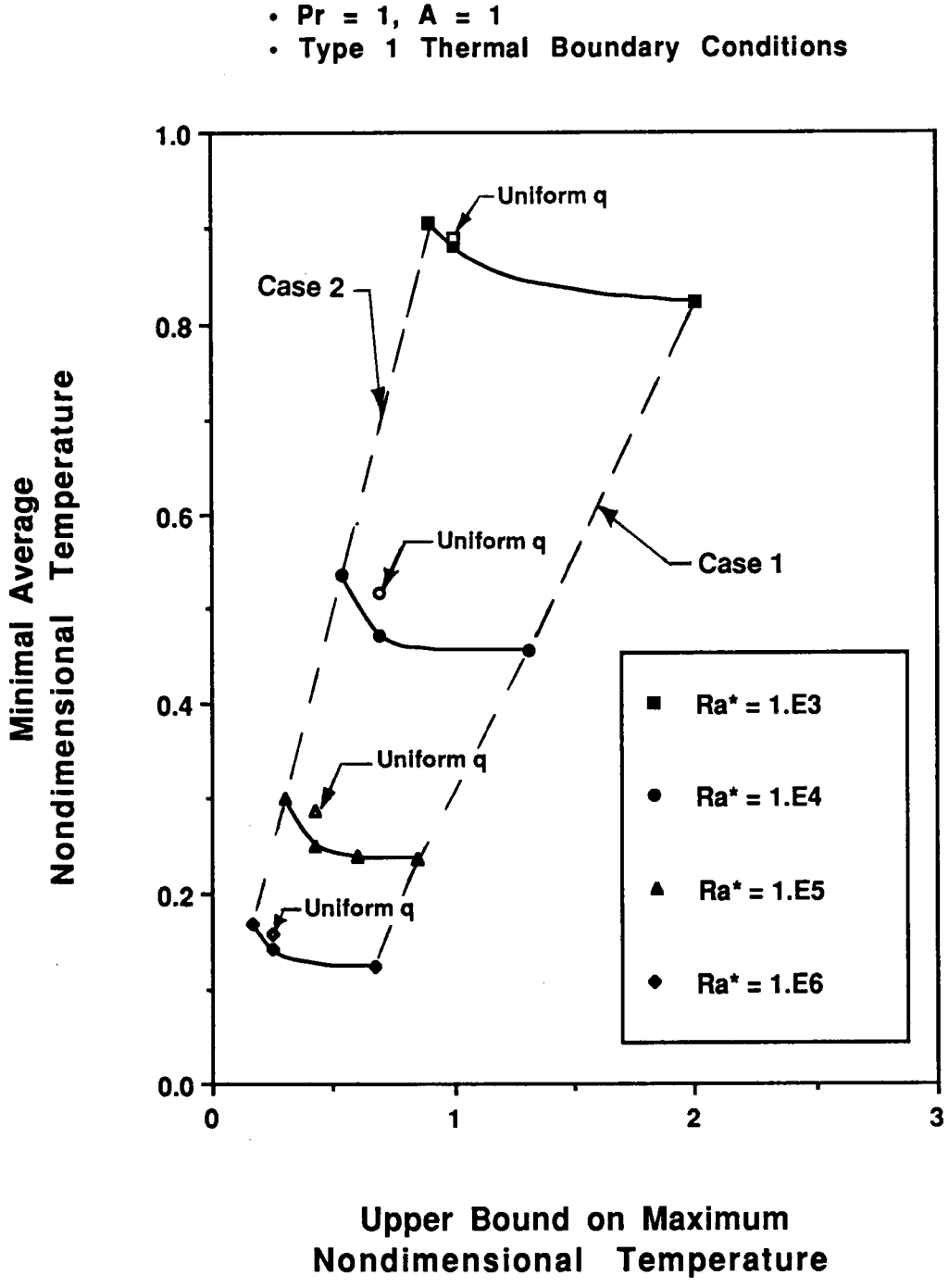


Figure 3-25. Optimal nondimensional temperatures on the LHVW for modified Rayleigh numbers from 10^3 to 10^6

Table 3-6. Summary of results for Rayleigh number sensitivity studies (Pr=1, A=1)

MODIFIED RAYLEIGH NUMBER	UNIFORM HEAT FLUX		CASE 1		CASE 2		CASE 3	
	AVE. NONDIM. TEMP	PEAK NONDIM. TEMP	MINIMAL AVE. NONDIM. TEMP	% REDUCTION AVE. NONDIM. TEMP	MINIMAL PEAK NONDIM. TEMP	% REDUCTION PEAK NONDIM. TEMP	MINIMAL AVE. NONDIM. TEMP	% REDUCTION AVE. NONDIM. TEMP
1.00E+03	0.888	1.004	0.823	7.3%	0.904	10.0%	0.864	2.7%
1.00E+04	0.517	0.688	0.455	12.0%	0.536	22.1%	0.471	8.8%
1.00E+05	0.287	0.426	0.237	17.4%	0.300	29.6%	0.249	13.3%
1.00E+06	0.158	0.249	0.123	22.2%	0.168	32.5%	0.133	15.7%

All other parameters were held at their nominal values, that is, Pr = 1, A = 1, and thermal boundary condition Type 1. These values of modified Rayleigh number span the range from the conduction dominated regime to the so-called laminar boundary layer regime.

The average nondimensional temperature of the LHVW is plotted in Figure 3-24 as a function of modified Rayleigh number for all three optimization cases. Based on its definition, the nondimensional temperature should approach a value of one (for A = 1) as the Rayleigh number approaches zero (conduction only). As shown in Figure 3-24, natural convection is relatively unimportant for $Ra^* = 10^3$. For this low value of modified Rayleigh number the average nondimensional temperatures range from about 0.82 to 0.90, depending on the constraint and objective functions (i.e., Cases 1, 2 or 3). At the highest modified Rayleigh numbers considered (10^6), natural convection dominates with average nondimensional temperatures ranging from about 0.12 to 0.17. It is interesting to note that the difference in average temperature between Cases 1 and 2 remains roughly the same for the entire range of modified Rayleigh numbers examined. However, since the values of the average temperature are much lower for high Ra^*, the relative difference between the average temperatures for Case 1 and Case 2 type optimizations is much greater for the highest values of Rayleigh number.

The curves defining the family of optimal solutions (Cases 1, 2, and 3) are shown in Figure 3-25 for the four values of modified Rayleigh number examined. This figure plots the average nondimensional temperature versus the peak nondimensional temperature obtained for the optimal solutions ranging from minimum average temperature (Case 1) to minimum peak temperature (Case 2). Results for a uniform heat flux distribution at each Rayleigh number are also shown in this figure for comparison. It is clear from this figure that relative to the results for a uniform heat flux distribution,

significant reduction in either peak or average temperatures are possible using either Case 2 or Case 1 type optimizations, respectively. Furthermore, if the peak temperature is considered to be excessive for the Case 1 optimization (minimum θ_{ave} with no upper limit on θ_{max}), then the Case 3 optimization with θ_{max} held at the same value as that for the uniform distribution can be used and significant reductions in the average temperature are still possible, especially at higher Rayleigh numbers. The reductions obtained for the optimal solutions compared with the uniform heat flux distribution are discussed quantitatively below. It is noteworthy that the Case 1 points and the Case 2 points shown in Figure 3-25 for the four values of modified Rayleigh number are nearly colinear. The nearly straight lines connecting these points form the boundary of possible optimal solutions for $10^3 < Ra^* < 10^6$.

As shown in Table 3-6, the reduction in objective function, either θ_{ave} or θ_{max}, relative to the results for the uniform heat flux distribution increases as the modified Rayleigh number is increased. The average temperature for the optimal distribution (Case 1) ranges from 7% to 22% less than that for the uniform distribution as the modified Rayleigh number is increased from 10^3 to 10^6. The relative reduction in the minimal peak temperature (Case 2) along the LHVW ranges from 10% to 33% over this same range of Rayleigh numbers. Constraining the peak temperature to remain below the value for the uniform heat flux distribution, significant reductions in the average temperature are still possible for the optimal distribution (Case 3). For this type of optimization, reductions in average temperature of more than 10% are possible for modified Rayleigh numbers greater than 10^5.

According to Berkovsky and Polevikov (1976), the average Nusselt number based on enclosure width, $\overline{Nu}_W$, for isothermal vertical walls (Case 2)

can be approximated by:

$$\overline{Nu_W} = 0.18 \; Ra_w^{0.29} \; [Pr / (Pr + 0.2)]^{0.29} \qquad (3\text{-}5)$$

$$1 < A < 2$$

$$Ra_w \; [Pr / (Pr+0.2)] > 10^3$$

$$10^{-3} < Pr < 10^5$$

where Ra_w is the Rayleigh number based on the temperature difference between the isothermal vertical walls and W, the width of the enclosure. The two Rayleigh numbers, Ra_w and Ra^*, are related by:

$$Ra^* = Ra_w \; \frac{q_{ave} \; H}{k \, (T_L - T_o)} \; A^{-3} \qquad (3\text{-}6)$$

where T_L is the temperature of the isothermal LHVW. In terms of the nondimensional variables, this relation is:

$$Ra^* = A^{-3} \; Ra_w / \theta_L \qquad (3\text{-}7)$$

Recalling equation 2-26, the Nusselt number based on enclosure width for this isothermal wall case is simply A/θ_L. Substituting this expression into equation 3-7 yields:

$$Ra^* = Ra_w \; \overline{Nu_W} \; A^{-4} \qquad (3\text{-}8)$$

By substituting this expression into equation 3-5, the following relationship between Ra^* and $\overline{Nu_W}$ is obtained:

$$\overline{Nu_W} = 0.265 \; A^{0.9} \; [Ra^* \; Pr / (Pr + 0.2)]^{0.225} \qquad (3\text{-}9)$$

Using this result, the average Nusselt number is plotted in Figure 3-26 for $10^3 < Ra^* < 10^6$ with Prandtl number and aspect ratio equal to unity. As shown in this figure, the numerical results for Case 2 of optimization problem number 1 (isothermal vertical walls) agree quite well with the values predicted using equation 3-9.

Streamline, heatline, and isothermal contour and heat flux distribution plots are presented in Appendix C for the four values of the modified Rayleigh

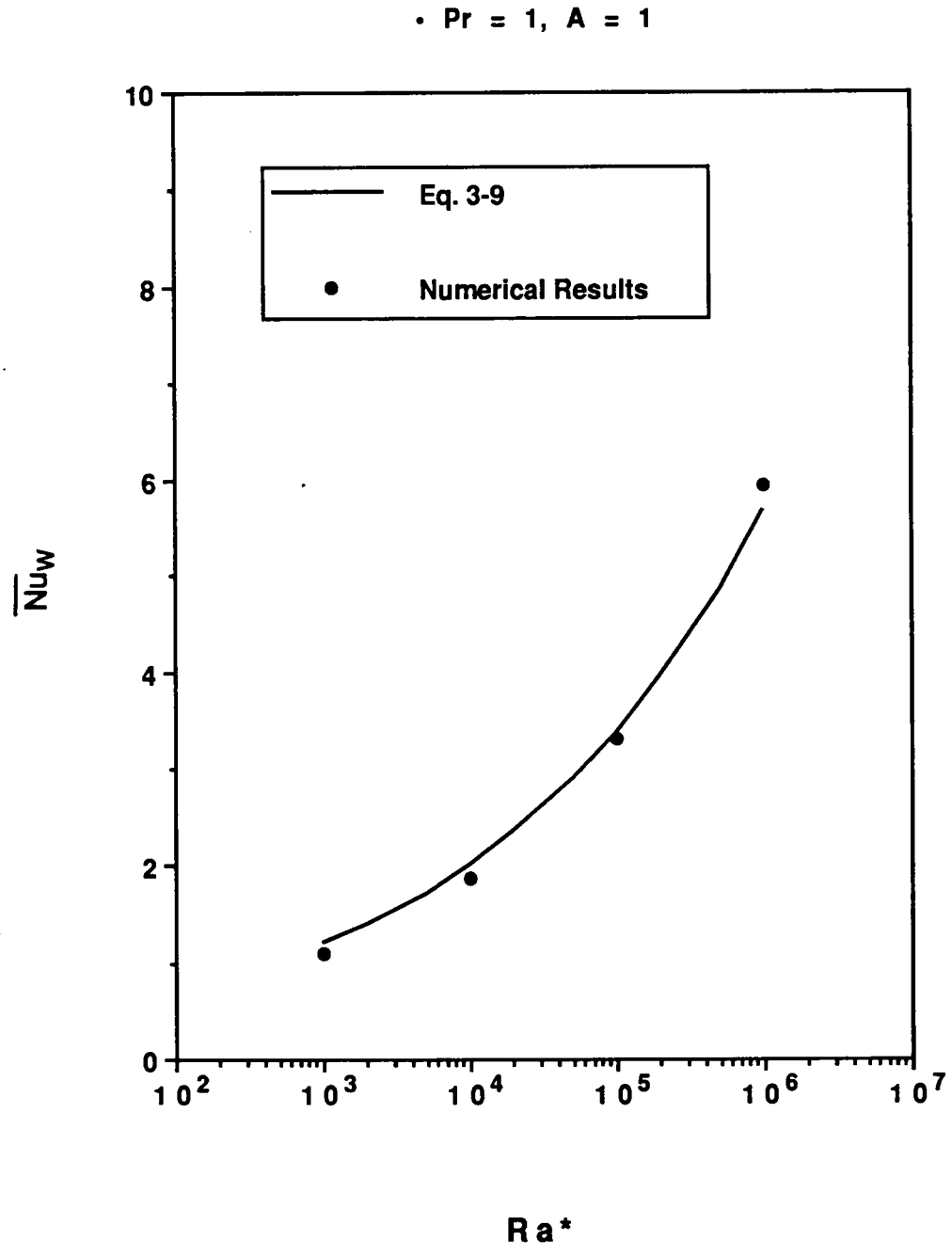


Figure 3-26. Comparison of numerically predicted values of Nusselt number with approximate relationship for isothermal vertical walls

number. The relatively low circulation rates, nearly horizontal heatline contours, and nearly vertical isothermal contours illustrate that conduction is the dominant mode of heat transfer for $Ra^* = 10^3$. The circulation rate for Case 2 (isothermal vertical walls) increases from $|\Psi|_{max}$=1.1 at $Ra^* = 10^3$ to 11.4 at $Ra^* = 10^6$. while the Nusselt number varies from 1.1 to 6.0 over this same range. The heatline and isothermal contours demonstrate that natural convection is the dominant heat transfer mechanism for the higher Rayleigh numbers.

The optimal heat flux distribution for Case1 (minimum θ_{ave}) varies only slightly over this range of modified Rayleigh numbers. For low modified Rayleigh numbers ($Ra^* = 10$ for example) the optimal Case 1 heat flux distribution was found to have all of the heat deposited on the node closest to the upper horizontal wall. Although the heat continues to be deposited at a single grid point in the upper region of the LHVW for higher Rayleigh numbers, the heated grid element shifts towards the midpoint of the LHVW. The grid point which is second from the top has the entire heat load for $Ra^* = 10^3$ and the grid point which is third from the top has the entire heating for $Ra^* = 10^4$ and 10^5. This is due to the increased importance of natural convection which at these intermediate values of Rayleigh numbers is an important heat transfer mechanism in the regions "far" from the horizontal walls. The optimal distribution shifts back toward the upper horizontal wall for $Ra^* = 10^6$, because the region with good convective flow is increased further up the the LHVW.

If conduction is the only heat transfer mechanism in the enclosure ($Ra^* \rightarrow 0$), the optimal Case 2 heat flux distribution is a uniform heat flux. The optimal Case 2 distribution is nearly uniform for $Ra^* = 10^3$, but more and more of the heat is deposited on the lower half of the wall as the Rayleigh number is increased.

It should be noted that difficulty in obtaining convergent solutions for $Ra^* > 10^6$ was encountered. Although it was possible to solve the natural convection problem for values somewhat greater than this with strong under relaxation, the number of iterations required to achieve a convergent solution was too large to perform optimization studies which typically required hundreds of solutions of the natural convection problem in order to determine the optimal heat flux distribution.

3.3.3 Sensitivity To The Prandtl Number. Results for Prandtl numbers ranging from 0.1 to 100 are plotted in Figures 3-27 and 3-28 and are summarized in Table 3-7. The results shown in Figure 3-27 indicate that the optimal value of the objective function (either θ_{ave} or θ_{max}) is insensitive to the value of the Prandtl number for $1 < Pr < 100$. For low Prandtl numbers, the objective function increases as the Prandtl number decreases. This result is consistent with the Nusselt number relationship presented by Berkovsky and Pelevikov (1976), which showed the dependence on Prandtl number indicated in equation 3-9. Although this expression was developed for the case of isothermal vertical walls, the sensitiviity with regard to Prandtl number is expected to remain the same for other nonuniformly heated vertical wall cases. From this relationship, it is clear that results for $Pr > 1$ should be insensitive to Pr number, whereas results for low Prandtl number should exhibit some slight dependence.

The average nondimensional temperature is plotted versus the peak nondimensional temperature in Figure 3-28 for the family of optimal solutions at all values of Prandtl number examined. As shown in Table 3-7, the reduction in average temperature for Case 1 type optimizations compared to the uniform heat flux distribution is roughly constant ranging from 15.7% for $Pr = 0.1$ to 17.8% for $Pr = 100$. With the upper limit on peak temperature set at the value obtained for the uniform heat flux distribution, reductions in average

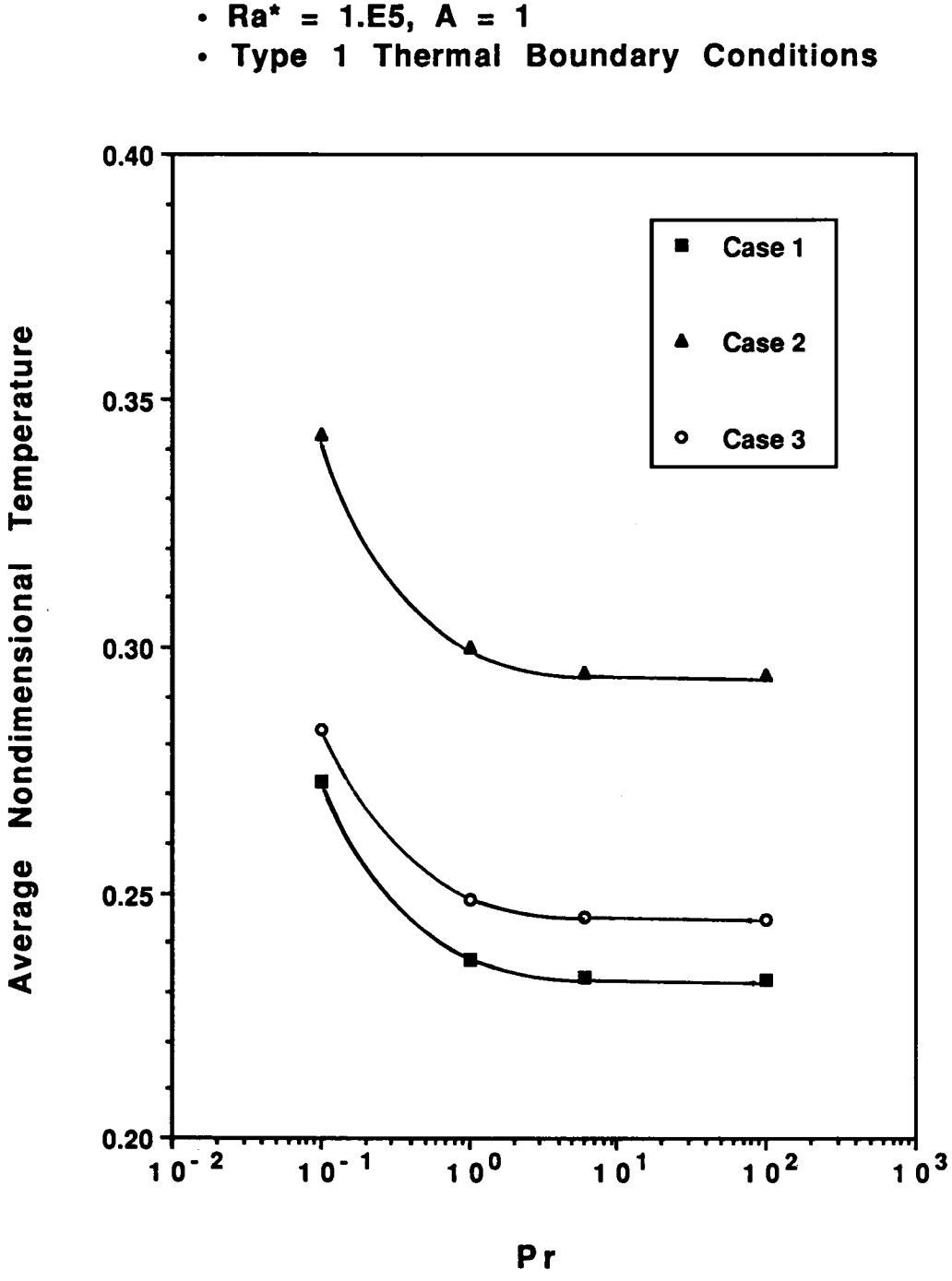


Figure 3-27. Sensitivity of the optimal average nondimensional temperatures on the LHVW to Prandtl number

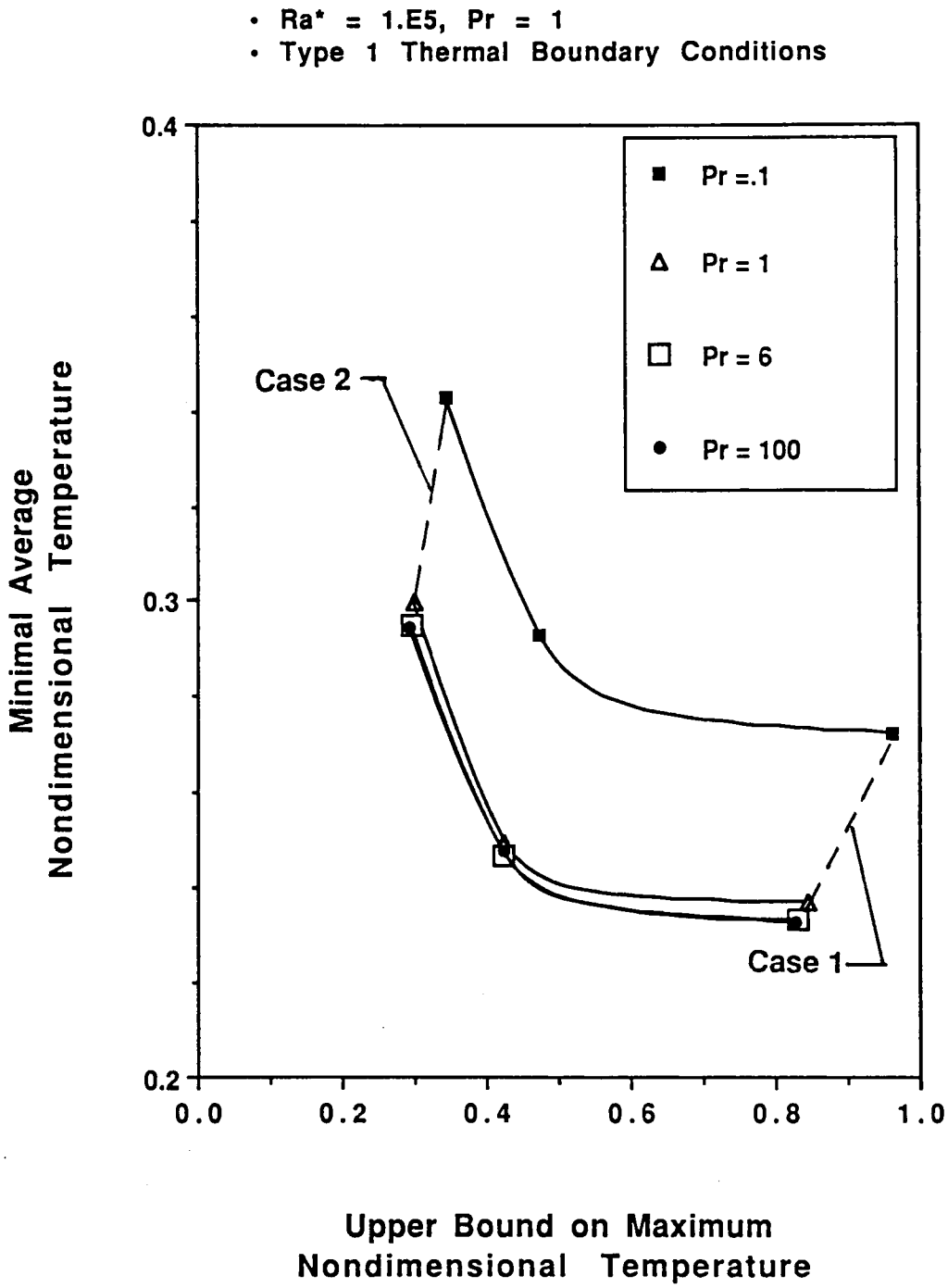


Figure 3-28. Optimal nondimensional temperatures on the LHVW for Prandtl numbers from .1 to 100

Table 3-7. Summary of results for Prandtl number sensitivity studies ($Ra^*=10^5$, A=1)

PRANDTL NUMBER	UNIFORM HEAT FLUX		CASE 1		CASE 2		CASE 3	
	AVE. NONDIM. TEMP	PEAK NONDIM. TEMP	MINIMAL AVE. NONDIM. TEMP	% REDUCTION AVE. NONDIM. TEMP	MINIMAL PEAK NONDIM. TEMP	% REDUCTION PEAK NONDIM. TEMP	MINIMAL AVE. NONDIM. TEMP	% REDUCTION AVE. NONDIM. TEMP
0.1	0.323	0.473	0.272	15.7%	0.343	27.5%	0.283	12.4%
1.0	0.287	0.426	0.237	17.4%	0.300	29.6%	0.249	13.2%
6.0	0.283	0.425	0.233	17.7%	0.295	30.6%	0.245	13.4%
100.0	0.283	0.425	0.233	17.8%	0.295	30.7%	0.245	13.5%

temperature of about 10% are possible. Reductions in peak temperature of about 30% are possible for the heat flux distibution which yields a minimum peak temperature (isothermal). As was the case for the modified Rayleigh number sensitivity, the boundary of possible temperatures for optimal solutions appears to be roughly a straight line.

Streamline, heatline and isothermal contours and heat flux distributions for all cases are presented in Appendix C. The streamline contour plots illustrate that the circulation rate is only weakly dependent on the Prandtl number, with circulation increasing slightly as the Prandtl number is increased. For isothermal vertical walls (Case 2) the value of $|\Psi|_{max}$ varies from 4.33 for Pr = 0.1 to 5.46 for Pr = 100.

The isothermal and heatline contours and optimal heat flux distributions are also relatively insensitive to the Prandtl number variation. This is consistent with equation 3-9, which showed that the Nusselt number (for isothermal vertical walls) has only a weak dependence on Prandtl number.

3.3.4 Sensitivity To The Enclosure Aspect Ratio. Sensitivity analysis results for aspect ratios from 0.2 to 5 are shown in Figures 3-29 and 3-30 and are summarized in Table 3-8. As shown in Figure 3-29 the average temperature for all optimization cases increases rapidly as the aspect ratio increases. However, the reason that the temperatures are much lower for low aspect ratios is not because of increased natural convection, but rather the decreased conduction path length from the heated LHVW to the cooled right-hand vertical wall. Examining the results for Case 2 (isothermal vertical walls) shown in Table 3-8, the nondimensional temperature difference between the two walls for A = 0.2 is seen to be 0.199 with $Ra^* = 10^5$, whereas, the temperature difference for the case of conduction only ($Ra^* = 0$) is 0.2. At the highest aspect ratio examined, A = 5, the nondimensional temperature difference between the isothermal verical walls is 0.481 with $Ra^* = 10^5$

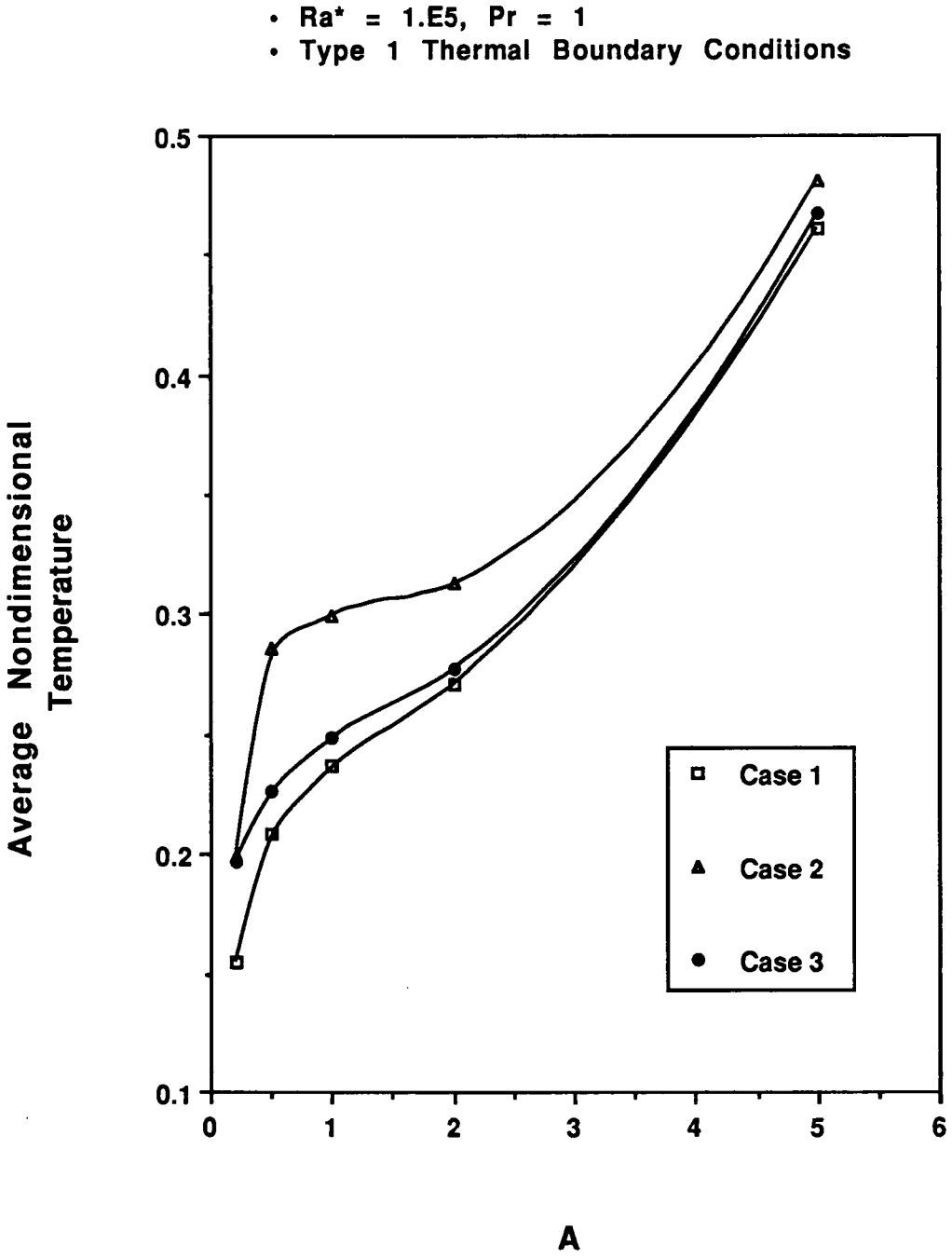


Figure 3-29. Sensitivity of the optimal average nondimensional temperatures on the LHVW to enclosure aspect ratio

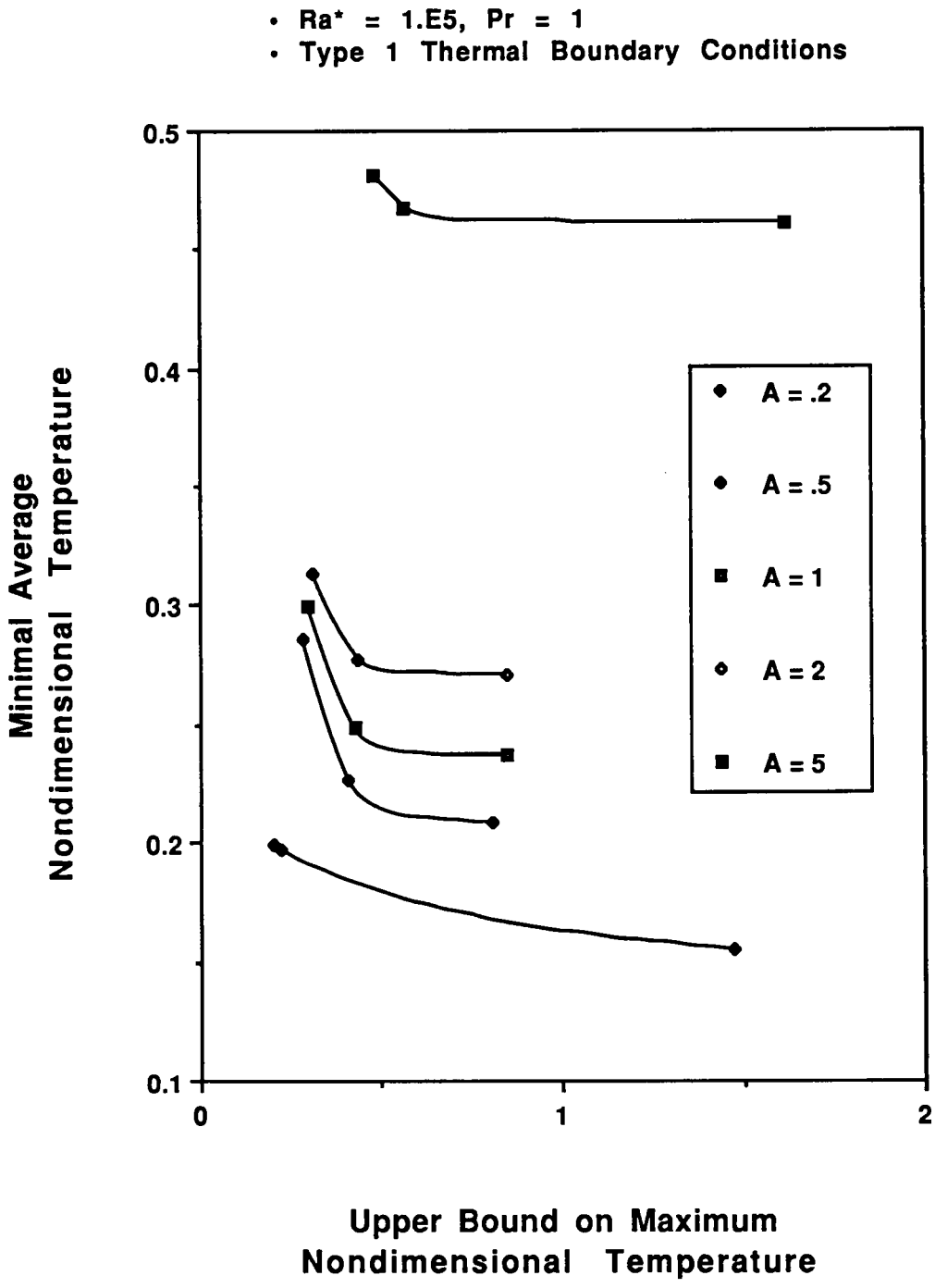


Figure 3-30. Optimal nondimensional temperatures on the LHVW for enclosure aspect ratios from .2 to 5

Table 3-8. Summary of results for enclosure aspect ratio sensitivity studies ($Ra^*=10^5$, Pr=1)

ASPECT RATIO	UNIFORM HEAT FLUX		CASE 1		CASE 2		CASE 3	
	AVE. NONDIM. TEMP	PEAK NONDIM. TEMP	MINIMAL AVE. NONDIM. TEMP	% REDUCTION AVE. NONDIM. TEMP	MINIMAL PEAK NONDIM. TEMP	% REDUCTION PEAK NONDIM. TEMP	MINIMAL AVE. NONDIM. TEMP	% REDUCTION AVE. NONDIM. TEMP
0.20	0.199	0.222	0.155	21.9%	0.199	10.3%	0.197	0.7%
0.50	0.268	0.410	0.209	22.0%	0.285	30.4%	0.226	15.5%
1.00	0.287	0.426	0.237	17.4%	0.300	29.6%	0.249	13.2%
2.00	0.305	0.434	0.271	11.1%	0.313	27.9%	0.277	9.1%
5.00	0.480	0.569	0.461	3.9%	0.481	15.4%	0.467	2.7%

compared to a nondimensional temperature of 5 for the case of conduction only. Further evidence of increased natural convection for large aspect ratios is shown in the streamline contour plots of Appendix C. The maximum absolute value of the streamfunction, $|\Psi|_{max}$, for the uniform heat flux case increases from 0.46 at A = 0.2 to 7.89 at A = 5. The values of the average Nusselt number based on enclosure width (ratio of natural convection heat transfer relative to the heat transfer if there were conduction only) calculated in this study for the case of isothermal verical walls (Case 2) are plotted in Figure 3-31 for aspect ratios from 0.2 to 5. Excellent agreement between these results and the numerically derived results of Berkovsky and Polovikov (1976) are shown in this figure.

The peak and average temperatures of the LHVW for the full range of optimal solutions are shown in Figure 3-30. Results summarized in Table 3-8 indicate that at the lower values of aspect ratio the reduction in average temperature for Case 1 type optimizations can be quite large compared to the values for a uniform heat flux distribution. For example, the reduction in average temperature for Case 1 type optimizations compared to the uniform heat flux case varies from 17.4% at A = 1 to 21.9% at A = 0.2. The reduction in peak temperature for Case 3 type optimizations are relatively close to those possible with the more extreme Case 1 type optimizations for all aspect ratios except the smallest (A = 0.2).

Streamline, heatline, and isothermal contour and heat flux distribution plots for all cases are provided in Appendix C. As mentioned above, the streamline contours shown in Appendix C demonstrate that the natural convection flow is more intense for large aspect ratios. Also, the heatline contours illustrate that a larger fraction of the total heat is transferred through the upper portions of the enclosure for large aspect ratios.

The optimal heat flux distributions shown in Appendix C for Case 1 type optimizations illustrate that the grid point which has the entire heat load is in

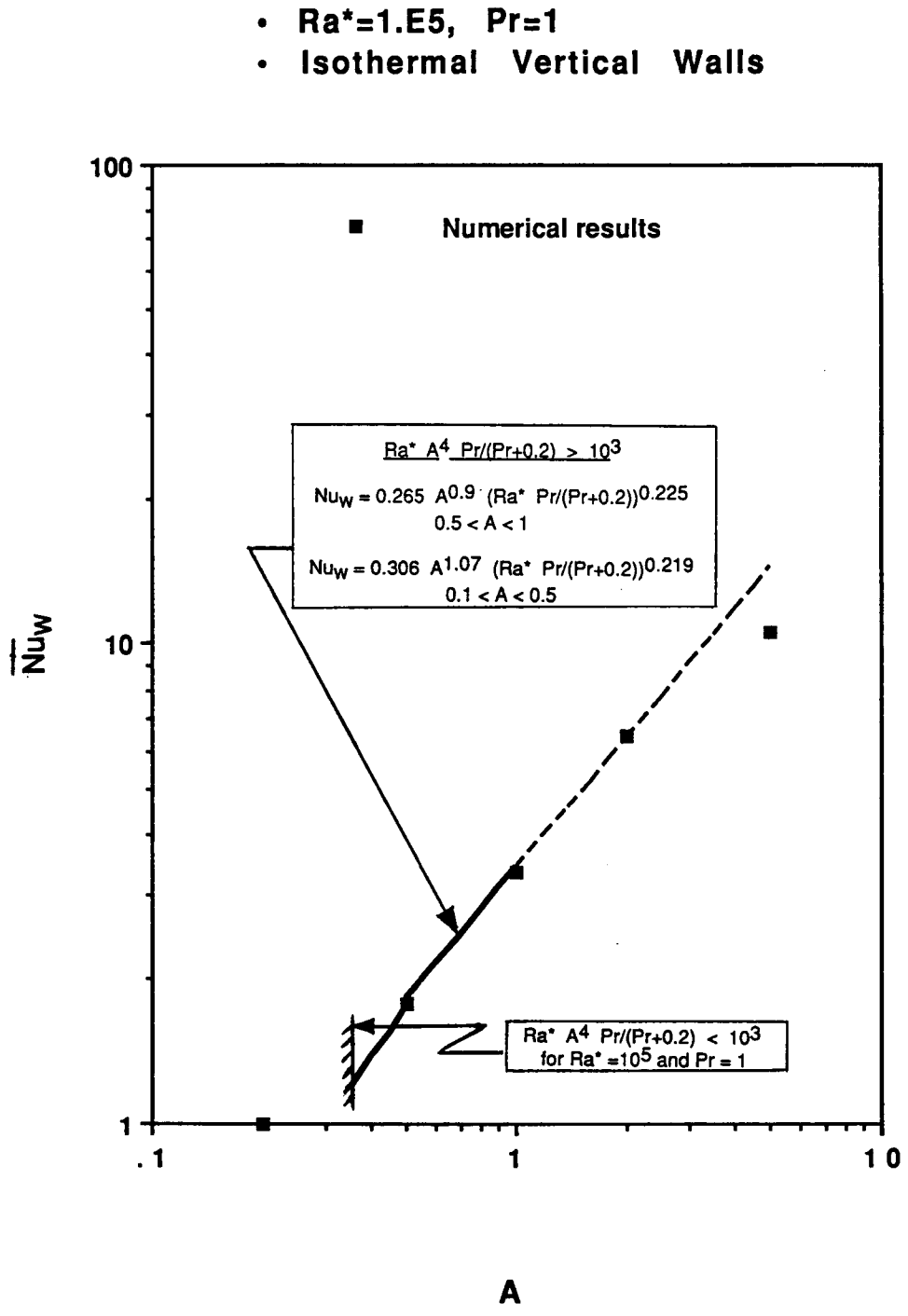


Figure 3-31. Comparison of numerically predicted Nusselt number dependence on enclosure aspect ratio with relationship derived by Berkovsky and Polevikov (1976)

the upper region of the LHVW for all aspect ratios examined, but is shifted towards the midpoint of the LHVW for larger aspect ratios. For Case 2, the heat flux distribution becomes less uniform with more of the heat deposited in the upper portions of the LHVW as the aspect ratio is increased. This is consistent with the suppression of natural convection at low aspect ratio. (Recall that the optimal Case 2 heat flux distribution for $Ra^* \rightarrow 0$ is a uniform heat flux).

3.3.5 Sensitivity To The Thermal Boundary Conditions. The two alternate boundary conditions, designated Type 2 and Type 3, are defined schematically in Figure 1-2. The reference Type 1 boundary conditions include adiabatic top and bottom horizontal walls and an isothermal right-hand vertical wall. Type 2 boundary conditions consist of an isothermal top horizontal wall and adiabatic right-hand vertical and bottom horizontal walls. The Type 3 boundary conditions include two isothermal and equal temperature surfaces at the top horizontal and right-hand vertical walls and an adiabatic bottom vertical wall. Results were computed for all three optimization cases for modified Rayleigh numbers ranging from 10^3 to 10^6.

Results for boundary conditions Type 2 and 3 are summarized in Figures 3-32 and 3-33. Results for Type 1 boundary conditions are shown in these figures for reference. Because of the closer proximity of the top horizontal wall to the heated LHVW, the temperatures for Type 2 boundary conditions are significantly lower than for the reference Type 1 thermal boundary conditions. The temperatures are slightly lower for Type 3 than Type 2 because of the additional isothermal wall.

For Case 1 type optimization, all of the heat is deposited on the uppermost grid point of the LHVW. This result is independent of the Rayleigh number. The results for Case 3 show that the minimum average temperature for the intermediate values of modified Rayleigh number ($Ra^* = 10^4$ and 10^5)

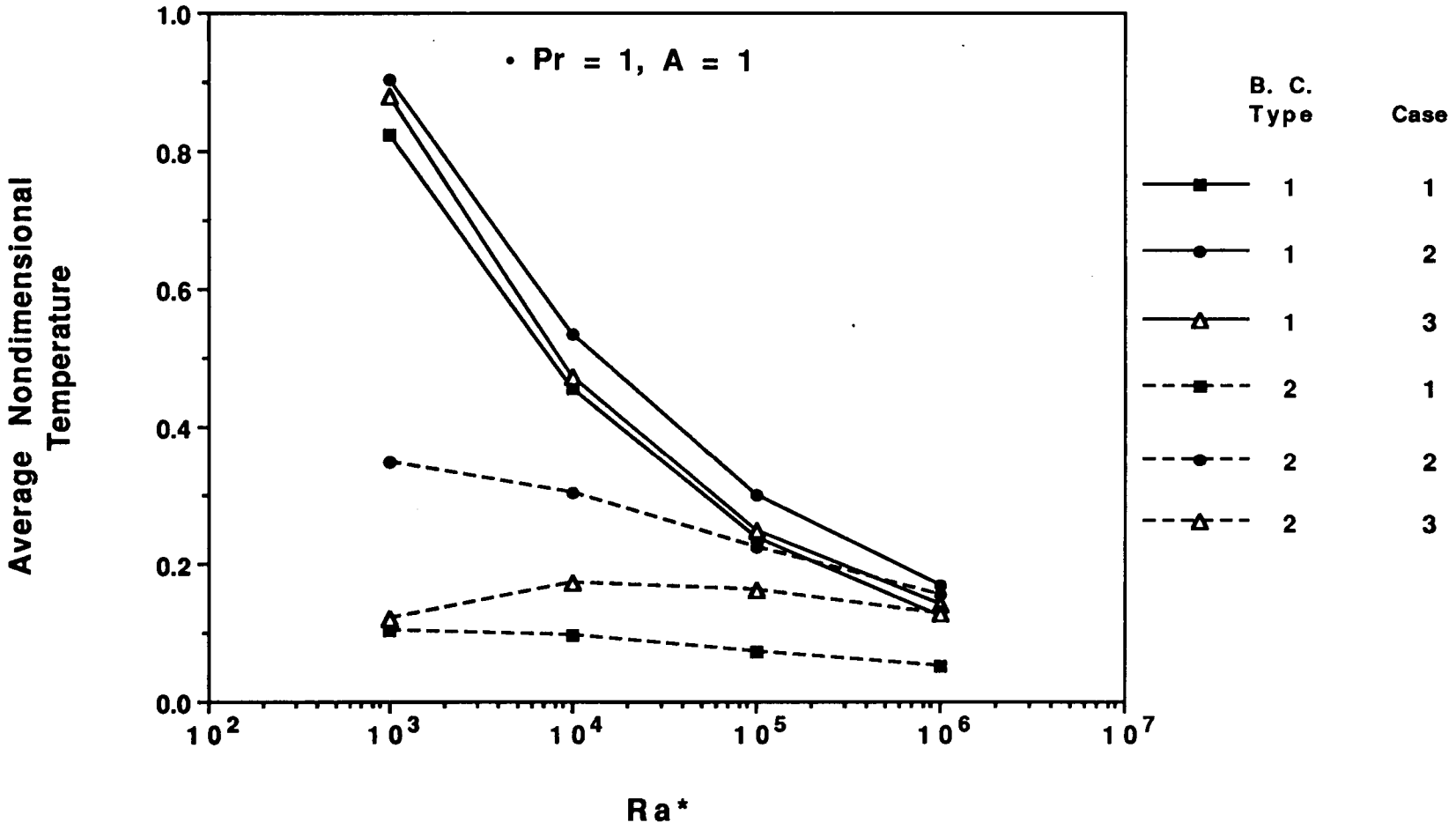


Figure 3-32. Sensitivity of the optimal temperatures on the LHVW to Rayleigh number for thermal boundary condition Type 2

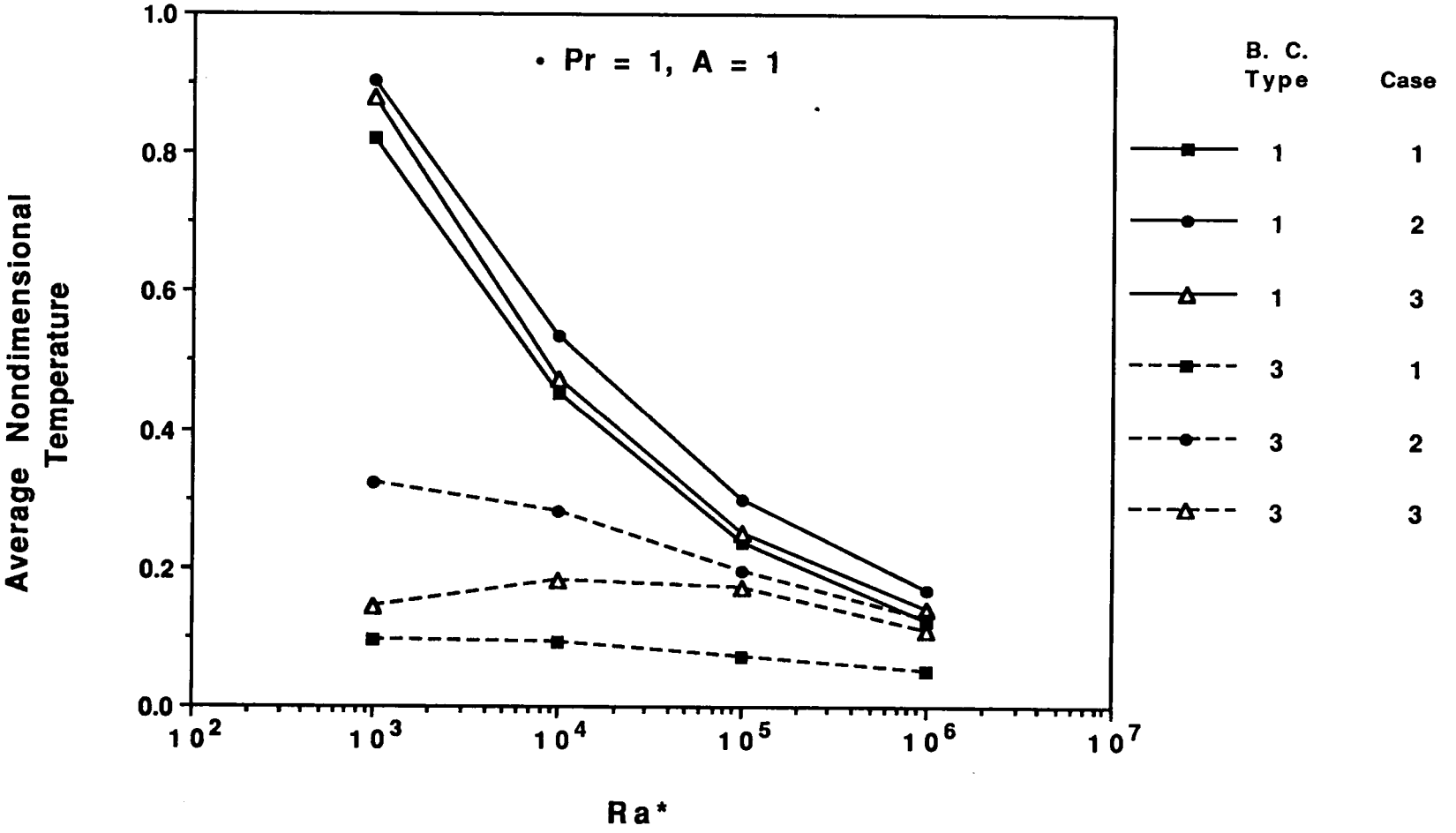


Figure 3-33. Sensitivity of the optimal temperatures on the LHVW to Rayleigh number for thermal boundary condition Type 3

is higher than that for the lowest modified Rayleigh number ($Ra^* = 10^3$). This is caused by the fact that the value of the upper limit on peak temperature ofthe LHVW is much higher for the $Ra^* = 10^3$ case (recall that the upper limit is set based on the calculated peak temperature for a uniform heat flux distribution), thus allowing more of the heating to be located close to the top isothermal wall.

Streamline, heatline, and isothermal contour and heat flux distribution plots are provided in Appendix C for all three types of boundary conditions. The heatline and isothermal contours are extremely closely spaced in the upper lefthand corner of the enclosure for Case 1 type optimizations with either boundary condition Type 2 or 3. This is due to the fact that the heat is deposited at the upper most grid point along the LHVW and is transferred essentially entirely by conduction to the upper isothermal (cooled) wall. The dominance of conduction for Case 1 with boundary conditions Type 2 or 3 is supported by the fact that circulation rates are very low, even at $Ra^* = 10^6$.

The circulation rates for boundary condition Type 2 are slightly higher than for Type 3 for all cases. By comparing the isothermal and heatline contours for boundary conditions Type 2 and 3, it can be concluded that the additional vertical isothermal (cooled) wall for Type 3 is relatively unimportant. Most of the heat transfer takes place between the LHVW and the upper isothermal wall.

CHAPTER 4

SUMMARY AND CONCLUSIONS

4.1 Numerical Model Validation And Grid Size Selection

A numerical natural convection model using the SIMPLER algorithm was constructed and successfully coupled with an existing numerical optimization code, called GRG2, to determine optimal heat flux distributions along a vertical wall of a rectangular enclosure. Optimal heat flux distributions were obtained for various constraint conditions, modified Rayleigh numbers (Ra*), Prandtl numbers (Pr), enclosure aspect ratios (A), and thermal boundary conditions. The conclusions drawn from the results of these studies are discussed below.

The natural convection model constructed for these studies was validated by comparing results with those obtained by: (1) de Vahl Davis (1983) for his "benchmark solution" of natural convection in a square enclosure with isothermal vertical walls; and (2) Kimura and Bejan (1984) for natural convection in a rectangular enclosure with uniform heating along both vertical walls.

A 13 x 13 nonuniformly spaced mesh was shown to be adequate for modeling the natural convection process for Newtonian fluids in the laminar flow regime. The peak and average nondimensional temperatures were within approximately 4% of the results obtained for a 31 x 31 grid. This same grid was shown to be of practical size for performing the optimization studies. The optimization results were shown to be relatively insensitive to grid size for meshes finer than 9 x 9.

Grids with significantly more than 13 x 13 grid points were shown to be impractical for optimization studies because of computer run time requirements. Using a CRAY-2 supercomputer, approximately one hour of CPU time is required to perform the simplest type of optimization with a 13 x

13 grid. The CPU time was shown to scale as $N^{2.86}$, where N is the number of grid points. Therefore, using only a marginally finer mesh of 15 x 15 grid points more than doubles the CPU time.

4.2 Optimal Heat Flux Distribution Studies For Various Approaches And Constraints

Using the heat flux at the grid points along the LHVW as the independent variables, results for three cases of optimization problem number 1, as well as for optimization problem number 2, were obtained for the reference set of parameters ($Ra^* = 10^5$, Pr = 1, A = 1) and thermal boundary conditions (Type 1 from Figure 1-2). Results for Case 1 of optimization problem number 1 demonstrate that the minimum average temperature of the LHVW, subject to a fixed total heating rate along the LHVW, is achieved for a heat flux distribution that has all of the heat deposited on a single boundary control volume located roughly 70% of the way up the LHVW. The average nondimensional temperature for Case 1 is about 17% lower than that obtained for a uniform heat flux distribution with the same total heating rate. The unconstrained peak temperature for this highly peaked heat flux distribution exceeds the uniform heat flux distribution case by about a factor of two for the 13 x 13 grid used in these studies.

Minimizing the peak temperature along the LHVW subject to a fixed total heating rate (optimization problem number 1, Case 2) was shown to result in an isothermal LHVW. The optimal heat flux dristribution is therefore the same as the heat flux distribution that yields an isothermal surface. The peak nondimensional temperature of the LHVW for Case 2 was determined to be 30% less than that for the corresponding uniform heat flux distribution case.

The results for Cases 1 and 2 of optimization problem number 1 were shown to be special cases of the more general (optimization problem number 1, Case 3) problem of determining the optimal heat flux distribution that

minimizes the average temperature of the LHVW subject to a fixed total heating rate and an upper limit on peak temperature. If the upper limit on peak temperature is greater than or equal to the peak temperature obtained for Case 1, then the Case 3 results are identical to the Case 1 results. If the upper limit on peak temperature is set at the value of the isothermal wall temperature obtained in Case 2, then the Case 3 results are identical to the Case 2 results. There is no solution for upper limits on peak temperature that are less than the isothermal wall temperature. The entire family of optimal solutions can be generated by setting the upper limit on peak temperature at values between the results obtained for Cases 1 and 2.

Setting the upper limit on peak temperature equal to the value obtained for a uniform heat flux distribution, the average nondimensional temperature for Case 3 is 13% lower than the average value for the corresponding uniform heat flux case. The magnitude of this reduction is only slightly less than the 17% reduction obtained for Case 1 (unconstrained peak temperature), and in contrast to the "singularity-like" heat flux distribution for Case 1, the heat flux distribution for the Case 3 type of optimization is a profile that should be reasonably simple to approximate in a real application.

Results for optimization problem number 2 demonstrated that using the total heating rate as the objective function to be maximized with constraints on average and/or peak temperatures of the LHVW is an equally valid approach for determining the optimal heat flux distribution. However, since this approach roughly doubles the required computing time, it is not recommended.

Results were obtained for Cases 1, 2, and 3 of optimization problem number 1 with the coefficients of polynomial heat flux distributions used as the independent variables for optimization. Optimal heat flux distributions were reasonably well approximated for Cases 2 and 3. The "singularity type" heat flux obtained for Case 1 is not well approximated by the polynomial

distributions. However, even for Case 1, the optimal LHVW temperatures obtained using the polynomial heat flux distributions approached those achieved with the grid point heat flux approach discussed above with polynomials of only third or fourth order. Computing times were roughly the same despite the fact that the number of independent variables was greatly reduced. This is due to the difficulty in satisfying the constraint that the heat flux along the LHVW must be greater than or equal to zero (i.e. no heat removal by the LHVW) for the polynomial heat flux approach.

4.3 Parametric Studies

Parametric studies were performed to determine the sensitivity of the optimal solutions to modified Rayleigh number, Prandtl number, enclosure aspect ratio, and thermal boundary conditions. Results for modified Rayleigh numbers ranging from 10^3 to 10^6 with Pr = 1, A = 1, and the reference set of thermal boundary conditions (Type 1) showed that reductions in average nondimensional LHVW temperatures of 7% to 22% compared to the corresponding uniform heat flux distribution solution are possible for optimization problem number 1 with the average nondimensional temperature of the LHVW set as the objective function to be minimized (Case 1). The optimal heat flux distribution for Case 1 varies only slightly over this range of Rayleigh numbers, with all of the heat deposited on a single grid element located in the upper portion of the LHVW.

The maximum nondimensional temperature of the LHVW is reduced by 10% to 33% compared to the values for a uniform heat flux distribution for optimization problem number 1 with the maximum nondimensional temperature of the LHVW set as the objective function (Case 2) to be minimized over this same range of Rayleigh numbers. At the lowest values of the modified Rayleigh number examined ($Ra^* = 10^3$), the heat flux distribution for Case 2 is nearly uniform. As the modified Rayleigh number is increased,

the optimal distribution has more and more of the heat deposited on the lower half of the LHVW.

For optimization problem number 1 with the maximum nondimensional temperature on the LHVW set as the objective function to be minimized subject to the constraint that the peak nondimensional temperature of the LHVW remain below the value obtained for the uniform heat flux distribution (Case 3), the reduction in average temperature of the LHVW was found to be only about 3% for $Ra^*=10^3$ but increased to roughly 16% for $Ra^*=10^6$.

Prandtl numbers ranging from 0.1 to 100 were examined. Results showed that the optimal heat flux and resulting temperature distributions were insensitive to Prandtl number for $1<Pr<100$. For low Prandtl numbers ($Pr<1$) the objective function, either peak or average temperature of the LHVW, increases as the Prandtl number is decreased. This is consistent with existing expressions for the Nusselt number which show negligible dependence on Prandtl number for $Pr>1$, but a relatively weak dependence for $Pr<1$.

The sensitivity of the optimal solutions to aspect ratio of the rectangular enclosure was examined for values ranging from 0.2 to 5.0. The average temperature of the LHVW increases rapidly as the aspect ratio increases. However, this is not due to increased natural convection, but rather the decreased conduction path length for small aspect ratios. In fact, the average Nusselt number based on enclosure width (Nu_W), i.e. ratio of natural convection heat transfer relative to conduction heat transfer, varies from near 1 at an aspect ratio of 0.2 to more than 10 at an aspect ratio of 5. The calculated Nusselt numbers were shown to be consistent with existing correlations. The shape of the optimal heat flux distribution was shown to vary significantly over this range of aspect ratios. For Case 1 of optimization problem number 1, the position where the highly peaked heat flux occurs is shifted towards the center of the LHVW for the larger aspect ratios. For Case 2 of optimization problem number 2 (leads to an isothermal LHVW), the heat flux

distribution becomes less uniform with more of the heat deposited in the upper portions of LHVW as the aspect ratio is increased. Since the optimal Case 2 distribution for conduction only is a uniform distribution, this is consistent with the lack of natural convection at low aspect ratios.

Alternate thermal boundary conditions were also examined. For these alternate thermal boundary conditions, the top horizontal wall was changed from adiabatic (Type 1) to isothermal and the right-hand vertical wall was either adiabatic (Type 2) or isothermal (Type 3). The shorter distance (essentially zero distance in the upper left-hand corner of the enclosure) from the heated LHVW to the top isothermal wall resulted in significantly lower temperatures for the Type 2 and 3 boundary condition cases compared to the corresponding Type 1 results. Since the top, cooled wall meets the left-hand, heated wall, all of the heat is deposited on the upper most grid point along the LHVW for the optimization that seeks a heat flux distribution that minimizes the average nondimensional temperature of the LHVW (Case 1 of optimization problem number 1). The heat transfer was dominated by conduction over a very small conduction path length.

4.4 Design Guidance For Optimum Placement Of Electronic Components On Circuit Boards Cooled By Natural Convection

In view of the results obtained in this study, some general guidelines can be formulated. This guidance should aid in the initial stages of the design process for arranging electronic components along a vertically oriented component board which forms one wall of a rectangular enclosure cooled by natural convection. It must be understood that these guidelines are valid only within the limitations expressed in Section 1.4. That is, it is assumed that the flow is steady state and laminar and the rectangular enclosure is completely filled with a Newtonian fluid. The design guidelines are listed below.

(1) If all components have the same sensitivity to operation at elevated temperature, heat sources should be arranged in a fashion which minimizes the peak temperature of the vertical surface that holds the components in place. Results have shown that this optimal heat source distribution is simply the distribution resulting in an isothermal wall.

(2) Achieving a minimal average temperature of the mounting surface could be of primary importance in some situations. For example, this could be the case if some highly temperature sensitive, non- or low-heat producing components are located on the same component board with components that are less sensitive to exposure to elevated temperatures but produce significant heating. For this case, a distribution which places the discrete heat sources in as concentrated a fashion as possible was found to be optimal. The optimal location for this concentrated heating is roughly 70% of the way up the heated vertical wall for all cases examined in this study.

(3) The most general application of this procedure is to arrange the heat sources in a fashion such that the average temperature of the heated vertical wall is minimized while ensuring that the peak temperature of the heated wall does not exceed a specified critical temperature (optimization problem number 1, Case 3). Results for this optimization process have shown that the optimal heat flux distribution varies between the range of distributions for the two cases discussed above.

(4) The relative benefit obtained by optimizing the heat flux distribution was shown to be larger for higher Rayleigh numbers with the

reference thermal boundary conditions (cool isothermal vertical wall opposite the heated vertical wall and adiabatic horizontal walls). Thus, in addition to the obvious benefit of inreasing the Rayleigh number on the cooling of the components, the higher Rayleigh number opens up the possibilities of further significant reductions in temperatures by the use of improved, i.e. optimal, heat flux distributions.

(5) The optimal heat flux distributions and their resulting temperatures were shown to be relatively insensitive to changes in the Prandtl number of the fluid that fills the enclosure Although there is a significant benefit to be gained by optimizing the heat source distribution for all values of the Prandtl number examined ($0.1 < Pr < 100$), the potential benefit is slightly larger at higher Prandtl numbers.

(6) The largest benefit for optimizing the heat source distribution occurs for intermediate values of the aspect ratio, that is, $0.5 < A < 2$. Because conduction is the dominant heat transfer mechanism at low values of the enclosure aspect ratio, there is less benefit to optimizing the heat flux distribution for $A < 0.2$. The natural convection heat transfer was found to be most intense at the highest values of aspect ratio examined ($A = 5$), however, there is less benefit to be gained in optimizing the heat source distribution at this high value of the aspect ratio compared to the intermediate values.

(7) If the top horizontal wall is maintained as a cool isothermal surface (Type 2 or 3 thermal boundary conditions), the conduction heat transfer dominates the natural convection heat transfer, even for the highest Rayleigh numbers examined. The importance of optimizing

the heat flux distribution is most significant for low Rayleigh numbers, where by placing the heat close to the upper cooled surface the heat is transferred by conduction through a very short path length. Therefore, although there is an obvious benefit to raising the Rayleigh number for these alternate thermal boundary conditions, optimizing the heat flux distribution becomes less important at higher Rayleigh numbers.

(8) In addition to the general guidance given above, the technique developed for this study could prove to be a useful tool for performing optimization studies as part of the initial design process. Alternate boundary conditions, enclosure shapes, and parameters (Rayleigh numbers, Prandtl numbers, and aspect ratios), or constraints could be analyzed. However, due to the computer resource intensive optimization process, applying this technique to study three-dimensional enclosures with complex shapes is likely to be, at best, limited to a few run cases, i.e. parametric studies of the type performed in this study would be impractical for such complex geometries given existing computing technologies.

LIST OF REFERENCES

Anderson, D. A., Tannehill, J. C., and Pletcher, R. H. (1984), Computational Fluid Mechanics and Heat Transfer, McGraw-Hill, New York.

Baker, A. J. (1983), Finite Element Computational Fluid Mechanics, McGraw-Hill, New York.

Berkovsky, B. M., Fertman, V. E., Nogotov, E. F., Lipkina, E. A., and Bashtovoi, V. G. (1971), "Free Convection," pp. 191-233 in Prog. In Heat and Mass Transfer, Vol. 4.

Berkovsky, B. M., and Polevikov, V. K. (1976), "Numerical Study of Problems on High-Intensive Free Convection," pp. 443-455 in Heat Transfer and Turbulent Buoyant Convection, edited by Spalding, D. B., and Afgan, H., Hemisphere, Washington, D.C.

Catton, I. (1978), "Natural Convection in Enclosures," Proc. 6th Int. Heat Transfer Conf., Vol. 6, pp. 13-31, Toronto.

Chao, P., Ozoe, H., and Churchill, S. W. (1981), "The Effect of Non-Uniform Surface Temperature on Laminar Natural Convection in a Rectangular Enclosure," Chem. Eng. Comm., Vol. 9, pp. 245-254.

Chu, H. H. S., Churchill, S. W., and Patterson, C. V. S. (1976), "The Effect of Heater Size, Aspect Ratio, and Boundary Conditions on Two-Dimensional, Laminar, Natural Convection in Rectangular Enclosures," ASME J. Heat Trans., Vol. 98, Series C, No. 2, pp. 194-201.

Churchill, S. W. (1983), "Free Convection in Layers and Enclosures," Section 2.5.8, Vol. 2, Heat Exchanger Design Handbook, Hemisphere, Washington, D.C.

Courant, R., Isaacson, E., and Rees, M. (1952), "On the Solution of Non-Linear Hyperbolic Differential Equations by Finite Differences, Comm. Pure Appl. Math., Vol. 5, pp. 243-252.

de Vahl Davis, G., and Jones, I. P. (1983), "Natural Convection in a Square Cavity: A Comparison Exercise," Int. J. for Numerical Methods in Fluids, Vol. 3, pp. 227-248.

de Vahl Davis, G. (1983), "Natural Convection of Air in a Square Cavity: A Bench Mark Numerical Solution," Int. J. for Numerical Methods in Fluids, Vol. 3, pp. 249-264.

Gebhart, B., Jaluria, Y., Mahajan, R. L., and Sammakia, B. (1988), Buoyancy-Induced Flows and Transport, Hemisphere, Washington, D.C.

Hoogendorn, C. J. (1986), "Natural Convection in Enclosures," Proc. 8th Int. Heat Transfer Conf., Vol. 1, pp. 111-120, San Francisco.

Jaluria, Y. (1980), Natural Convection Heat and Mass Transfer, Pergamon, Oxford.

Jaluria Y., and Torrance K. E. (1986), Computational Heat Transfer, Hemisphere, Washington, D.C.

Kelleher, M. D., Knock, R. H., and Yang, K. T. (1987), "Laminar Natural Convection in a Rectangular Enclosure Due to a Heated Protrusion on One Vertical Wall - Part 1: Experimental Investigation," Proc. of the 2nd ASME/JSME Thermal Engineering Conference, Vol. II, pp. 169-178, Honolulu.

Kimura, S., and Bejan, A. (1983), "The "Heatline" Visualization of Convective Heat Transfer," ASME J. of Heat Transfer, Vol.105, pp. 916-919.

Kimura, S., and Bejan, A. (1984), "The Boundary Layer Natural Convection Regime in a Rectangular Cavity with Uniform Heat Flux from the Side," ASME J. of Heat Transfer, Vol. 106, pp. 98-103.

Lasdon, L. S., Waren, A. D., Jain, A., and Ratner, M. (1978), "Design of a Generalized Reduced Gradient Code for Nonlinear Programming," ACM Trans. on Mathematical Software, Vol. 4, No. 1, pp.34-50.

Lasdon, L. S., and Waren A. D. (1986), "GRG2 Users Guide."

Lee, J. J., Liu, K. V., Yang, K. T., and Kelleher, M. D. (1987), "Laminar Natural Convection in a Rectangular Enclosure Due to a Heated Protrusion on One Vertical Wall - Part II: Numerical Simulations," Proc. of the 2nd ASME/JSME Thermal Engineering Conference, Vol. II, pp. 179-185, Honolulu.

Liu, K. V., Yang, K. T., and Kelleher, M. D. (1987), "Three Dimensional Natural Convection Cooling of an Array of Heated Protrusions in an Enclosure Filled with a Dielectric Fluid," Proc. of the Int. Electronics Cooling Symposium, pp. 486-497, Honolulu.

Oktay, S., Hannemann, R., Bar-Cohen, A. (1986), "High Heat from a Small Package," Mechanical Engineering, March, pp. 36-42.

Ostrach, S. (1972), "Natural Convection in Enclosures," pp. 161-227 in Advances in Heat Transfer, Vol. 8, Academic, New York.

Ostrach, S. (1982), "Natural Convection Heat Transfer in Cavities and Cells," Proc. 7th Int. Heat Transfer Conf., Vol. 1, pp. 365-379, Munich.

Ozoe, H., Miyachi, H., and Imai, K. (1987), "The Development of a Computational Scheme for Natural Convection in an Enclosure with Multiple Isolated Heat Sources," Proc. of the Int. Electronics Cooling Symposium, pp. 522-534, Honolulu.

Patankar, S. V. (1978), "A Numerical Method for Conduction in Composite Materials, Flow in Irregular Geometries, and Conjugate Heat Transfer," Proc. 6th Int. Heat Transfer Conf., Vol. 3, pp. 297-302, Toronto.

Patankar S. V. (1980), Numerical Heat Transfer and Fluid Flow, McGraw-Hill, New York.

Patankar, S. V. (1981), "A Calculation Procedure for Two-Dimensional Elliptic Situations," Numerical Heat Transfer, Vol. 4, pp. 409-425.

Reklaitis G. V., Ravindran A., and Ragsdell K. M. (1983), Engineering Optimization Methods and Applications, Wiley, New York.

Siddall J. N. (1982), Optimal Engineering Design, Marcel Dekker, New York.

Spalding, D. B. (1972), "A Novel Finite-Difference Formulation for Differential Expressions Involving Both First and Second Derivatives," Int. J. Num. Methods Eng., Vol. 4, pp. 551-562.

Torrance, K. E., Orloff, L., and Rockett, J. A. (1969), "Experiments on Natural Convection in Enclosures with Localized Heating from Below," J. Fluid Mech., Vol. 36, pp. 21-31.

Torrance, K. E., and Rockett, J. A. (1969), "Numerical Study of Natural Convection in an Enclosure with Localized Heating from Below - Creeping Flow to the Onset of Laminar Instability," J. Fluid Mech., Vol. 36, pp. 33-54.

Turner, B. L., and Flack, R. D. (1980), "The Experimental Measurement of Natural Convective Heat Transfer in Rectangular Enclosures with Concentrated Energy Sources," ASME J. Heat Transfer, Vol. 102, pp. 236-241.

Vanderplaats G. N. (1984), Numerical Optimization Techniques for Engineering Design: With Applications, McGraw-Hill, New York.

APPENDIXES

APPENDIX A

DESCRIPTION OF THE ALGORITHM USED FOR THE NUMERICAL SOLUTION OF THE NATURAL CONVECTION FLOWS

This appendix describes the SIMPLER algorithm of Patankar (1980, 1981), which was used to perform the numerical solutions of the natural convection flows of interest. The finite volume approach employed by this algorithm, the resulting discretization equations, and the solution procedure used to construct the FORTRAN program listed in Appendix B are all discussed below.

The governing equations for heat and mass transfer are essentially statements of the conservation of mass, energy, and chemical species and of Newton's second law. For steady state, all of these equations can be written in the form of the general differential equation given by:

$$\frac{\partial}{\partial x_i}\left(\rho u_i \phi\right) = \frac{\partial}{\partial x_i}\left(\Gamma \frac{\partial \phi}{\partial x_i}\right) + S \qquad \text{(A-1)}$$

where Cartesian-tensor notation has been used, ϕ is the dependent variable, ρ is the density, u_i is the velocity in the x_i direction, Γ is the diffusion coefficient, and S is a "source term" which usually represents only the generation or annihilation of ϕ. The term on the left-hand side of this equation is referred to as the convective term since it represents the flux of ϕ that is carried by the flow. The first term on the right-hand side is the diffusion term. By expanding the definition of S to represent any term not covered by the convective or diffusion term, any physical process can be represented by equation A-1.

The four governing equations for this study are the continuity equation, Newton's second law in the x- and y-directions, and the energy conservation equation. The correspondence between the variables and parameters in the governing equations (equations 1-1 through 1-4 and 1-24 through 1-27) and equation (A-1) is shown in Chart A-1.

To apply the finite volume approach, the calculation region is discretized into a set of control volumes. Each of the terms in Equation A-1 is formulated

Chart A-1. Correspondence between variables and parameters in the governing equations and those in the general differential equation (A-1).

DIMENSIONAL FORM OF GOVERNING EQUATION

Parameter in the General Equation (A-1)	Continuity Equation (1-1)	x-Direction Momentum Equation (1-2)	y-Direction Momentum Equation(1-3)	Energy Equation (1-4)
ρ	ρ	ρ	ρ	ρc_p
Γ	0	μ	μ	k
ϕ	1	u	v	T
x_i	x,y	x,y	x,y	x,y
u_i	u,v	u,v	u,v	u,v
S	0	$-\frac{\partial p_d}{\partial x}$	$-\frac{\partial p_d}{\partial y} + g\beta (T-T_o)$	0

NONDIMENSIONAL FORM OF GOVERNING EQUATION

Parameter in the General Equation (A-1)	Continuity Equation (1-24)	x-Direction Momentum Equation (1-25)	y-Direction Momentum Equation(1-26)	Energy Equation (1-27)
ρ	1	1	1	1
Γ	0	Pr	Pr	1
ϕ	1	U	V	θ
x_i	X,Y	X,Y	X,Y	X,Y
u_i	U,V	U,V	U,V	U,V
S	0	$-\frac{\partial P}{\partial X}$	$-\frac{\partial P}{\partial Y} + Ra^* Pr\ \theta$	0

in terms of a conservation principle for each of the control volumes. In other finite difference approaches the conservation principles may hold only in the limits as the grid size approaches zero; however, since conservation principles are used to form the discretization equations for the finite volume approach, the conservation principles remain valid regardless of the grid size. This is an especially important feature for this problem because, when coupling the natural convection model with the numerical optimization (GRG2) code, the use of the minimum number of grid points is necessary to maintain the computer usage time within reasonable limits. The general grid geometry and nomenclature for grid spacing and dimensions of individual nodal volumes are shown in Figure A-1. The distances between adjacent nodes $(\delta x)_e$, $(\delta x)_w$, $(\delta x)_n$, and $(\delta x)_s$ are, in general, not equal. In fact, in the studies descibed in this dissertation the grid spacing is increased as distance from the wall is increased. This allows improved resolution of variables which have large gradients near the wall while minimizing the computing resource requirements.

For the discretization approach used herein, the grid points are located at the center of the control volumes. This ensures that the value of a variable at a grid point is representative of the value for the entire control volume. The control volumes at the boundaries (i.e. walls of the 2-D enclosure) have zero thickness as shown in Figure A-2. This allows direct application of the boundary condition information. Both Dirichlet (specified value) and Neumann (specified normal derivative) type boundary conditions are employed in this study. Examples of these types of boundary conditions are given below:

Dirichlet type: $$\phi_b = C_1 \qquad \text{(A-2)}$$

Neumann type: $$\phi_b = \phi_{b+1} + C_2 / (\delta x)_b \qquad \text{(A-3)}$$

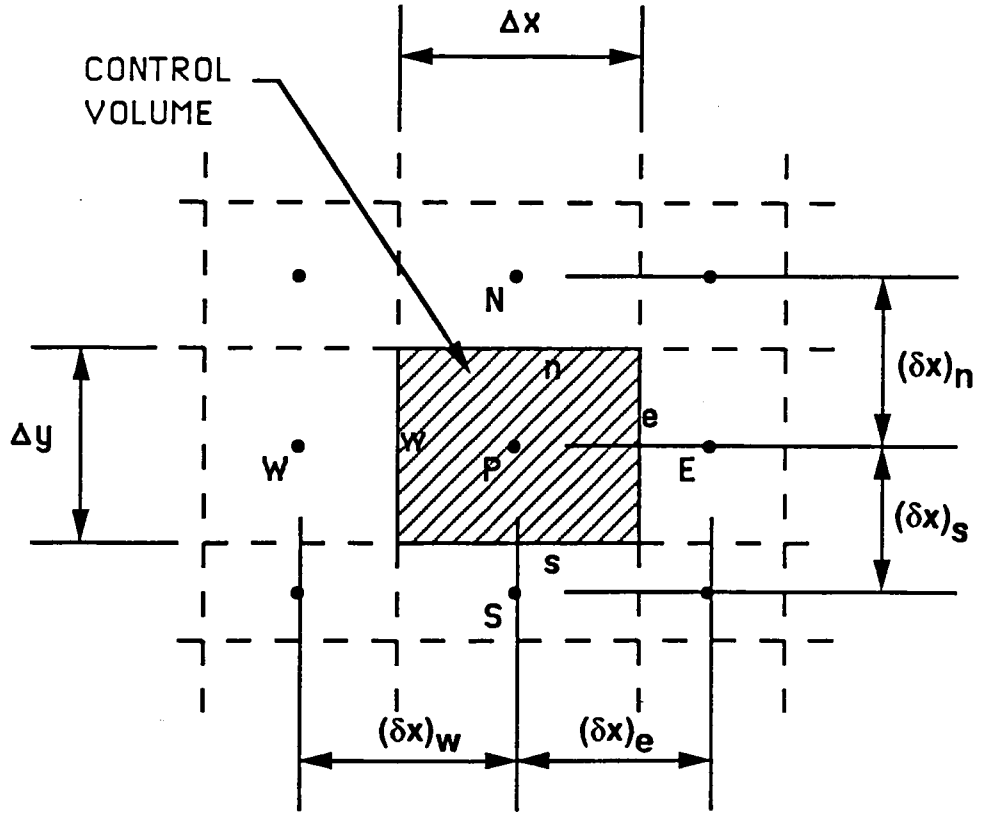


Figure A-1. Nomenclature for the computational grid

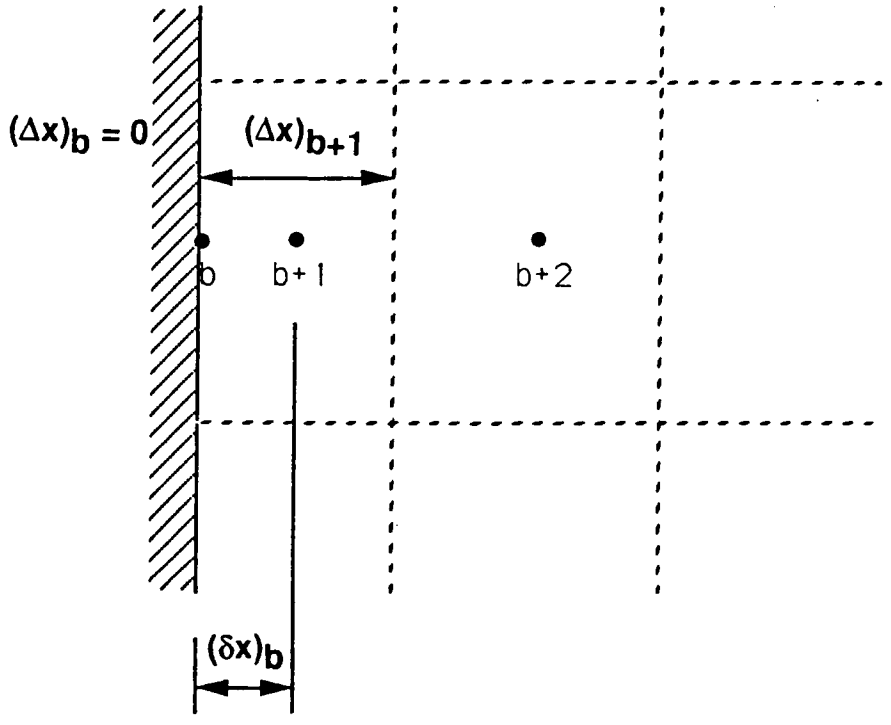


Figure A-2. Boundary control volume geometry

where C1 and C2 are constants, ϕ_b and ϕ_{b+1} are the values of ϕ at the boundary and at the grid point directly adjacent to the boundary, respectively, and $(\delta x)_b$ is the distance between grid points b and b+1.

Using the finite volume approach, each of the terms in equation A-1 is integrated over the control volume. In one dimension, the diffusion term integrated over the control volume P is given by:

$$\text{net diffusion into control volume P} = \int_P \frac{\partial}{\partial x}\left(\Gamma \frac{\partial \phi}{\partial x}\right) dx \qquad \text{(A-4)}$$

$$= \left(\Gamma \frac{\partial \phi}{\partial x}\right)_e - \left(\Gamma \frac{\partial \phi}{\partial x}\right)_w \qquad \text{(A-5)}$$

where the nomenclature for the grid point geometry is defined in Figure A-1. The grid points E and W, which refer to east and west, are located to the right and left, respectively, of the grid point P. The lower case letters e and w refer to the boundaries between control volumes. Evaluating the derivatives in equation A-5, in a piecewise linear fashion yields:

$$\int_P \frac{\partial}{\partial x}\left(\Gamma \frac{\partial \phi}{\partial x}\right) dx = \frac{\Gamma_e(\phi_E - \phi_P)}{(\delta x)_e} - \frac{\Gamma_w(\phi_P - \phi_W)}{(\delta x)_w}. \qquad \text{(A-6)}$$

Since Γ is, in general, not constant the values of Γ_e and Γ_w must be determined. The most straightforward procedure for obtaining the interface diffusion coefficient is to assume a linear variation of Γ between each two adjacent grid points. However, as pointed out by Patankar (1978), this leads to incorrect results in limiting cases such as an abrupt change in diffusion coefficient that occurs in composite materials. A more well behaved formulation for the interface conductivity recommended by Patankar (1978) is given by:

$$\Gamma_e = \left(\frac{1 - f_e}{k_P} + \frac{f_e}{k_E} \right)^{-1} \qquad \text{(A-7)}$$

where: $$f_e = \frac{\Delta x_E}{2\ (\delta x)_e} \ . \qquad \text{(A-8)}$$

Including the convective term along with the diffusion terms in equation A-1, and integrating over the control volume P gives

$$(\rho\, u\, \phi)_e - (\rho\, u\, \phi)_w = D_e\ (\phi_E - \phi_P) - D_w\ (\phi_P - \phi_W) \qquad \text{(A-9)}$$

where: $D_e = \Gamma_e / (\delta x)_e$ (A-10)

and,

$$D_w = \Gamma_w / (\delta x)_w \ . \qquad \text{(A-11)}$$

The selection of the "proper" profile for ϕ that is necessary to determine the quantities ϕ_e and ϕ_w for given values of ϕ_W, ϕ_P, and ϕ_E is an important consideration in modelling convection-diffusion processes. This subject has received considerable attention in the computatiuonal fluid mechanics literature. Simply using a central difference approach as is used for the $\partial\phi/\partial x$ derivative in the diffusion term results in an unacceptable discretization equation which for some cases leads to numerical instability and does not yield the correct results for the simple problem of one-dimensional convection-diffusion with a constant diffusion coefficient.

The upwind scheme was proposed by Courant et al (1952) to resolve the problems inherent in the central difference scheme as applied to convection-diffusion problems. In the upwind scheme, the diffusion term is still calculated assuming a linear variation for ϕ between adjacent grid points, but for the purpose of calculating the convection term the value of ϕ at the interface between control volumes is set equal to the value of ϕ at the grid point on the upwind side of the interface. For example, if $(\rho u)_e > 0$, then $\phi_e =$

ϕ_P, and if $(\rho u)_e < 0$, then $\phi_e = \phi_E$. Although this scheme eliminates the problems of physically unrealistic solutions which are possible under certain conditions for the central difference scheme, the upwind scheme overestimates diffusion. This excessive diffusion is sometimes referred to as "false" or "numerical" diffusion.

Spalding (1972) introduced the "exponential" scheme to develop the discretization equations for convection-diffusion problems. This scheme is extracted directly from the exact solution of the one-dimensional convection-diffusion problem with constant diffusion coefficients and no source terms. Therefore, for the one dimensional convection-diffusion problem with constant Γ and no source terms, the exponential scheme yields results that are in complete agreement with the exact solution for all values of the coefficients in equation A-9 and for all grid sizes. However, this scheme is not usually used because (1) it is "expensive" to compute exponentials, and (2) it is not exact for two- or three-dimensional situations, non-zero source terms, or variable diffusion coefficients. Schemes which have the same behavior as the exponential scheme but are more easily computed are generally used.

The so-called "power-law scheme", which was introduced by Patankar (1980, 1981) and recommended for use in the SIMPLER algorithm, is used in this study. It closely approximates the exponential scheme and also has the property of being easily computed. The formulation of the power-law scheme is given by the following relations

$$a_P \phi_P = a_E \phi_E + a_W \phi_W , \qquad \text{(A-12)}$$

$$a_E = D_e \left[\left| 0, \left(1 - \frac{0.1 |F_e|}{D_e} \right)^5 \right| \right] + \left[\left| 0, -F_e \right| \right] , \qquad \text{(A-13)}$$

$$a_W = D_w \left[\left| 0, \left(1 - \frac{0.1 |F_w|}{D_w} \right)^5 \right| \right] + \left[\left| 0, -F_w \right| \right] , \qquad \text{(A-14)}$$

$$a_P = a_E + a_W , \qquad \text{(A-15)}$$

$$F_e = (\rho u)_e \ , \qquad \text{(A-16)}$$

and,

$$F_w = (\rho u)_w \ , \qquad \text{(A-17)}$$

where the operator $[|\ A,B\ |]$ is used to denote the greater of A and B.

A key feature of the SIMPLER algorithm is the use of "staggered" grids for the calulation of the velocities. If the velocities are calculated at the same grid points as the pressure, the pressure field can be "wavy" due to the fact that the discretization for first derivatives will include information only on alternate grid points and not at adjacent ones. By using a "staggered" grid for the velocities and locating the velocity grid points at the interfaces between grid points for the other variables, this problem is resolved. Examples of "staggered" grids for the velocity components u and v are shown in Figure A-3. The x-direction velocity component (u) is staggered only in the x-direction, while the y-direction velocity component (v) is staggered only in the y-direction.

The iterative procedure defined by the SIMPLER algorithm consists of eight steps. The first step is to estimate the velocity field. For the initial call to subroutine GCOMP (in an optimization run) the estimate is either that all velocities are zero or the final results of a previous run are used. The velocities that resulted from the previous call to subroutine GCOMP are used as the initial guesses for subsequent solutions of the natural convection problem.

The discretized x-direction momentum equation can be written in the form:

$$u_e = \hat{u}_e + d_e\ (P_P - P_E) \qquad \text{(A-18)}$$

where P_P and P_E are the values of the pressure at grid points P and E, $\hat{u}_e$ is the so-called "pseudovelocity", and

$$d_e = \frac{[|\ 0,\ [(1\ -\ 0.1\ |F_e|\ )/D_e]^5\ |]}{a_e} \ . \qquad \text{(A-19)}$$

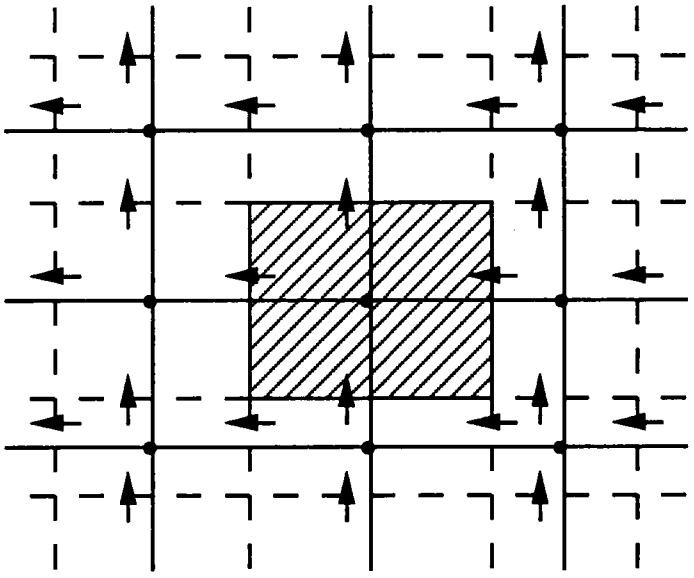


Figure A-3. Staggered grid for velocities

The pseudovelocity, $\hat{u}_e$, is defined as

$$\hat{u}_e = \frac{\sum a_{nb} u_{nb} + b}{a_e} \qquad \text{(A-20)}$$

where u_{nb} and a_{nb} represent the values of the velocities and their coefficients for the four neighboring grid points in the staggered grid arrangement used for the x-direction velocities. A similar equation is written for the y-direction velocity to determine the pseudovelocity $\hat{v}$. The second step of the SIMPLER algorithm consists of substituting the coefficients and the velocity estimates into the equations for $\hat{u}$ and $\hat{v}$ to determine the pseudovelocities.

The continuity equation can be written as:

$$[(\rho u)_e - (\rho u)_w] \Delta y + [(\rho v)_n - (\rho v)_s] \Delta x = 0 . \qquad \text{(A-21)}$$

Substituting for u (equation A-18) and v in terms of the pseudovelocities yields

$$a_P P_P = a_E P_E + a_W P_W + a_N P_N + a_S P_S + b , \qquad \text{(A-22)}$$

where: $a_E = \rho_e d_e \Delta y$, (A-23)

$$a_W = \rho_w d_w \Delta y , \qquad \text{(A-24)}$$

$$a_N = \rho_n d_n \Delta x , \qquad \text{(A-25)}$$

$$a_S = \rho_s d_s \Delta x , \qquad \text{(A-26)}$$

$$a_P = a_E + a_W + a_N + a_S , \qquad \text{(A-27)}$$

and,

$$b = [(\rho \hat{u})_w - (\rho \hat{u})_e] \Delta y + [(\rho \hat{v})_s - (\rho \hat{v})_n] \Delta x . \qquad \text{(A-28)}$$

The third step in the SIMPLER algorithm is to calculate the above coefficients and solve equation A-22 to obtain the pressure field. This new pressure field, which is denoted by P^*, will be treated as an estimate of the solution pressure field.

The fourth step of the SIMPLER algorithm is performed by using the estimated pressure field to solve the momentum equation, thus obtaining a

velocity field denoted by u^* and v^* and given by

$$a_e u_e^* = \Sigma a_{nb} u_{nb}^* + b + (P_P^* - P_E^*) \Delta y \qquad \text{(A-29)}$$

and,

$$a_n v_n^* = \Sigma a_{nb} v_{nb}^* + b + (P_P^* - P_N^*) \Delta x \; . \qquad \text{(A-30)}$$

The corrected pressure, P, is obtained from the equation:

$$P = P^* + P' \qquad \text{(A-31)}$$

where P' is the pressure correction. Similarly the corrected velocities are given by

$$u = u^* + u' \qquad \text{(A-32)}$$

and,

$$v = v^* + v' \; . \qquad \text{(A-33)}$$

Substituting equations A-29 and A-30 for the starred velocities (u^* and v^*) into the continuity equation (Equation A-21) and rearranging yields the following equation for P'

$$a_P P_P' = a_E P_E' + a_W P_W' + a_N P_N' + a_S P_S' + b \qquad \text{(A-34)}$$

where: $a_E = \rho_e d_e \Delta y \; ,$ (A-35)

$$a_W = \rho_w d_w \Delta y \; , \qquad \text{(A-36)}$$

$$a_N = \rho_n d_n \Delta x \; , \qquad \text{(A-37)}$$

$$a_S = \rho_s d_s \Delta x \; , \qquad \text{(A-38)}$$

$$a_P = a_E + a_W + a_N + a_S \; , \qquad \text{(A-39)}$$

and,

$$b = [(\rho u^*)_w - (\rho u^*)_e] \Delta y + [(\rho v^*)_s - (\rho v^*)_n] \Delta x \; . \qquad \text{(A-40)}$$

The final term, b, in this equation consists of the left-hand side of the continuity equation written in terms of the starred velocities (velocity estimates). If b is equal to zero, the starred velocities satisfy the continuity equation, and no further correction is needed. However, if b is nonzero (or, in

practice, has an absolute value greater than some previously set convergence tolerance), it represents a "mass source". Thus, the iterations must be continued until this "mass source" is annihilated by repeated correction of the velocity and pressure field.

The fifth step in the SIMPLER algorithm is to calculate this mass source term and thus solve for the pressure correction P'. Substituting equations A-32 and A-33 into equation A-34 yields the following relationship between the velocity and pressure corrections:

$$a_e u_e' = (P_P' - P_E') \Delta y + \Sigma a_{nb} u_{nb}' . \qquad \text{(A-41)}$$

The SIMPLER algorithm proceeds by dropping the final term in this equation. If this term was retained, the velocity correction would not only depend on the pressure correction but also the velocity corrections at the neighboring points. To solve this set of equations would involve the simultaneous and direct solution of the coupled set of momentum and continuity equations. By eliminating the term, the pressure correction can be solved with no other variables treated simultaneously. The letters, S-I-M-P-L-E-R, in SIMPLER refer to semi-implicit pressure linked equations - revised. The words semi-implicit acknowledge that the final term in equation A-41 is omitted. The neighboring velocities are not allowed to indirectly (or implicitly) influence the pressure correction. Thus, this omission serves as a means to simplify the process of updating the velocities during each iteration. The omission of this term is not a problem, however, since for the final iteration (converged solution) the pressure and velocity corrections are zero, that is, the omitted term will be zero for the solution velocity field.

With the term under discussion omitted, equation A-56 becomes:

$$a_e u_e' = (P_P' - P_E') \Delta y . \qquad \text{(A-42)}$$

Substituting this equation into equation A-42 yields:

$$u = u^* + (P_P' - P_E') \Delta y / a_e . \qquad \text{(A-43)}$$

Similarly the equation for the y-direction velocity can be written in terms of the

pressure correction as:

$$v = v^{*} + (P_P' - P_N') \, \Delta x / a_n \, . \qquad \text{(A-44)}$$

The sixth step in the SIMPLER algorithm is to correct the velocity field using the pressure correction in equations A-43 and A-44. The pressure, however, is not corrected at this point.

The seventh step in the SIMPLER algorithm is to solve for other ϕ's. In this case, the temperatures at all grid points are determined using the updated velocity field. Because of the buoyancy term in the equation for Newton's second law in the y-direction, this updated temperature field will have a "feedback" effect on the velocity and pressure fields.

The updated velocity and temperature fields are used in returning to the second step of the SIMPLER procedure and this process is repeated until convergence is achieved. Convergence of the solution is determined based on annihilating the mass source term (b in equation A-22) within some allowable tolerance. A discussion of the convergence tolerances that are required to accurately predict the optimal heat flux distribution is presented in Chapter 2.

APPENDIX B

FORTRAN PROGRAM LISTINGS

This appendix includes the FORTRAN program listings of:

(1) the main program portion of the GRG2 code that was modified from its usual form to read the input data which includes specification of the optimization type, natural convection parameter values, relaxation coefficients, "mass source" tolerance, grid locations, and initial values for all variables;

(2) subroutine GCOMP, which contains the natural convection model and the calculations of the objective and constraint functions;

(3) all subroutines and function subprograms called by subroutine GCOMP, including subroutines TAB, TDMA2D, MAXMIN, FCA, and REPORT;

(4) typical examples of the input files required to execute an optimization run, including files named "OPTIN", "GRID", and "CASE", as well as an example of the information that is input in an interactive fashion.

These are the essential elements of the computer program that were specifically created to perform the studies documented in this dissertation. Except for minor modifications to adapt them for use on the CRAY-2 computers, the standard GRG2 subroutines described by Lasdon et al (1978) and Lasdon and Waren (1986) were not modified, and therefore, are not listed in this appendix.

GRG2 Main Program

```
c
c            GRG2  -  Numerical Optimization Program
c
c
      real z
      dimension z(7500)
      integer ncore
c
      dimension ueold(51,51),vnold(51,51),told(51,51),pold(51,51)
      dimension xdist(51),y(51),dx(51),dy(51),delx(51),dely(51)
      dimension ue(51,51),vn(51,51),t(51,51),p(51,51)
      dimension uue(51,51),vvn(51,51),tt(51,51),pp(51,51)
      real u(51,51),v(51,51),bpc(51,51),xmult(51)
       real gmult(51),qt(4),qlhvw(51),xx(51),yy(51)
         integer isid(4)
c
      common /inp/ eps,ra,pr,ar,nx,ny,rf,rft,nrest,xmult,
     1           ntype,ncase,nord,isid,qt,gmult,nbc
c
c  pstep defines the size of the step in x taken to determine the
c  derivative dg/dx, where dx = pstep * x
       common /grad/ pstep
c
c
      common /ans/ qlhvw,u,v,t,p,xdist,y,dx,dy,bpc,tbar
c
      common /old/ ueold,vnold,pold,told
      common /start/ delx,dely,ue,vn
c
      data ncore/7500/
c
c.....................................................
c      Input files:
c       optin - input file which includes the standard grg2
c               input data in addition to defining the
c               optimization type, thermal boundary conditions,
c               perturbation size for computing the numerical
c               derivatives, and scaling factors for variables
c               and functions
c
c       grid - calculation grid info including number of nodes
c              in each direction, aspect ratio, node dimensions,
c              and distance between adjacent nodes
c
c       case - initial values for all variables (file is created
c              as an output file called rest from a previous run)
c
c
c      Output files:
```

```
c        outg - the main output file which lists the values of
c               all variables at each grid point
c
c        postin - file which gives the value of the stream-
c                 function, heatline, temperature, and pressure
c                 for each grid point.  This file is used to
c                 create contour plots.
c
c        rest - includes the values of all variables at the final
c                    iteration for use in restarting the run
c
c.....................................................................
c
      call link("unit5=(optin),unit6=(outg,create,text),in2=case,
     1 unit7=(dump),unit4=(tty),unit15=(postin,create,text),
     2 in3=grid,unit3=(in2,open),unit13=(rest,create,text),
     3   unit22=(in3,open),//")
c
c.....................................................................
c        ivar = number of variables
c        xmult(i) = scaling factors for variables
c        gmult(i) = scaling factors for functions
c        pstep = variable perturbation size used to evaluate grad
c        ntype = tpye of variables used for optimization
c              = 1 - nodal heat fluxes used as variables
c              = 2 - coefficients of polynomial used as variables
c        nord = order of polynomial for ntype = 2
c        ncase = optimization case number
c            = 1 - minimize average temp. for fixed total heat
c            = 2 - minimize max temp for fixed total heat
c            = 3 - minimize average temp for fixed total heat and
c                  max temp less than upper bound
c            = 4 - maximize total heat for max temp and average
c                  temp less than or equal to upper bounds
c
c.....................................................................
c
c
         write(4,*) ' restart=1, no restart=0'
         read(4,*)nrest
         write(4,*) 'input eps,ra,pr'
         read(4,*) eps,ra,pr
         write(4,*) 'input rf,rft'
         read(4,*) rf,rft
c
         read(5,*) ncase,ntype,nord
         read(5,*) (isid(i),i=1,4)
         read(5,*) (qt(i),i=1,4)
         read(5,*) pstep
         read(5,*) (gmult(i),i=1,4)
        read(5,*)ivar
        read(5,*)(xmult(i),i=1,ivar)
```

```
c
c
c
      if(isid(2) .ne. 1) then
      nbc = 1
      else
          if(isid(3) .ne. 1) then
          nbc = 2
          else
          nbc = 3
          endif
      endif
c
c.............  read/define grid parameters  .................
c
               read(22,8601)nx,ny,ar
               read(22,8602)(xdist(i),i=1,nx)
               read(22,8602)(dx(i),i=1,nx)
               read(22,8602)(y(j),j=1,ny)
               read(22,8602)(dy(j),j=1,ny)
c
        write(4,*)'grid and property data read ok'
8601   format(1x,2i4,f10.4)
8602   format(1x,5e16.6)
c
         do 8001 i=1,nx-1
         delx(i)=xdist(i+1)-xdist(i)
8001     continue
c
         do 8002 j=1,ny-1
         dely(j)=y(j+1)-y(j)
8002     continue
c         delx(nx)=1.
c         dely(ny)=1.
c
c
c.....................................................
c
        write(6,707) ra,pr,ar,eps,nx,ny,rf,rft
707     format(t5,'<<<results for:ra=',1x,
     *  f7.0,1x,'pr=',1x,f8.3,1x,'aspect ratio=',1x,
     *  f7.2,/,t5,'eps=',1x,e12.3,2x,'nx=',i2,2x,'ny=',i2,/,
     *  'relaxation factors:  velocities=',f7.4,4x,'temp.=',f7.4,
     *  4x,'>>>',//)
c
c
      if(nrest.ne.0)then
c..... restart option ..................................
c
      read(3,*)rra,ppr,aar,nnx,nny
        do 7001 i=1,nnx
        do 7001 j=1,nny
```

```
154         read(3,7601)xx(i),yy(j),uue(i,j),vvn(i,j),tt(i,j),pp(i,j)
155 c       write(6,7601)xx(i),yy(j),uue(i,j),vvn(i,j),tt(i,j),pp(i,j)
156 7001        continue
157 c
158          do 7002 i=1,nx
159 c
160          if(i.eq.1)then
161          ii=1
162          else
163          if(i.eq.nx)then
164              ii=nnx-1
165             else
166          ii=0
167 7010     ii=ii+1
168            if(xx(ii)-xdist(i))7010,7010,7012
169 7012     ii=ii-1
170             endif
171          endif
172          do 7002 j=1,ny
173          if(j.eq.1)then
174          jj=1
175          else
176          if(j.eq.ny)then
177              jj=nny-1
178             else
179              jj=0
180 7011     jj=jj+1
181             if(yy(jj)-y(j))7011,7011,7013
182 7013     jj=jj-1
183             endif
184          endif
185 c
186 c
187          difx=(xdist(i)-xx(ii))/(xx(ii+1)-xx(ii))
188          dify=(y(j)-yy(jj))/(yy(jj+1)-yy(jj))
189          int1=1.-difx-dify+difx*dify
190          int2=difx-difx*dify
191          int3=dify-difx*dify
192          int4=difx*dify
193 c
194        ue(i,j)=uue(ii,jj)*int1+uue(ii+1,jj)*int2+uue(ii,jj+1)*int3
195       1           +uue(ii+1,jj+1)*int4
196        vn(i,j)=vvn(ii,jj)*int1+vvn(ii+1,jj)*int2+vvn(ii,jj+1)*int3
197       1           +vvn(ii+1,jj+1)*int4
198        t(i,j)=tt(ii,jj)*int1+tt(ii+1,jj)*int2+tt(ii,jj+1)*int3
199       1           +tt(ii+1,jj+1)*int4
200        p(i,j)=pp(ii,jj)*int1+pp(ii+1,jj)*int2+pp(ii,jj+1)*int3
201       1           +pp(ii+1,jj+1)*int4
202 c
203             ueold(i,j)=ue(i,j)
204             vnold(i,j)=vn(i,j)
205             told(i,j)=t(i,j)
```

```
206              pold(i,j)=p(i,j)
207 7002    continue
208 7601    format(1x,6(1pe16.8))
209 c
210         write(4,*)'restart data read ok'
211 c
212           endif
213 c
214 c
215         call grg(z,ncore)
216 c
217 c
218              call timer (4)
219              call timer (6)
220 c
221 c
222         stop
223         end
224 c
225 c
226 c ____________________________________________________________________
227 c
```

```
      subroutine gcomp(g,x)
        dimension g(1),x(1)
c
c
c   This program uses Patankar's SIMPLER algorithm to obtain the
c   velocity and temperature fields for a natural convection
c   problem.  The problem of interest is the nat. conv. in a
c   rectangular enclosure with a heat flux distribution on the
c   LHVW.  The boundary conditions on the other walls may be a
c   specified heat flux or temperature.
c
c         Nonuniform grid version
c
c
c      list of variables:
c            aep(i,j): coeff. ap for the x-momentum[node:(i,j)]
c            anp(i,j): coeff. ap for the y-momentum[node:(i,j)]
c            ue(i,j) : staggered x-direction velocity
c            vn(i,j) : staggered y-direction velocity
c            app(i,j): coeff. for pressure equation
c            p(i,j)  : pressure for the regular grid points
c            atp(i,j): coeff. ap for the energy equation
c            t(i,j)  : temperature for the regular grid points
c            be(i,j) : constant term for the x-momentum
c            bn(i,j) : constant term for the y-momentum
c            bp(i,j) : constant term for the pressure equation
c            bpc(i,j): the mass source term in pressure correc-
c                      tion equation
c            bt(i,j) : constant term in the energy equation
c            f**(i,j): convective coefficients of general
c                      variable phi
c            pr      : the Prandtl number
c            ra      : the Rayleigh number
c            nx      : number of grid points in x-direction
c            ny      : number of grid points in y-direction
c            ar      : the aspect ratio
c            isid(k) : boundary cond. type for wall k (1-LHVW,
c                      2-top, 3-RHVW, 4-bottom)= 1 - fixed temp
c                      = 2 - specified heat flux
c            qt(k)   : specified temp or heat flux on wall k
c
c
c
c
c-----------------------------------------------------------------
c
      external  fca
      character*10 lblt,lblu,lblv,lblx,lbly,lblm,lblp,lbls
      character*10 lblpc,lblc,lblh
      real xmult(51) t(51,51),
```

```
      real ue(51,51),vn(51,51),p(51,51),pc(51,51),ups(51,51)
      real vps(51,51),aep(51,51),aee(51,51),aew(51,51),aen(51,51)
      real aes(51,51),be(51,51),anp(51,51),ane(51,51),anw(51,51)
      real ann(51,51),ans(51,51),app(51,51),ape(51,51),apw(51,51)
      real apn(51,51),aps(51,51),bp(51,51),bpc(51,51),atp(51,51)
      real ate(51,51),atw(51,51),atn(51,51),ats(51,51),bt(51,51)
      real fee(51,51),few(51,51),fen(51,51),fes(51,51),fne(51,51)
      real fnw(51,51),fnn(51,51),fns(51,51),fte(51,51),ftw(51,51)
      real y(51),maxso,minso,qlhvw(51),xdist(51)
      real ftn(51,51),fts(51,51),bn(51,51),u(51,51),v(51,51)
      real ueold(51,51),vnold(51,51),told(51,51),pold(51,51)
      real delx(51),dx(51),dy(51),dely(51),qt(4)
      real xx(51),yy(51),uue(51,51),vvn(51,51),tt(51,51)
      real pp(51,51),nulh(51),nurh(51),nubar
      real gmult(51)
      integer flgp(51,51),fle2d(51,51),fln2d(51,51),flt2d(51,51)
      integer count,flag,isid(4)
      real int1,int2,int3,int4
c
c
      common /inp/ eps,ra,pr,ar,nx,ny,rf,rft,nrest,xmult,
     1           ntype,ncase,nord,isid,qt,gmult,nbc
c
      common /ans/ qlhvw,u,v,t,p,xdist,y,dx,dy,bpc,tbar
c
      common /old/ ueold,vnold,pold,told
      common /start/ delx,dely,ue,vn
      common /prop/ cond,dencp,dens
c
c.....entering the parameters of the problem
c
      lblpc= 'pres. corr'
      lblp = 'pressure  '
      lbls = 'str. func.'
      lblh = 'heatlines '
      lblc = 'p correct.'
        lblu='vel. x-dir'
        lblv='vel. y-dir'
        lblt='temp.     '
c
       count = 0
c
c       flgp(2,2)=1
        flag=1
c.....................................................
c
      if (ntype.eq.1)then
c
c.....  heat flux for type 1
c
      do 33 j=1,ny
33    qlhvw(j)=x(j)/xmult(j)
```

```
c
      else
c
c.....  heat flux for type 2
c
       qlhvw(1) = 0.0
       qlhvw(ny)=0.0
       qqq=0.0
          do 1034 k=1,nord
        qqq=qqq+x(k)/xmult(k)*((y(2)+dy(2)/2.)**k)/dy(2)/k
1034       continue
      qlhvw(2)=qqq
c
        do 1035 j=3,ny-1
        ye = y(j) + dy(j)/2.
        yw = y(j) -dy(j) / 2.
         qqq=0.0
             do 34 k=1,nord
        qqq = qqq + x(k)/xmult(k) * (ye**k - yw**k)/dy(j)/k
34      continue
       qlhvw(j)=qqq
1035    continue
      end if
c....... problem parameters and properties
       vis=pr
       dens=1.
       csu=0.0
       csv=ra*pr
       cond=1.
       dencp=1.
       cst=0.0
c.........................................
c
c
c                     STEP 1 OF SIMPLER ALGORITHM
c
c.....initialize velocities and temperatures
        do 10 i=1,nx
          do 10 j=1,ny
         do 11 k=1,4
         if (isid(k).eq.2)go to 10
         if (k.eq.1)then
         flt2d(1,j)=1
         told(1,j)=qt(1)
         t(1,j)=qt(1)
        end if
         if (k.eq.2) then
         flt2d(i,ny)=1
         told(i,ny)=qt(2)
         t(i,ny)=qt(2)
        end if
         if (k.eq.3) then
```

```
381           flt2d(nx,j)=1
382           told(nx,j)=qt(3)
383           t(nx,j)=qt(3)
384          end if
385           if (k.eq.4) then
386           flt2d(i,1)=1
387           told(i,1)=qt(4)
388           t(i,1)=qt(4)
389          end if
390   11       continue
391   10      continue
392  c
393  c
394          do 1155 i=1,nx-1
395            do 1155 j=1,ny
396              if(i.eq.1) then
397                aee(i,j)=0.
398                aew(i,j)=0.
399                aen(i,j)=0.
400                aes(i,j)=0.
401                aep(i,j)=1.
402                be(i,j)=0.
403              else if(i.eq.nx-1) then
404                aee(i,j)=0.
405                aew(i,j)=0.
406                aen(i,j)=0.
407                aes(i,j)=0.
408                aep(i,j)=1.
409                be(i,j)=0.
410              else if(j.eq.1) then
411                aee(i,j)=0.
412                aew(i,j)=0.
413                aen(i,j)=0.
414                aes(i,j)=0.
415                aep(i,j)=1.
416                be(i,j)=0.
417              else if(j .eq. ny) then
418                aee(i,j)=0.
419                aew(i,j)=0.
420                aen(i,j)=0.
421                aes(i,j)=0.
422                aep(i,j)=1.
423                be(i,j)=0.
424              else
425              end if
426  1155      continue
427  c
428  c
429          do 1157 i=1,nx
430            do 1157 j=1,ny-1
431              if(i.eq.1) then
432                ane(i,j)=0.
```

```
433               anw(i,j)=0.
434               ann(i,j)=0.
435               ans(i,j)=0.
436               anp(i,j)=1.
437               bn(i,j)=0.
438             else if(i.eq.nx) then
439               ane(i,j)=0.
440               anw(i,j)=0.
441               ann(i,j)=0.
442               ans(i,j)=0.
443               anp(i,j)=1.
444               bn(i,j)=0.
445             else if(j.eq.1) then
446               ane(i,j)=0.
447               anw(i,j)=0.
448               ann(i,j)=0.
449               ans(i,j)=0.
450               anp(i,j)=1.
451               bn(i,j)=0.
452             else if(j .eq. ny-1) then
453               ane(i,j)=0.
454               anw(i,j)=0.
455               ann(i,j)=0.
456               ans(i,j)=0.
457               anp(i,j)=1.
458               bn(i,j)=0.
459             else
460             end if
461 1157      continue
462 c
463 c.....coeff. for the boundaries.
464 c         this is required by the tdma2d subroutine
465         do 111 i=1,nx
466           do 111 j=1,ny
467             fle2d(1,j)=1
468             fle2d(nx-1,j)=1
469             fle2d(i,1)=1
470             fle2d(i,ny)=1
471             fln2d(1,j)=1
472             fln2d(nx,j)=1
473             fln2d(i,1)=1
474             fln2d(i,ny-1)=1
475 111     continue
476 c
477 c.....
478         do 1150 i=1,nx
479           do 1150 j=1,ny
480             if(i.eq.1) then
481 c.....heat flux distribution on lhvw
482                if(isid(1).eq.1) then
483               atw(i,j)=0.
484               ate(i,j)=0.
```

```
485               atn(i,j)=0.
486               ats(i,j)=0.
487               atp(i,j)=1.
488               bt(i,j)=qt(1)
489             else
490               ate(i,j)=cond/delx(i)
491               atw(i,j)=0.
492               atn(i,j)=0.
493               ats(i,j)=0.
494               atp(i,j)=cond/delx(i)
495               bt(i,j)=qlhvw(j)
496             end if
497               else if(i.eq.nx) then
498 c
499                 if(isid(3).eq.1) then
500               atw(i,j)=0.
501               ate(i,j)=0.
502               atn(i,j)=0.
503               ats(i,j)=0.
504               atp(i,j)=1.
505               bt(i,j)=qt(3)
506             else
507               atw(i,j)=cond/delx(i-1)
508               ate(i,j)=0.
509               atn(i,j)=0.
510               ats(i,j)=0.
511               atp(i,j)=cond/delx(i-1)
512               bt(i,j)=qt(3)
513             end if
514               else if(j.eq.1) then
515 c
516                 if(isid(4).eq.1) then
517               atw(i,j)=0.
518               ate(i,j)=0.
519               atn(i,j)=0.
520               ats(i,j)=0.
521               atp(i,j)=1.
522               bt(i,j)=qt(4)
523             else
524               atn(i,j)=cond/dely(j)
525               ate(i,j)=0.
526               atw(i,j)=0.
527               ats(i,j)=0.
528               atp(i,j)=cond/dely(j)
529               bt(i,j)=qt(4)
530           end if
531             else if(j .eq. ny) then
532 c
533                 if(isid(2).eq.1) then
534               atw(i,j)=0.
535               ate(i,j)=0.
536               atn(i,j)=0.
```

```
537               ats(i,j)=0.
538               atp(i,j)=1.
539               bt(i,j)=qt(2)
540             else
541               ats(i,j)=cond/dely(j-1)
542               ate(i,j)=0.
543               atw(i,j)=0.
544               atn(i,j)=0.
545               atp(i,j)=cond/dely(j-1)
546               bt(i,j)=qt(2)
547             end if
548               else
549             end if
550 1150        continue
551 c
552 c
553 c                     END OF STEP 1
554 c
555 c......start the iteration
556 170      continue
557 c
558        if(count .eq. 0)goto 145
559          if(flag .eq. 0) goto 165
560 c
561 c
562 c                        START OF STEP 2 OF SIMPLER ALGORITHM
563 c
564 c
565 c.....calculating the coefficients of momentum equation
566           do 155 i=2,nx-2
567             do 155 j=2,ny-1
568 c
569 c
570 c
571               dee=vis*dy(j)/dx(i+1)
572               dew=vis*dy(j)/dx(i)
573               den=vis*delx(i)/dely(j)
574               des=vis*delx(i)/dely(j-1)
575 c
576               fee(i,j)=((ue(i+1,j)+ue(i,j))/(2.))*dy(j)*dens
577               few(i,j)=((ue(i-1,j)+ue(i,j))/(2.))*dy(j)*dens
578               fintfe=dx(i+1)/delx(i)/2.
579 c
580 c
581 c
582             fen(i,j)=(fintfe*vn(i,j)+(1.-fintfe)*vn(i+1,j))
583      1                      *dens*delx(i)
584             fes(i,j)=(fintfe*vn(i,j-1)+(1.-fintfe)*vn(i+1,j-1))
585      1                      *dens*delx(i)
586             aee(i,j)=dee*fca(abs(fee(i,j)/dee))+amax1(-fee(i,j),0.)
587             aew(i,j)=dew*fca(abs(few(i,j)/dew))+amax1(few(i,j),0.)
588             aen(i,j)=den*fca(abs(fen(i,j)/den))+amax1(-fen(i,j),0.)
```

```
589           aes(i,j)=des*fca(abs(fes(i,j)/des))+amax1(fes(i,j),0.)
590           aep(i,j)=aee(i,j)+aew(i,j)+aen(i,j)+aes(i,j)
591           be(i,j)=0.
592 155       continue
593          do 157 i=2,nx-1
594           do 157 j=2,ny-2
595 c
596               dnn=vis*dx(i)/dy(j+1)
597               dns=vis*dx(i)/dy(j)
598               dne=vis*dely(j)/delx(i)
599               dnw=vis*dely(j)/delx(i-1)
600 c
601               fnn(i,j)=((vn(i,j+1)+vn(i,j))/(2.))*dx(i)*dens
602               fns(i,j)=((vn(i,j-1)+vn(i,j))/(2.))*dx(i)*dens
603               fintfe=dy(j+1)/dely(j)/2.
604 c
605 c
606            fne(i,j)=(fintfe*ue(i,j)+(1.-fintfe)*ue(i,j+1))
607      1                    *dens*dely(j)
608            fnw(i,j)=(fintfe*ue(i-1,j)+(1.-fintfe)*ue(i-1,j+1))
609      1                    *dens*dely(j)
610           ane(i,j)=dne*fca(abs(fne(i,j)/dne))+amax1(-fne(i,j),0.)
611           anw(i,j)=dnw*fca(abs(fnw(i,j)/dnw))+amax1(fnw(i,j),0.)
612           ann(i,j)=dnn*fca(abs(fnn(i,j)/dnn))+amax1(-fnn(i,j),0.)
613           ans(i,j)=dns*fca(abs(fns(i,j)/dns))+amax1(fns(i,j),0.)
614           anp(i,j)=ane(i,j)+anw(i,j)+ann(i,j)+ans(i,j)
615           fintt=dy(j+1)/2./dely(j)
616 c
617 c
618            tn=fintt*t(i,j)+(1.-fintt)*t(i,j+1)
619 c
620 c
621 c
622           bn(i,j)=(csv*tn)*dx(i)*dy(j)
623  157      continue
624 c.....calculating the pseudovelocties
625          do 40 i=2,nx-2
626           do 40 j=2,ny-1
627          ups(i,j)=(aee(i,j)*ue(i+1,j)+aew(i,j)*ue(i-1,j)+aen(i,j)*
628      *            ue(i,j+1)+aes(i,j)*ue(i,j-1)+be(i,j))/aep(i,j)
629 40       continue
630          do 45  i=2,nx-1
631           do 45 j=2,ny-2
632          vps(i,j)=(ane(i,j)*vn(i+1,j)+anw(i,j)*vn(i-1,j)+ann(i,j)*
633      *             vn(i,j+1)+ans(i,j)*vn(i,j-1)+bn(i,j))/anp(i,j)
634 45       continue
635 c.....
636 c
637 c                              END OF STEP 2
638 c
639 c
640 c                              START OF STEP 3 OF SIMPLER ALGORITHM
```

```
641 c
642 c
643 c.....calculating the coefficients for the pressure equation.
644         do 50 j=2,ny-1
645           do 50 i=2,nx-1
646 c
647             ape(i,j)=dy(j)**2/aep(i,j)*dens
648             apw(i,j)=dy(j)**2/aep(i-1,j)*dens
649             apn(i,j)=dx(i)**2/anp(i,j)*dens
650             aps(i,j)=dx(i)**2/anp(i,j-1)*dens
651             if (i .eq. 2 ) apw(i,j)=0.
652             if(i .eq. nx-1) ape(i,j)=0.
653             if(j .eq. 2) aps(i,j)=0.
654             if(j .eq. ny-1) apn(i,j)=0.
655             app(i,j)=ape(i,j)+apw(i,j)+apn(i,j)+aps(i,j)
656       bbp=(ups(i-1,j)-ups(i,j))*dy(j)+(vps(i,j-1)-vps(i,j))*dx(i)
657       bp(i,j)=bbp*dens
658 50      continue
659 c
660 c.....
661 c.....call tdma2d to get pressure solution.
662 c
663         call tdma2d(app,apn,aps,ape,apw,
664      *              bp,p,flgp,2,nx-1,2,ny-1,2.e-9,0,lblp,1.)
665 c
666         do 371 j=1,ny
667         do 371 i=1,nx
668         pold(i,j)=p(i,j)
669 371     continue
670 c
671 c
672 c                              END OF STEP 3
673 c
674 c
675 c
676 c                              START OF STEP 4 OF SIMPLER ALGORITHM
677 c
678 c
679 c.
680 c.....solve the momentum equations
681         do 60 i=2,nx-2
682           do 60 j=2,ny-1
683             be(i,j)=be(i,j)+(p(i,j)-p(i+1,j))*dy(j)
684 60      continue
685         do 70 i=2,nx-1
686           do 70 j=2,ny-2
687             bn(i,j)=bn(i,j)+(p(i,j)-p(i,j+1))*dx(i)
688 70      continue
689 c.....call tdma2d to obtain velocity field
690         call tdma2d(aep,aen,aes,aee,aew,
691      *              be,ue,fle2d,1,nx-1,1,ny,2.e-11,0,lblu,1.0)
692 c
```

```
693          call tdma2d(anp,ann,ans,ane,anw,
694       *              bn,vn,fln2d,1,nx,1,ny-1,2.e-11,0,lblv,1.0)
695  c
696          do 531 i=2,nx-1
697           do 532 j=2,ny-1
698             u(i,j)=(ue(i-1,j)+ue(i,j))/2.
699             v(i,j)=(vn(i,j-1)+vn(i,j))/2.
700  532     continue
701  531     continue
702  c
703  c
704  c                        END OF STEP 4
705  c
706  c
707  c
708  c               START OF STEP 5 OF SIMPLER ALGORITHM
709  c
710  c
711  c
712  c.....calculate the mass source term for the pressure correction
713  c.....eq.flag is used to designate whether bpc(i,j) .lt. eps
714          flag=0
715          minso=0.
716          maxso=0.
717          nflag=0
718          do 120 i=2,nx-1
719            do 120 j=2,ny-1
720          pc(i,j)=0.0
721          bpc(i,j)=((ue(i-1,j)-ue(i,j))*dy(j)+(vn(i,j-1)-vn(i,j))
722       1          *dx(i))*dens
723  c
724  c              CONVERGENCE TEST FOR SIMPLER
725  c
726            if(bpc(i,j) .gt. maxso) maxso=bpc(i,j)
727            if(bpc(i,j) .lt. minso) minso=bpc(i,j)
728            if(abs(bpc(i,j)).gt.eps) then
729              flag=1
730            endif
731            if(count.ge.100) then
732           flag=0
733           nflag=1
734           endif
735  c
736  120     continue
737  c
738          if(flag.eq.0) go to 160
739  c....
740  c.....call tdma2d to get pressure corrections.
741          call tdma2d(app,apn,aps,ape,apw,bpc,
742       *    pc,flgp,2,nx-1,2,ny-1,2.e-6,0,lblc,1.0)
743  c
744  c
```

```
745 c                              END OF STEP 5
746 c
747 c
748 c
749 c                    START OF STEP 6 OF SIMPLER ALGORITHM
750 c
751 c
752 c
753 c.....
754 c.....correct the velocity field with the pressure corrections.
755         do 130 i=2,nx-2
756           do 130 j=2,ny-1
757             ue(i,j)=ue(i,j)+(pc(i,j)-pc(i+1,j))*(dy(j)/aep(i,j))
758 c.....relaxation of updated x- velocity
759             ue(i,j)= ueold(i,j) * (1.-rf) + ue(i,j) * rf
760             ueold(i,j) = ue(i,j)
761 130     continue
762         do 140 i=2,nx-1
763           do 140 j=2,ny-2
764             vn(i,j)=vn(i,j)+(pc(i,j)-pc(i,j+1))*(dx(i)/anp(i,j))
765 c.........relaxation of updated y-velocity
766            vn(i,j) = vnold(i,j) * (1.-rf) + rf * vn(i,j)
767            vnold(i,j) = vn(i,j)
768 140     continue
769 c.....
770 145     continue
771 c
772 c
773 c                              END OF STEP 6
774 c
775 c
776 c                    START OF STEP 7 OF SIMPLER ALGORITHM
777 c
778 c
779 c.....solve the energy equation.
780         do 150 i=2,nx-1
781           do 150 j=2,ny-1
782         dte=dy(j)/delx(i)*cond
783         fte(i,j)=ue(i,j)*dy(j)*dencp
784         ate(i,j)=dte*fca(abs(fte(i,j)/dte))+amax1(-fte(i,j),0.)
785         dtw=dy(j)/delx(i-1)*cond
786         ftw(i,j)=ue(i-1,j)*dy(j)*dencp
787         atw(i,j)=dtw*fca(abs(ftw(i,j)/dtw))+amax1(ftw(i,j),0.)
788         dtn=dx(i)/dely(j)*cond
789         ftn(i,j)=vn(i,j)*dx(i)*dencp
790         atn(i,j)=dtn*fca(abs(ftn(i,j)/dtn))+amax1(-ftn(i,j),0.)
791         dts=dx(i)/dely(j-1)*cond
792         fts(i,j)=vn(i,j-1)*dx(i)*dencp
793         ats(i,j)=dts*fca(abs(fts(i,j)/dts))+amax1(fts(i,j),0.)
794 573         continue
795 c
796 c
```

```
797               atp(i,j)=ate(i,j)+atw(i,j)+atn(i,j)+ats(i,j)
798               bt(i,j)=0.
799 150       continue
800 c.....call tdma2d to get the temperature.
801           call tdma2d(atp,atn,ats,ate,atw,
802      *                bt,t,flt2d,1,nx,1,ny,5.e-9,0,lblt,1.0)
803 c
804        do 341 j=1,ny
805        do 341 i=1,nx
806        t(i,j)=t(i,j) * rft + told(i,j) * (1.-rft)
807 341    told(i,j)=t(i,j)
808 c.......
809 c
810 c
811 c                                END OF STEP 7
812 c
813 c
814         count=count+1
815 c           write(21,621)count,maxso,minso,tbar
816 c 621       format(1x,i4,4x,3(e12.4,2x))
817          go to 170
818 c
819 160      continue
820 c
821 c.......
822 c
823 c    ************************************************************
824 c
825 c           determine values of functions
826 c
827 c
828 c       g(1) = total heating rate along LHVW
829 c       g(2) = average temp along LHVW
830 c       g(3) = peak temp along LHVW
831 c       g(4) = minimum heat flux along LHVW
832 c
833 c
834          sumq=0.0
835          sum =0.0
836 c
837            g(4) = 9999.
838         if (ntype .eq. 1) then
839          do 925 j=2,ny-1
840          if (g(4) .gt. qlhvw(j)) g(4) = qlhvw(j)
841 925      continue
842 c
843              else
844 c
845           dyyy=1./1000.
846           yyy=0.0
847 c
848         do 1101 i=1,998
```

```
849         yyy=yyy+dyyy
850          qqq = 0.0
851               do 1102 k=1,nord
852               qqq = qqq + x(k) * yyy**(k-1)
853 1102        continue
854         if (qqq .lt. g(4))  g(4) = qqq
855 1101    continue
856 c
857        endif
858 c
859 c
860         g(3)=t(1,2)
861 c
862 c
863        do 110 j = 2,ny-1
864 c
865          sum = sum + t(1,j)*dy(j)
866          sumq = sumq + qlhvw(j)*dy(j)
867 c
868 c
869         if (t(1,j) .gt. g(3)) g(3) = t(1,j)
870 c
871 c
872 110    continue
873 c
874        tbar = sum / 1.
875        g(2)=tbar * gmult(2)
876        g(1) = sumq /1. * gmult(1)
877          g(3)=g(3)* gmult(3)
878          g(4) = g(4) * gmult(4)
879 c
880 c    ************************************************
881 c
882        if(nflag .eq. 1) then
883        write(6,*) '*****  THIS IS NOT A CONVERGED SOLUTION *****'
884        endif
885 c
886        write(6,671) tbar,count
887        write(4,671) tbar,count
888 671    format(/,1x,'Average LHVW temperature =',f12.8,
889       1 2x,'No. of iterations =',i4)
890        if (ntype .eq. 1) then
891            write(4,1671)(x(k),k=1,ny)
892            write(6,1671)(x(k),k=1,ny)
893          else
894            write(4,1671)(x(k),k=1,nord)
895            write(6,1671)(x(k),k=1,nord)
896          endif
897          write(4,1671)(g(k),k=1,4)
898          write(6,1671)(g(k),k=1,4)
899 1671       format(1x,10f12.6)
900 c
```

```
c
c
c
  165  return
       end
c-----------------------------------------------------------------
c
```

Subroutine TAB

```
      subroutine tab(z,nx,ny,lbl)
c
c....This subroutine prints the values of the variable (z) at all
c     grid points in the rectangular enclosure.  The values are
c     printed at their corresponding location in the enclosure.
c     That is, the values of the variables along the top
c     horizontal surface are printed across the top of the table,
c     the values of the variables along the right-hand, vertical
c     surface are arranged from top to bottom along the right-
c     hand side of the table, etc.
c.....................................................................
c
      character*10 lbl
      dimension z(51,51)
      write(6,602)
      write(6,*)lbl
      write(6,*)'-----------------------------------------------'
      do 1 j=ny,1,-1
      write(6,601)(z(i,j),i=1,nx)
    1 continue
  601 format(1x,10e12.4)
      write(6,602)
  602 format(////)
c
      return
      end
c
c
c
c---------------------------------------------------------------------
c
c
```

Subroutine TDMA2D

```
      subroutine tdma2d(ap,an,as,ae,aw,bb,phi2d,flg2d,
     $              imin,imax,jmin,jmax,maxrd,flg20,lble,alpha)
c
c  input:  ap(i,j),an(i,j),as(i,j),ae(i,j),aw(i,j),bb(i,j)
c          phi2d(i,j),flg2d(i,j)
c            for i=imin,imax; j=jmin,jmax
c          imin,imax,jmin,jmax,maxrd
c          note: phi2d contains data at specified locations.
c  output: phi2d(i,j)
c-----------------------------------------------------------------
c  this is the tri-diagonal matrix algorithm for 1-dimension:
c  input:  a(k),b(k),c(k),d(k), for k=1 to nk
c      where a(k),b(k),c(k), and d(k) are the coefficients of the
c      linear set of nk independent equations and nk unknowns
c      a(k)*phi(k)=b(k)*phi(k+1)+c(k)*phi(k-1)+d(k).
c
c  output: phi(k) for k=1 to nk.
c
c  note: (1) p(k) and q(k) are the coefficients of the recurrence
c            relation
c            phi(k)=p(k)*phi(k+1)+q(k).
c
c  reference:"numerical heat transfer and fluid flow,"
c             suhas v. patankar, mc-graw hill, 1980, p.52-3.
c-----------------------------------------------------------------
c  the algorithm was modified to account for internal boundaries
c  where phi2d is specified.  the array "flg2d(i,j)" defines the
c  points where phi2d is fixed. phi2d is not to be modified at
c  these points.
c  the program searches for the first point (i,j) where phi2d
c  is specified row by row, starting from i=imin and j=jmin.  the
c  i- and j-values of the point are assigned to icstrt and jcstrt
c  respectively.  rows jc's are swept first starting with
c  jc=jcstrt.  columns ic's are swept starting with ic=icstrt.
c  rows move to the top by increments jcstep=1 and columns to the
c  right by increments icstep=1 until a boundary is encountered.
c  once the row at the top is swept, jc is assigned the value
c  "jcstrt-1" and jcstep the value "-1" so that sweeping of rows
c  moves to the bottom. same logic is used for the columns--once
c  the column at the right is swept, ic is assigned the value
c  "icstrt-1" and icstep the value "-1" so that sweeping of
c  columns moves to the left. after either all rows and all
c  columns are swept a test for convergence is performed. the
c  subroutine returns the values of phi2d(i,j)if the test is
c  passed; otherwise, it continues execution.
c     when all rows are swept, jc is assigned the starting value
c  "jcstrt" and jcstep the value +1 to return to the original
c  sweeping mode.
c     when all columns are swept, ic is assigned the starting
```

```
 989 c  value"icstrt" and icstep the value +1 to return to the
 990 c  original sweeping mode.
 991 c-----------------------------------------------------------------
 992 c
 993 c   variable        description
 994 c
 995 c    alpha        relaxation factor
 996 c    count        counter for number of points wherephi2d is fixed
 997 c    flg2         switch (flag) no. 2 for test of convergence
 998 c                 request:
 999 c                        1 (on)= test required
1000 c                        0 (off)= test not required
1001 c    flg3         switch (flag) no. 3 for notification of
1002 c                 finding of a fixed phi2d (known) point:
1003 c                        1 (on)= point of known phi2d found
1004 c                        0 (off)= point of known phi2d not found
1005 c    ic           i-control: control of columns
1006 c    icount       counter for number of columns swept
1007 c    icstep       value of increment in ic
1008 c    imax         maximum vavue of ic
1009 c    imin         minimum vavue of ic
1010 c    jc           j-control: control of rows
1011 c    jcount       counter for number of rows swept
1012 c    jcstep       value of increment in jc
1013 c    jmax         maximum vavue of jc
1014 c    jmin         minimum vavue of jc
1015 c    kmax         maximum vavue of k(n)
1016 c    kmin         minimum vavue of k(n)
1017 c    m            dummy variable
1018 c    maxrd        maximum relative difference allowed between
1019 c                 the new and old value of phi2d
1020 c    n            direction of tdma application
1021 c                        1 for row (x-dir)
1022 c                        2 for row (x-dir)
1023 c    np(n)        number of points in a specified direction
1024 c                   np(1) : number of points in x-dir
1025 c                   np(2) : number of points in x-dir
1026 c    p(m)         coefficient of phi(m+1) in recurrence relation
1027 c    phi(m)       one-dimensional array of unknowns for use
1028 c                 during computations in tdma
1029 c    phi2d(i,j)   two-dimensional array of unknowns
1030 c    phi2do(i,j)  "old" two-dimensional array of unknowns
1031 c    q(m)             term in recurrence relation
1032 c
1033 c    coefficients of discretization equation
1034 c
1035 c    a(m)             coefficient of phi(m)
1036 c    b(m)             coefficient of phi(m+1)
1037 c    c(m)             coefficient of phi(m-1)
1038 c    d(m)             constant term in the phi-equation
1039 c
1040 c    ap(i,j)          coefficient of phi2d(i,j)
```

```
c     an(i,j)          coefficient of phi2d(i,j+1)
c     as(i,j)          coefficient of phi2d(i,j-1)
c     ae(i,j)          coefficient of phi2d(i+1,j)
c     aw(i,j)          coefficient of phi2d(i-1,j)
c     bb(i,j)          constant term in the phi2d-equation
c
c-----------------------------------------------------------------
      character*10 lble
        integer flg20
        integer flg2d(51,51),k(2),np(2),count,flg2,flg3
        integer flg11,flg12,flg13,flg14
        real p(51),q(51),maxrd,var
        real a(51),b(51),c(51),d(51),phi(51),phi2do(51,51)
        real an(51,51),as(51,51),ae(51,51),aw(51,51),
     $       ap(51,51),bb(51,51),phi2d(51,51)
c-----------------------------------------------------------------
c  1. initialize parameters.
      niter =0
        np(1)=imax-imin+1
        np(2)=jmax-jmin+1
        icstep=1
        jcstep=1
        icount=0
        jcount=0
        flg2=0
        flg3=0
        n=2
        phimax=phi2d(imin,jmin)
        phimin=phimax
c-----------------------------------------------------------------
c  2.   check if ae(imax,j)=aw(imin,j)=an(i,jmax)=as(i,jmin)=0.
        do  2 i=imin,imax
        if(an(i,jmax).ne.0.) then
       write(6,*)' subroutine tdma2d.....................'
       write(6,*)' an(i,jmax) is not equal to 0. need to either'
       write(6,*)' extend the solution domain to [i,jmax+1] and'
       write(6,*)' specify phi2d(i,jmax+1) or set an(i,jmax)=0.'
          stop
        end if
        if(as(i,jmin).ne.0.) then
        write(6,*)' subroutine tdma2d.....................'
        write(6,*)' as(i,jmin) is not equal to 0. need to either'
        write(6,*)' extend the solution domain to [i,jmin-1] and'
        write(6,*)' specify phi2d(i,jmin-1) or set as(i,jmin)=0.'
          stop
        end if
2       continue
        do  4 j=jmin,jmax
        if(ae(imax,j).ne.0.) then
        write(6,*)' subroutine tdma2d.....................'
        write(6,*)' ae(imax,j) is not equal to 0. need to either'
        write(6,*)' extend the solution domain to [imax+1,j] and'
```

```
1093          write(6,*)' specify phi2d(imax+1,j) or set ae(imax,j)=0.'
1094            stop
1095          end if
1096          if(aw(imin,j).ne.0.) then
1097          write(6,*)' subroutine tdma2d.....................'
1098          write(6,*)' aw(imin,j) is not equal to 0. need to either'
1099          write(6,*)' extend the solution domain to [imin-1,j] and'
1100          write(6,*)' specify phi2d(imin-1,j) or set aw(imin,j)=0.'
1101            stop
1102          end if
1103 4        continue
1104 c-------------------------------------------------------------------
1105 c  3. find point where phi2d is known and initialize phi2do(i,j).
1106 c        also search for phimin and phimax.
1107              icstrt=imin
1108              jcstrt=jmax
1109          do 10 j=jmin,jmax
1110          do 10 i=imin,imax
1111          if (flg2d(i,j).eq.1) then
1112            phi2do(i,j)=phi2d(i,j)
1113            if(flg3.eq.0) then
1114              icstrt=i
1115              jcstrt=j
1116              flg3=1
1117            end if
1118          else
1119            phi2do(i,j)=0.
1120          end if
1121          ii=i
1122          jj=j
1123          call maxmin(phi2d,phimin,phimax,ii,jj)
1124 10       continue
1125          ic=icstrt
1126          jc=jcstrt
1127 c-------------------------------------------------------------------
1128 c  4. check position of row and column of tdma application
1129 c  4.1. check row
1130 20       if((jc.gt.jmax).or.(jc.lt.jmin)) then
1131            jcstep=-jcstep
1132            if(jcount.ge.np(2)) then
1133              jcstep=1
1134              jcount=0
1135              flg2=1
1136              jc=jcstrt
1137            else
1138              jc=jcstrt-1
1139            end if
1140          end if
1141 c  4.2. check column
1142          if((ic.gt.imax).or.(ic.lt.imin)) then
1143            icstep=-icstep
1144            if(icount.ge.np(1)) then
```

```
1145              icstep=1
1146              icount=0
1147              flg2=1
1148              ic=icstrt
1149            else
1150              ic=icstrt-1
1151            end if
1152          end if
1153 c-------------------------------------------------------------------
1154 c  5. check convergence.
1155          if(flg2.eq.1) then
1156            flg2=0
1157          if(abs(phimax-phimin).lt.1.e-8) then
1158          write(6,*)
1159          write(6,*)' tdma2d......'
1160          write(6,*)' <<<warning>>>'
1161          write(6,*)' phimax=phimin... uniform phi2d distribution.'
1162          write(6,*)' convergence test is not possible'
1163            return
1164          end if
1165        niter = niter +1
1166        if(niter.gt.201) then
1167 c       write(6,625)lble,maxrd,reldif,niter
1168          return
1169 c 625    format(1x,a10,
1170 c     1 'Eq. not satisfied, tol=',1pe12.3,
1171 c     2 'rel. dif.=',1pe12.3,'No. of iters.=',i4)
1172        endif
1173 c.....................................................................
1174              do 30 i=imin,imax
1175              do 30 j=jmin,jmax
1176            reldif=abs((phi2d(i,j)-phi2do(i,j))/(phimax-phimin))
1177              if(reldif.gt.maxrd) goto 40
1178 30           continue
1179              return
1180            end if
1181 c-------------------------------------------------------------------
1182 c  6. initialize parameters according to direction of tdma
1183 40         if(n.eq.2) then
1184 c  6.1. row
1185              n=1
1186              k(2)=jc
1187              kmin=imin
1188              kmax=imax
1189              jc=jc+jcstep
1190              jcount=jcount+1
1191            else
1192 c  6.2. column
1193              n=2
1194              k(1)=ic
1195              kmin=jmin
1196              kmax=jmax
```

```
1197            ic=ic+icstep
1198            icount=icount+1
1199          end if
1200          count=0
1201 c-------------------------------------------------------------------
1202 c  7. redefine coefficients for 1-dim.
1203          do 50 m1=kmin,kmax
1204          k(n)=m1
1205          if(flg2d(k(1),k(2)).eq.1) then
1206            a(m1)=1.
1207            b(m1)=0.
1208            c(m1)=0.
1209            d(m1)=phi2d(k(1),k(2))
1210            count=count+1
1211          else
1212            if(ap(k(1),k(2)).eq.0.)then
1213        write(6,*)' tdma2d...'
1214        write(6,*)' <<<warning>>>'
1215        write(6,*)' ap=0 at point (',k(1),k(2),').'
1216        write(6,*)' phi2d(',k(1),k(2),') was assigned zero value.'
1217        write(6,*)' ap(',k(1),k(2),') was assigned the value of 1.'
1218              ap(k(1),k(2))=1.
1219              a(m1)=1.
1220              b(m1)=0.
1221              c(m1)=0.
1222              d(m1)=0
1223            else
1224              a(m1)=ap(k(1),k(2))
1225              if(n.eq.1) then
1226 c              define coefficients for tdma applied to a row.
1227               b(m1)=ae(k(1),k(2))
1228               c(m1)=aw(k(1),k(2))
1229               d(m1)=bb(k(1),k(2))+an(k(1),k(2))*phi2d(k(1),k(2)+1)
1230      $                           +as(k(1),k(2))*phi2d(k(1),k(2)-1)
1231              else
1232 c              define coefficients for tdma applied to a column.
1233               b(m1)=an(k(1),k(2))
1234               c(m1)=as(k(1),k(2))
1235               d(m1)=bb(k(1),k(2))+ae(k(1),k(2))*phi2d(k(1)+1,k(2))
1236      $                           +aw(k(1),k(2))*phi2d(k(1)-1,k(2))
1237              end if
1238            end if
1239          end if
1240 c        define the one-dimensional "phi".
1241          phi(m1)=phi2d(k(1),k(2))
1242 50       continue
1243          if(count.ge.np(n)) goto 20
1244 c-------------------------------------------------------------------
1245 c  8. apply tdma.
1246 c  8.1. compute p and q.
1247 c          write(21,*)'1 ok'
1248          do 60 m=kmin,kmax
```

```
1249          k(n)=m
1250 c        write(21,*)'n,k(n)=',n,k(n)
1251          aaaa=a(m)-c(m)*p(m-1)
1252          if(aaaa.lt.1.e-10) then
1253          p(m)=1.0
1254          q(m)=0.0
1255          else
1256          p(m)=b(m)/(aaaa)
1257 c         write(21,*)'p(m)=',p(m)
1258          q(m)=(d(m)+c(m)*q(m-1))/(aaaa)
1259          endif
1260 c         write(21,*)'q(m)=',q(m)
1261 60       continue
1262 c          write(21,*)'2 ok'
1263 c  8.2. compute phi2d
1264          do 70 m=kmax,kmin,-1
1265          k(n)=m
1266 c         write(21,*)'k(n)=',k(n)
1267          if(flg2d(k(1),k(2)).ne.1) then
1268            phi2do(k(1),k(2))=phi2d(k(1),k(2))
1269            phi2d(k(1),k(2))=(p(m)*phi(m+1)+q(m)) * alpha
1270       1                          + (1.-alpha)*phi2do(k(1),k(2))
1271          ii=k(1)
1272          jj=k(2)
1273
1274          call maxmin(phi2d,phimin,phimax,ii,jj)
1275          end if
1276 c         write(21,*)'3 ok'
1277 70       continue
1278          goto 20
1279 c-----------------------------------------------------------------
1280 999    write(5,*)' execution halted while in tdma2d. reason: '
1281        write(5,*)'condition flg3=',flg3,'. a unique solution '
1282        write(5,*)'does not exist for the specified domain.'
1283          stop
1284          end
1285 c-----------------------------------------------------------------
```

Subroutine MAXMIN

```
1286          subroutine maxmin(eta,etamin,etamax,i,j)
1287 c
1288 c....This subroutine determines the maximum and minimum value
1289 c     of the array eta(i,j).
1290 c
1291          real eta(51,51)
1292          if(eta(i,j).gt.etamax) etamax=eta(i,j)
1293          if(eta(i,j).lt.etamin) etamin=eta(i,j)
1294          return
1295          end
1296 c-------------------------------------------------------------------
1297 c
1298 c
```

Subroutine FCA

```
1299          real function fca(x)
1300 c
1301 c....This function subroutine computes the function A(|P|)
1302 c     which is a coefficient in the discretization equation
1303 c     for the general differential equation for convection
1304 c     and diffusion.  This coefficient is defined on pp.92-94
1305 c     of the book "Numerical Heat Transfer and Fluid Flow," by
1306 c     Suhas V. Patankar, McGraw-Hill, 1980.  In this appilication
1307 c     the coefficient A is the function fca and the Peclet
1308 c     number (P) corresponds to the parameter x.  The so-called
1309 c     "power law scheme" is used in this function subroutine to
1310 c     determine the coefficient.
1311 c.....................................................
1312 c
1313          x1=1.-0.1*abs(x)
1314          fca=amax1(0.,x1**5)
1315          return
1316          end
1317 c-------------------------------------------------------------
1318 c
```

Subroutine REPORT

```
      subroutine report(g,x,mp1,n,con,var,x0)
c
c....This subroutine writes the input and output data to files
c    called "outg", "postin", and "rest".  The values of the
c    stream function and heat function are also computed in this
c    subroutine using the finite volume approach.  The files
c    are defined below.
c
c    Output files:
c      outg - the main output file which lists the values of all
c             variables at each grid point
c
c      postin - file which gives the value of the stream-
c               function, heatline, temperature, and pressure
c               for each grid point.  This file is used to
c               create contour plots.
c
c      rest - includes the values of all variables at the final
c             iteration for use in restarting the run
c
c
c.....................................................................
c
      dimension x(n),g(mp1)
      dimension var(n),con(mp1),x0(n)
         integer isid(4)
        character*10 lblt,lblu,lblv,lblx,lbly,lblm,lblp,lbls,lblh
        character*10 lblpc,lblc
      real t(51,51),p(51,51),nulh(51),nurh(51),nubar
      real xdist(51),y(51),qlhvw(51)
      real u(51,51),v(51,51),qt(4),bpc(51,51),xmult(51)
      real gmult(51)
      real appsi(51,51),aepsi(51,51),awpsi(51,51)
      real anpsi(51,51),aspsi(51,51),psi(51,51),bpsi(51,51)
      real aph(51,51),ash(51,51),anh(51,51),aeh(51,51),awh(51,51)
      real bh(51,51),h(51,51),dx(51),dy(51)
      real delx(51),dely(51),ue(51,51),vn(51,51)
      integer flgpsi(51,51),flgh(51,51)
      common /inp/ eps,ra,pr,ar,nx,ny,rf,rft,nrest,xmult,
     1           ntype,ncase,nord,isid,qt,gmult,nbc
c
      common /ans/ qlhvw,u,v,t,p,xdist,y,dx,dy,bpc,tbar
      common /initbk/ init
      common /start/ delx,dely,ue,vn
      common /prop/ cond,dencp,dens
c
      if (init.eq.1) then
         write(6,707) ra,pr,ar,eps,nx,ny,rf,rft
 707    format(t5,'<<<results for:ra=',1x,
```

```
1368      * f7.0,1x,'pr=',1x,f8.3,1x,'aspect ratio=',1x,
1369      * f7.2,/,t5,'eps=',1x,f7.4,2x,'nx=',i2,2x,'ny=',i2,/,
1370      * 'relaxation factors:  velocities=',f7.4,4x,'temp.=',f7.4,
1371      * 4x,'>>>',//)
1372 c
1373        else
1374 c
1375 c
1376 c.............output results
1377 c
1378 c
1379         call gcomp(g,x)
1380 c
1381       g1 = g(1) / gmult(1)
1382       g2 = g(2) / gmult(2)
1383       g3 = g(3) / gmult(3)
1384       g4 = g(4) / gmult(4)
1385 c
1386         write(6,601)ncase
1387 c
1388        if(ncase .eq. 2) go to 32
1389        if(ncase .eq. 3) go to 33
1390        if(ncase .eq. 4) go to 34
1391 31      write(6,634)
1392         write(6,633)
1393         go to 35
1394 32      write(6,635)
1395         write(6,633)
1396         go to 35
1397 33      write(6,634)
1398         write(6,633)
1399         write(6,636)
1400         go to 35
1401 34      write(6,637)
1402         write(6,638)
1403         write(6,636)
1404 c
1405 35      continue
1406 634   format('Objective Function:  Minimal average temperature',
1407      1      ' of LHVW')
1408 635   format('Objective Function:  Minimal maximum temperature ',
1409      1      'of LHVW',//)
1410 637   format('Objective Function:  Maximal total heating rate ',
1411      1      'along LHVW',//)
1412 c
1413 633   format('Constraints:  Fixed total heating rate along lhvw')
1414 636   format(14x,'Maximum temp of lhvw < ','upper bound')
1415 638   format('Constraints: Average temp of lhvw <','upper bound')
1416 c
1417 c
1418 601    format(////,'****************************************',
1419      1 '*********',//,20x,'Optimization Case',i2,//)
```

```
1420 c
1421          if(ntype.eq.1) then
1422         write(6,642)
1423          else
1424         write(6,643)
1425          endif
1426 642      format(///,'nodal heat fluxes used as variables ',
1427     1    'for optimization',//)
1428 643      format(///,'coefficients of polynomial series ',
1429     1    'used as variables for optimization',//)
1430 c
1431       write(6,621)
1432 621    format(/,10x,'Boundary Conditions',//,8x,'Wall',3x,
1433     1 'Condition',7x,'Value',/)
1434         do 100 k=2,4
1435           abc=8htemp
1436           if(isid(k) .eq. 2) abc=8hheat flx
1437         aside =8hTop
1438         if (k .eq. 3) aside =8hRHVW
1439         if (k .eq. 4) aside =8hBottom
1440         write(6,602) aside,abc,qt(k)
1441 100     continue
1442 602     format(5x,a8,2x,a8,2x,f10.2)
1443 c
1444         write(6,603)
1445 603     format(////,20x,'OPTIMAL HEAT FLUX AND TEMPERATURE ',/,
1446     1 17x,'DISTRIBUTION ALONG LEFT-HAND VERTICAL WALL',/,)
1447       write(6,631)
1448 631     format(14x,'y',6x,'Heat Flux',4x,'Temp.',/)
1449         do 101 j=2,ny-1
1450         write(6,604) y(j),qlhvw(j),t(1,j)
1451 101     continue
1452 604     format(10x,3f10.4)
1453 c
1454 c
1455         write(6,605) g1
1456 605     format(////,'Total Heating Rate Along LHVW =',f10.4)
1457          write(6,606) g2
1458 606     format(/,'Average Temp. of LHVW =',f10.4)
1459          write(6,607) g3
1460 607     format(/,'Maximum Temp. of LHVW =',f10.4,//////)
1461 c
1462         write(6,608)
1463 608     format('Values of Variables and Functions from GRG2',
1464     1   ///,11x,'i',8x,'g(i)',7x,'multiplier',/)
1465         do 102 k=1,4
1466         write(6,609) k,g(k),gmult(k)
1467 102     continue
1468 609      format(10x,i2,3x,2f12.4)
1469         nxx=nx
1470         if (ntype .eq. 2) nxx=nord
1471         write(6,610)
```

```
1472 610     format(//,11x,'i',8x,'x(i)',7x,'multiplier',/)
1473         do 103 k=1,nxx
1474         write(6,609)k,x(k),xmult(k)
1475 103     continue
1476         write(6,611)
1477 611     format(/,'*********************************************',
1478      1 '******',////)
1479 c
1480 c
1481 c
1482 c
1483       lblpc= 'pres. corr'
1484       lblp = 'pressure  '
1485       lbls = 'str. func.'
1486       lblh = 'heatlines '
1487       lblc = 'p correct.'
1488         lblu='vel. x-dir'
1489         lblv='vel. y-dir'
1490         lblt='temp.      '
1491         write(6,*) (t(1,j),j=1,ny)
1492         write(6,909)
1493 909     format(//t20,'<<<<the converged solution is>>>>')
1494         write(6,802) count
1495 802   · format(//t10,'iteration no.:',i3)
1496         write(6,*) '-------------------------------------------
1497      *--------------------'
1498              write(6,803)
1499 803     format(/'   the mass source is:')
1500         write(6,809)
1501 809     format('   _____________________')
1502         lblx='x-position'
1503         lbly='y-position'
1504         lblm='mass so.  '
1505 c
1506            do 2 j=ny-1,2,-1
1507             write(6,800) (bpc(i,j),i=2,nx-1)
1508 800     format(1x,10(1pe12.3))
1509 2          continue
1510 632      continue
1511 c
1512 c
1513 c
1514         write(6,1001)
1515 1001    format(3x,'x(i)',t14,'y(j)',t23,'t(i,j)',t33,'u(i,j)'
1516      *          t43,'v(i,j)'t53,'p(i,j)'7x,'i',6x,'j')
1517         write(6,*) '-------------------------------------------
1518      *-----------------------'
1519         do 535 i=1,nx
1520           do 535 j=1,ny
1521       write(6,1000) xdist(i),y(j),t(i,j),u(i,j),v(i,j),p(i,j),i,j
1522 1000    format(1x,f8.4,2x,f8.4,2x,f8.4,2x,f8.4,2x,f8.4,2x,f10.2
1523      *         ,3x,i3,3x,i3)
```

```
1524 535     continue
1525 c
1526
1527       call tab(p,nx,ny,lblp)
1528       call tab(u,nx,ny,lblu)
1529       call tab(v,nx,ny,lblv)
1530       call tab(t,nx,ny,lblt)
1531 c
1532 c.............calculate average temp of LHVW
1533 c.............also calculate max and min temps of LHVW
1534 c
1535        tmin = 9999.
1536        tmax = -9999.
1537          do 1 j = 2, ny-1
1538        if (t(1,j) .gt. tmax) tmax = t(1,j)
1539        if (t(1,j) .lt. tmin) tmin = t(1,j)
1540 1        continue
1541 c
1542       write(6,671) tbar,tmax,tmin
1543 671   format(//,1x,'Average LHVW temperature =',f8.4,//,
1544      1  1x,'Maximum LHVW temperature =',f8.4,//,
1545      2  1x,'Minimum LHVW temperature =',f8.4,//)
1546 c
1547 c
1548 20     continue
1549 c
1550 c
1551 c......calculate stream function
1552 c
1553       do 231 i=2,nx-1
1554       do 231 j=2,ny-1
1555       aepsi(i,j)=dy(j)/delx(i)
1556       awpsi(i,j)=dy(j)/delx(i-1)
1557       anpsi(i,j)=dx(i)/dely(j)
1558       aspsi(i,j)=dx(i)/dely(j-1)
1559 c
1560          fints=dy(j)/2./dely(j-1)
1561          fintn=dy(j)/2./dely(j)
1562          finte=dx(i)/2./delx(i)
1563          fintw=dx(i)/2./delx(i-1)
1564       bbb=fintn*u(i,j+1)-fints*u(i,j-1)+(fints-fintn)*u(i,j)
1565       bb1=finte*v(i+1,j)-fintw*v(i-1,j)+(fintw-finte)*v(i,j)
1566       bpsi(i,j)=-(bbb/dy(j)-bb1/dx(i)) * dx(i)*dy(j)
1567 c
1568 231   appsi(i,j)=aepsi(i,j)+awpsi(i,j)+anpsi(i,j)+aspsi(i,j)
1569 c
1570 c
1571       do 230 i=1,nx
1572       flgpsi(i,1)=1
1573       flgpsi(i,ny)=1
1574       psi(i,1)=0.
1575       psi(i,ny)=0.
```

```
1576         appsi(i,1)=1.
1577         appsi(i,ny)=1.
1578 230    continue
1579        do 232 j=1,ny
1580        flgpsi(1,j)=1
1581        flgpsi(nx,j)=1
1582        psi(1,j)=0.0
1583         appsi(1,j)=1.
1584         appsi(nx,j)=1.
1585 232       psi(nx,j)=0.0
1586 c
1587 c
1588 c
1589        call tdma2d(appsi,anpsi,aspsi,aepsi,awpsi,bpsi,psi,flgpsi,
1590       1 1,nx,1,ny,0.0000001,0,1bls,1.)
1591 cc
1592 c
1593 c
1594 c........ calculate heatlines
1595 c
1596         do 240 i =1,nx
1597           do 240 j=1,ny
1598             aeh(i,j)=0.0
1599             awh(i,j)=0.0
1600             anh(i,j)=0.0
1601             ash(i,j)=0.0
1602             aph(i,j)=0.0
1603             bh(i,j)=0.0
1604 240     continue
1605 c
1606 c
1607 c      determine bulk temperature
1608 c
1609           tsum = 0.0
1610           vsum = 0.0
1611         do 5432 i=1,nx
1612         do 5432 j=1,ny
1613         tsum = tsum + t(i,j) * dy(j) * dx(i)
1614         vsum = vsum + dy(j) * dx(i)
1615 5432    continue
1616 c
1617         tbulk = tsum / vsum
1618         write (6,*) 'Bulk Temp =',tbulk
1619         write (4,*) 'Bulk Temp =',tbulk
1620 c
1621 c
1622 c
1623        flgh(1,1)=1
1624        h(1,1)=0.0
1625          do 241 i=2,nx-1
1626          do 241 j=2,ny-1
1627          aeh(i,j)=dy(j)/delx(i)
```

```
1628          awh(i,j)=dy(j)/delx(i-1)
1629          ash(i,j)=dx(i)/dely(j-1)
1630          anh(i,j)=dx(i)/dely(j)
1631           fints=dy(j)/2./dely(j-1)
1632           fintn=dy(j)/2./dely(j)
1633           finte=dx(i)/2./delx(i)
1634           fintw=dx(i)/2./delx(i-1)
1635         sutp=u(i,j)*(t(i,j) - tbulk) * dencp
1636         sutn=u(i,j+1)*(t(i,j+1) - tbulk) * dencp
1637         suts=u(i,j-1)*(t(i,j-1) - tbulk) * dencp
1638         svte=v(i+1,j)*(t(i+1,j) - tbulk) * dencp
1639         svtw=v(i-1,j)*(t(i-1,j)-tbulk) * dencp
1640         svtp=v(i,j)*(t(i,j) - tbulk) * dencp
1641         bbb=fintn*sutn-fints*suts+(fints-fintn)*sutp
1642         bb1=finte*svte-fintw*svtw+(fintw-finte)*svtp
1643         bh(i,j)=-(bbb/dy(j)-bb1/dx(i)) * dx(i)*dy(j)
1644         aph(i,j)=aeh(i,j)+awh(i,j)+anh(i,j)+ash(i,j)
1645 241       continue
1646 c
1647          do 242 i=3,nx-1
1648          awh(i,1)=1.0
1649          aph(i,1)=1.0
1650          awh(i,ny)=1.0
1651          aph(i,ny)=1.0
1652           ba=cond*dx(i-1)/2.*(t(i-1,2)-t(i-1,1))/dely(1)
1653           bb=cond*dx(i)/2.*(t(i,2)-t(i,1))/dely(1)
1654           bh(i,1)=ba+bb
1655           bc=cond*dx(i-1)/2.*(t(i-1,ny)-t(i-1,ny-1))
1656           bd=cond*dx(i)/2.*(t(i,ny)-t(i,ny-1))
1657           bh(i,ny)=(bc+bd)/dely(ny-1)
1658 242            continue
1659 c
1660          do 243 j=3,ny-1
1661          ash(1,j)=1.0
1662          aph(1,j)=1.0
1663          ash(nx,j)=1.0
1664          aph(nx,j)=1.0
1665           ba=cond*dy(j-1)/2.*(t(2,j-1)-t(1,j-1))/delx(1)
1666           bb=cond*dy(j)/2.*(t(2,j)-t(1,j))/delx(1)
1667               bh(1,j)=-(ba+bb)
1668           bc=cond*dy(j-1)/2.*(t(nx,j-1)-t(nx-1,j-1))
1669           bd=cond*dy(j)/2.*(t(nx,j)-t(nx-1,j))
1670           bh(nx,j)=-(bc+bd)/delx(nx-1)
1671 243            continue
1672 c
1673          awh(2,1)=1.0
1674          aph(2,1)=1.0
1675          bh(2,1)=(t(2,2)-t(2,1))/dely(1)*cond*dx(2)/2.
1676          awh(nx,1)=1.0
1677          aph(nx,1)=1.0
1678          bh(nx,1)=(t(nx-1,2)-t(nx-1,1))/dely(1)*cond*dx(nx-1)
1679       1                  /2.
```

```
1680          awh(2,ny)=1.0
1681          aph(2,ny)=1.0
1682          bh(2,ny)=(t(2,ny)-t(2,ny-1))/dely(ny-1)*cond*dx(2)
1683       1                  /2.
1684          awh(nx,ny)=1.0
1685          aph(nx,ny)=1.0
1686          bh(nx,ny)=(t(nx-1,ny)-t(nx-1,ny-1))/dely(ny-1)*cond
1687       1                   *dx(nx-1)/2.
1688          ash(1,2)=1.0
1689          aph(1,2)=1.0
1690          bh(1,2)=-(t(2,2)-t(1,2))/delx(1)*cond*dy(2)/2.
1691          ash(1,ny)=1.0
1692          aph(1,ny)=1.0
1693          bh(1,ny)=-(t(2,ny-1)-t(1,ny-1))/delx(1)*cond*dy(ny-1)
1694       1                  /2.
1695          ash(nx,2)=1.0
1696          aph(nx,2)=1.0
1697          bh(nx,2)=-(t(nx,2)-t(nx-1,2))/delx(nx-1)*cond*dy(2)
1698       1                  /2.
1699  c
1700  c
1701  c.....................................
1702  c
1703          call tdma2d(aph,anh,ash,aeh,awh,bh,h,flgh,1,nx,1,ny,
1704       1  1.e-7,0,lblh,1.0)
1705  c.....................................
1706  c
1707  c         create file for contour plotting
1708  c
1709          write(15,616)nx,ny,ra,pr,ar,ncase,nbc
1710  616     format (1x,2i3,3(1pe14.5),2i3)
1711  c
1712        do 236 i=1,nx
1713        do 236 j=1,ny
1714        write(15,615)xdist(i),y(j),u(i,j),v(i,j),psi(i,j),h(i,j),
1715       1             t(i,j),p(i,j)
1716  236   continue
1717  615   format(1x,8(1pe14.5))
1718  c
1719  c
1720  c
1721  c..... nusselt number calculations .....
1722          write(6,6620)
1723          do 776 j=2,ny-1
1724          nurh(j)=(t(nx-1,j)-t(nx,j))/delx(nx-1)/tbar * ar
1725           nulh(j) = qlhvw(j)/t(1,j) * ar
1726  c
1727          write(6,6621)j,y(j),nulh(j),nurh(j)
1728  776     continue
1729  6620  format(//,5x,'Local Nusselt Number Distribution Along ',
1730       1'Vertical Walls',/,1x,'Node    y     Nu LHVW    Nu RHVW',/)
1731  6621    format(1x,i5,f10.4,2f10.4)
```

```
1732 c
1733           nubar=ar/tbar
1734           write(6,6623)nubar
1735 6623      format(///,1x,'AVERAGE NUSSELT NUMBER =',f10.4,///)
1736 c.....-....    create restart file  .................
1737 c
1738        write(13,*)ra,pr,ar,nx,ny
1739         do 7020 i=1,nx
1740         do 7020 j=1,ny
1741          write(13,7601)xdist(i),y(j),ue(i,j),vn(i,j),t(i,j),p(i,j)
1742 7020    continue
1743 7601    format(1x,6(1pe16.8))
1744 c.................................................
1745 c
1746 c
1747 c
1748        end if
1749 c
1750        return
1751        end
1752 c-------------------------------------------------------------
```

Input File "OPTIN"

The input file called "OPTIN" contains the speciification of the optimization problem number/case (i.e., Case 1, 2, or 3 for the three variations of optimization problem number 1 or optimization problem number 2 which is designated as Case 4 for the purposes of this input file), type of variables used to define the heat flux along the left-hand vertical wall (either discrete values at all grid points along the wall or coefficints of a polynomial), the order of the polynomial that defines the heat flux if that type of heat flux profile is being used, the thermal boundary conditions on each wall (either fixed temperature or fixed heat flux), the perturbation size to be used for computing the gradient, scaling factors for the functions, the number of variables and the scaling factors for each of the variables, and the standard input information required for GRG2. The standard input data required for GRG2 is explained in the GRG2 Users Manual (Lasdon and Waren, 1986). A typical "OPTIN" input file is listed below.

```
1,1,1
2,2,1,2
1.,0.,0.,0.
1.e-2
10.,10.,10.,10.
13
1.,10.,10.,10.,10.,10.,10.,10.,10.,10.,10.,10.,1.
   13    4
name heat flux distribution that minimizes temp of lhvw
rows
 e   1      10.
 o   2
 l   3      100.
 g   4      0.0
end
bounds
 e   1      0.0
 g   2  12   0.0
 e  13      0.0
end
```

```
initial
separate
     2   12   10.
end
print
ipr       3
end
met
fdc
end
eps
epnewt     1.e-6
epinit      1.e-4
eptop      1.e-5
end
go
```

Input File "GRID"

The input file called "GRID" is required to define the coordinates of the calculation grid points to be used for determining the velocity components, temperature, and pressure for the natural convection problem. The first line of this file contains the number of grid points in the x-direction (nx), number of grid points in the y-direction (ny), and aspect ratio of the enclosure (A). The group of lines following the first line contains the x coordinates of the grid points in the rectangular grid. The next group of lines contain the x-direction thickness of each finite volume. The final two groups of lines contain the y coordinates of the grid points and y-direction thicknesses of the finite volumes, respectively.

```
   13  13   1.0000
     0.              0.287827e-01    0.921048e-01    0.168091e+00
0.259275e+00
     0.368695e+00    0.500000e+00    0.631305e+00    0.740725e+00
0.831909e+00
     0.907895e+00    0.971217e+00    0.100000e+01
     0.              0.575655e-01    0.690786e-01    0.828943e-01
0.994732e-01
     0.119368e+00    0.143241e+00    0.119368e+00    0.994732e-01
0.828943e-01
     0.690786e-01    0.575655e-01    0.
     0.              0.287827e-01    0.921048e-01    0.168091e+00
0.259275e+00
     0.368695e+00    0.500000e+00    0.631305e+00    0.740725e+00
0.831909e+00
     0.907895e+00    0.971217e+00    0.100000e+01
     0.              0.575655e-01    0.690786e-01    0.828943e-01
0.994732e-01
     0.119368e+00    0.143241e+00    0.119368e+00    0.994732e-01
0.828943e-01
     0.690786e-01    0.575655e-01    0.
```

Input File "CASE"

The input file called "CASE" is required for restarting a run or to provide an initial guess for all "primitive" variables calculated in the SIMPLER algorithm. The first line contains the Rayleigh number, Prandtl number, enclosure aspect ratio, number of x-direction grid points, and number of y-direction grid points for this input file. The file is formatted so that, following the first line, each line contains the x and y coordinates, x and y-direction velocity components, temperature, and pressure at a grid point. (This grid does not necessarily have to be the same as the calculation grid defined in the input file "GRID". If the grid is different, the values of the variables will be interpolated from the values at the grid points in the "CASE" file to the grid locations defined in the "GRID" file.) The final step in an optimization run is the creation of an output file called "REST" which is a file that can be renamed "CASE" and used for the initial guess in a future run. A typical example of a "CASE" input file is listed below.

```
 100000.0 , 1.0 , 1.0 , 13 , 13
   0.              0.              0.              0.
1.96029678e-01  0.
   0.              2.87827000e-02  0.              0.
2.24812378e-01  0.
   0.              9.21048000e-02  0.              0.
2.23267400e-01  0.
   0.              1.68091000e-01  0.              0.
2.24695581e-01  0.
   0.              2.59275000e-01  0.              0.
2.31444976e-01  0.
   0.              3.68695000e-01  0.              0.
2.44787162e-01  0.
   0.              5.00000000e-01  0.              0.
2.65779638e-01  0.
   0.              6.31305000e-01  0.              0.
2.90552492e-01  0.
   0.              7.40725000e-01  0.              0.
3.22140079e-01  0.
   0.              8.31909000e-01  0.              0.
3.63420744e-01  0.
```

```
   0.              9.07895000e-01  0.              0.
4.04249331e-01  0.
   0.              9.71217000e-01  0.              0.
4.25849722e-01  0.
   0.              1.00000000e+00  0.              0.
3.97067022e-01  0.
   2.87827000e-02  0.              0.              0.
1.96029677e-01  0.
   2.87827000e-02  2.87827000e-02 -3.82642943e+00  3.82642948e+00
1.96029677e-01 -6.41394210e+03
   2.87827000e-02  9.21048000e-02 -4.82869521e+00  9.62086385e+00
1.94484700e-01 -5.45995956e+03
   2.87827000e-02  1.68091000e-01 -3.79002547e+00  1.50784994e+01
1.95912881e-01 -4.62933628e+03
   2.87827000e-02  2.59275000e-01 -2.27386485e+00  1.90077388e+01
2.02662276e-01 -3.83711066e+03
   2.87827000e-02  3.68695000e-01 -8.52378757e-01  2.07752343e+01
2.16004462e-01 -2.90410512e+03
   2.87827000e-02  5.00000000e-01  5.84311236e-03  2.07606953e+01
2.36996938e-01 -1.55486036e+03
   2.87827000e-02  6.31305000e-01  1.22718321e+00  1.82160047e+01
2.61769791e-01  7.43614789e+02
   2.87827000e-02  7.40725000e-01  2.19990729e+00  1.44145647e+01
2.93357379e-01  3.17162409e+03
   2.87827000e-02  8.31909000e-01  3.32461777e+00  9.62711666e+00
3.34638044e-01  5.71324467e+03
   2.87827000e-02  9.07895000e-01  4.63145627e+00  4.06936970e+00
3.75466631e-01  8.31369418e+03
   2.87827000e-02  9.71217000e-01  4.06937002e+00  0.
3.97067022e-01  1.08724481e+04
   2.87827000e-02  1.00000000e+00  0.              0.
3.97067022e-01  0.
   9.21048000e-02  0.              0.              0.
1.41050004e-01  0.
   9.21048000e-02  2.87827000e-02 -7.20239374e+00  2.81330366e+00
1.41050004e-01 -6.27931063e+03
   9.21048000e-02  9.21048000e-02 -1.12428483e+01  9.22745686e+00
1.38155666e-01 -5.47832277e+03
   9.21048000e-02  1.68091000e-01 -1.05635189e+01  1.73556471e+01
1.39316393e-01 -4.70061517e+03
   9.21048000e-02  2.59275000e-01 -7.61342298e+00  2.50446122e+01
1.47086336e-01 -3.90846189e+03
   9.21048000e-02  3.68695000e-01 -3.80150776e+00  3.01407150e+01
1.62065588e-01 -2.95341085e+03
   9.21048000e-02  5.00000000e-01 -4.04328180e-01  3.09912440e+01
1.84613246e-01 -1.57029140e+03
   9.21048000e-02  6.31305000e-01  3.29635647e+00  2.74157073e+01
2.10462576e-01  7.33648017e+02
   9.21048000e-02  7.40725000e-01  6.69755338e+00  2.09390959e+01
2.42989449e-01  3.17594129e+03
   9.21048000e-02  8.31909000e-01  1.02570863e+01  1.26201361e+01
2.86281821e-01  5.72118736e+03
```

```
   9.21048000e-02  9.07895000e-01  1.28740858e+01  4.37750718e+00
3.30224927e-01  8.28462477e+03
   9.21048000e-02  9.71217000e-01  9.32237917e+00  0.
3.52858337e-01  1.07131457e+04
   9.21048000e-02  1.00000000e+00  0.              0.
3.52858337e-01  0.
   1.68091000e-01  0.              0.              0.
9.91521182e-02  0.
   1.68091000e-01  2.87827000e-02 -7.77895017e+00  4.00386580e-01
9.91521182e-02 -5.99787183e+03
   1.68091000e-01  9.21048000e-02 -1.47037595e+01  3.28448009e+00
9.63436268e-02 -5.39536066e+03
   1.68091000e-01  1.68091000e-01 -1.59802168e+01  8.70117811e+00
9.75057135e-02 -4.72792687e+03
   1.68091000e-01  2.59275000e-01 -1.31401791e+01  1.53332881e+01
1.05850265e-01 -3.97907472e+03
   1.68091000e-01  3.68695000e-01 -7.69280713e+00  2.09367688e+01
1.22243792e-01 -3.02736374e+03
   1.68091000e-01  5.00000000e-01 -1.32839130e+00  2.25335458e+01
1.47201034e-01 -1.62278364e+03
   1.68091000e-01  6.31305000e-01  5.19357156e+00  1.98015510e+01
1.76028476e-01  6.58812983e+02
   1.68091000e-01  7.40725000e-01  1.13931359e+01  1.41668497e+01
2.12139005e-01  3.08342336e+03
   1.68091000e-01  8.31909000e-01  1.71114089e+01  7.31252731e+00
2.58248579e-01  5.58856890e+03
   1.68091000e-01  9.07895000e-01  1.94135987e+01  1.86293252e+00
3.00746240e-01  8.05326761e+03
   1.68091000e-01  9.71217000e-01  1.20050020e+01  0.
3.19827722e-01  1.02927330e+04
   1.68091000e-01  1.00000000e+00  0.              0.
3.19827722e-01  0.
   2.59275000e-01  0.              0.              0.
7.61806143e-02  0.
   2.59275000e-01  2.87827000e-02 -7.16222607e+00 -3.56900379e-01
7.61806143e-02 -5.72881839e+03
   2.59275000e-01  9.21048000e-02 -1.57723133e+01  3.85150769e-01
7.52808438e-02 -5.26868348e+03
   2.59275000e-01  1.68091000e-01 -1.88721417e+01  2.79508714e+00
7.81753422e-02 -4.70732067e+03
   2.59275000e-01  2.59275000e-01 -1.65182188e+01  6.17312671e+00
8.78010395e-02 -4.01534870e+03
   2.59275000e-01  3.68695000e-01 -1.02150913e+01  9.19987141e+00
1.05073630e-01 -3.08360361e+03
   2.59275000e-01  5.00000000e-01 -1.82674005e+00  9.91749109e+00
1.31540692e-01 -1.68136778e+03
   2.59275000e-01  6.31305000e-01  6.69008075e+00  8.12167713e+00
1.64082073e-01  5.66365998e+02
   2.59275000e-01  7.40725000e-01  1.47371051e+01  4.77770767e+00
2.03720486e-01  2.95090105e+03
   2.59275000e-01  8.31909000e-01  2.11112979e+01  1.44446842e+00
2.48196786e-01  5.38609001e+03
```

```
   2.59275000e-01  9.07895000e-01  2.17331311e+01 -1.66317217e-01
2.82643632e-01  7.71922591e+03
   2.59275000e-01  9.71217000e-01  1.17176063e+01  0.
2.95593523e-01  9.77245438e+03
   2.59275000e-01  1.00000000e+00  0.              0.
2.95593523e-01  0.
   3.68695000e-01  0.              0.              0.
6.48844411e-02  0.
   3.68695000e-01  2.87827000e-02 -7.22666338e+00  3.10751280e-02
6.48844411e-02 -5.52078863e+03
   3.68695000e-01  9.21048000e-02 -1.68627477e+01  6.62112681e-01
6.56131720e-02 -5.13406856e+03
   3.68695000e-01  1.68091000e-01 -2.06469434e+01  1.89461168e+00
7.07532356e-02 -4.64961125e+03
   3.68695000e-01  2.59275000e-01 -1.79907077e+01  3.12168394e+00
8.29667347e-02 -4.01255410e+03
   3.68695000e-01  3.68695000e-01 -1.06572664e+01  3.56385865e+00
1.02613750e-01 -3.10510640e+03
   3.68695000e-01  5.00000000e-01 -1.07155411e+00  2.65763863e+00
1.31081409e-01 -1.71186161e+03
   3.68695000e-01  6.31305000e-01  8.19122204e+00  1.15649680e+00
1.66857992e-01  5.15887706e+02
   3.68695000e-01  7.40725000e-01  1.66319769e+01 -4.22561190e-01
2.06293119e-01  2.85979701e+03
   3.68695000e-01  8.31909000e-01  2.22449072e+01 -1.20978841e+00
2.43906352e-01  5.20559856e+03
   3.68695000e-01  9.07895000e-01  2.09410617e+01 -7.51415278e-01
2.68593115e-01  7.39549288e+03
   3.68695000e-01  9.71217000e-01  1.01594698e+01  0.
2.76416893e-01  9.29365808e+03
   3.68695000e-01  1.00000000e+00  0.              0.
2.76416893e-01  0.
   5.00000000e-01  0.              0.              0.
5.70815346e-02  0.
   5.00000000e-01  2.87827000e-02 -8.49798005e+00  5.10915128e-01
5.70815346e-02 -5.30700345e+03
   5.00000000e-01  9.21048000e-02 -1.88935312e+01  1.49026946e+00
5.88733050e-02 -4.96995269e+03
   5.00000000e-01  1.68091000e-01 -2.21151615e+01  2.33993475e+00
6.63308052e-02 -4.55483341e+03
   5.00000000e-01  2.59275000e-01 -1.84672329e+01  2.67085576e+00
8.18492754e-02 -3.98512278e+03
   5.00000000e-01  3.68695000e-01 -1.01801566e+01  2.27326221e+00
1.04664729e-01 -3.11717377e+03
   5.00000000e-01  5.00000000e-01  2.55483489e-01  9.46223987e-01
1.35099612e-01 -1.73203558e+03
   5.00000000e-01  6.31305000e-01  9.83737197e+00 -4.25573860e-01
1.71720501e-01  4.97784376e+02
   5.00000000e-01  7.40725000e-01  1.77224407e+01 -1.18284273e+00
2.07911263e-01  2.80615442e+03
   5.00000000e-01  8.31909000e-01  2.21239075e+01 -1.11281947e+00
2.37842841e-01  5.05623147e+03
```

```
   5.00000000e-01  9.07895000e-01  1.95943625e+01 -4.63367694e-01
2.54859297e-01  7.11337301e+03
   5.00000000e-01  9.71217000e-01  9.00646644e+00  0.
2.59548738e-01  8.88903313e+03
   5.00000000e-01  1.00000000e+00  0.              0.
2.59548738e-01  0.
   6.31305000e-01  0.              0.              0.
4.87927231e-02  0.
   6.31305000e-01  2.87827000e-02 -9.47702347e+00  4.72146105e-01
4.87927231e-02 -5.01081704e+03
   6.31305000e-01  9.21048000e-02 -1.93260956e+01  7.22472455e-01
5.17656372e-02 -4.73642079e+03
   6.31305000e-01  1.68091000e-01 -2.13713461e+01  2.05934862e-01
6.24329216e-02 -4.40564574e+03
   6.31305000e-01  2.59275000e-01 -1.74618722e+01 -6.31864746e-01
8.24002734e-02 -3.92420239e+03
   6.31305000e-01  3.68695000e-01 -9.94218198e+00 -8.69839732e-01
1.08778283e-01 -3.11829652e+03
   6.31305000e-01  5.00000000e-01 -2.29309650e-01 -2.88090921e-01
1.39759190e-01 -1.75495286e+03
   6.31305000e-01  6.31305000e-01  9.94699646e+00 -3.97715814e-01
1.74485905e-01  4.77022324e+02
   6.31305000e-01  7.40725000e-01  1.75650545e+01 -2.66560990e-01
2.06470089e-01  2.75788404e+03
   6.31305000e-01  8.31909000e-01  2.16868756e+01  3.69328564e-02
2.30969084e-01  4.93041662e+03
   6.31305000e-01  9.07895000e-01  1.94202762e+01  1.37677225e-01
2.43631323e-01  6.88489604e+03
   6.31305000e-01  9.71217000e-01  9.29195481e+00  0.
2.46597184e-01  8.57129581e+03
   6.31305000e-01  1.00000000e+00  0.              0.
2.46597184e-01  0.
   7.40725000e-01  0.              0.              0.
3.99300624e-02  0.
   7.40725000e-01  2.87827000e-02 -8.54799342e+00 -5.37632932e-01
3.99300624e-02 -4.66248233e+03
   7.40725000e-01  9.21048000e-02 -1.60673507e+01 -2.80064979e+00
4.42285775e-02 -4.46416902e+03
   7.40725000e-01  1.68091000e-01 -1.71163321e+01 -6.34649331e+00
5.78097052e-02 -4.21062387e+03
   7.40725000e-01  2.59275000e-01 -1.42635088e+01 -9.54485680e+00
8.07943779e-02 -3.80182674e+03
   7.40725000e-01  3.68695000e-01 -9.26289597e+00 -1.03600014e+01
1.08673203e-01 -3.05622632e+03
   7.40725000e-01  5.00000000e-01 -2.46817630e+00 -7.13604293e+00
1.39449919e-01 -1.73590384e+03
   7.40725000e-01  6.31305000e-01  7.09089354e+00 -3.70871513e+00
1.74201458e-01  4.74725519e+02
   7.40725000e-01  7.40725000e-01  1.47868830e+01 -9.30543738e-01
2.02777663e-01  2.73282751e+03
   7.40725000e-01  8.31909000e-01  1.96955400e+01  7.28901936e-01
2.22958463e-01  4.83773419e+03
```

```
   7.40725000e-01  9.07895000e-01  1.93219215e+01  7.97203956e-01
2.32230602e-01  6.68694433e+03
   7.40725000e-01  9.71217000e-01  1.06695238e+01  0.
2.33192081e-01  8.27077290e+03
   7.40725000e-01  1.00000000e+00  0.              0.
2.33192081e-01  0.
   8.31909000e-01  0.              0.              0.
2.94511369e-02  0.
   8.31909000e-01  2.87827000e-02 -5.28516847e+00 -2.26585109e+00
2.94511369e-02 -4.34310768e+03
   8.31909000e-01  9.21048000e-02 -9.46912604e+00 -7.76437279e+00
3.42067633e-02 -4.21967166e+03
   8.31909000e-01  1.68091000e-01 -1.00598454e+01 -1.48208595e+01
4.78095348e-02 -4.01568502e+03
   8.31909000e-01  2.59275000e-01 -8.94438392e+00 -2.12038120e+01
6.90921703e-02 -3.64295304e+03
   8.31909000e-01  3.68695000e-01 -6.87906883e+00 -2.46365292e+01
9.40899873e-02 -2.92987177e+03
   8.31909000e-01  5.00000000e-01 -3.73326233e+00 -2.24504660e+01
1.22393424e-01 -1.63151309e+03
   8.31909000e-01  6.31305000e-01  2.38708896e+00 -1.56769757e+01
1.57048858e-01  5.43061803e+02
   8.31909000e-01  7.40725000e-01  8.54312573e+00 -8.18446406e+00
1.84900865e-01  2.76976707e+03
   8.31909000e-01  8.31909000e-01  1.38843545e+01 -2.37327841e+00
2.03200390e-01  4.79936990e+03
   8.31909000e-01  9.07895000e-01  1.61456481e+01  2.73616867e-01
2.09726585e-01  6.50067737e+03
   8.31909000e-01  9.71217000e-01  1.10635322e+01  0.
2.07435137e-01  7.88457532e+03
   8.31909000e-01  1.00000000e+00  0.              0.
2.07435137e-01  0.
   9.07895000e-01  0.              0.              0.
1.74114336e-02  0.
   9.07895000e-01  2.87827000e-02 -1.60707743e+00 -3.06507576e+00
1.74114336e-02 -4.16507781e+03
   9.07895000e-01  9.21048000e-02 -2.90165959e+00 -9.63254208e+00
2.06509164e-02 -4.09320952e+03
   9.07895000e-01  1.68091000e-01 -3.13168328e+00 -1.79463345e+01
2.96519031e-02 -3.91049041e+03
   9.07895000e-01  2.59275000e-01 -3.06251710e+00 -2.64162241e+01
4.36862398e-02 -3.54050311e+03
   9.07895000e-01  3.68695000e-01 -2.84449774e+00 -3.33879734e+01
6.06839119e-02 -2.82375022e+03
   9.07895000e-01  5.00000000e-01 -2.32775785e+00 -3.63024196e+01
8.10085752e-02 -1.49721721e+03
   9.07895000e-01  6.31305000e-01 -2.99148383e-01 -3.16605944e+01
1.07376464e-01  6.75044896e+02
   9.07895000e-01  7.40725000e-01  2.20565725e+00 -2.25346383e+01
1.30175750e-01  2.88852495e+03
   9.07895000e-01  8.31909000e-01  5.14996887e+00 -1.20533780e+01
1.46487817e-01  4.85177185e+03
```

```
   9.07895000e-01  9.07895000e-01  7.64922397e+00 -3.55695376e+00
1.52515157e-01  6.37646632e+03
   9.07895000e-01  9.71217000e-01  6.79518787e+00  0.
1.48887261e-01  7.42499908e+03
   9.07895000e-01  1.00000000e+00  0.              0.
1.48887261e-01  0.
   9.71217000e-01  0.              0.              0.
5.57301079e-03  0.
   9.71217000e-01  2.87827000e-02  0.             -1.60707739e+00
5.57301079e-03 -4.14644338e+03
   9.71217000e-01  9.21048000e-02  0.             -5.08906883e+00
6.53536757e-03 -4.10326261e+03
   9.71217000e-01  1.68091000e-01  0.             -9.59869158e+00
9.24680583e-03 -3.93026928e+03
   9.71217000e-01  2.59275000e-01  0.             -1.48907219e+01
1.36070581e-02 -3.55090592e+03
   9.71217000e-01  3.68695000e-01  0.             -2.07890811e+01
1.91245821e-02 -2.81430677e+03
   9.71217000e-01  5.00000000e-01  0.             -2.65812718e+01
2.60996591e-02 -1.44561590e+03
   9.71217000e-01  6.31305000e-01  0.             -2.72015867e+01
3.57029461e-02  7.60577136e+02
   9.71217000e-01  7.40725000e-01  0.             -2.33902102e+01
4.45940305e-02  3.00872610e+03
   9.71217000e-01  8.31909000e-01  0.             -1.59742567e+01
5.16394213e-02  4.97556119e+03
   9.71217000e-01  9.07895000e-01  0.             -6.79518791e+00
5.49608539e-02  6.40715314e+03
   9.71217000e-01  9.71217000e-01  0.              0.
5.37536621e-02  7.15392096e+03
   9.71217000e-01  1.00000000e+00  0.              0.
5.37536621e-02  0.
   1.00000000e+00  0.              0.              0.              0.
           0.
   1.00000000e+00  2.87827000e-02  0.              0.              0.
           0.
   1.00000000e+00  9.21048000e-02  0.              0.              0.
           0.
   1.00000000e+00  1.68091000e-01  0.              0.              0.
           0.
   1.00000000e+00  2.59275000e-01  0.              0.              0.
           0.
   1.00000000e+00  3.68695000e-01  0.              0.              0.
           0.
   1.00000000e+00  5.00000000e-01  0.              0.              0.
           0.
   1.00000000e+00  6.31305000e-01  0.              0.              0.
           0.
   1.00000000e+00  7.40725000e-01  0.              0.              0.
           0.
   1.00000000e+00  8.31909000e-01  0.              0.              0.
           0.
```

```
1.00000000e+00  9.07895000e-01  0.              0.              0.
        0.
1.00000000e+00  9.71217000e-01  0.              0.              0.
        0.
1.00000000e+00  1.00000000e+00  0.              0.              0.
        0.
```

Interactive Input Required To Run The Optimization Program

The following is a typical example of the type of information that must be input to the computer in an interactive fashion to run the optimization program. The prompts, i.e. statements printed on the terminal by the computer, are shown in italics.

restart=1, no restart=0
1
input eps,ra,pr
1.e-7,1.e5,1.
input rf,rft
0.55,0.45

APPENDIX C

CONTOUR PLOTS

Appendix C consists of streamline, heatline, and isotherm contour plots and optimal heat flux distribution plots for each set of parameters specified in Table 3-5. These sensitivity studies examine the effects of varying the modified Rayleigh number, the Prandtl number, the aspect ratio of the rectangular enclosure, and the type of thermal boundary conditions.

MODIFIED RAYLEIGH NUMBER
SENSITIVITY STUDIES

Ra^* varied from 10^3 to 10^6

Pr = 1

A = 1

Thermal Boundary Condition Type 1

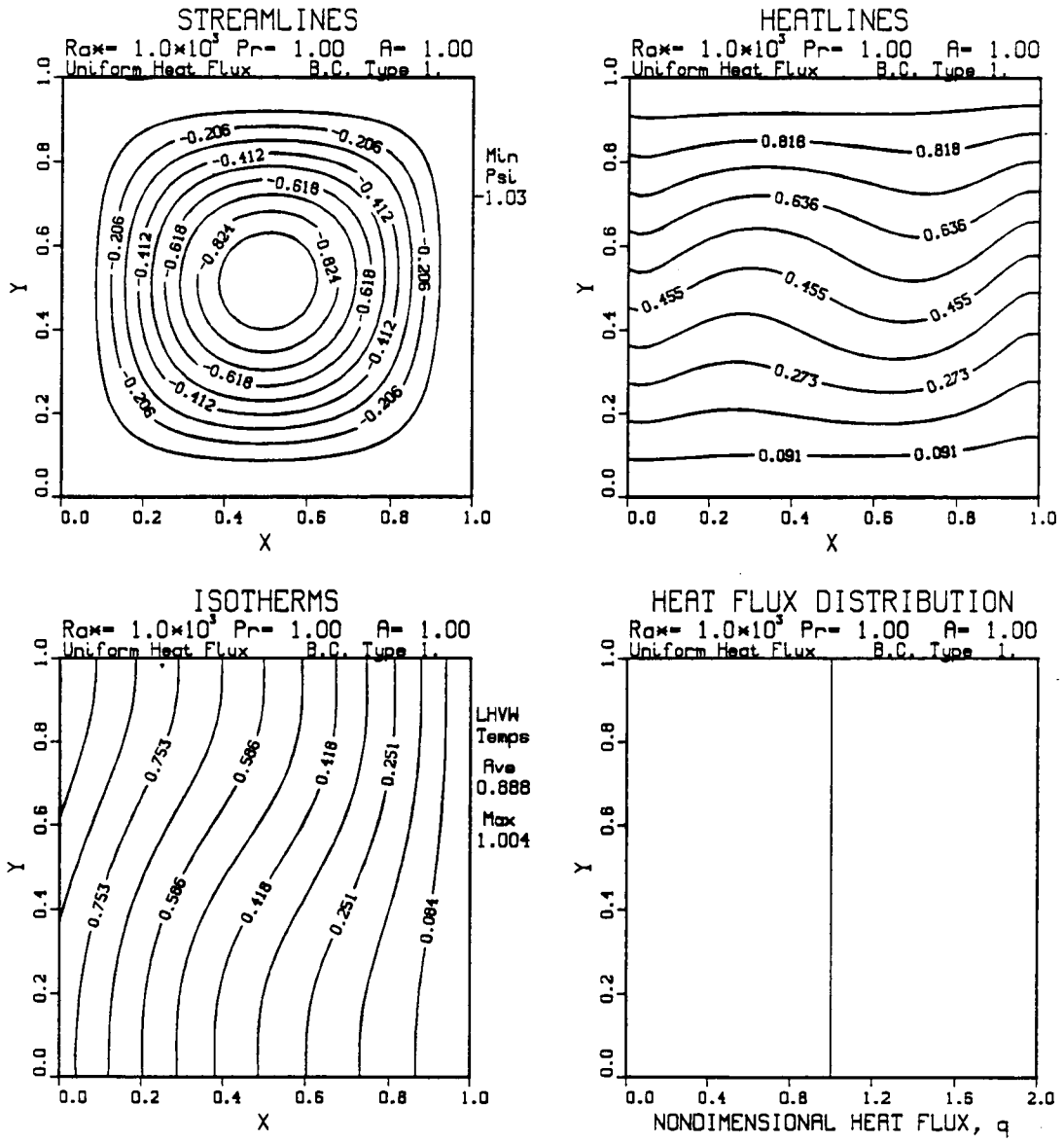


Figure C-1. Summary of results from modified Rayleigh number sensitivity studies for uniform heat flux distribution with $Ra^* = 10^3$

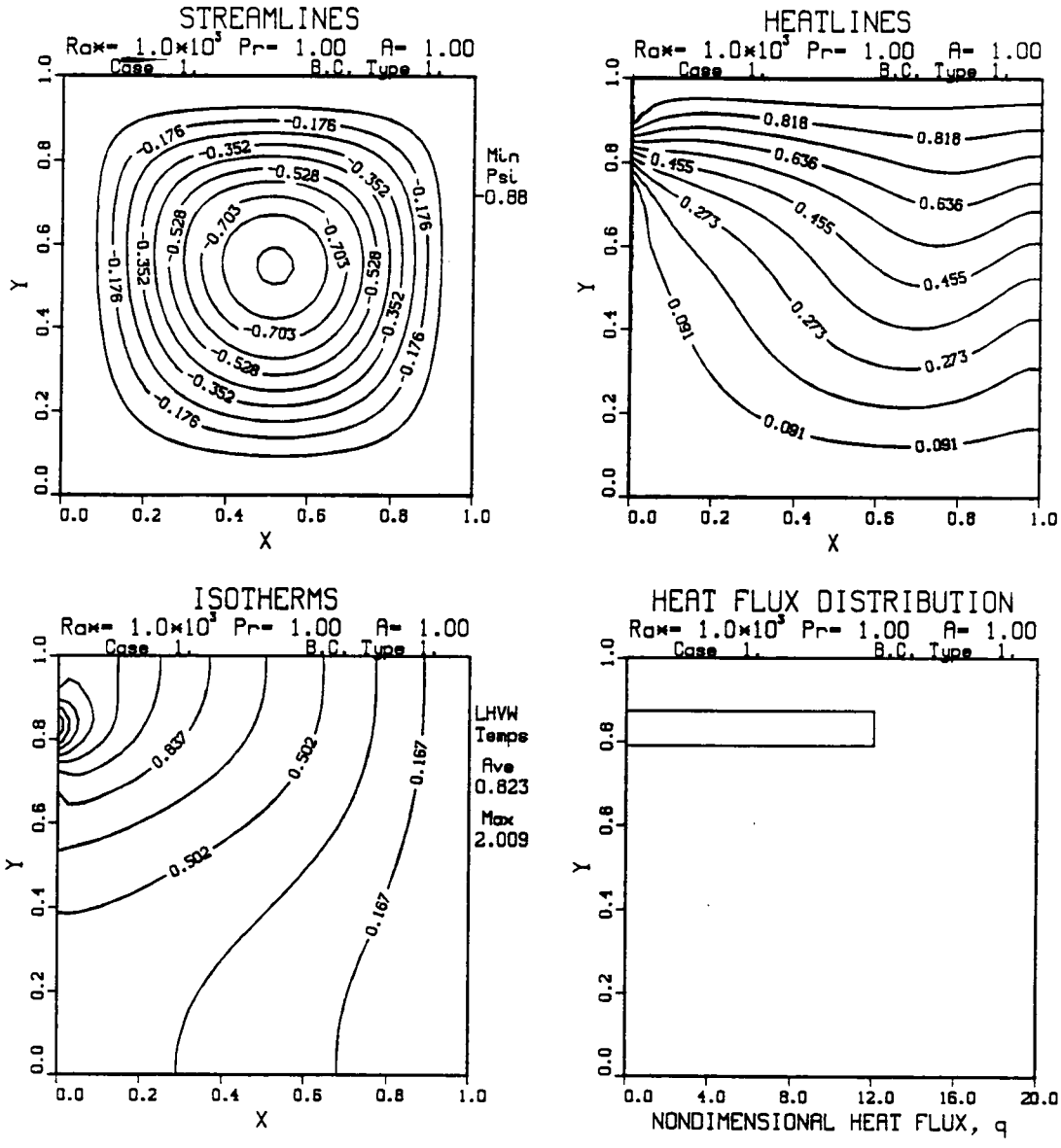


Figure C-2. Summary of results from modified Rayleigh number senstivity studies for Case 1 type optimization with $Ra^*=10^3$

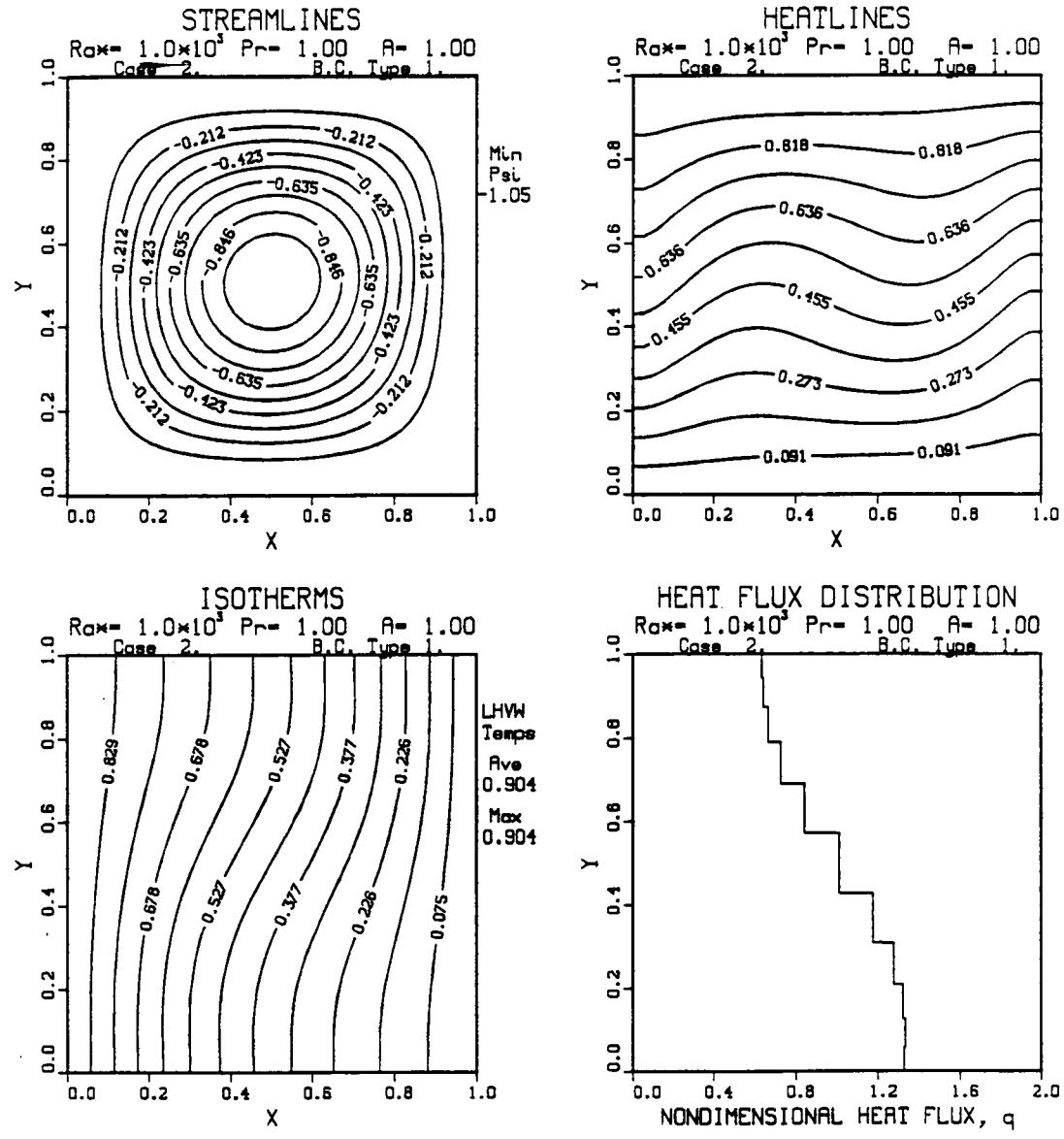


Figure C-3. Summary of results from modified Rayleigh number sensitivity studies for Case 2 type optimization with $Ra^*=10^3$

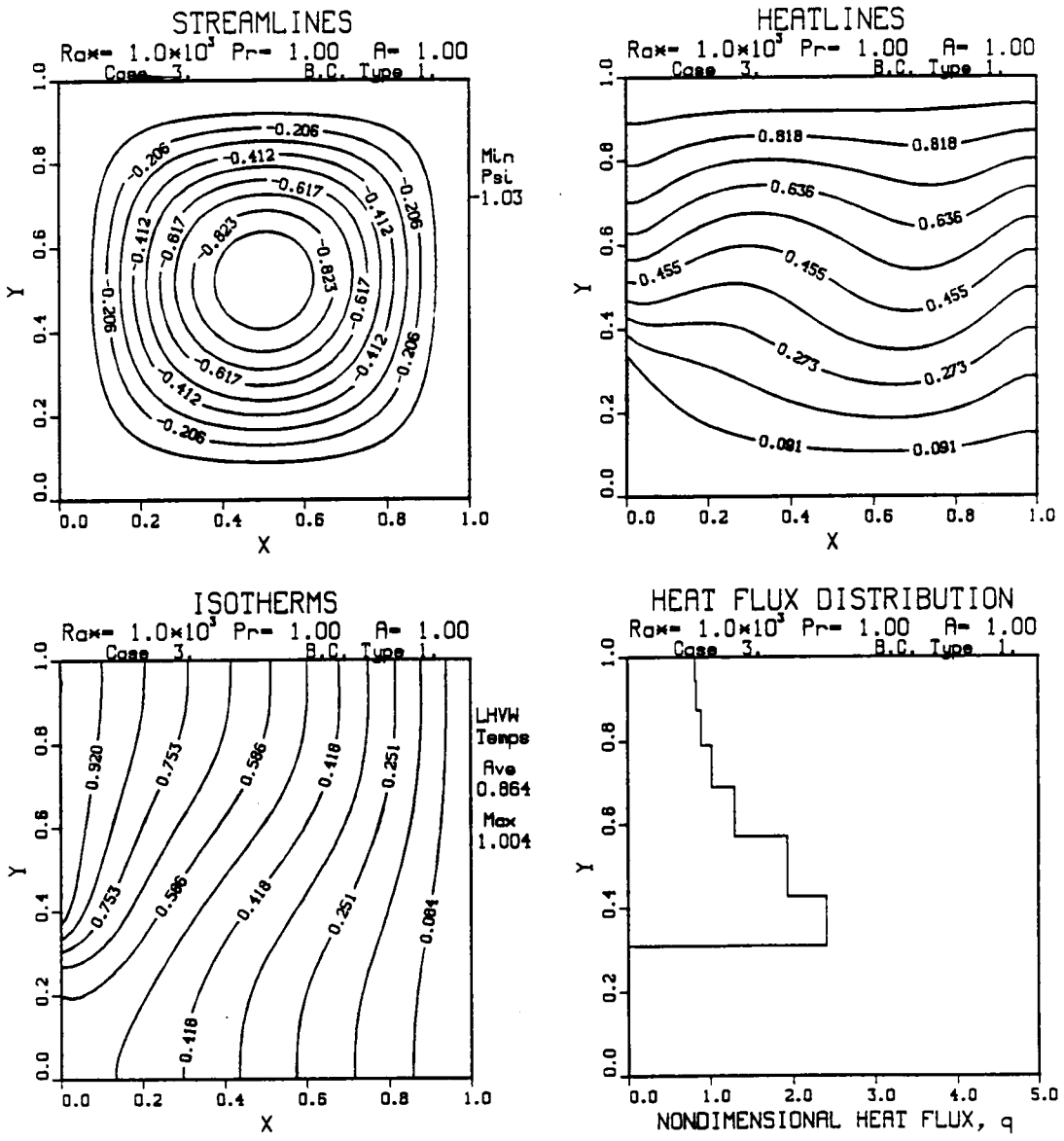


Figure C-4. Summary of results from modified Rayleigh number sensitivity studies for Case 3 type optimization with $Ra^*=10^3$

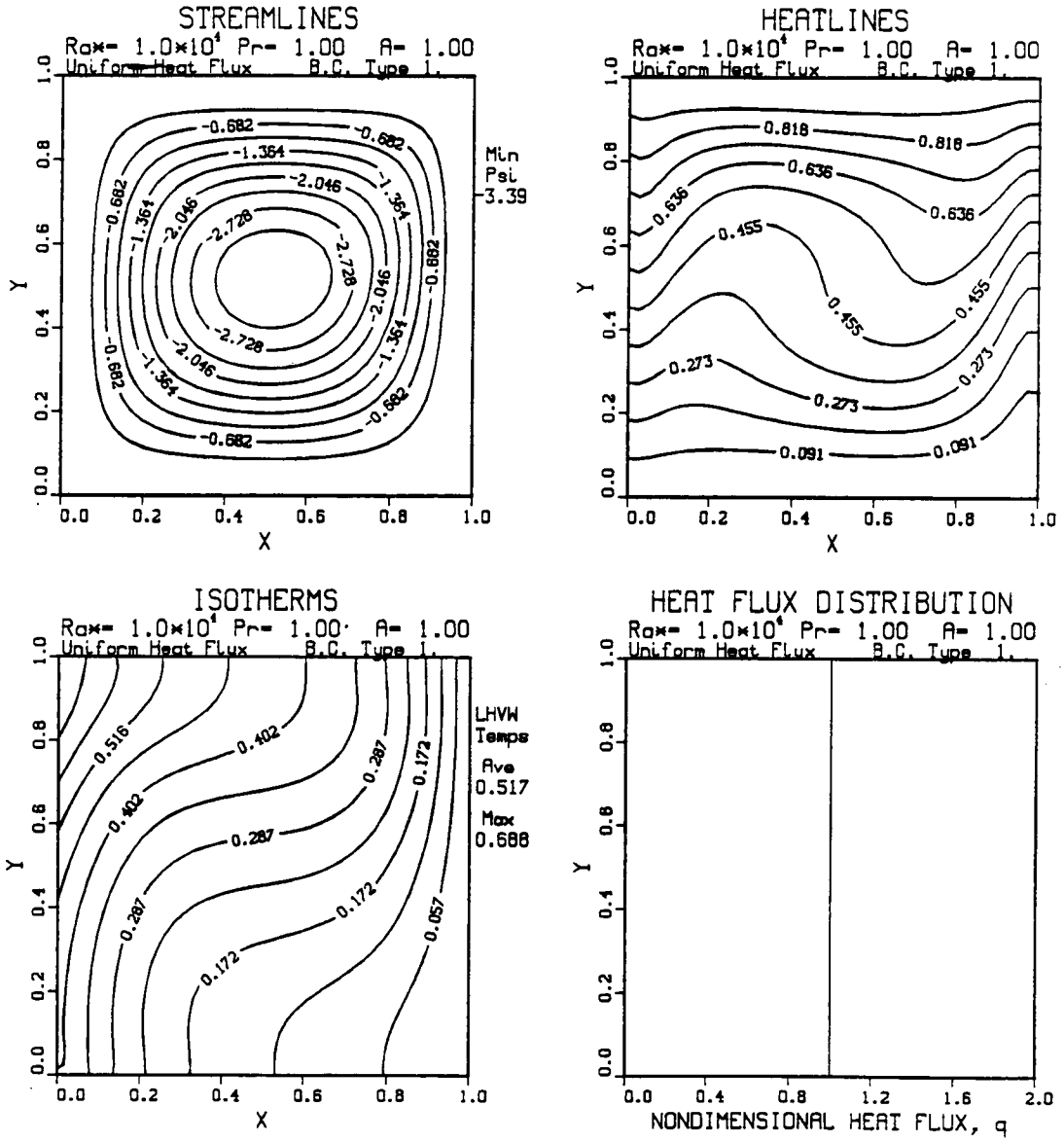


Figure C-5. Summary of results from modified Rayleigh number sensitivity studies for uniform heat flux distribution with $Ra^* = 10^4$

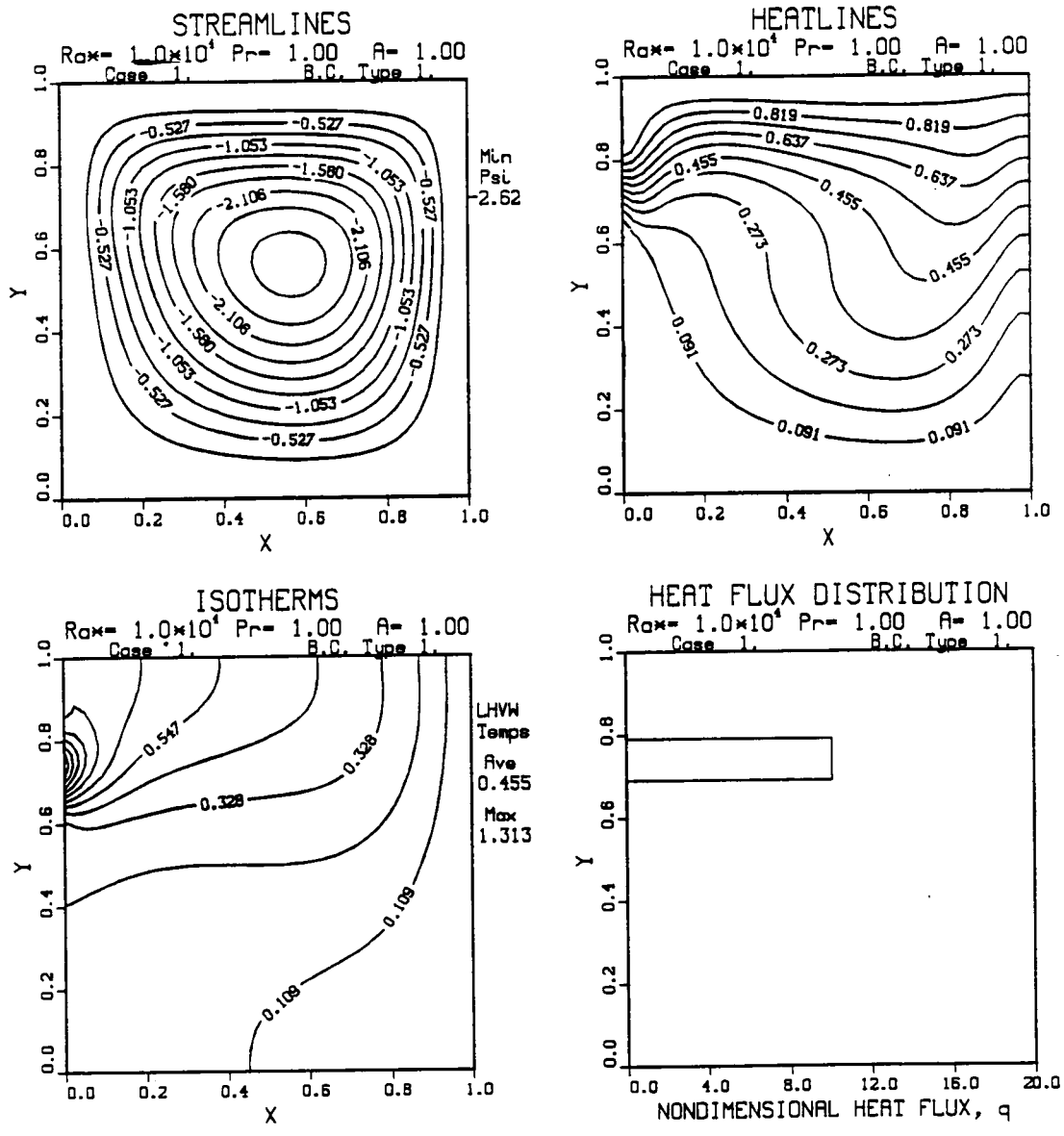


Figure C-6. Summary of results from modified Rayleigh number senstivity studies for Case 1 type optimization with $Ra^*=10^4$

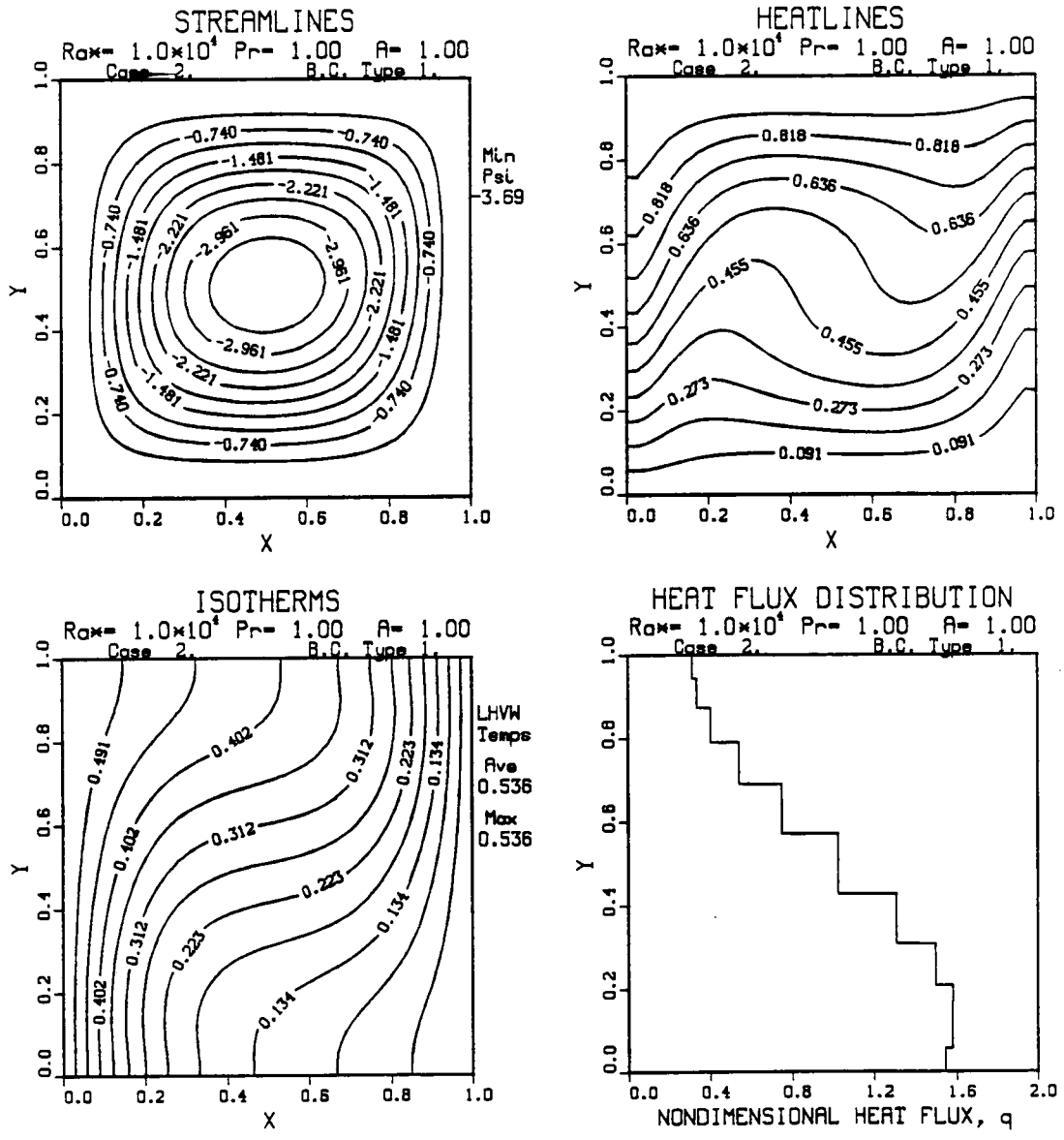


Figure C-7. Summary of results from modified Rayleigh number sensitivity studies for Case 2 type optimization with $Ra^*=10^4$

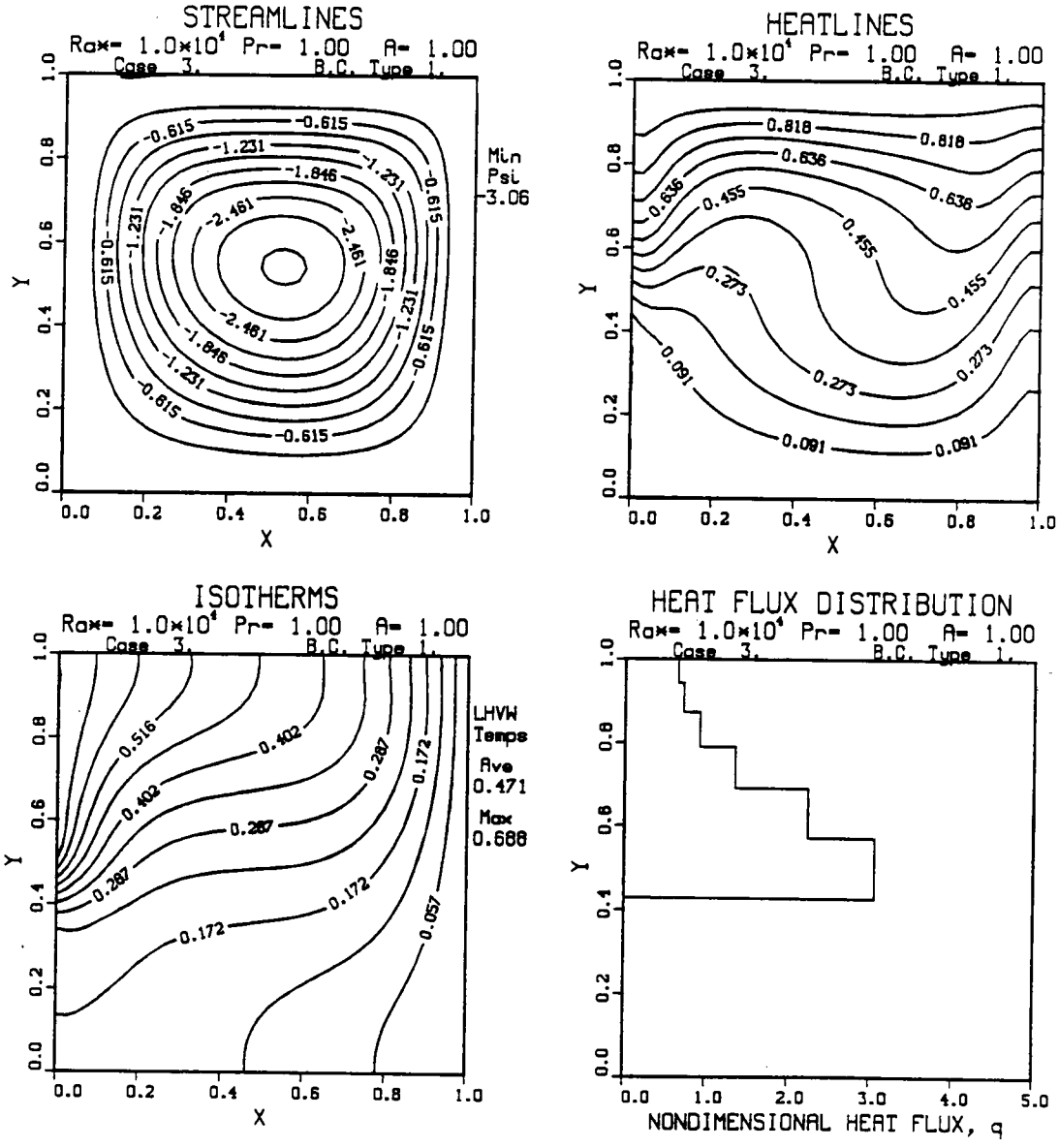


Figure C-8. Summary of results from modified Rayleigh number sensitivity studies for Case 3 type optimization with $Ra^*=10^4$

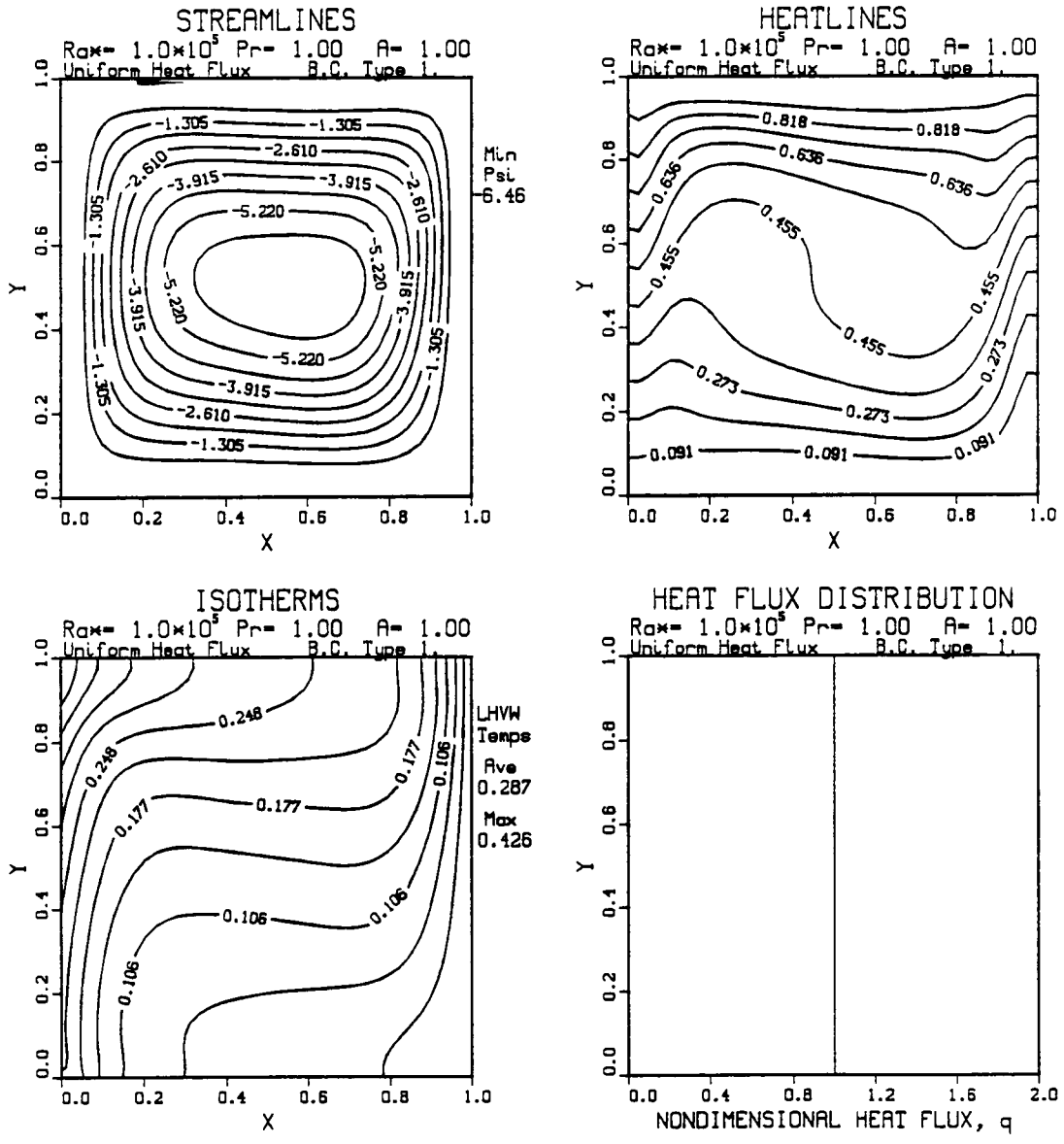


Figure C-9. Summary of results from modified Rayleigh number sensitivity studies for uniform heat flux distribution with $Ra^* = 10^5$

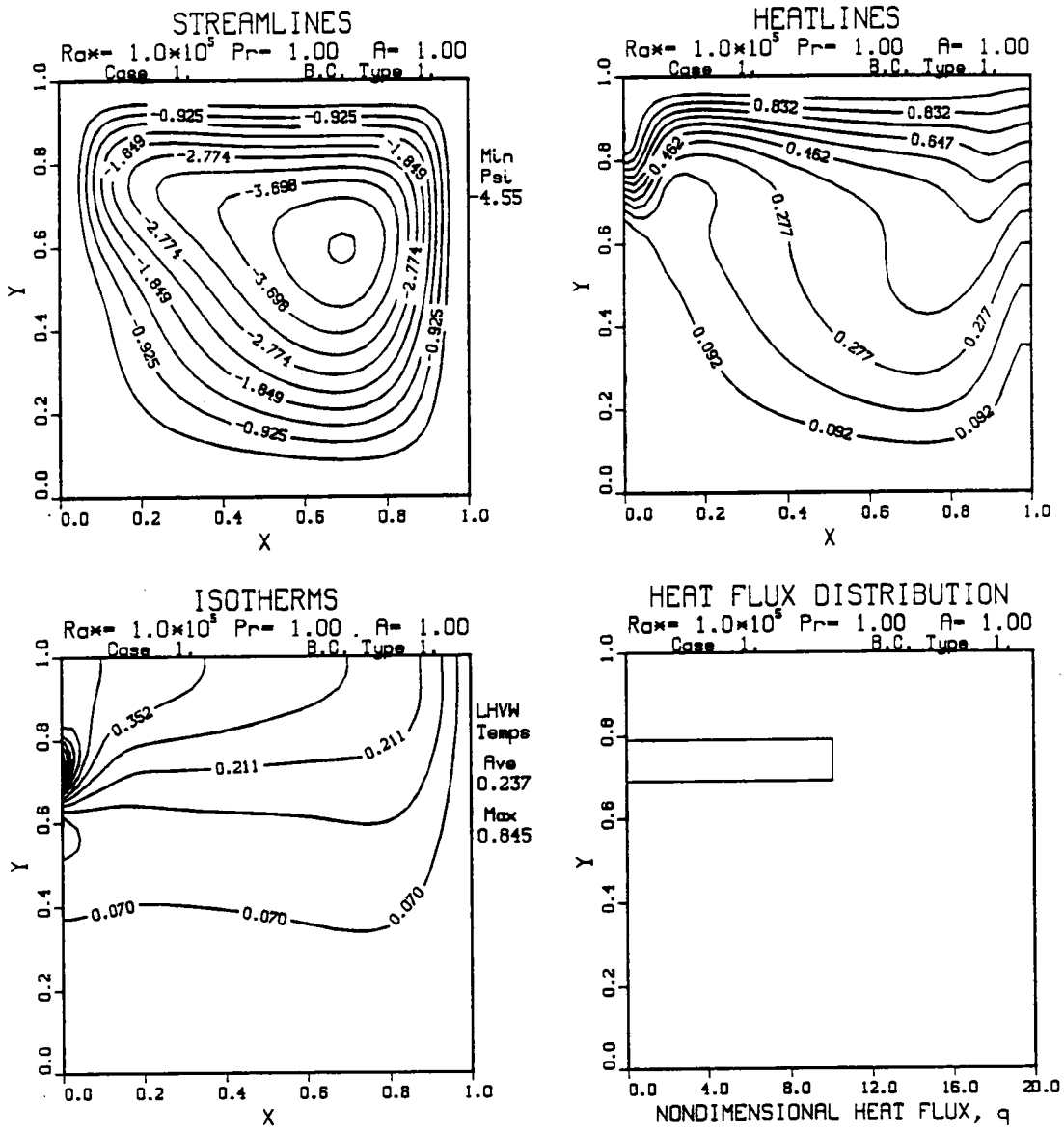


Figure C-10. Summary of results from modified Rayleigh number senstivity studies for Case 1 type optimization with $Ra^*=10^5$

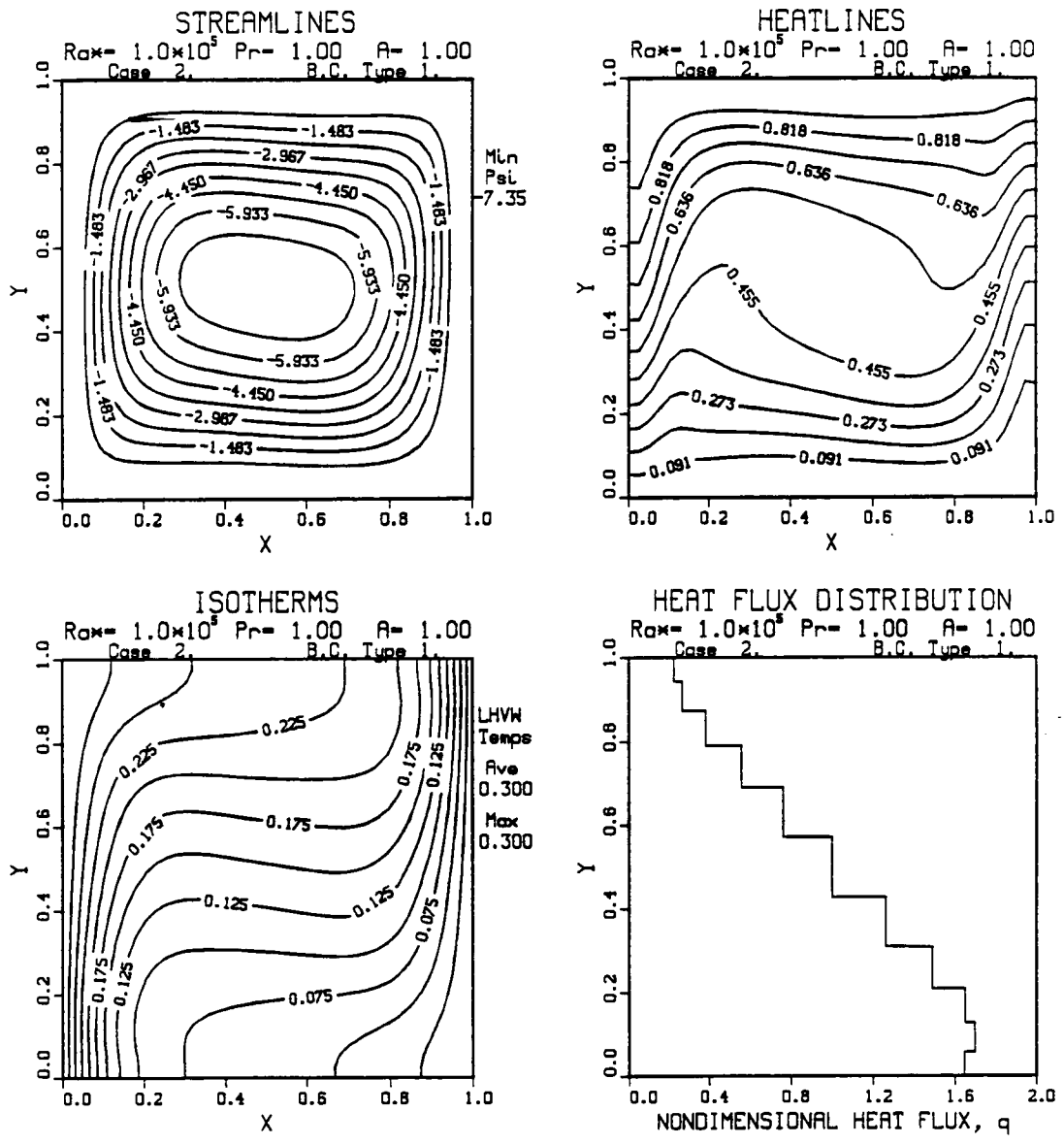


Figure C-11. Summary of results from modified Rayleigh number sensitivity studies for Case 2 type optimization with $Ra^*=10^5$

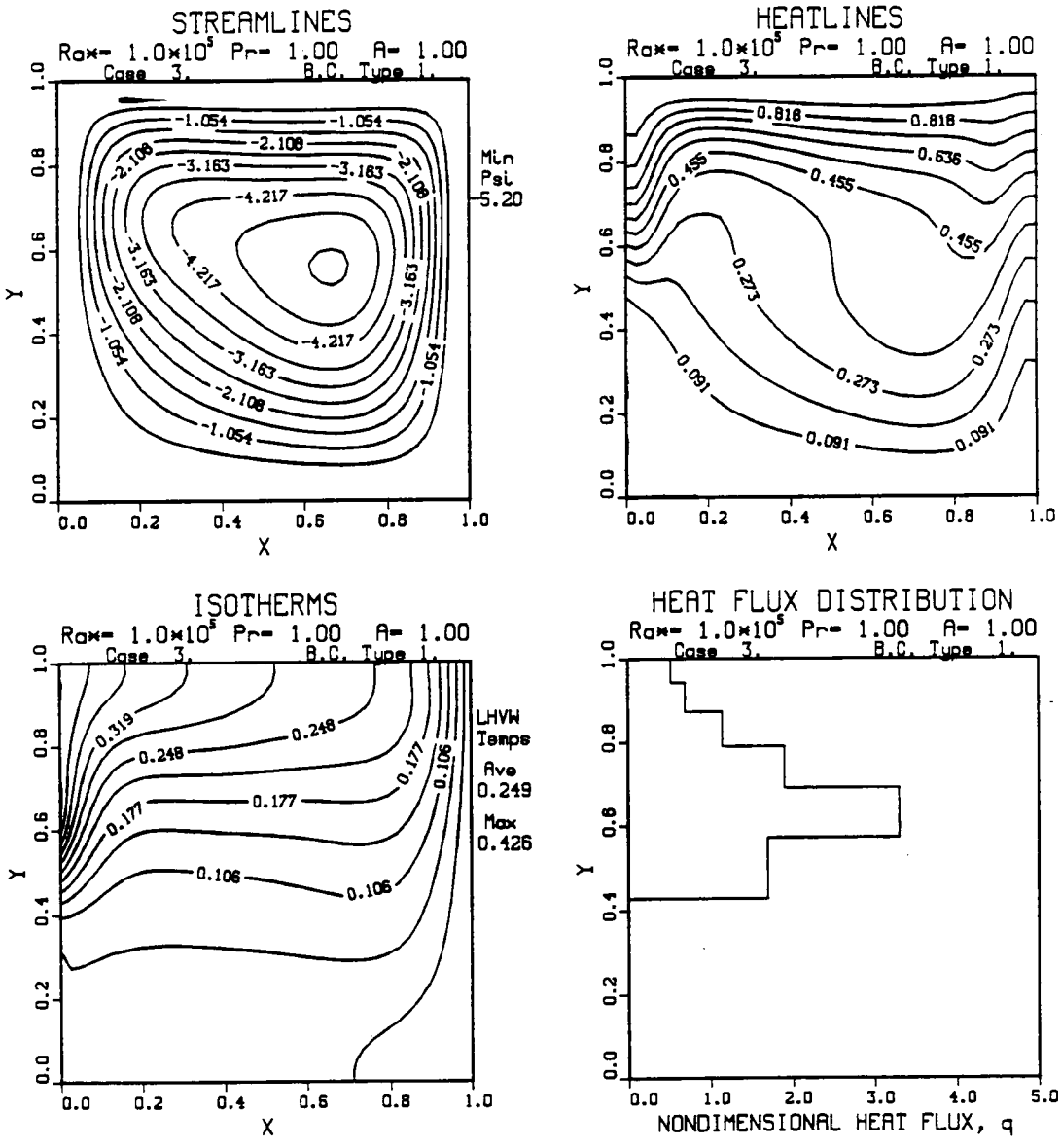


Figure C-12. Summary of results from modified Rayleigh number sensitivity studies for Case 3 type optimization with $Ra^*=10^5$

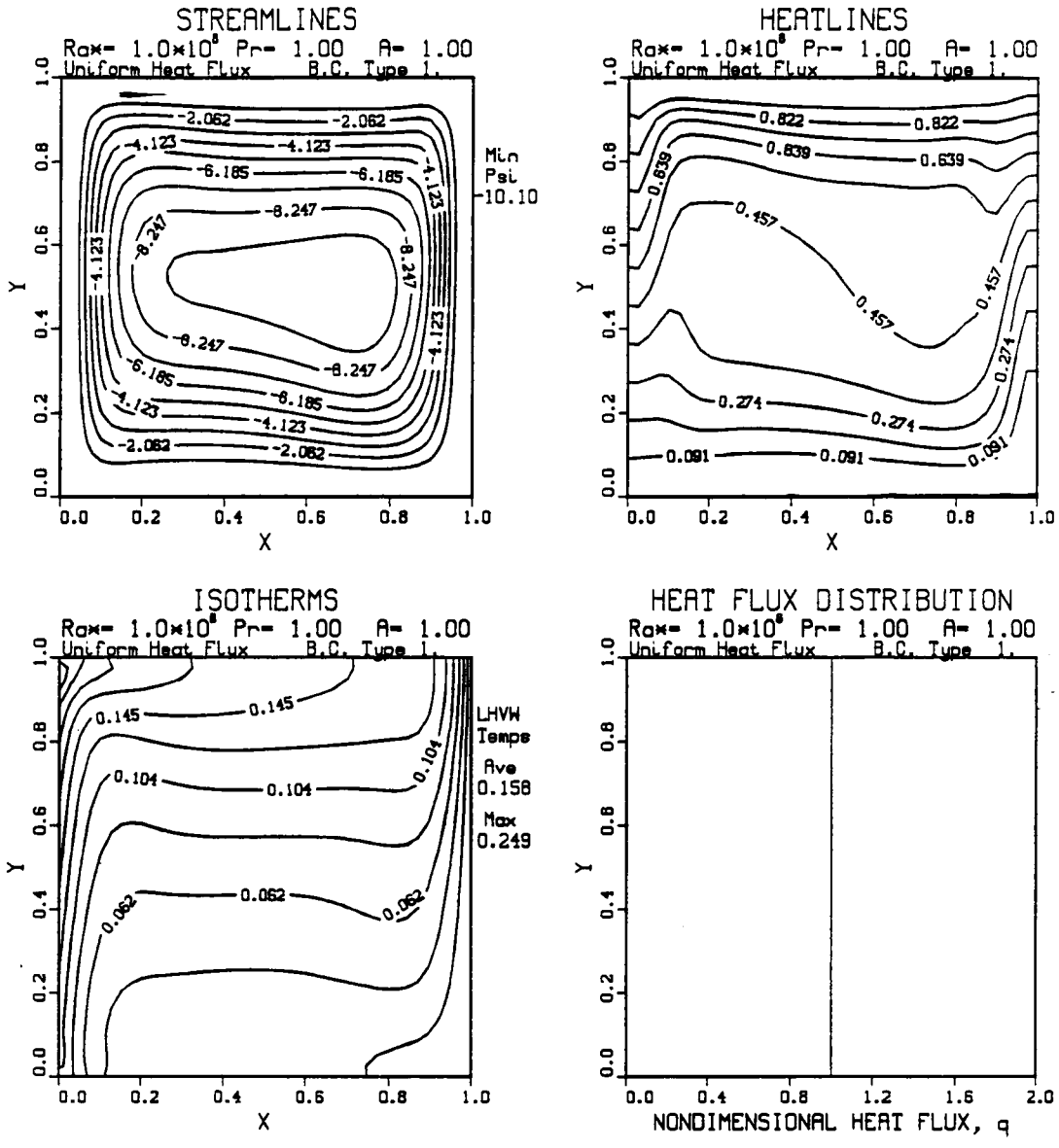


Figure C-13. Summary of results from modified Rayleigh number sensitivity studies for uniform heat flux distribution with $Ra^* = 10^6$

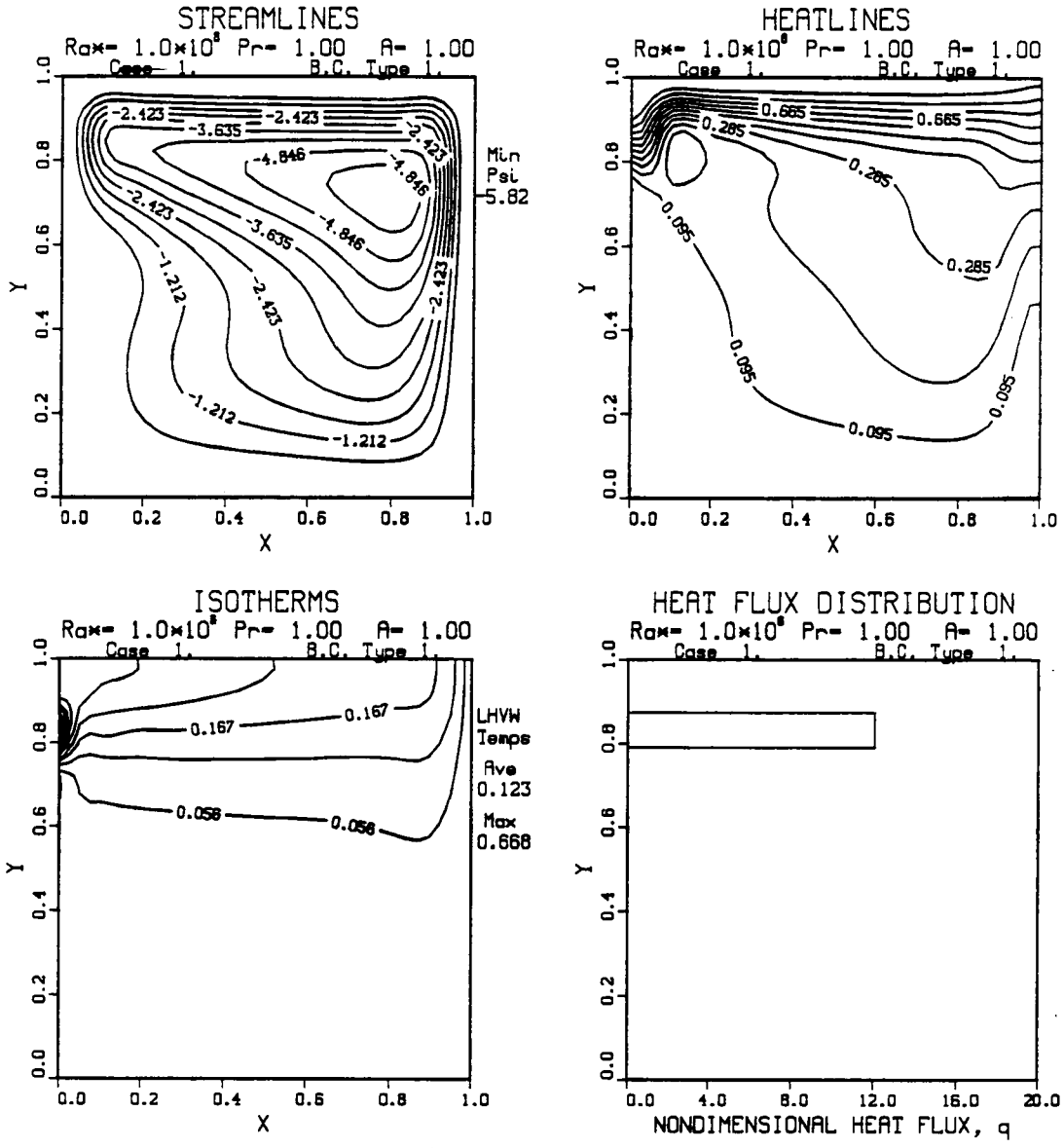


Figure C-14. Summary of results from modified Rayleigh number senstivity studies for Case 1 type optimization with $Ra^*=10^6$

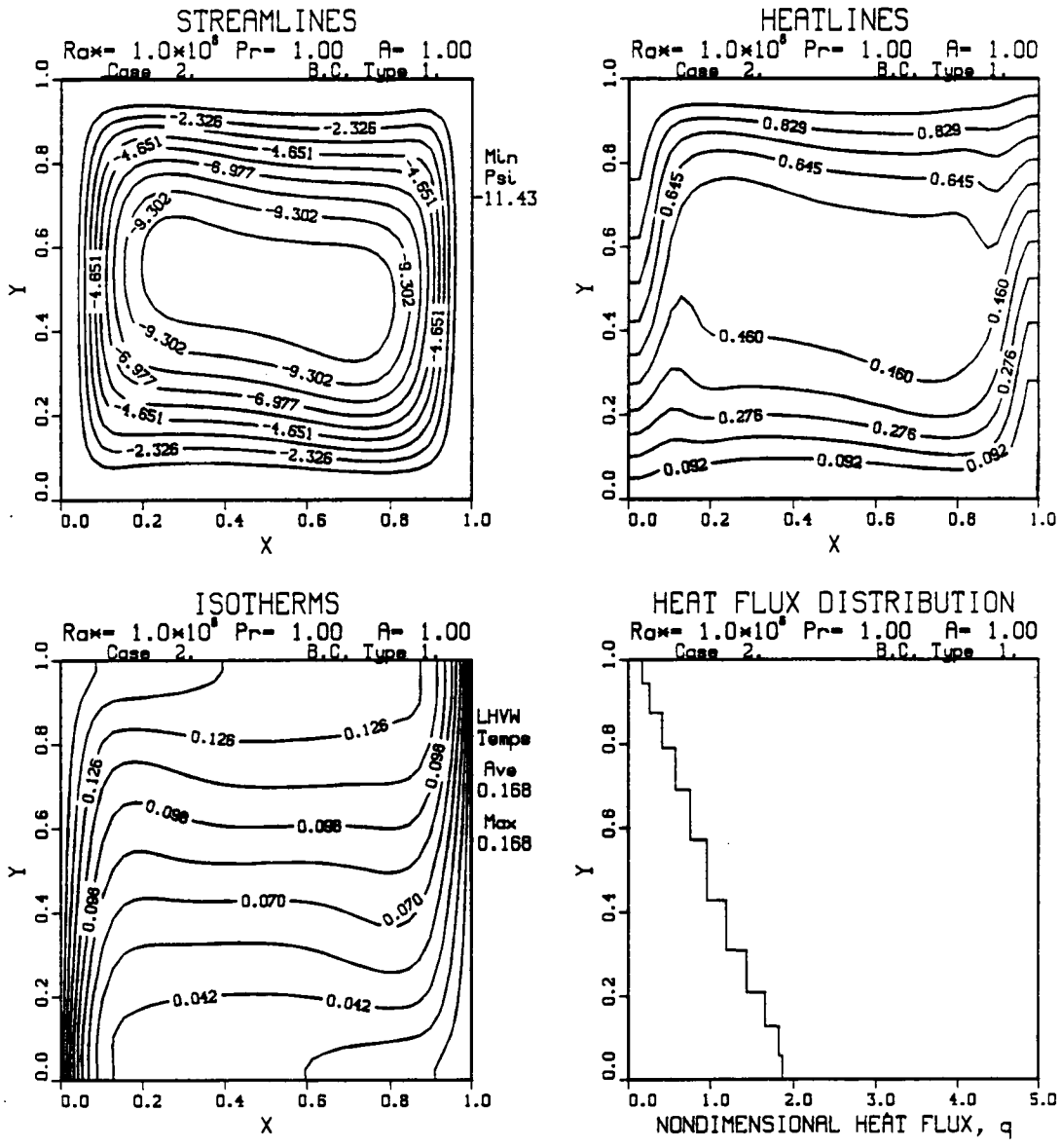


Figure C-15. Summary of results from modified Rayleigh number sensitivity studies for Case 2 type optimization with $Ra^*=10^6$

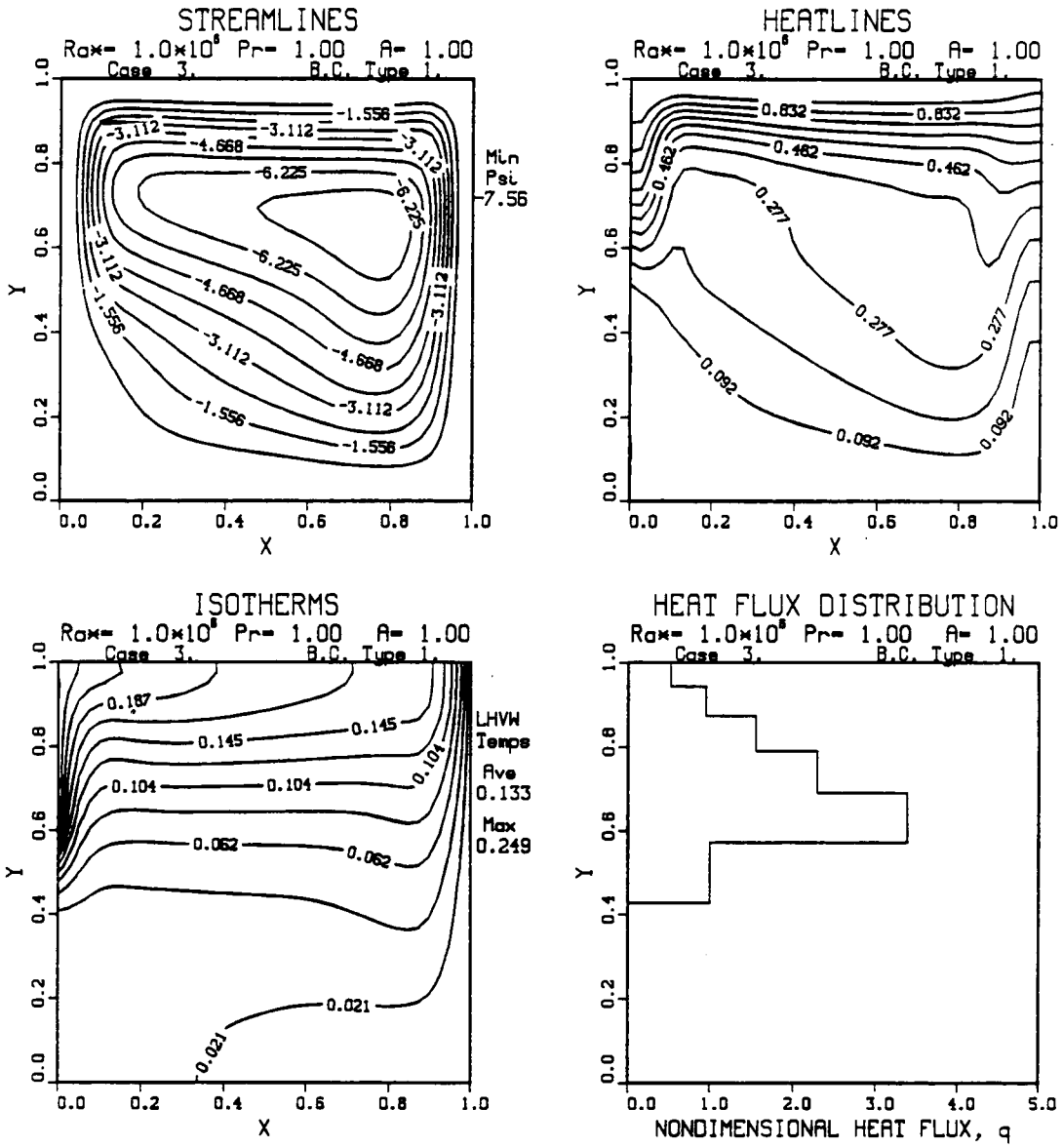


Figure C-16. Summary of results from modified Rayleigh number sensitivity studies for Case 3 type optimization with $Ra^*=10^6$

PRANDTL NUMBER
SENSITIVITY STUDIES

Pr varied from 0.1 to 100

$Ra^* = 10^5$

$A = 1$

Thermal Boundary Condition Type 1

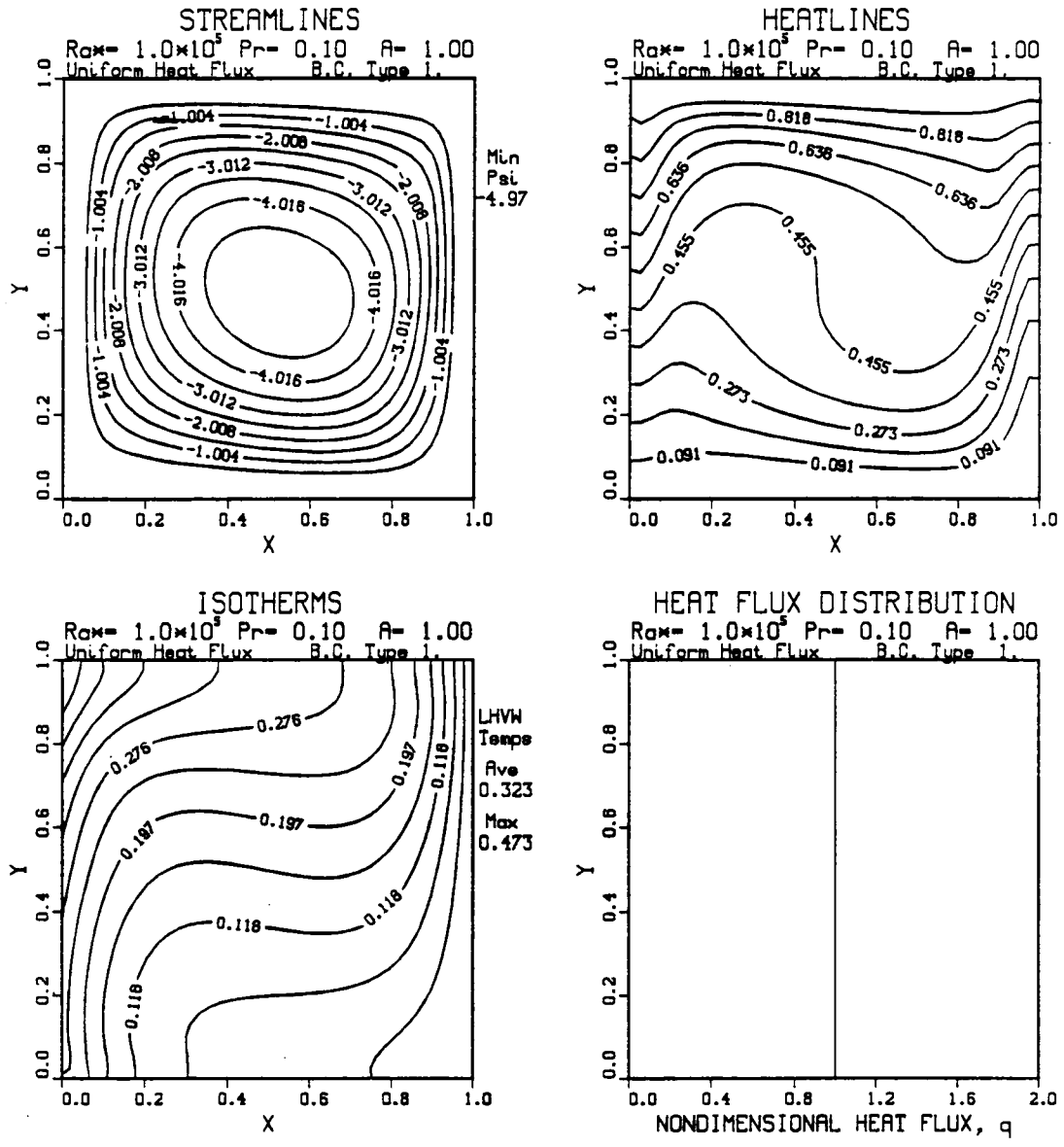


Figure C-17. Summary of results from Prandtl number sensitivity studies for uniform heat flux distribution with Pr = 0.1

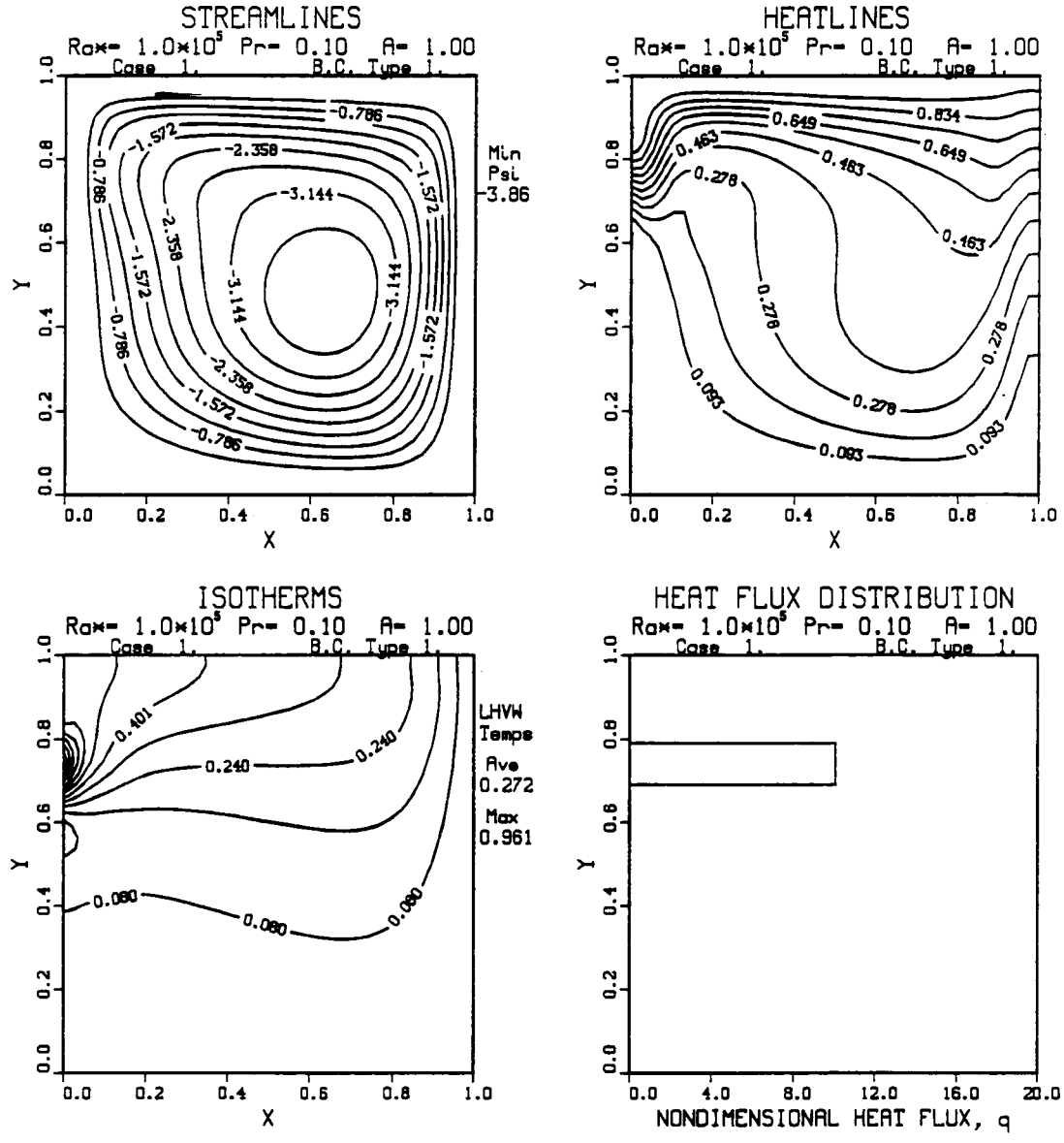


Figure C-18. Summary of results from Prandtl number senstivity studies for Case 1 type optimization with Pr = 0.1

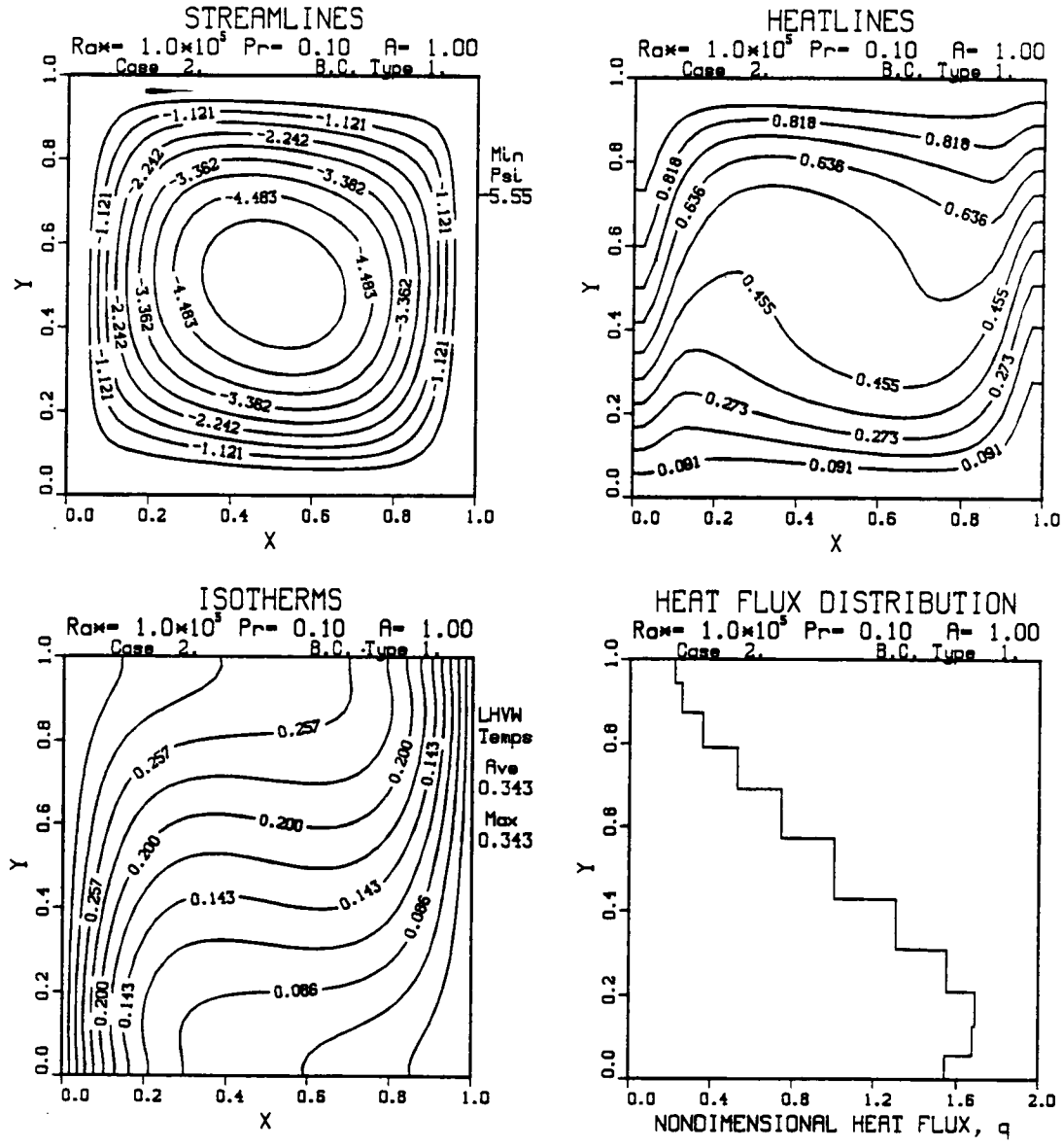


Figure C-19. Summary of results from Prandtl number sensitivity studies for Case 2 type optimization with Pr = 0.1

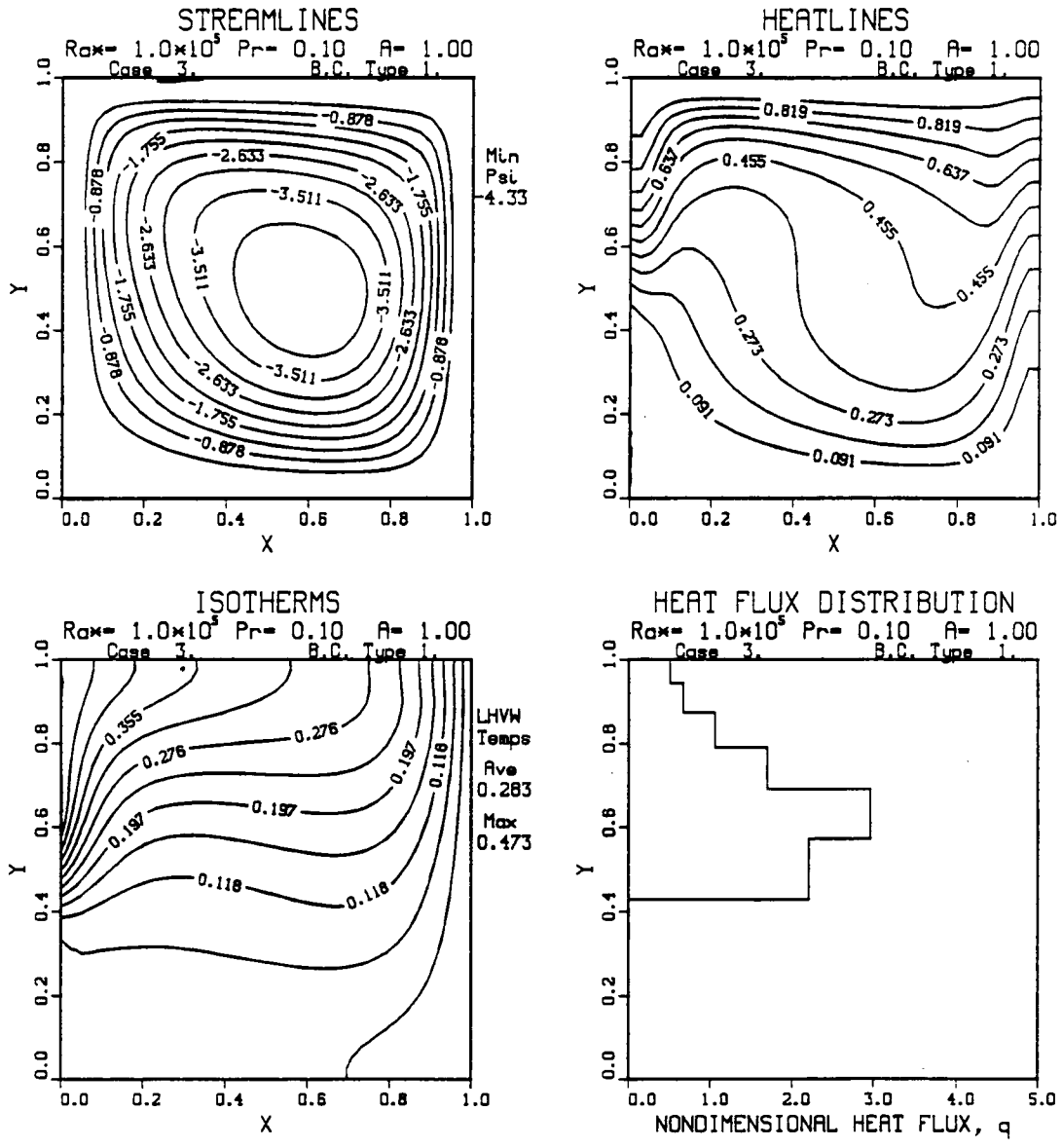


Figure C-20. Summary of results from Prandtl number sensitivity studies for Case 3 type optimization with Pr = 0.1

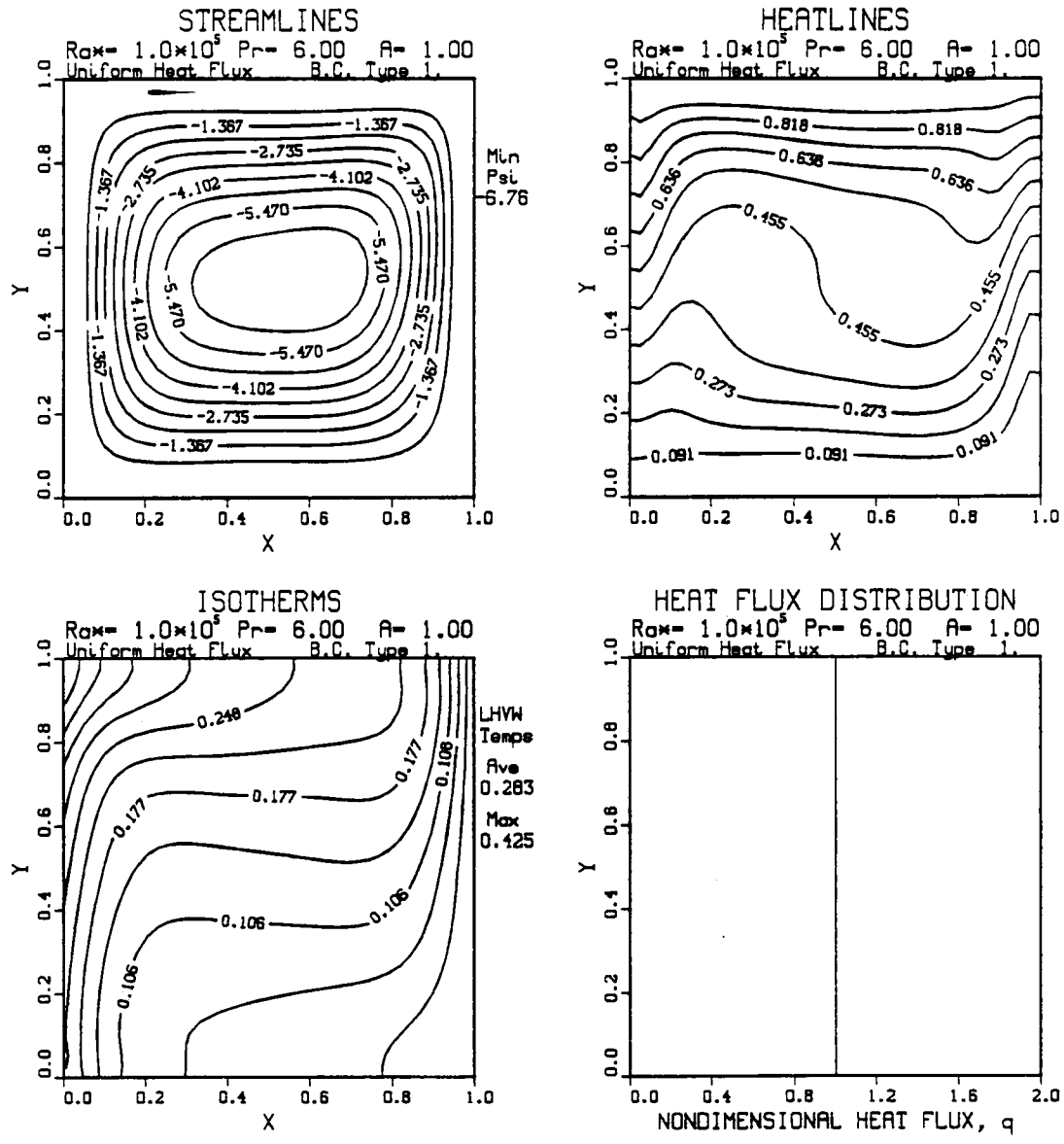


Figure C-21. Summary of results from Prandtl number sensitivity studies for uniform heat flux distribution with Pr = 6

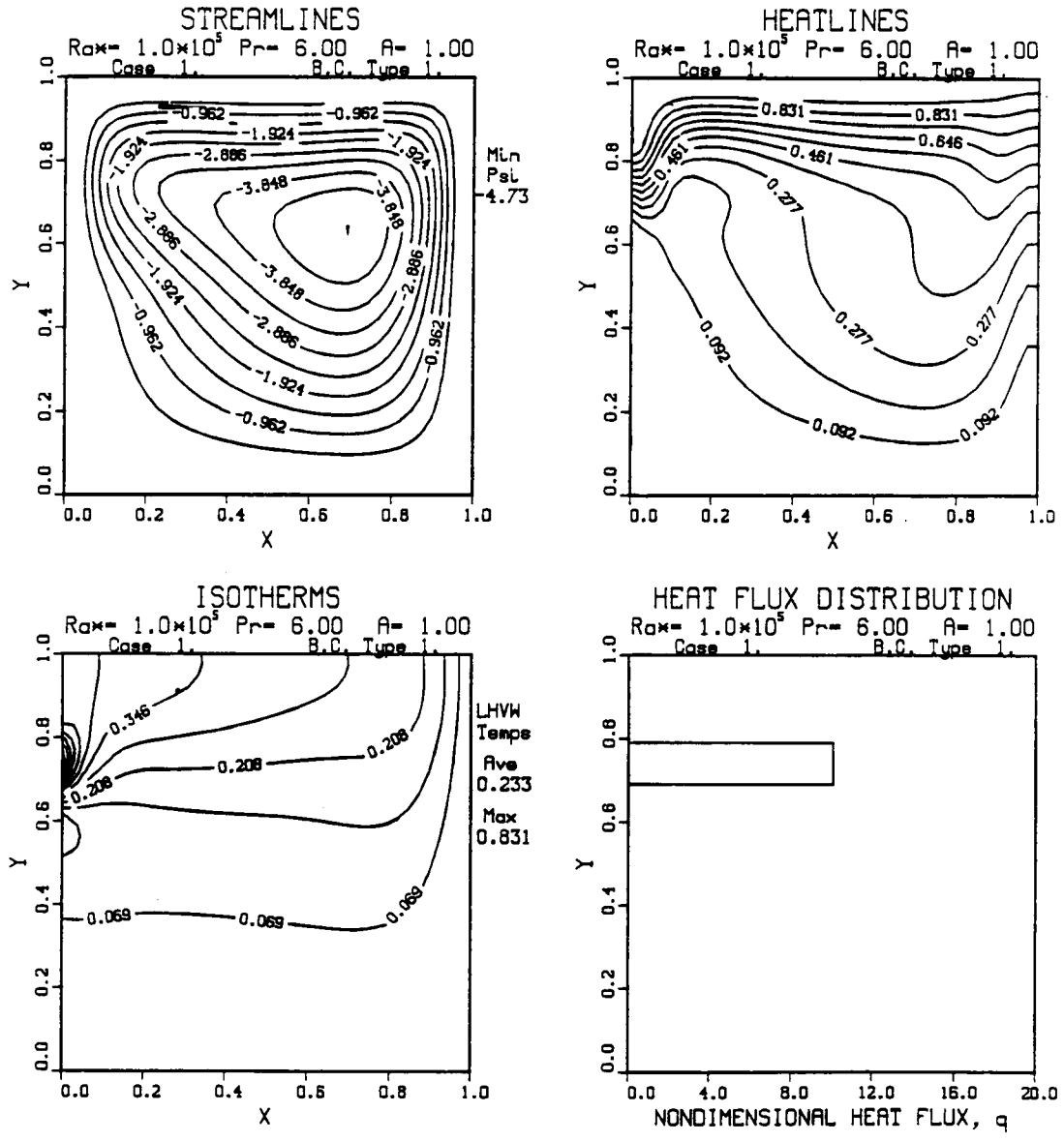


Figure C-22. Summary of results from Prandtl number senstivity studies for Case 1 type optimization with Pr = 6

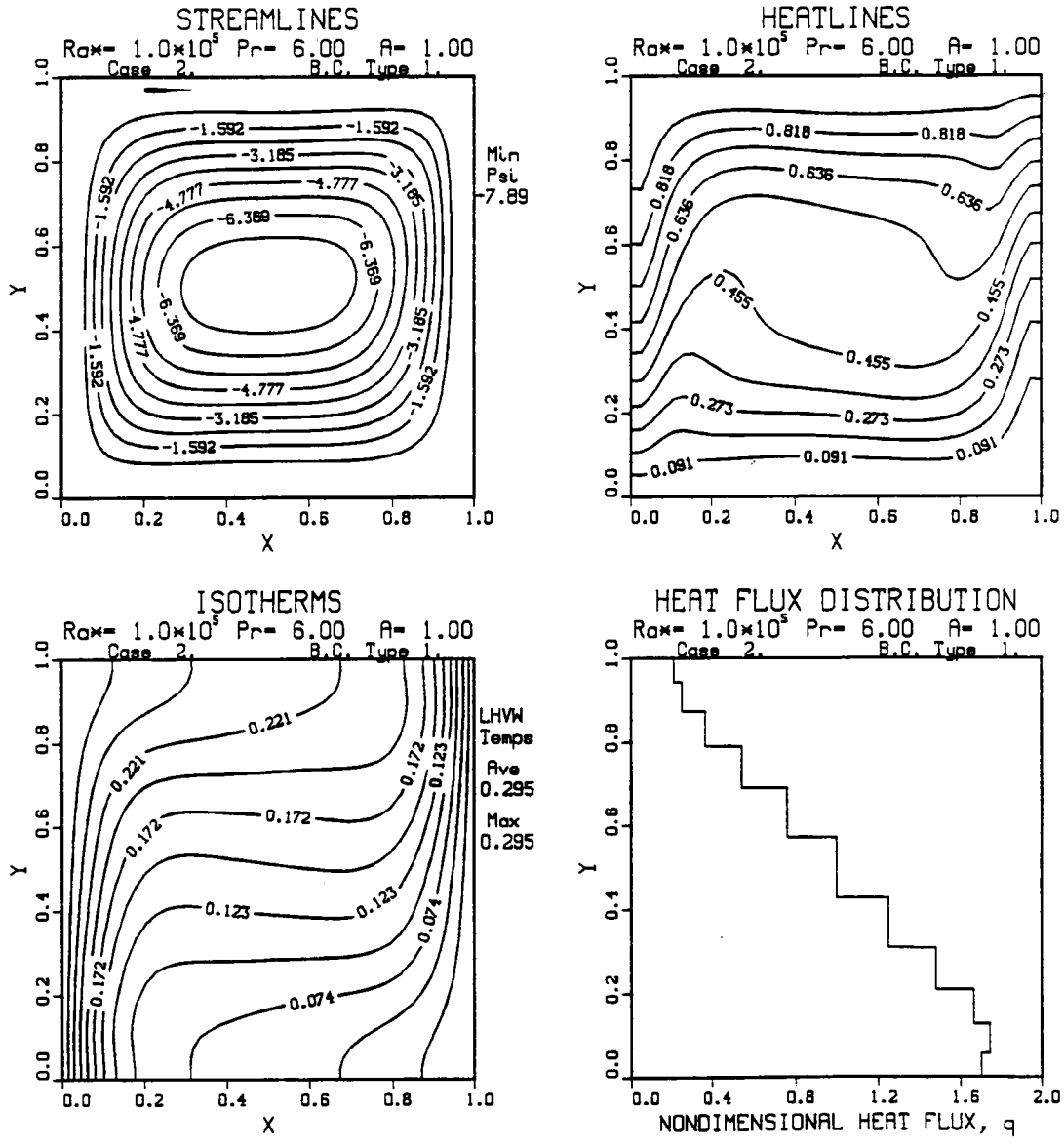


Figure C-23. Summary of results from Prandtl number sensitivity studies for Case 2 type optimization with Pr = 6

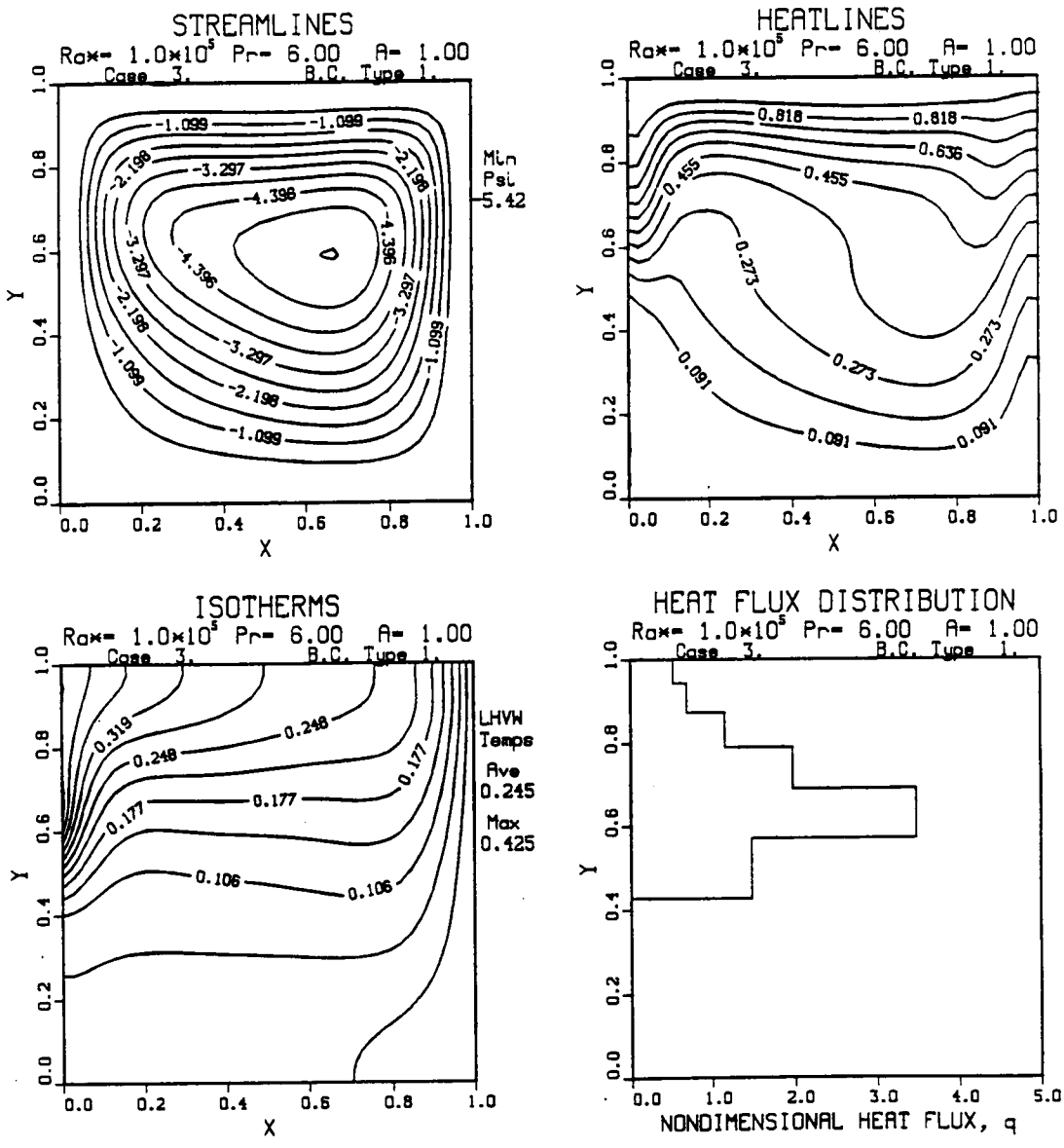


Figure C-24. Summary of results from Prandtl number sensitivity studies for Case 3 type optimization with Pr = 6

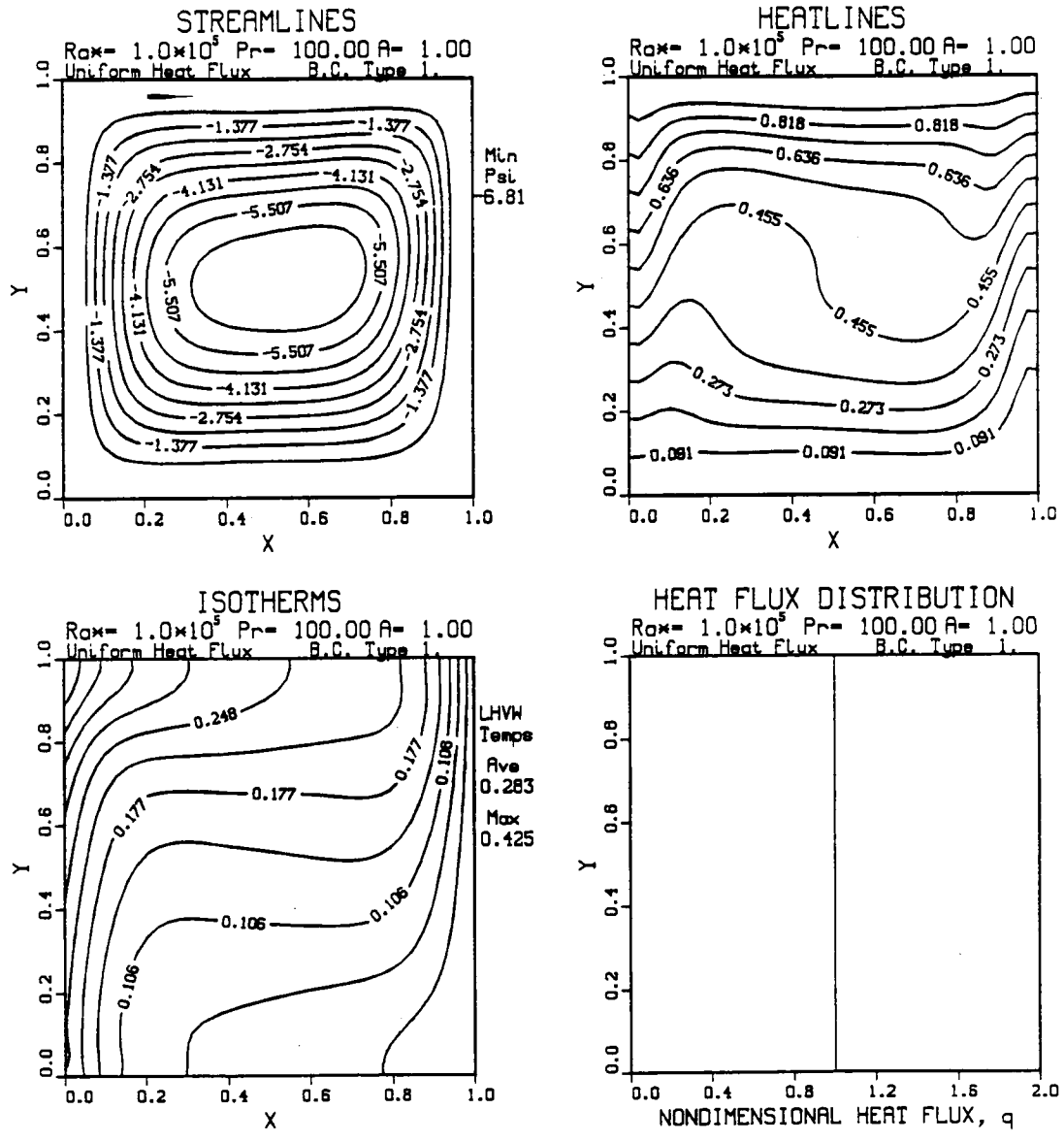


Figure C-25. Summary of results from Prandtl number sensitivity studies for uniform heat flux distribution with Pr = 100

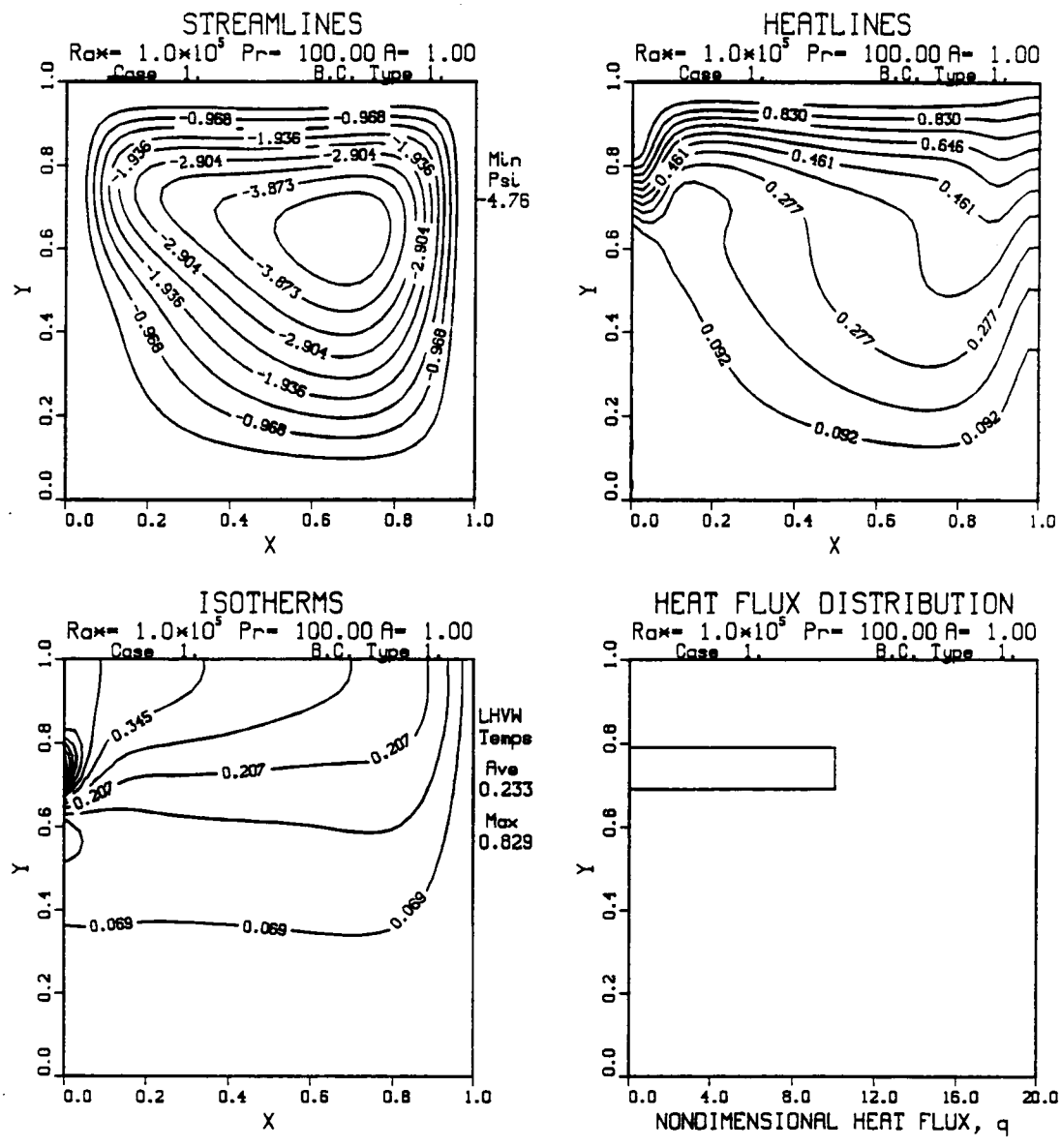


Figure C-26. Summary of results from Prandtl number senstivity studies for Case 1 type optimization with Pr = 100

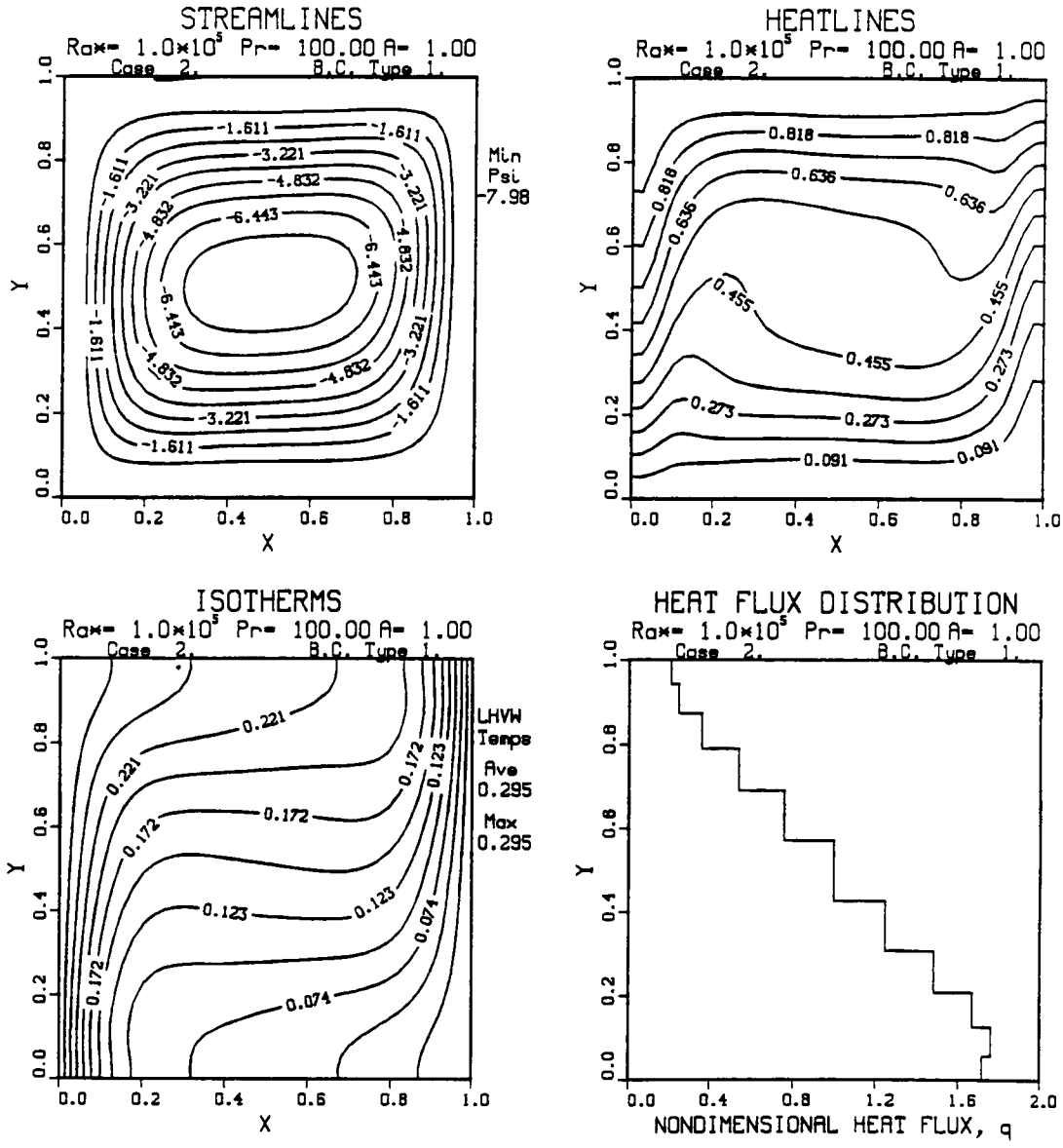


Figure C-27. Summary of results from Prandtl number sensitivity studies for Case 2 type optimization with Pr = 100

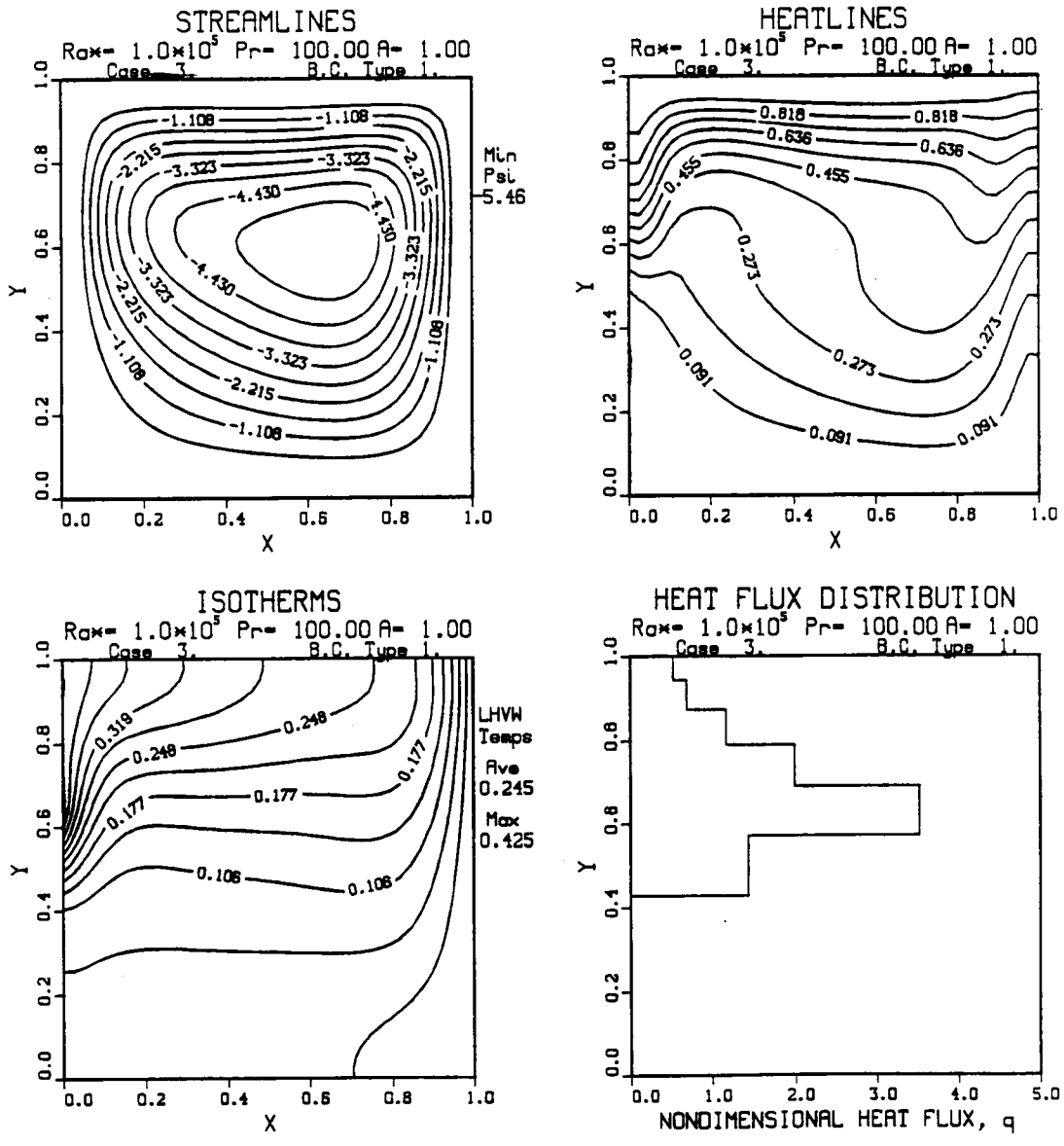


Figure C-28. Summary of results from Prandtl number sensitivity studies for Case 3 type optimization with Pr = 100

ASPECT RATIO

SENSITIVITY STUDIES

A varied from 0.2 to 5.0

$Ra^* = 10^5$

Pr = 1

Thermal Boundary Condition Type 1

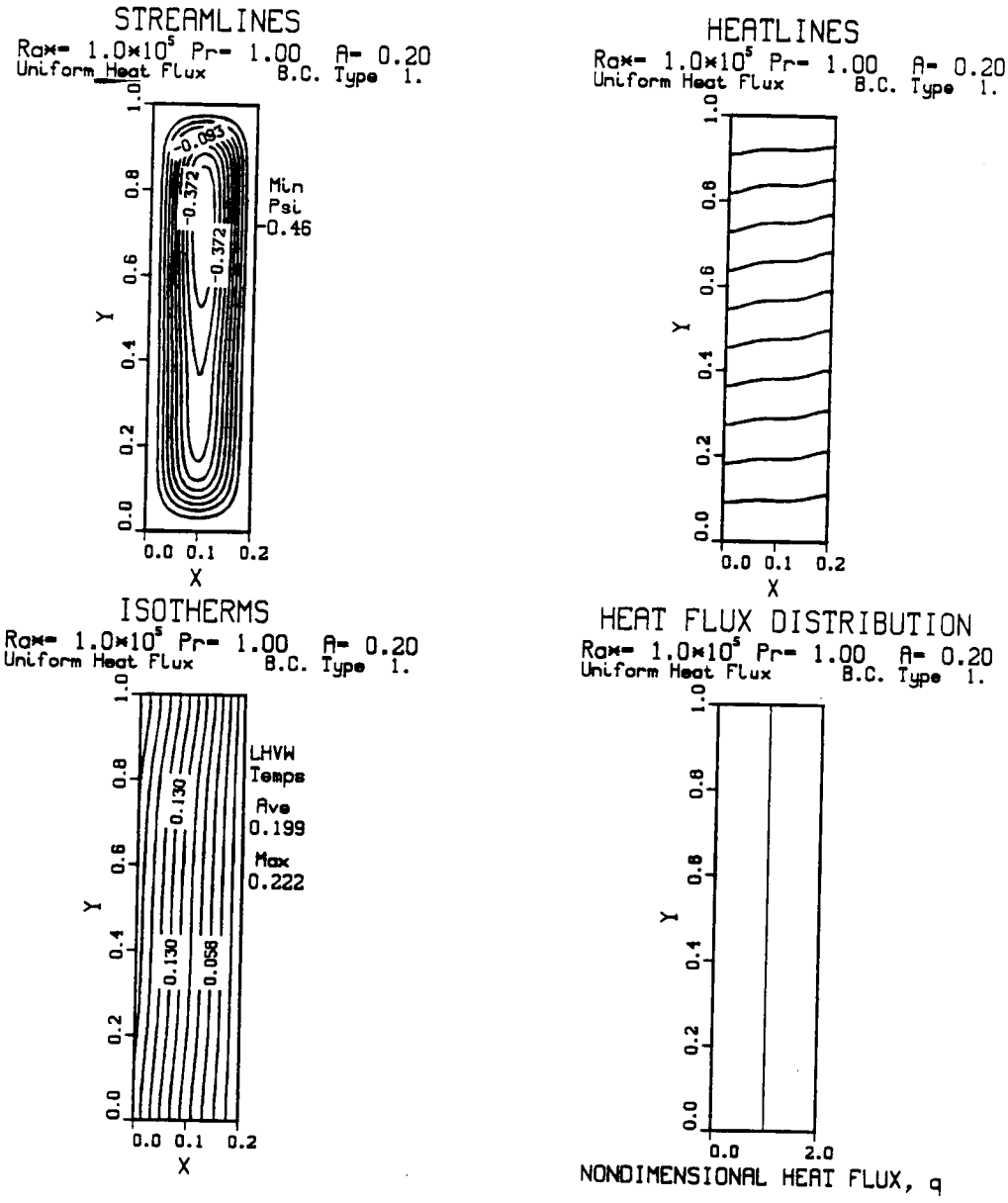


Figure C-29. Summary of results from aspect ratio sensitivity studies for uniform heat flux distribution with A = 0.2

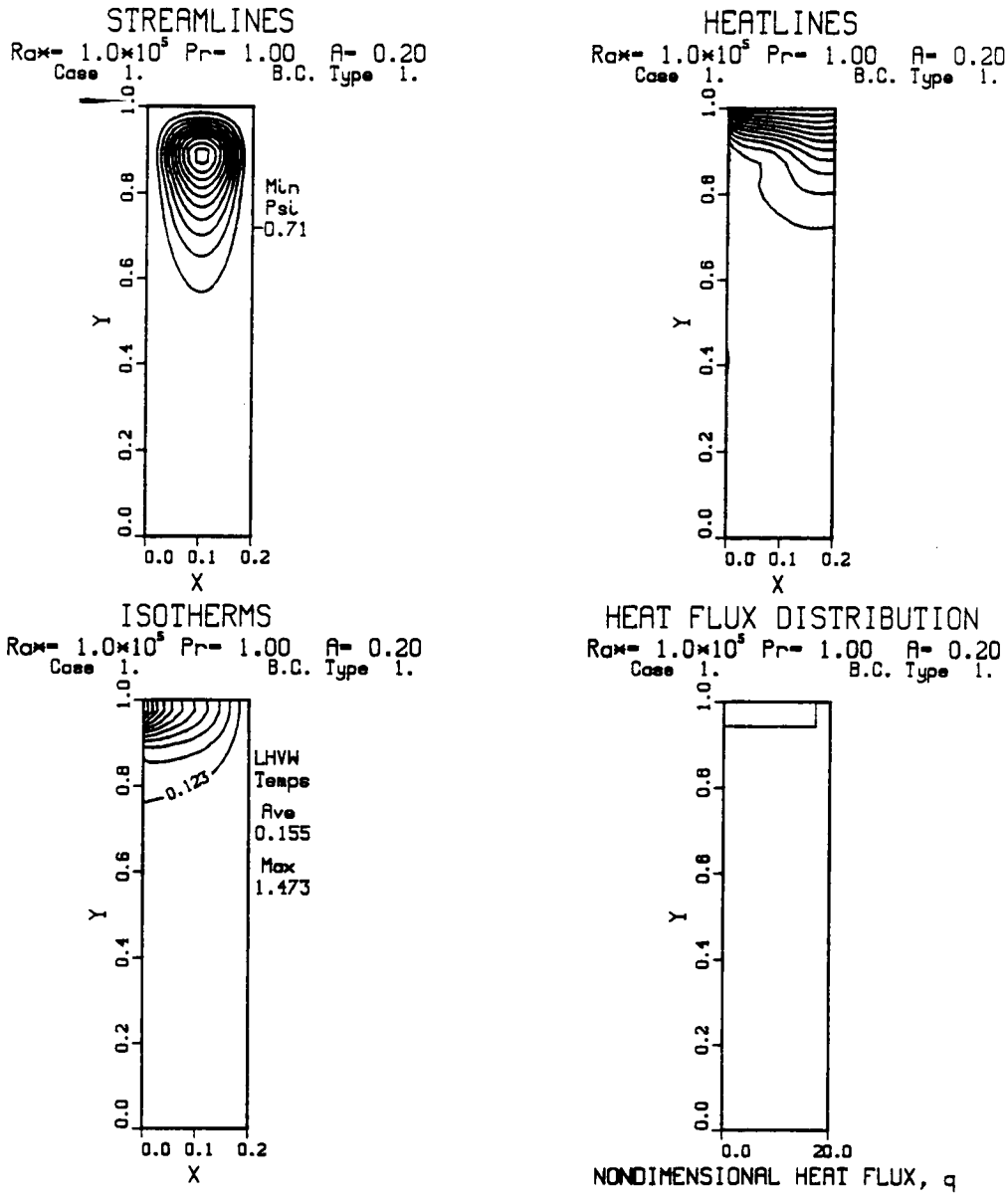


Figure C-30. Summary of results from aspect ratio senstivity studies for Case 1 type optimization with A = 0.2

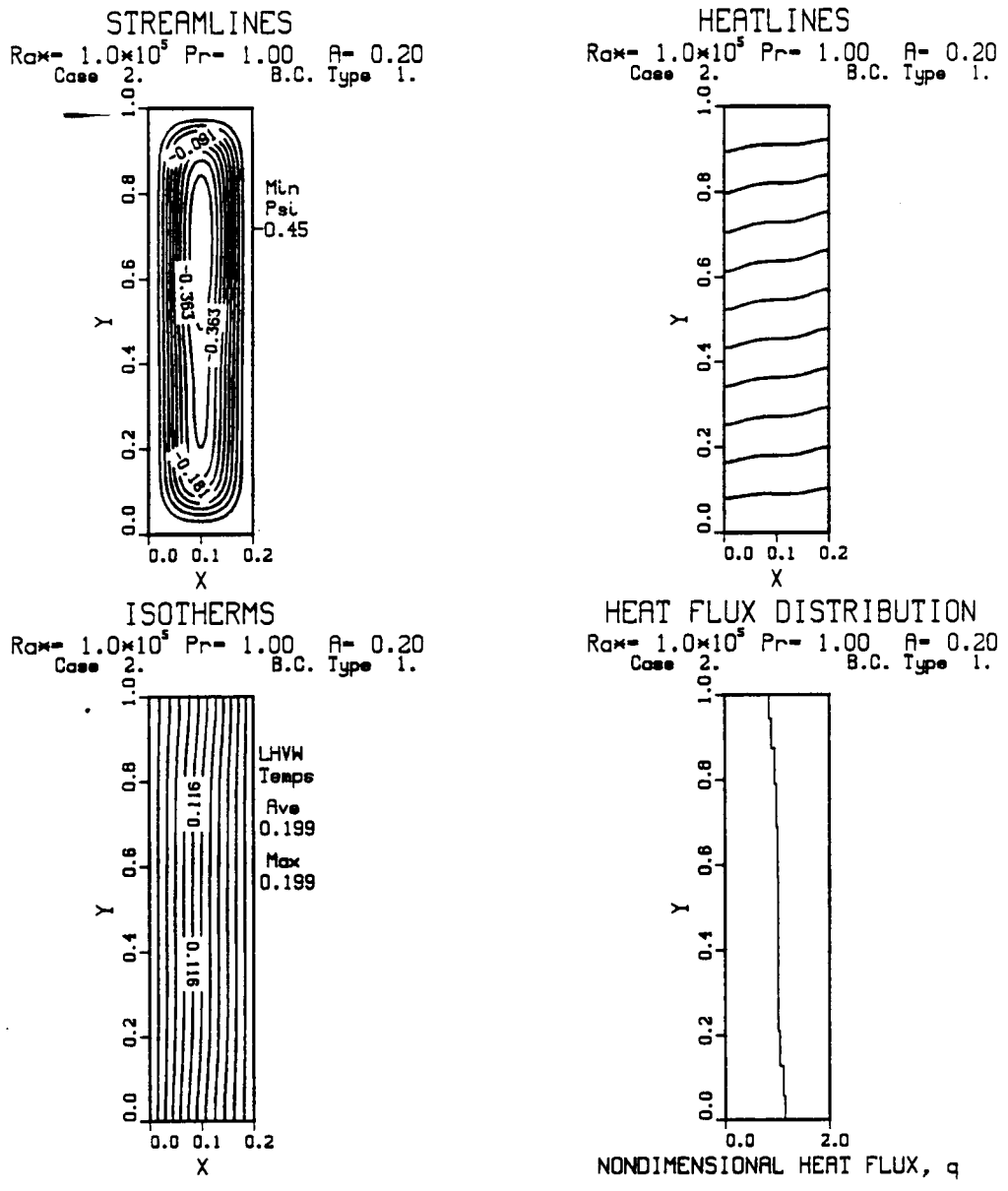


Figure C-31. Summary of results from aspect ratio sensitivity studies for Case 2 type optimization with A = 0.2

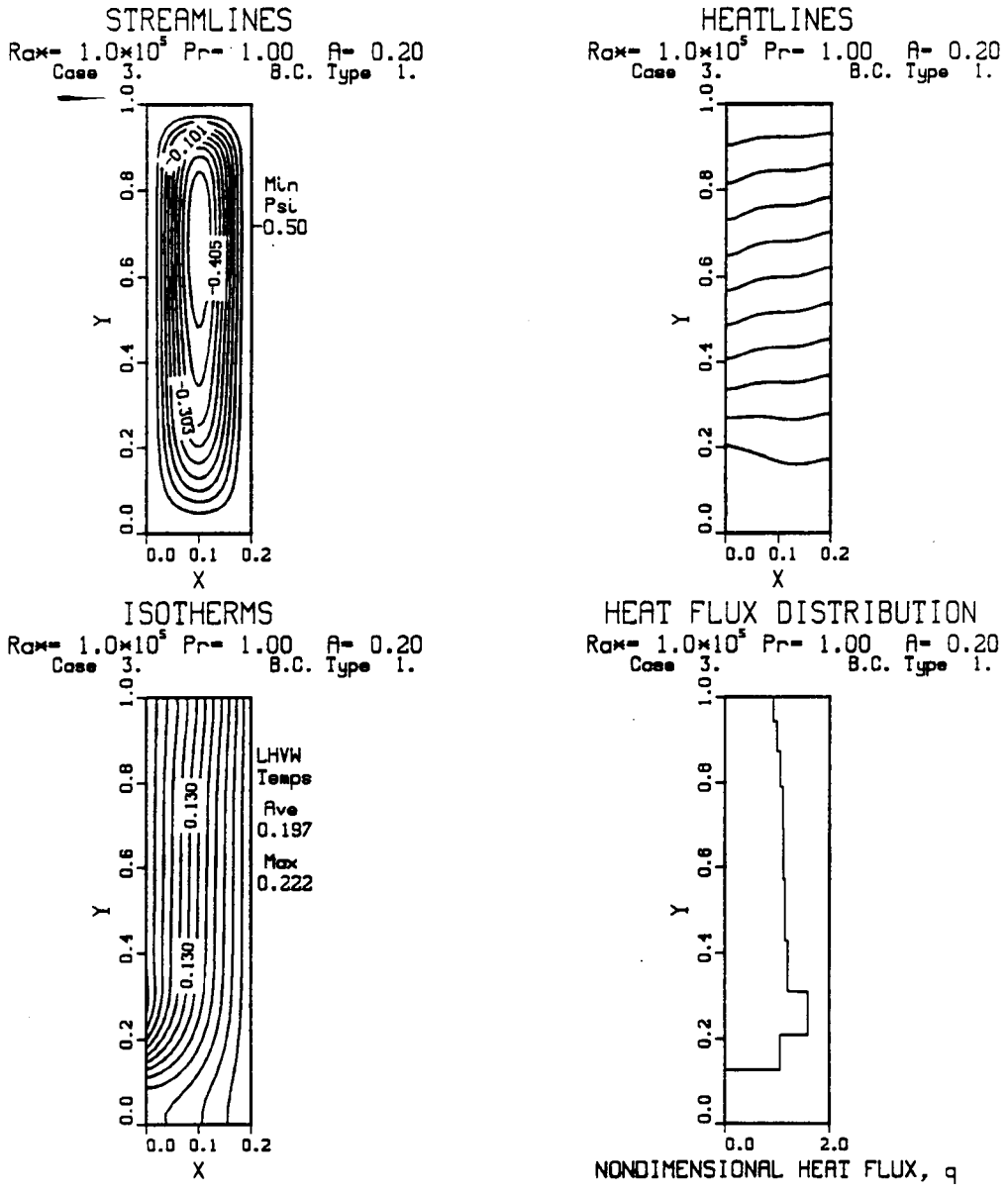


Figure C-32. Summary of results from aspect ratio sensitivity studies for Case 3 type optimization with A = 0.2

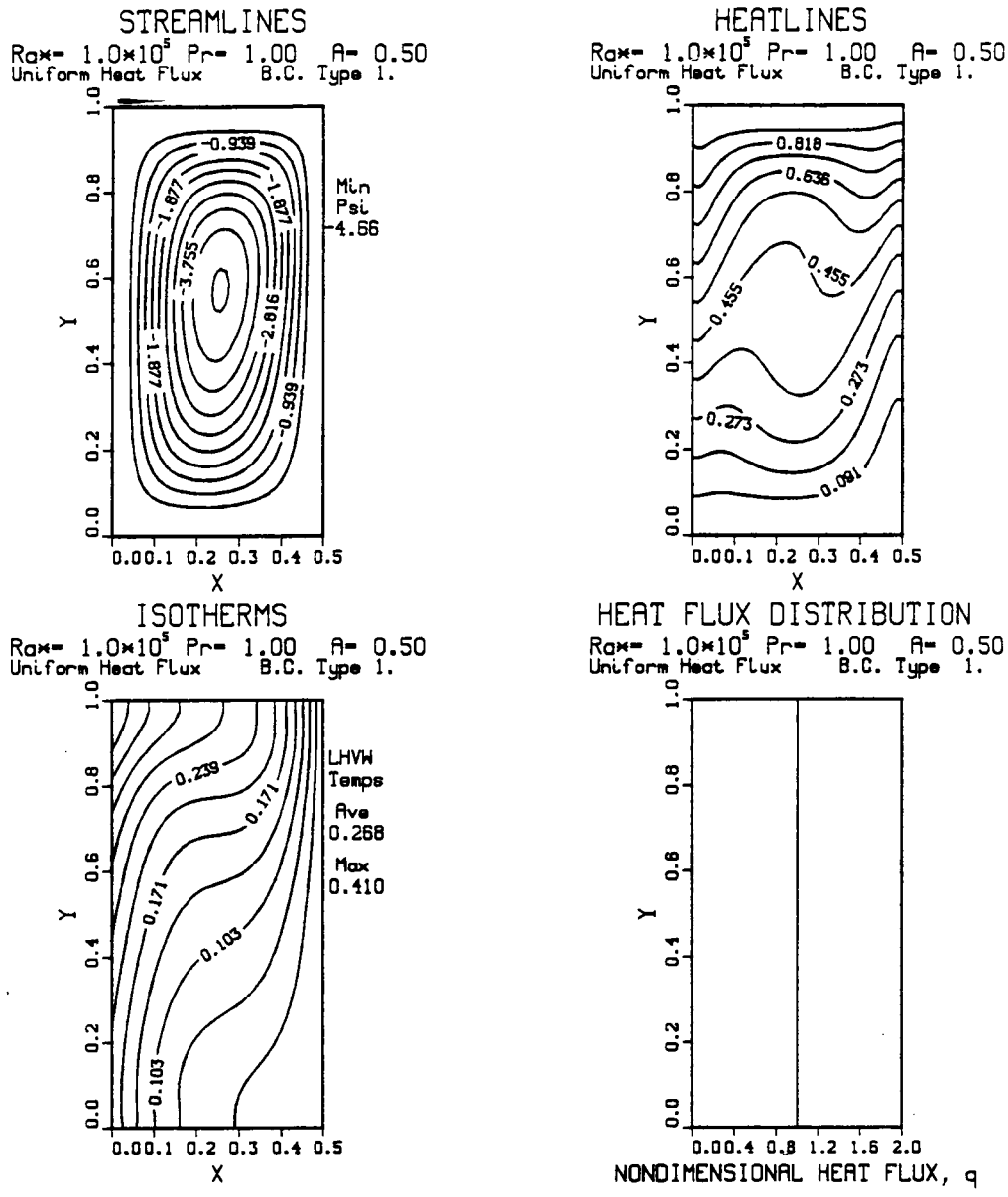


Figure C-33. Summary of results from aspect ratio sensitivity studies for uniform heat flux distribution with A = 0.5

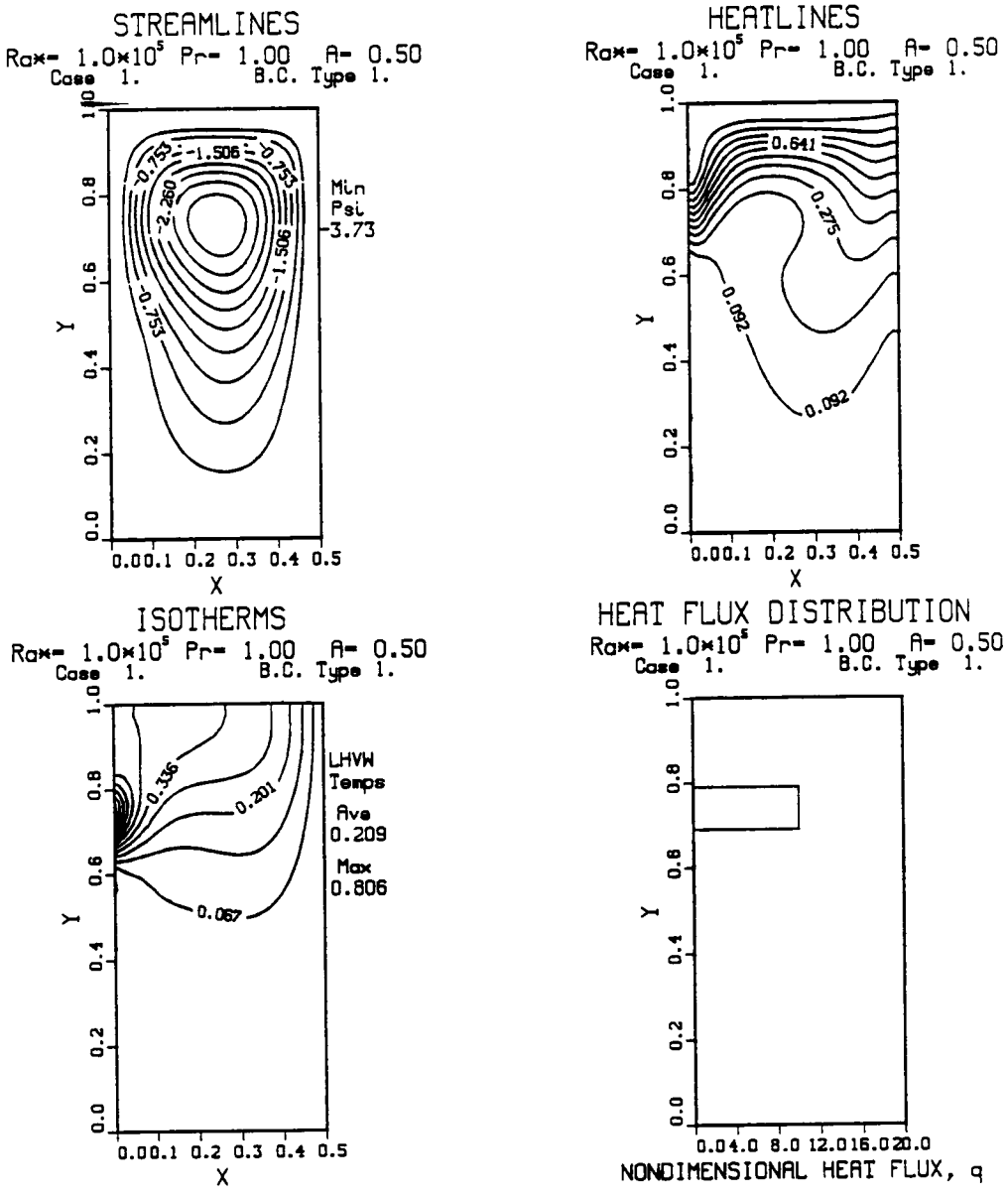


Figure C-34. Summary of results from aspect ratio senstivity studies for Case 1 type optimization with A = 0.5

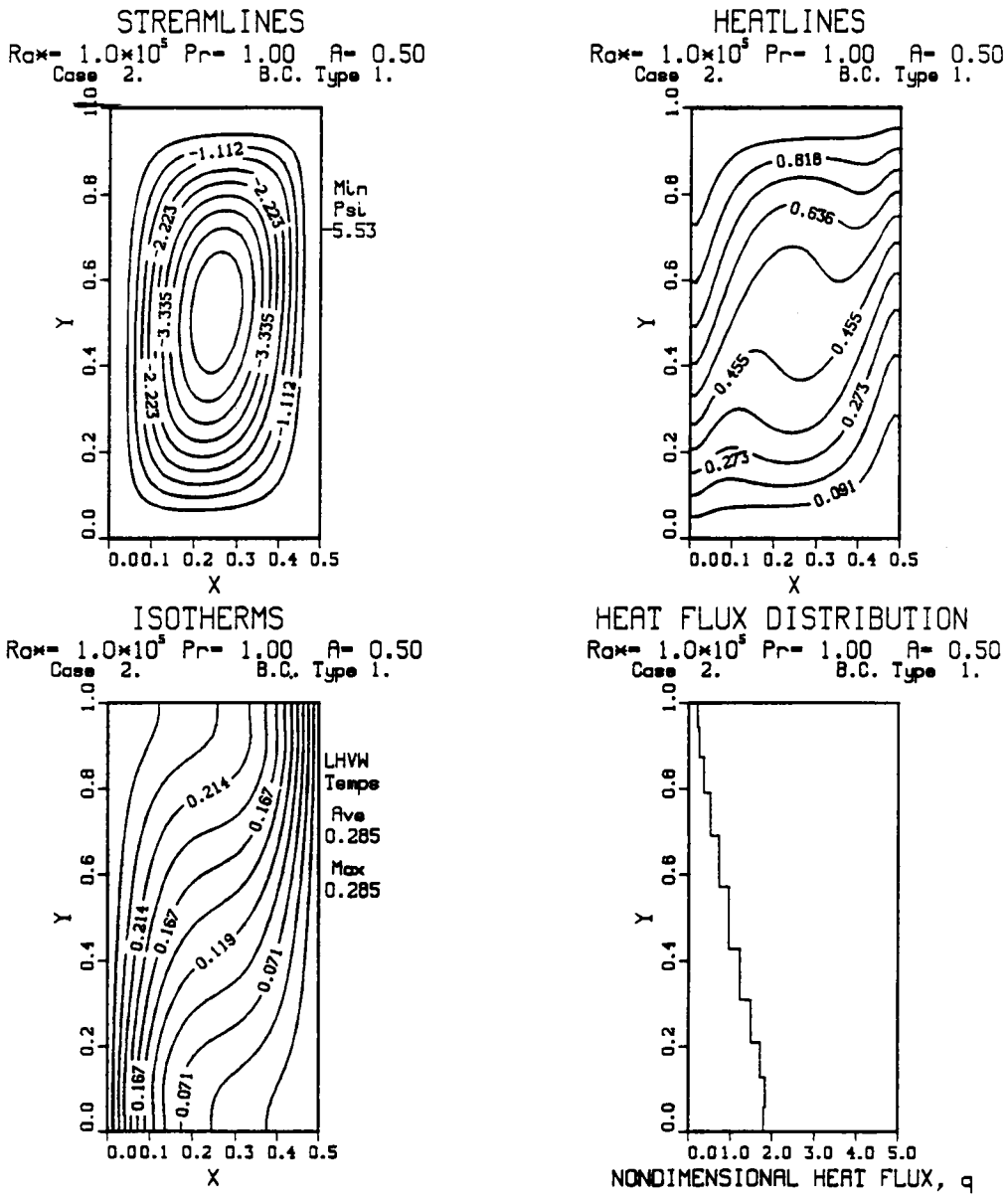


Figure C-35. Summary of results from aspect ratio sensitivity studies for Case 2 type optimization with A = 0.5

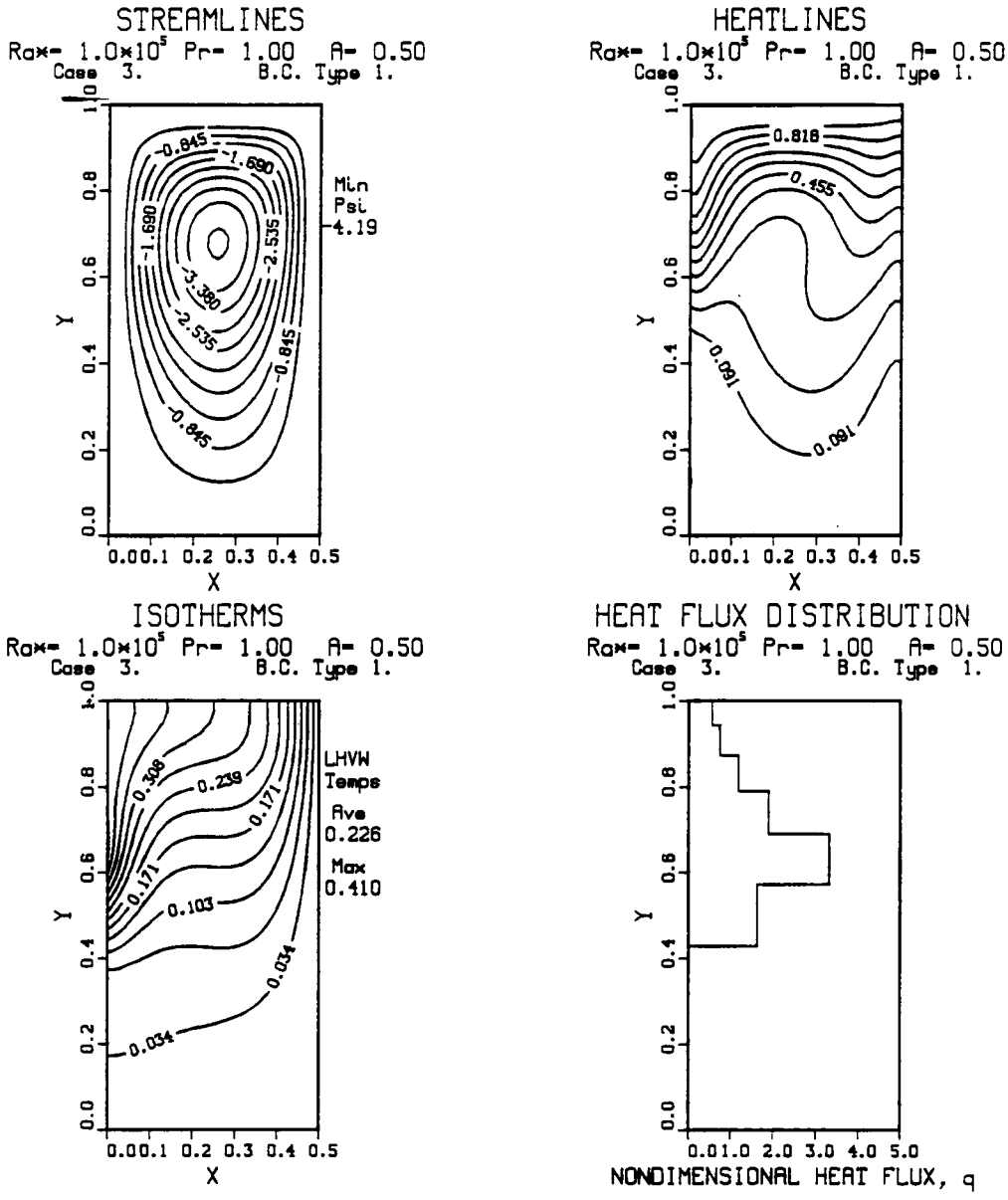


Figure C-36. Summary of results from aspect ratio sensitivity studies for Case 3 type optimization with A = 0.5

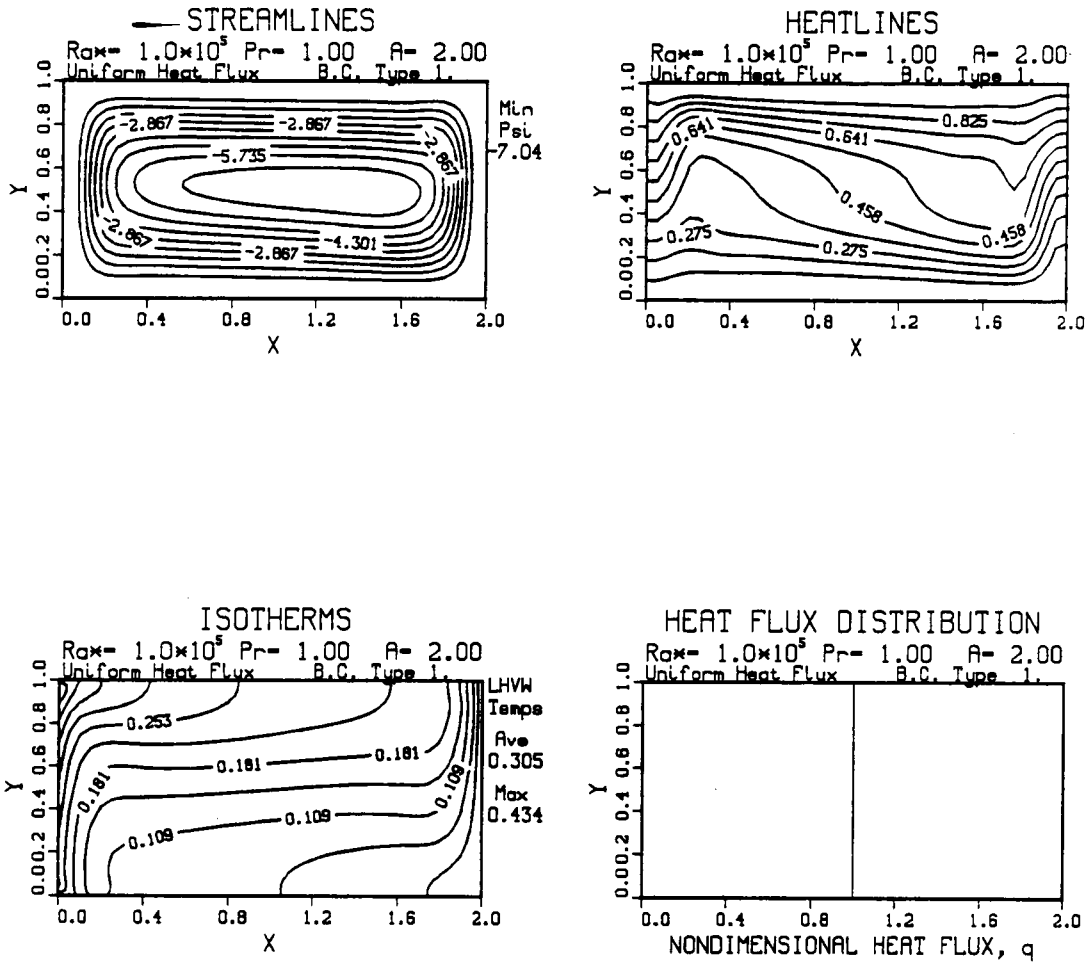


Figure C-37. Summary of results from aspect ratio sensitivity studies for uniform heat flux distribution with A = 2

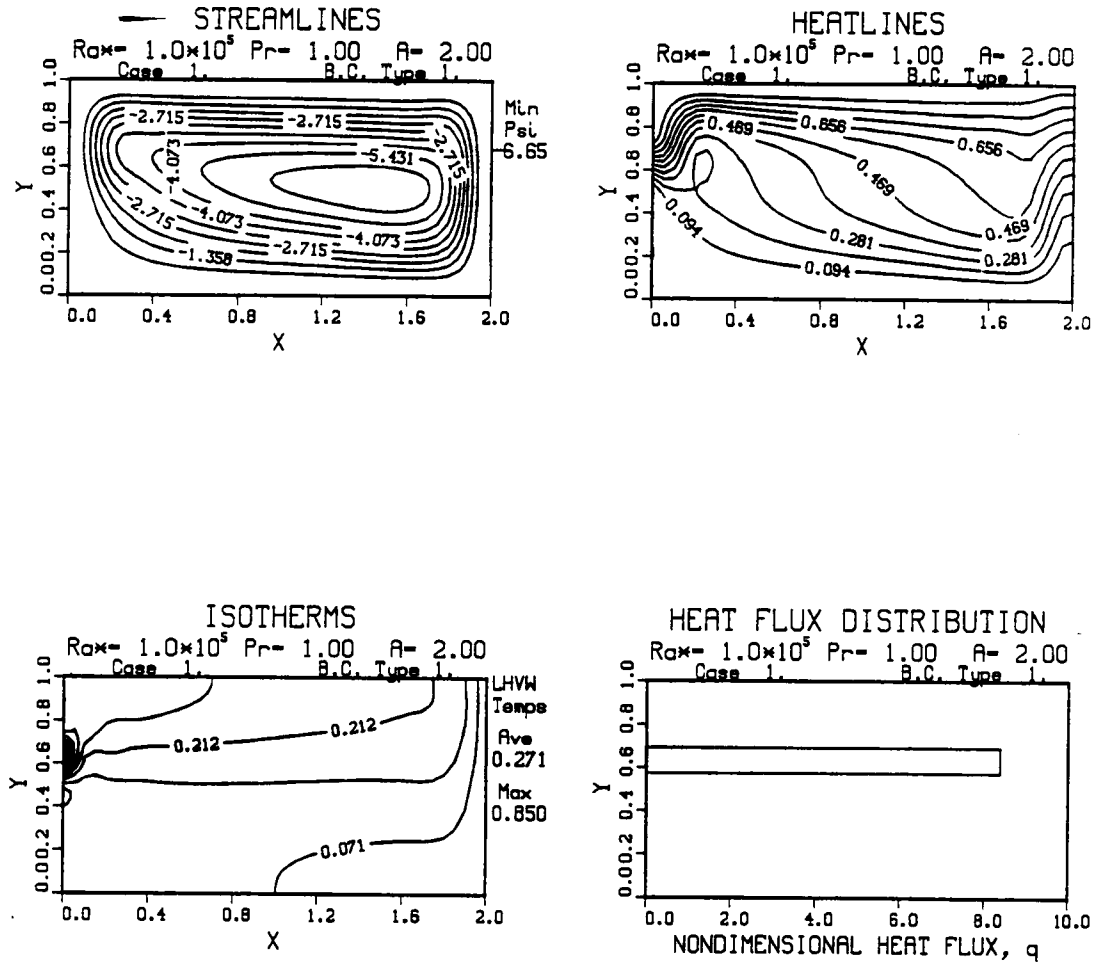


Figure C-38. Summary of results from aspect ratio senstivity studies for Case 1 type optimization with A = 2

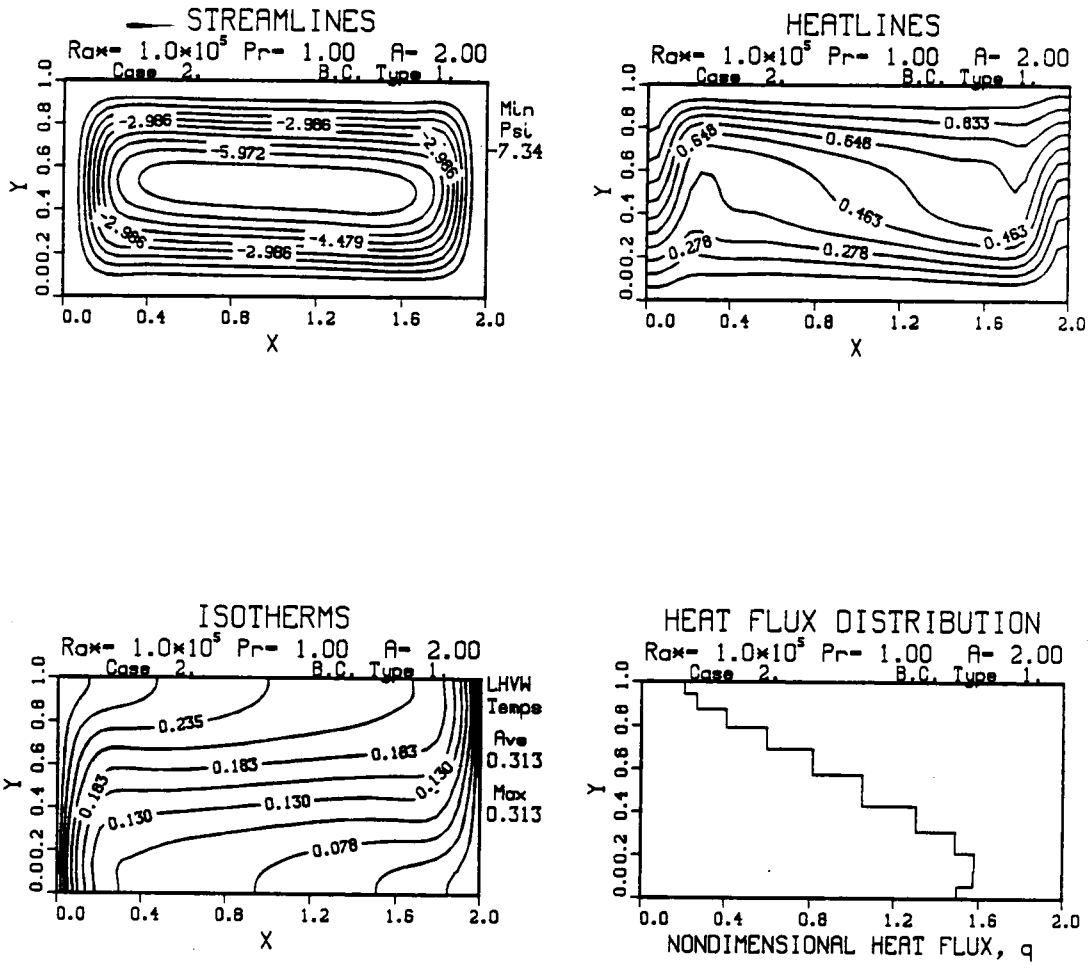


Figure C-39. Summary of results from aspect ratio sensitivity studies for Case 2 type optimization with A = 2

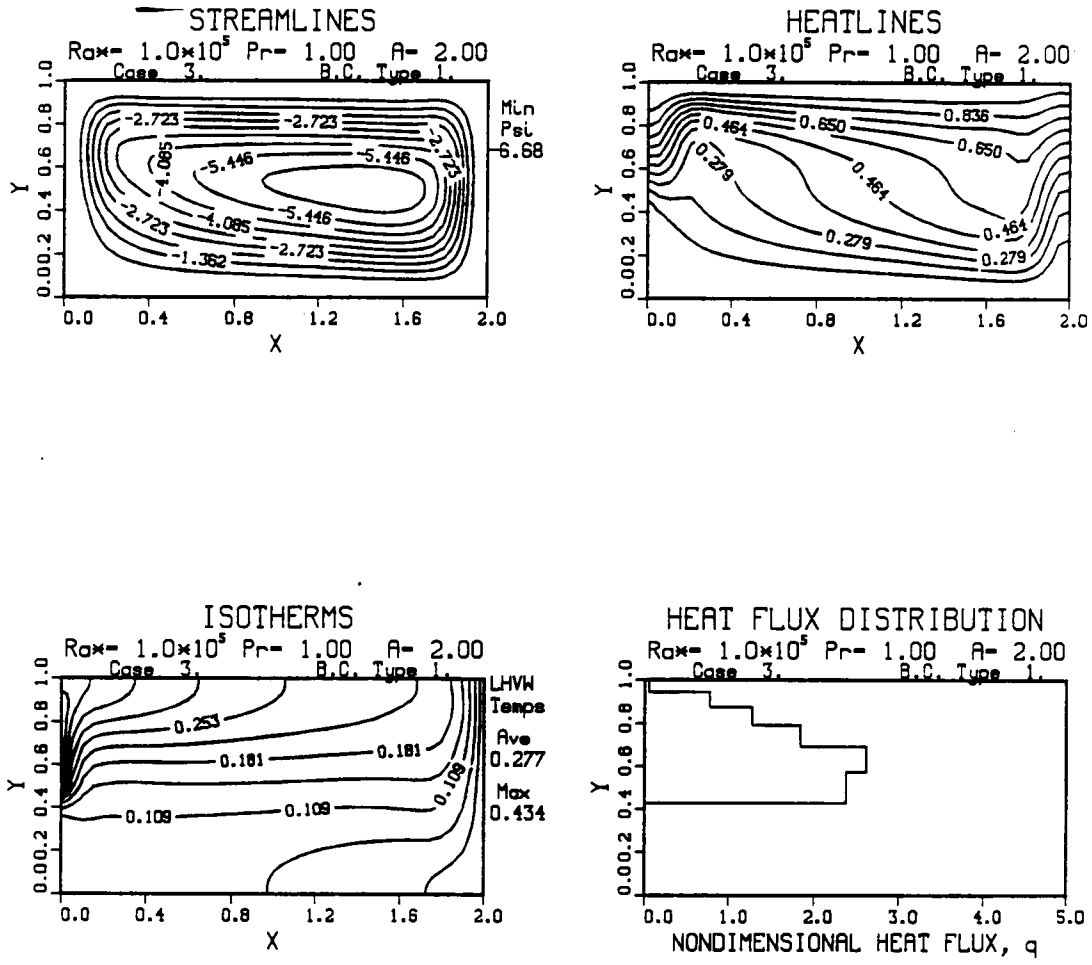


Figure C-40. Summary of results from aspect ratio sensitivity studies for Case 3 type optimization with A = 2

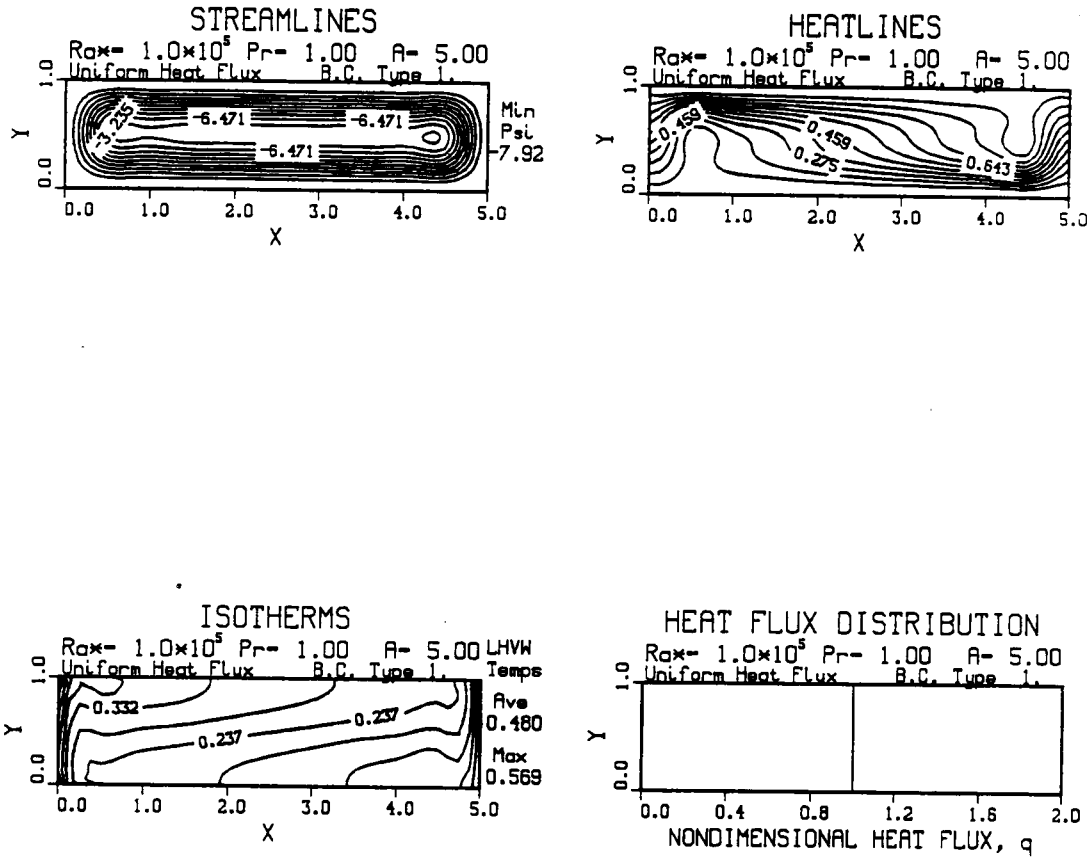


Figure C-41. Summary of results from aspect ratio sensitivity studies for uniform heat flux distribution with A = 5

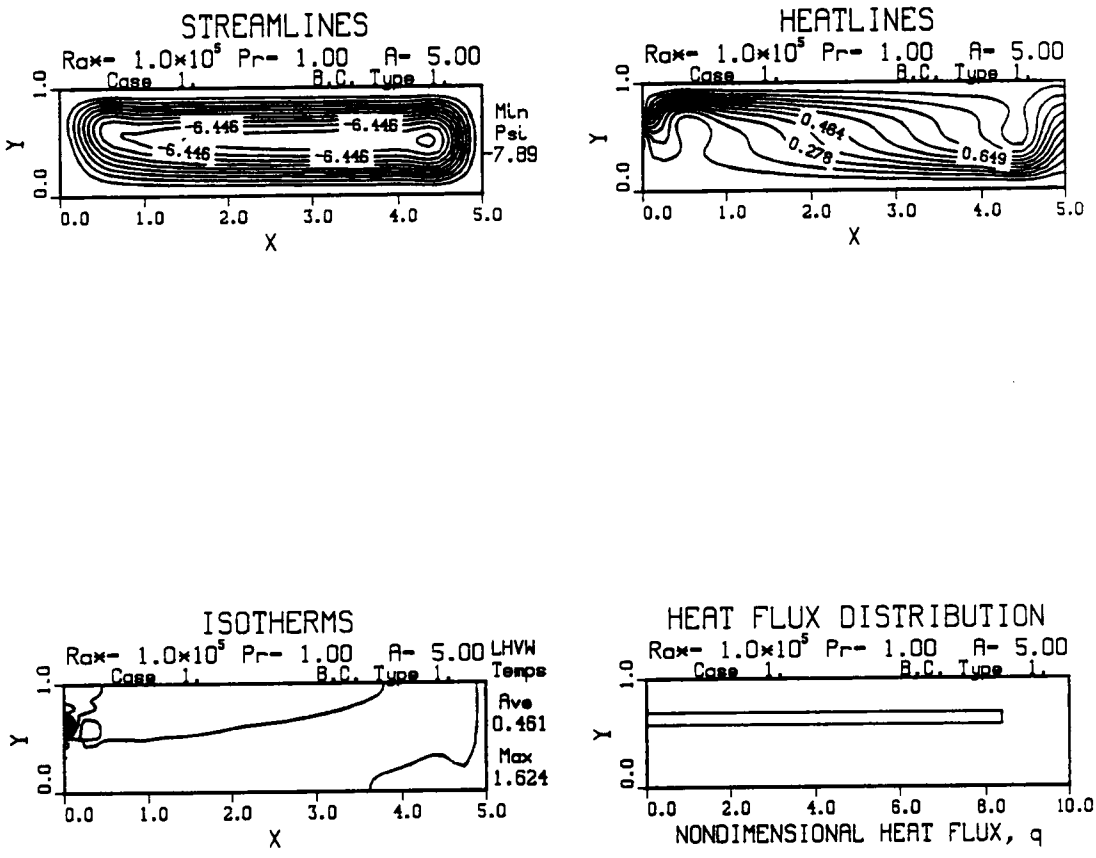


Figure C-42. Summary of results from aspect ratio senstivity studies for Case 1 type optimization with A = 5

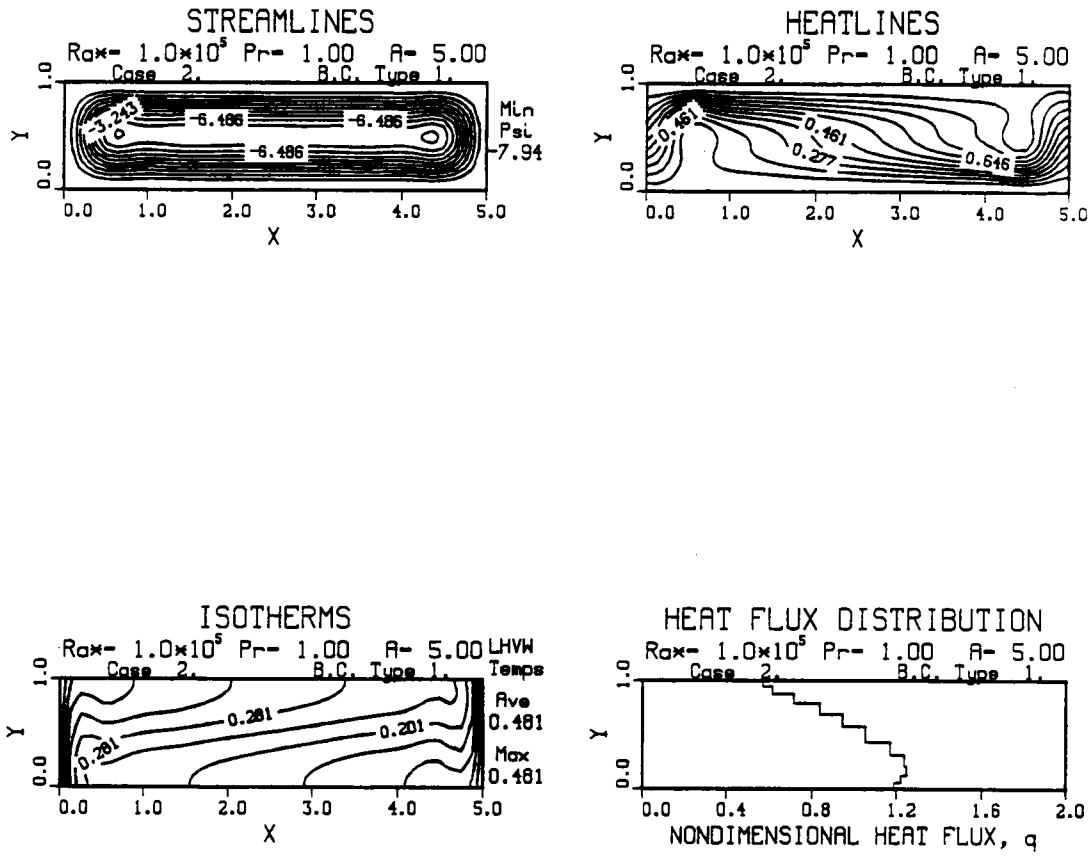


Figure C-43. Summary of results from aspect ratio sensitivity studies for Case 2 type optimization with A = 5

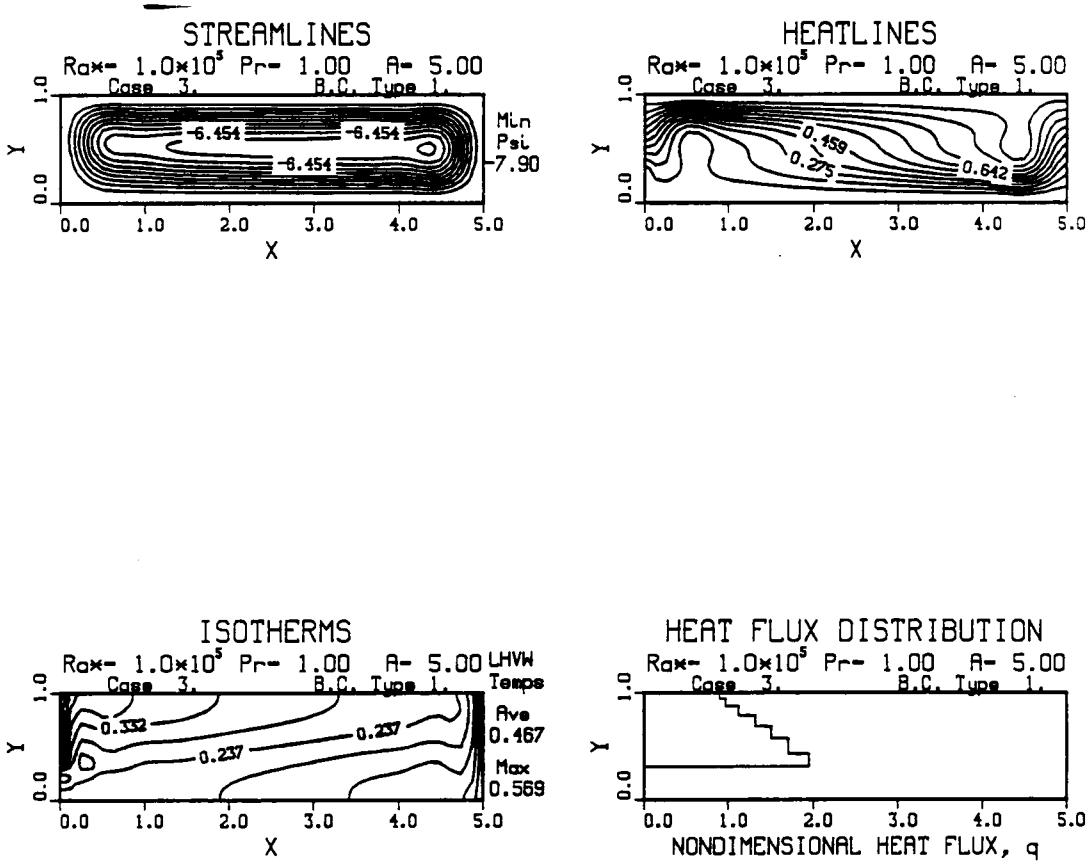


Figure C-44. Summary of results from aspect ratio sensitivity studies for Case 3 type optimization with A = 5

THERMAL BOUNDARY CONDITION
SENSITIVITY STUDIES

Ra^* varied from 10^3 to 10^6

Thermal Boundary Conditions Type 2 and 3

$Pr = 1$

$A = 1$

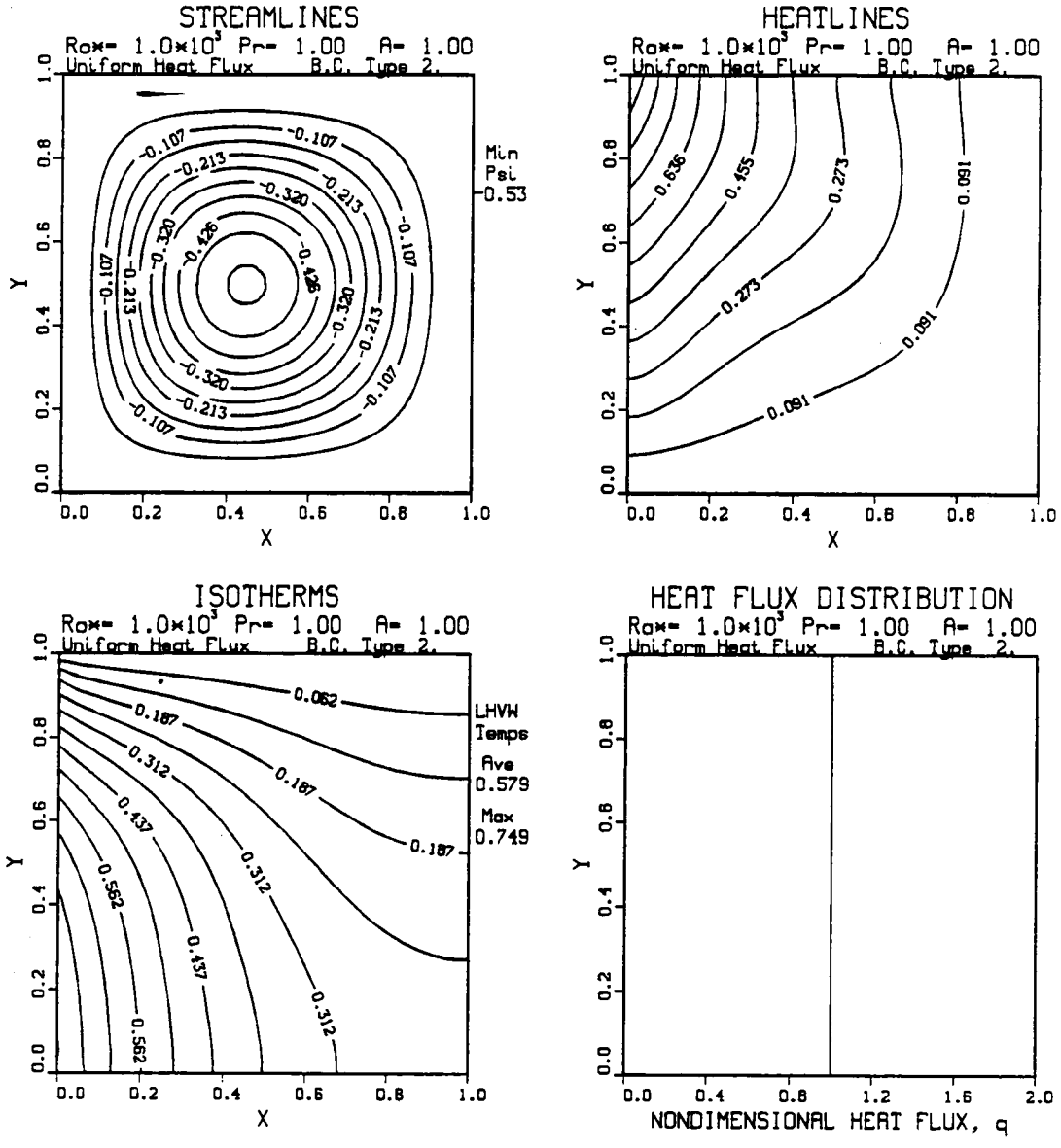


Figure C-45. Summary of results from thermal boundary condition sensitivity studies for uniform heat flux distribution with thermal boundary condition Type 2 and $Ra^* = 10^3$

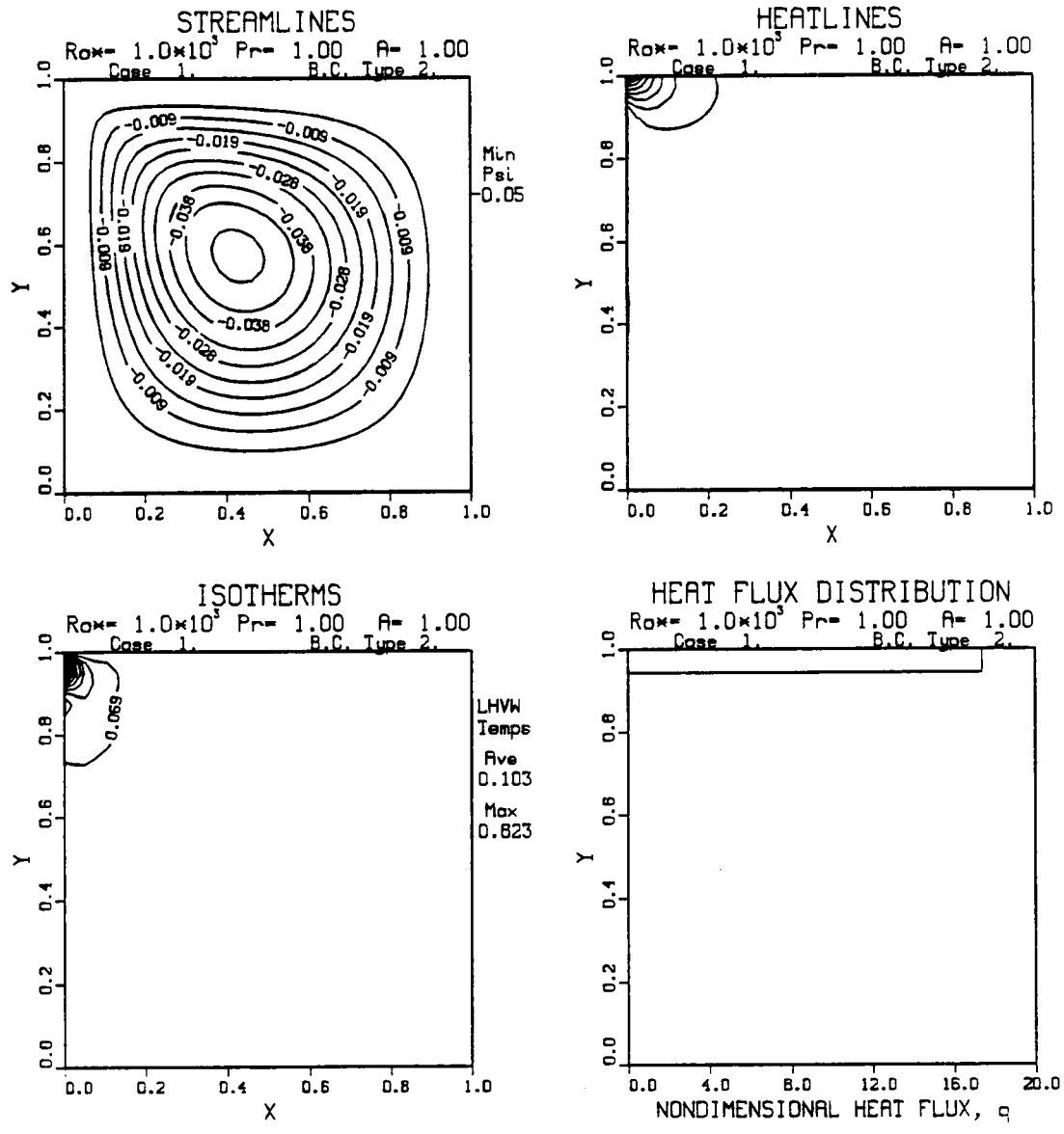


Figure C-46. Summary of results from thermal boundary condition sensitivity studies for Case 1 type optimization with thermal boundary condition Type 2 and $Ra^*=10^3$

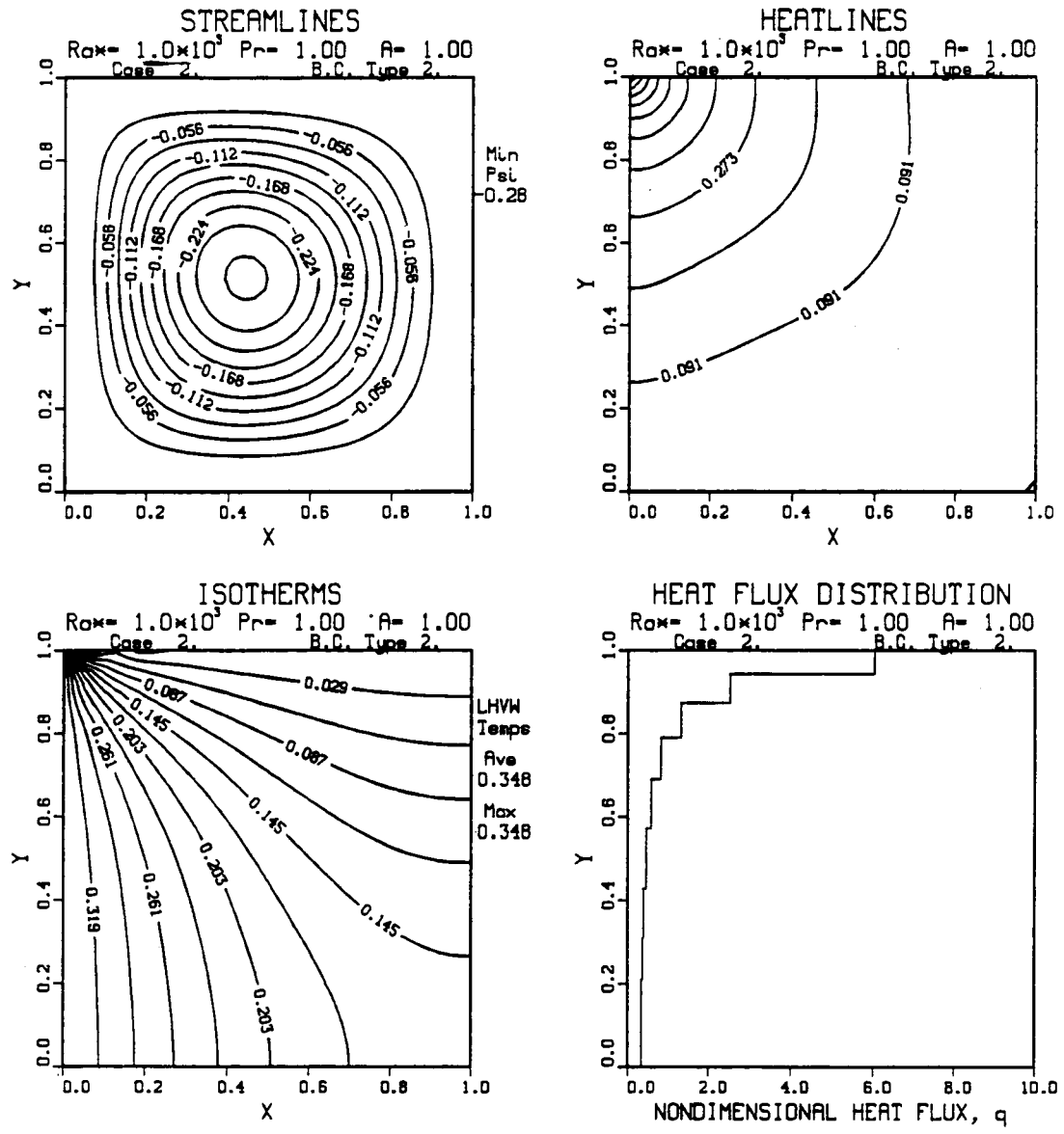


Figure C-47. Summary of results from thermal boundary condition sensitivity studies for Case 2 type optimization with thermal boundary condition Type 2 and $Ra^*=10^3$

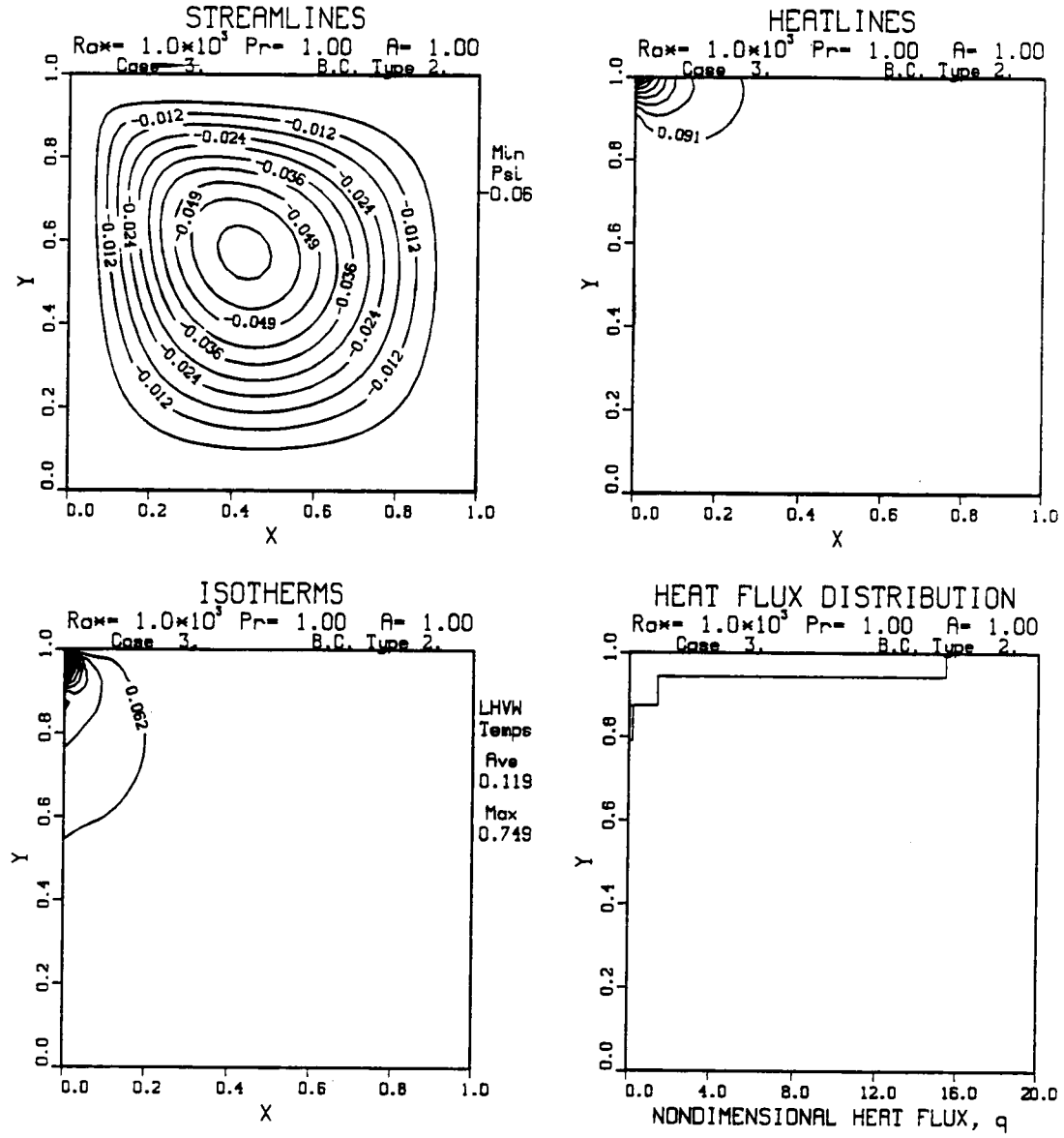


Figure C-48. Summary of results from thermal boundary condition sensitivity studies for Case 3 type optimization with thermal boundary condition Type 2 and $Ra^*=10^3$

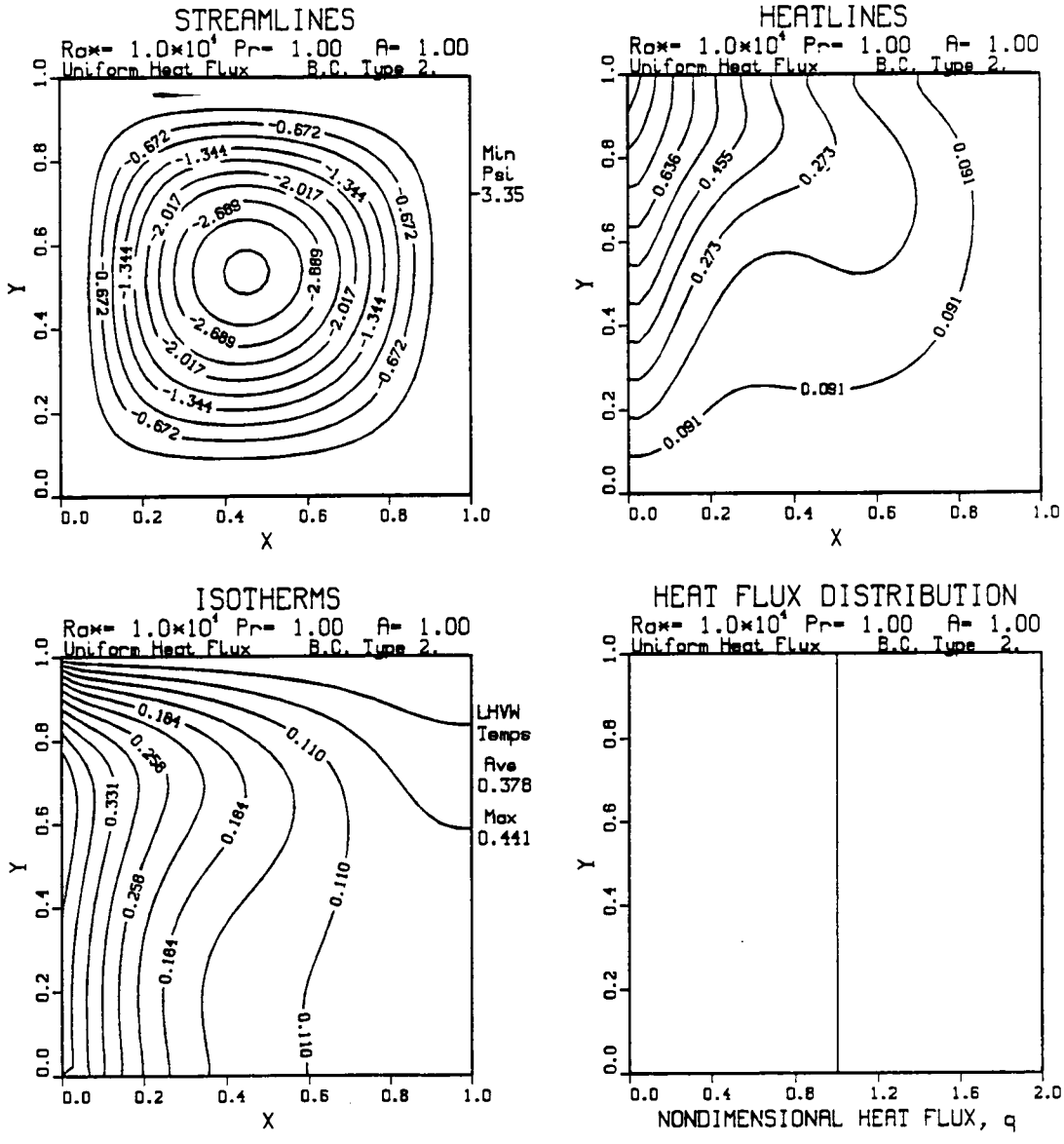


Figure C-49. Summary of results from thermal boundary condition sensitivity studies for uniform heat flux distribution with thermal boundary condition Type 2 and $Ra^* = 10^4$

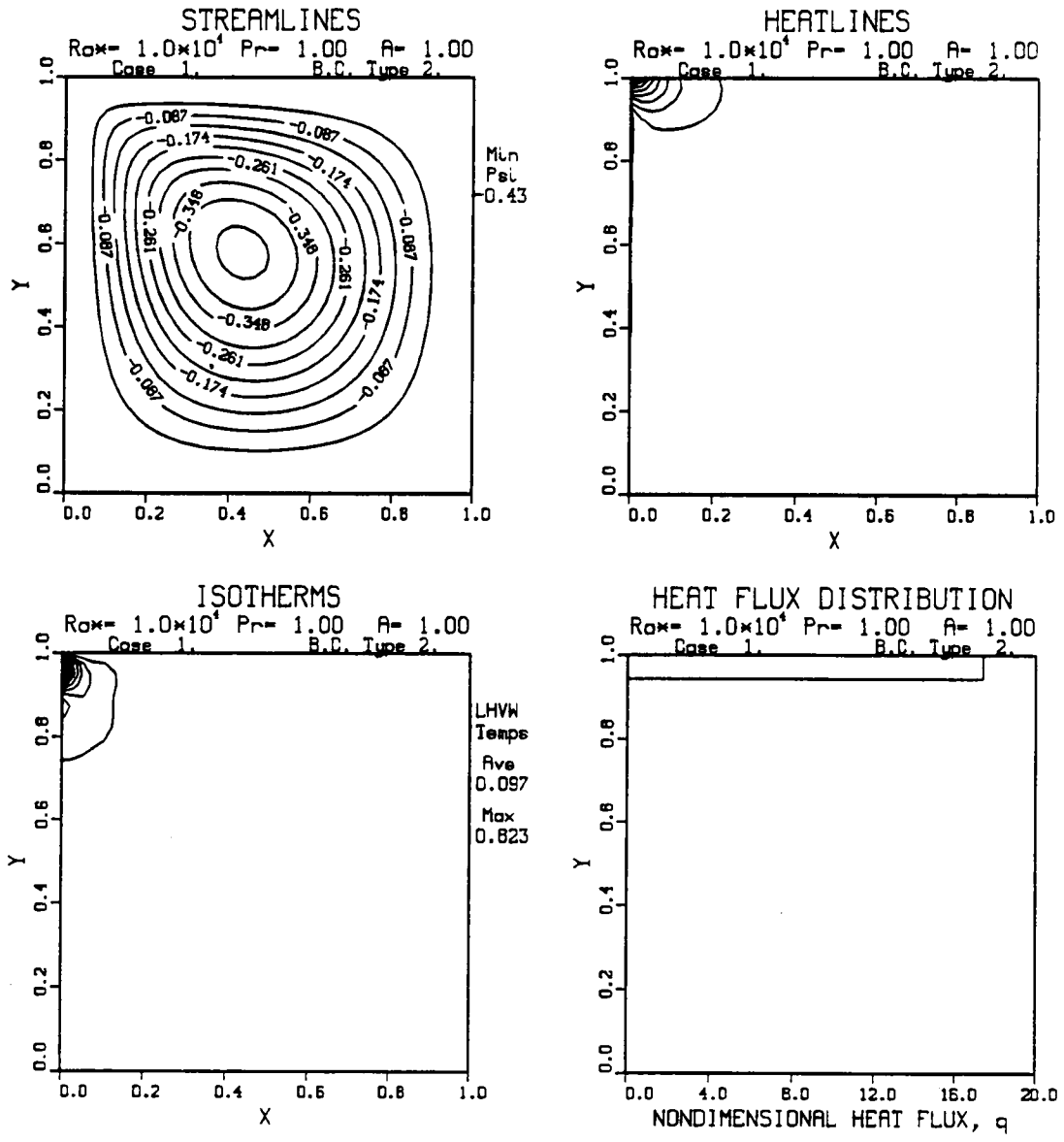


Figure C-50. Summary of results from thermal boundary condition sensitivity studies for Case 1 type optimization with thermal boundary condition Type 2 and $Ra^*=10^4$

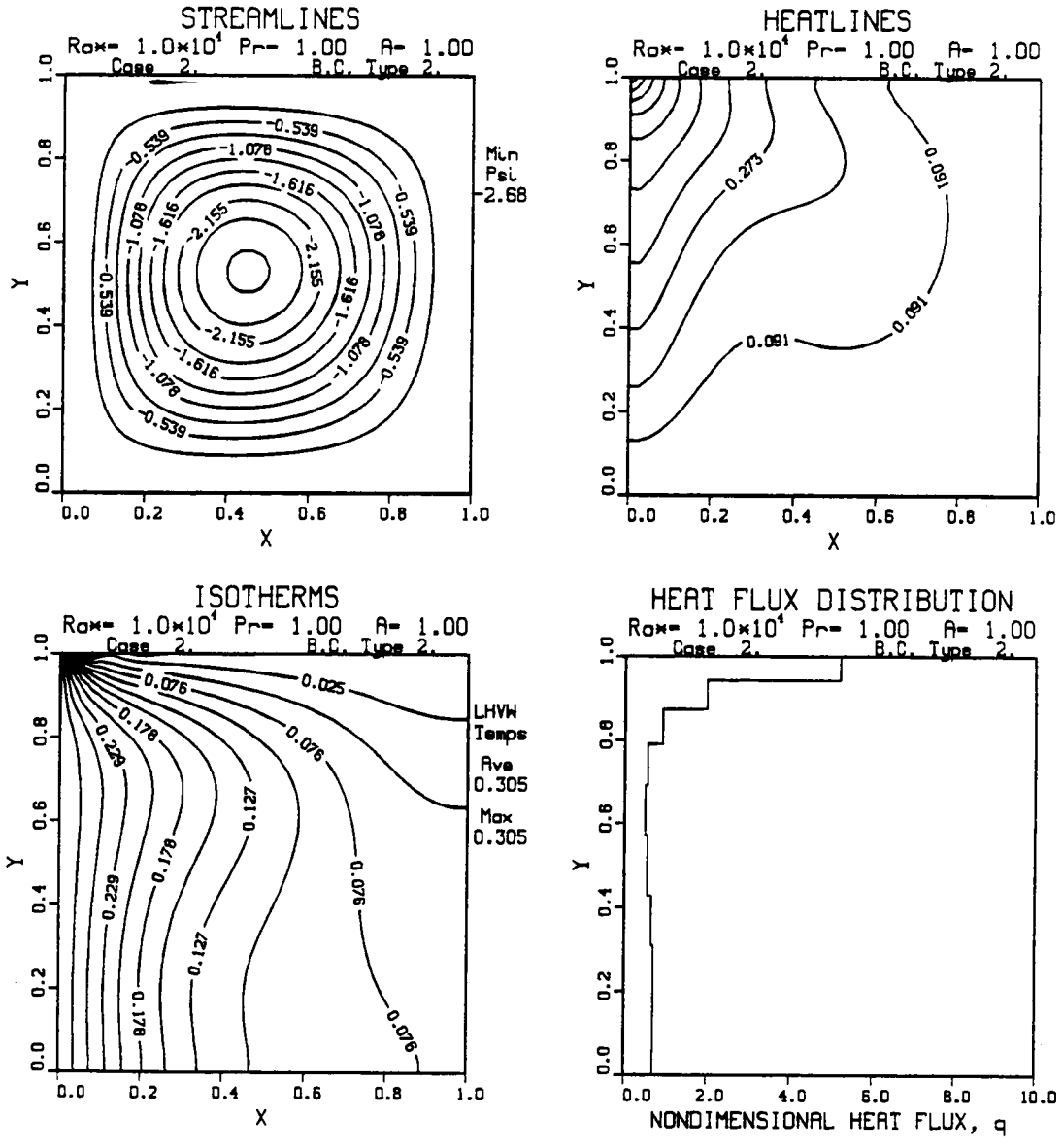


Figure C-51. Summary of results from thermal boundary condition sensitivity studies for Case 2 type optimization with thermal boundary condition Type 2 and $Ra^*=10^4$

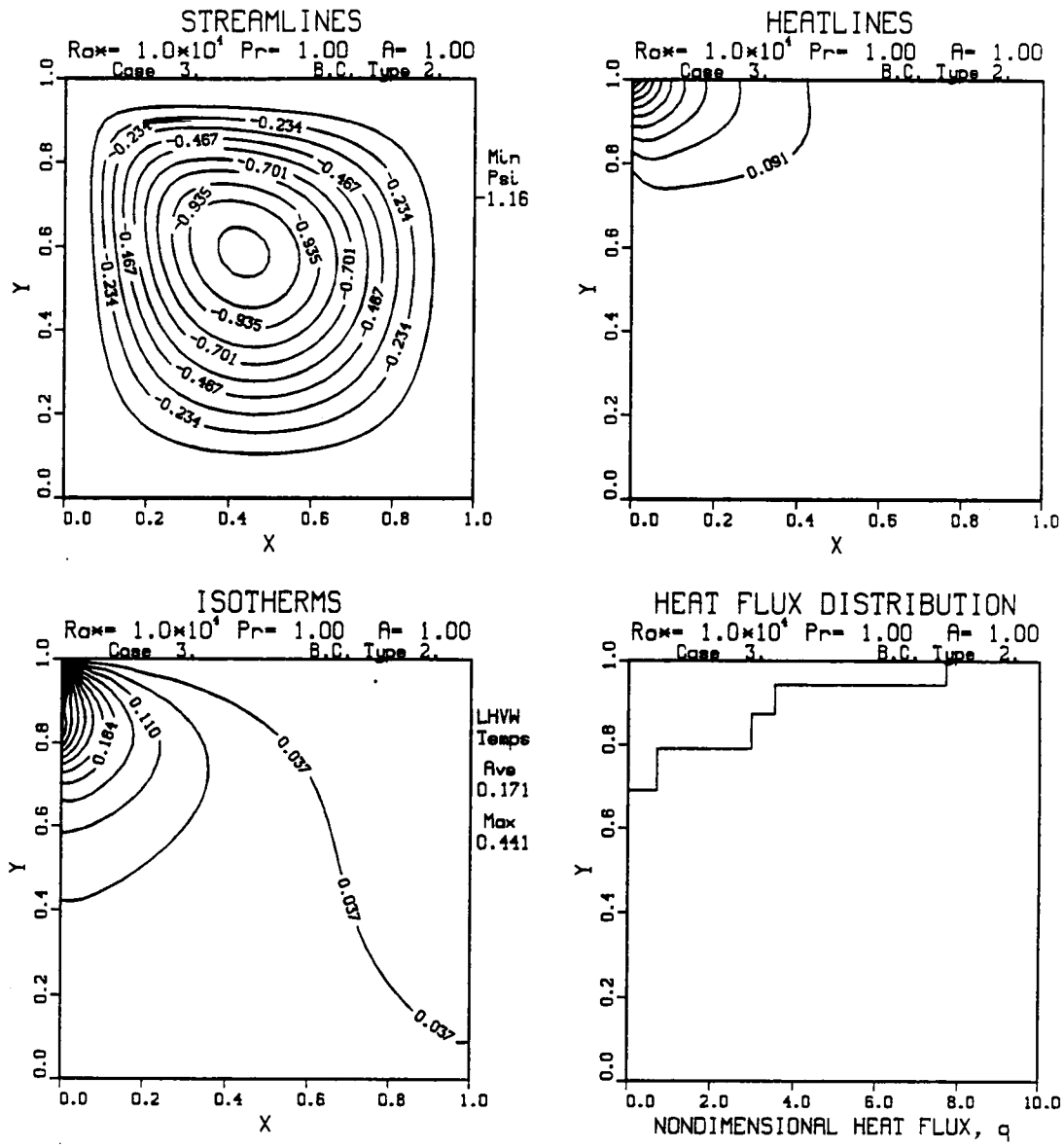


Figure C-52. Summary of results from thermal boundary condition sensitivity studies for Case 3 type optimization with thermal boundary condition Type 2 and $Ra^*=10^4$

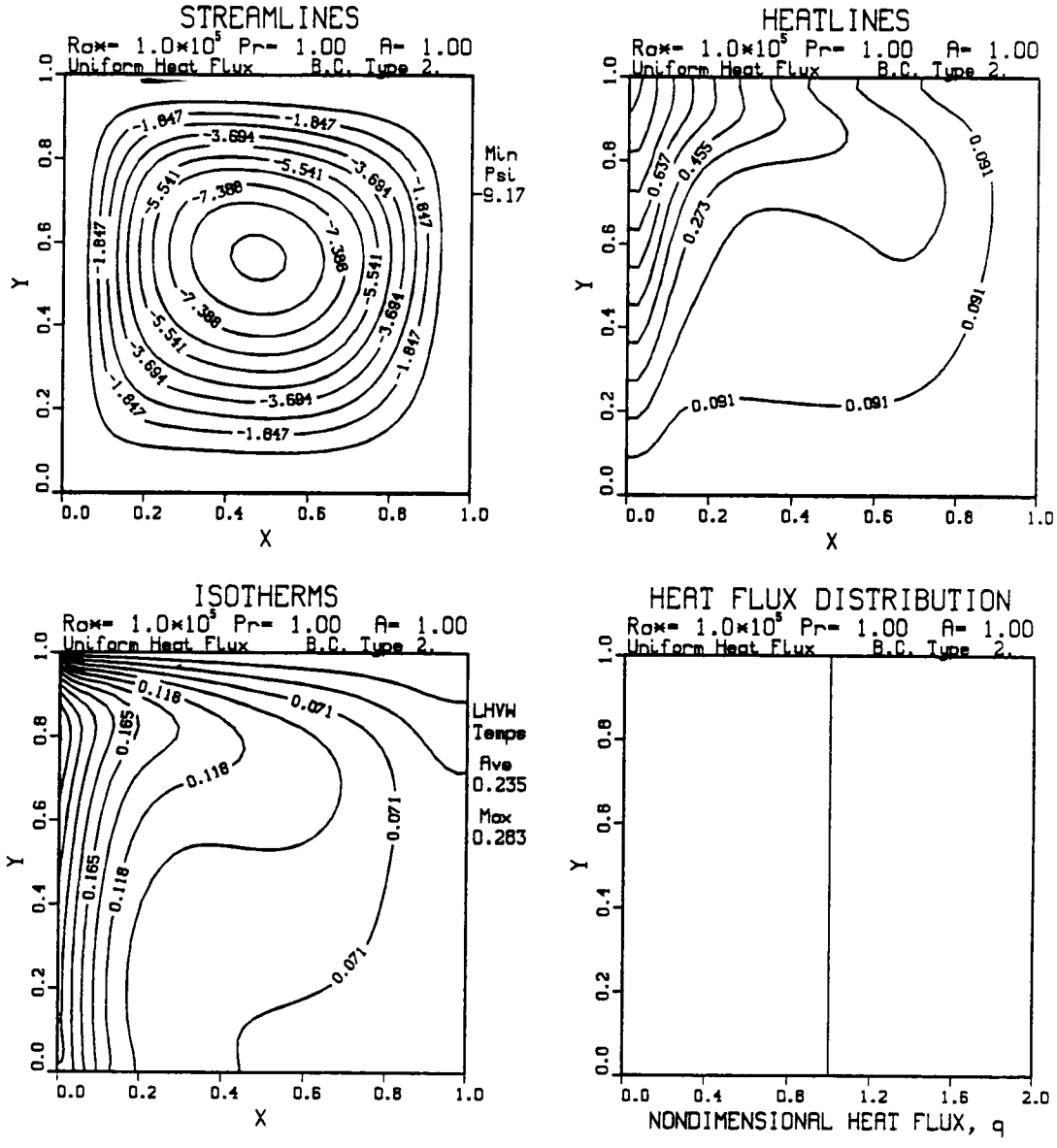


Figure C-53. Summary of results from thermal boundary condition sensitivity studies for uniform heat flux distribution with thermal boundary condition Type 2 and $Ra^* = 10^5$

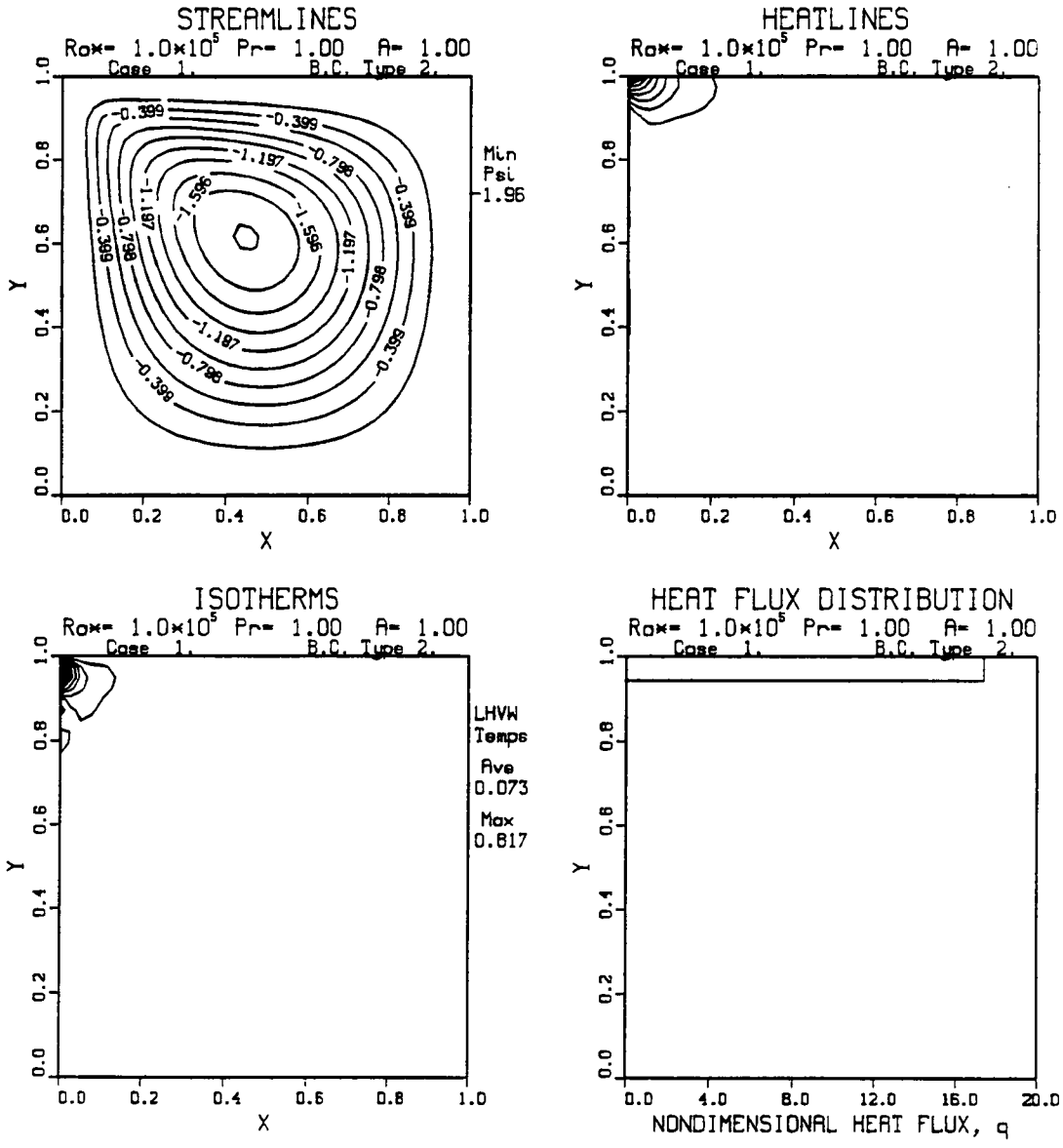


Figure C-54. Summary of results from thermal boundary condition sensitivity studies for Case 1 type optimization with thermal boundary condition Type 2 and $Ra^*=10^5$

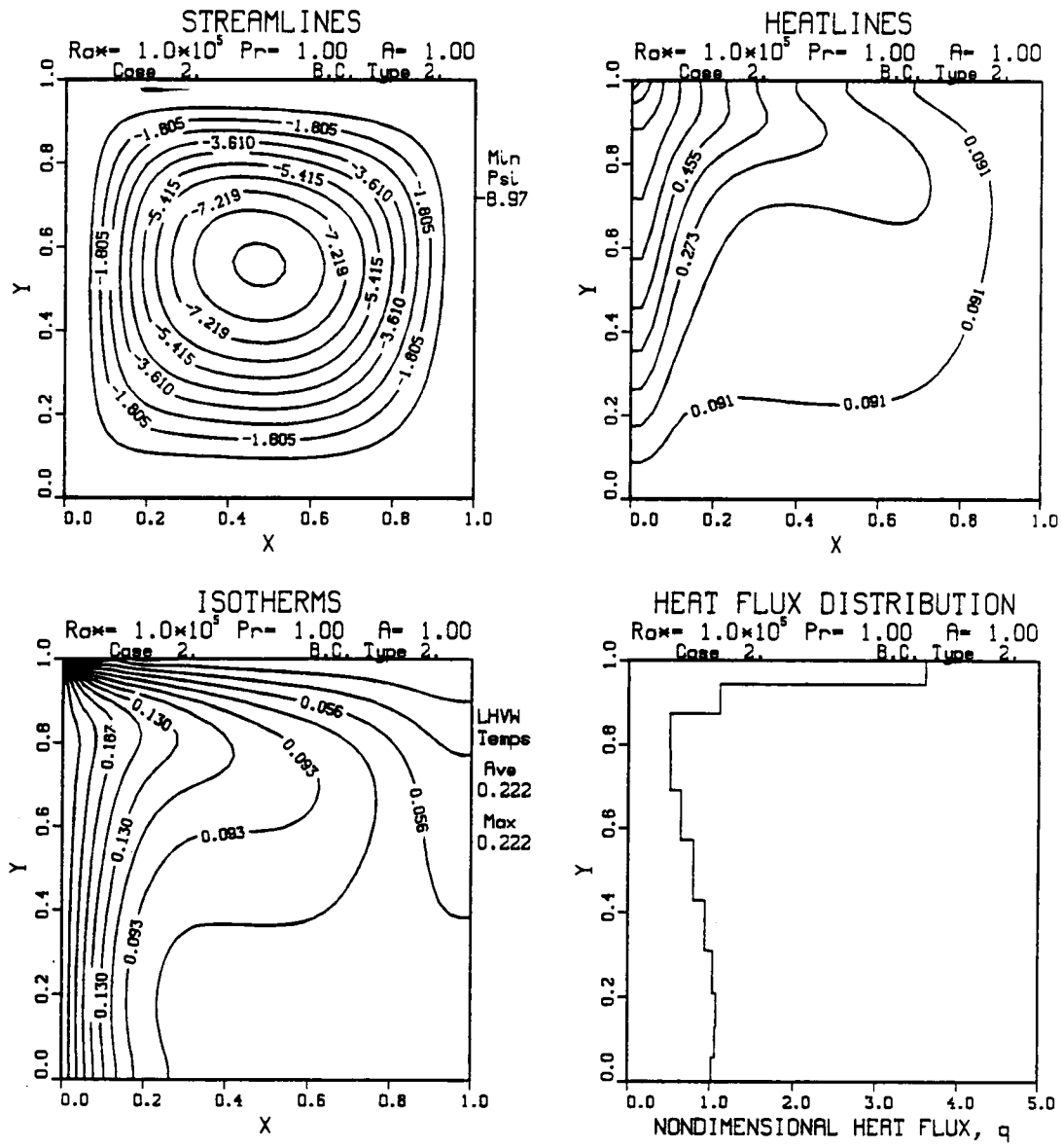


Figure C-55. Summary of results from thermal boundary condition sensitivity studies for Case 2 type optimization with thermal boundary condition Type 2 and $Ra^*=10^5$

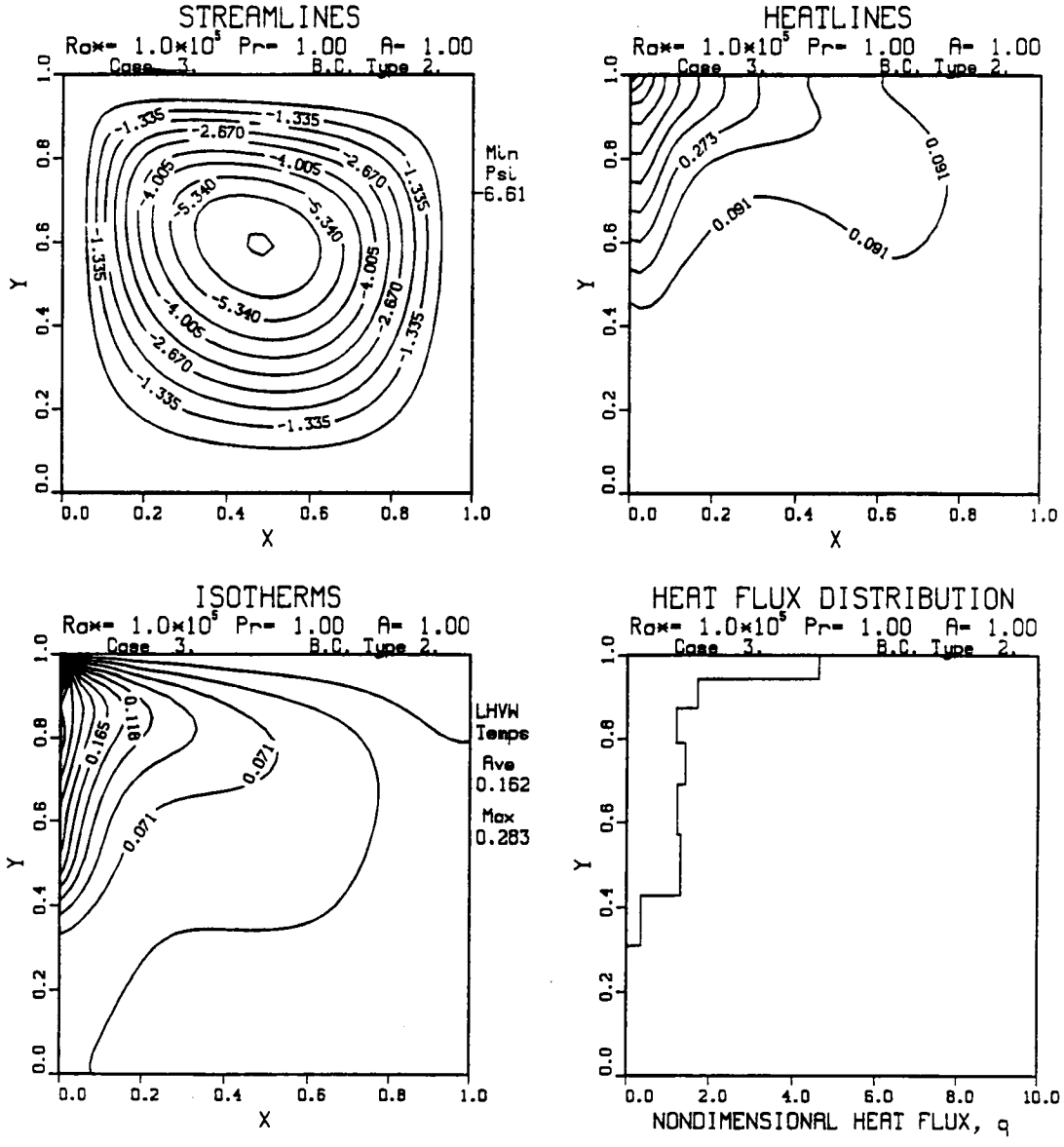


Figure C-56. Summary of results from thermal boundary condition sensitivity studies for Case 3 type optimization with thermal boundary condition Type 2 and $Ra^*=10^5$

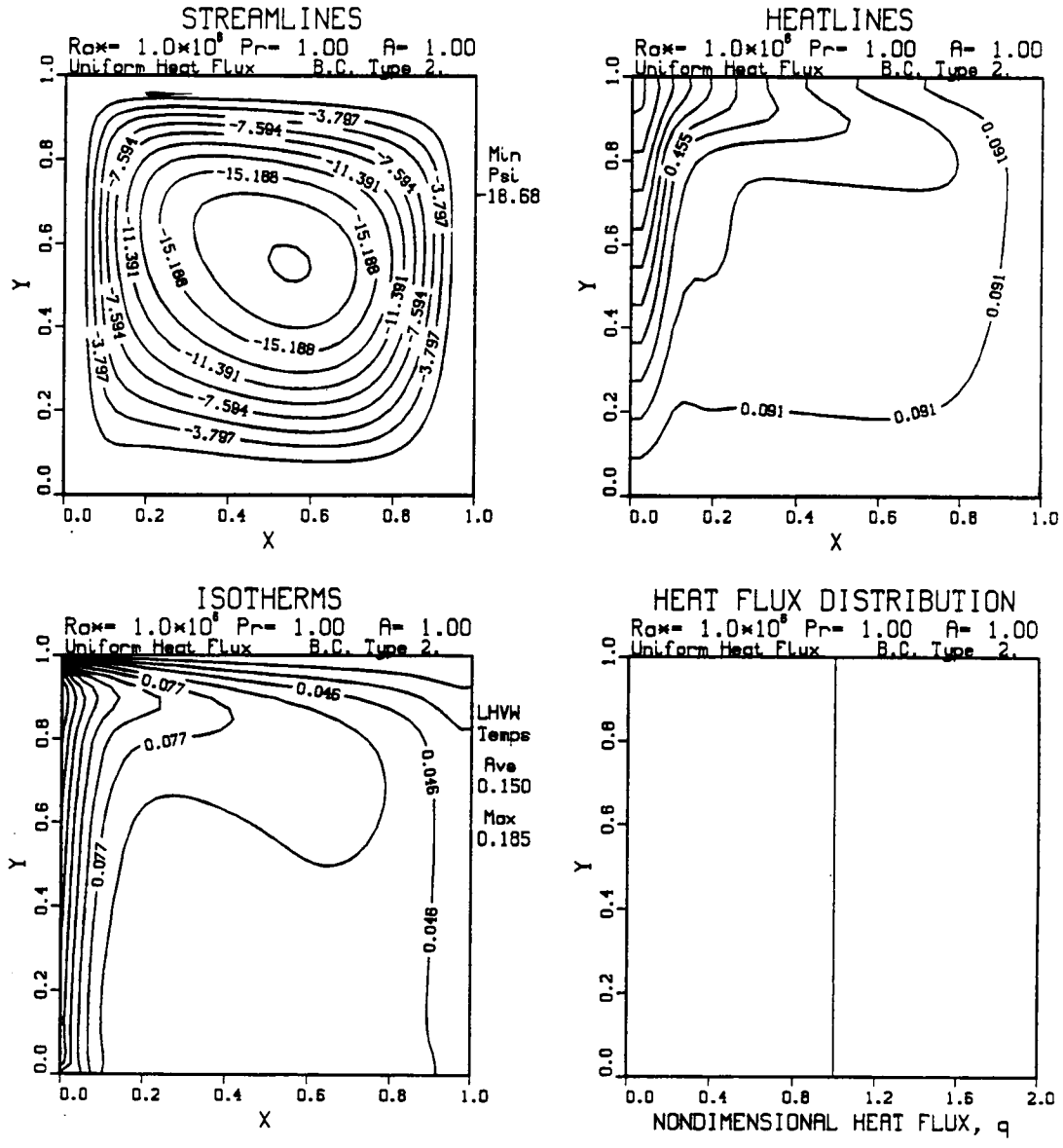


Figure C-57. Summary of results from thermal boundary condition sensitivity studies for uniform heat flux distribution with thermal boundary condition Type 2 and $Ra^* = 10^6$

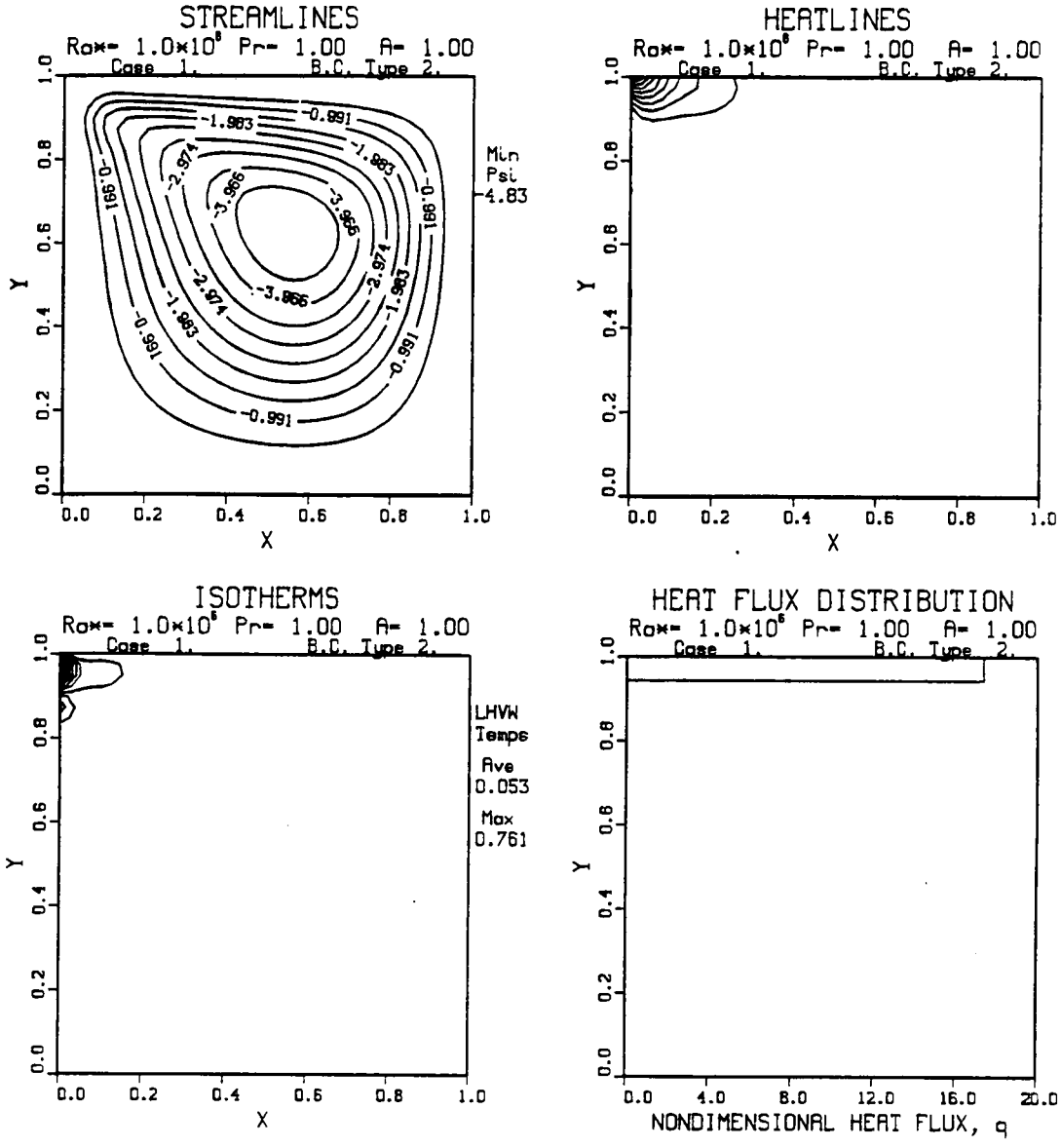


Figure C-58. Summary of results from thermal boundary condition sensitivity studies for Case 1 type optimization with thermal boundary condition Type 2 and $Ra^*=10^6$

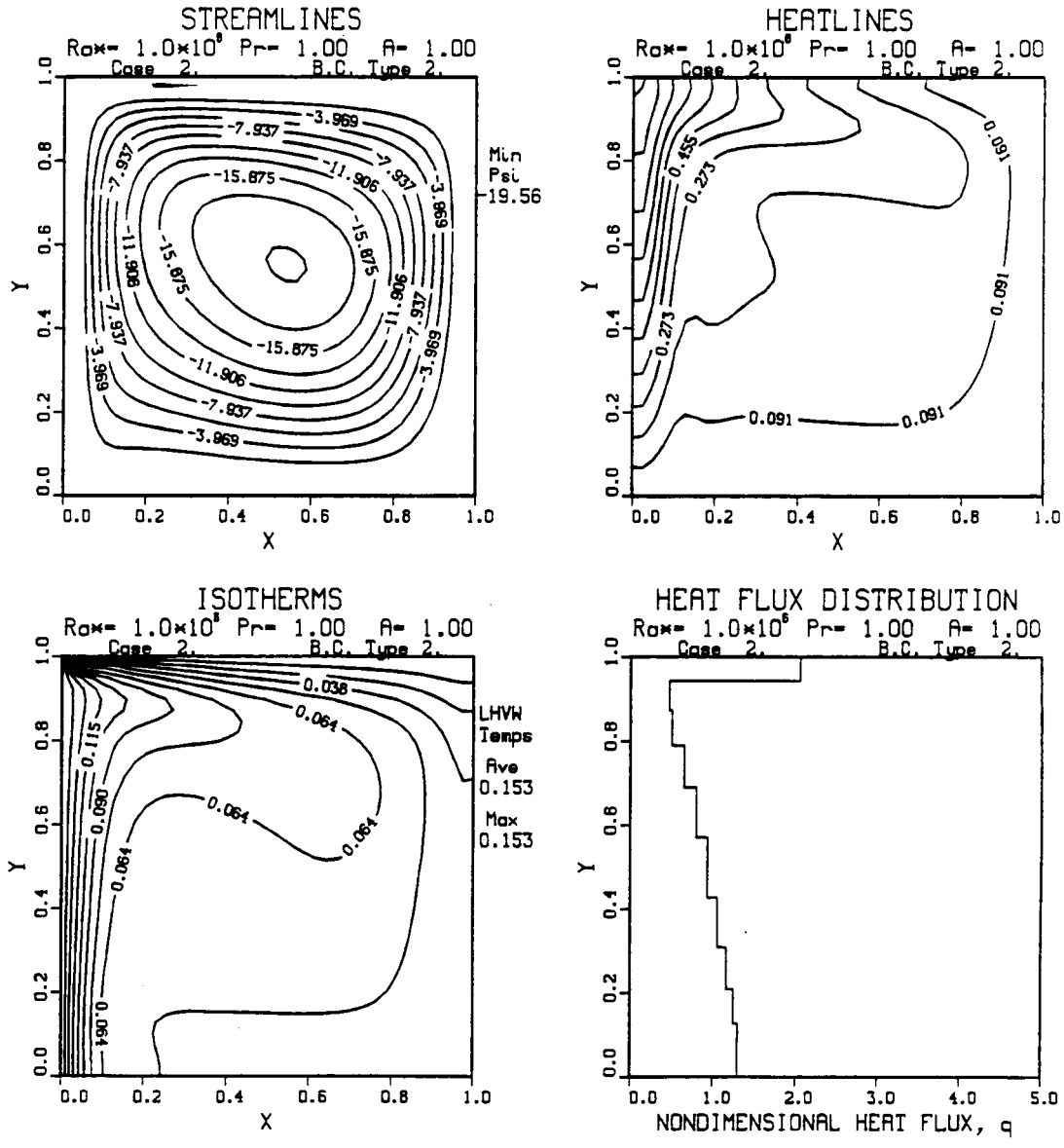


Figure C-59. Summary of results from thermal boundary condition sensitivity studies for Case 2 type optimization with thermal boundary condition Type 2 and $Ra^*=10^6$

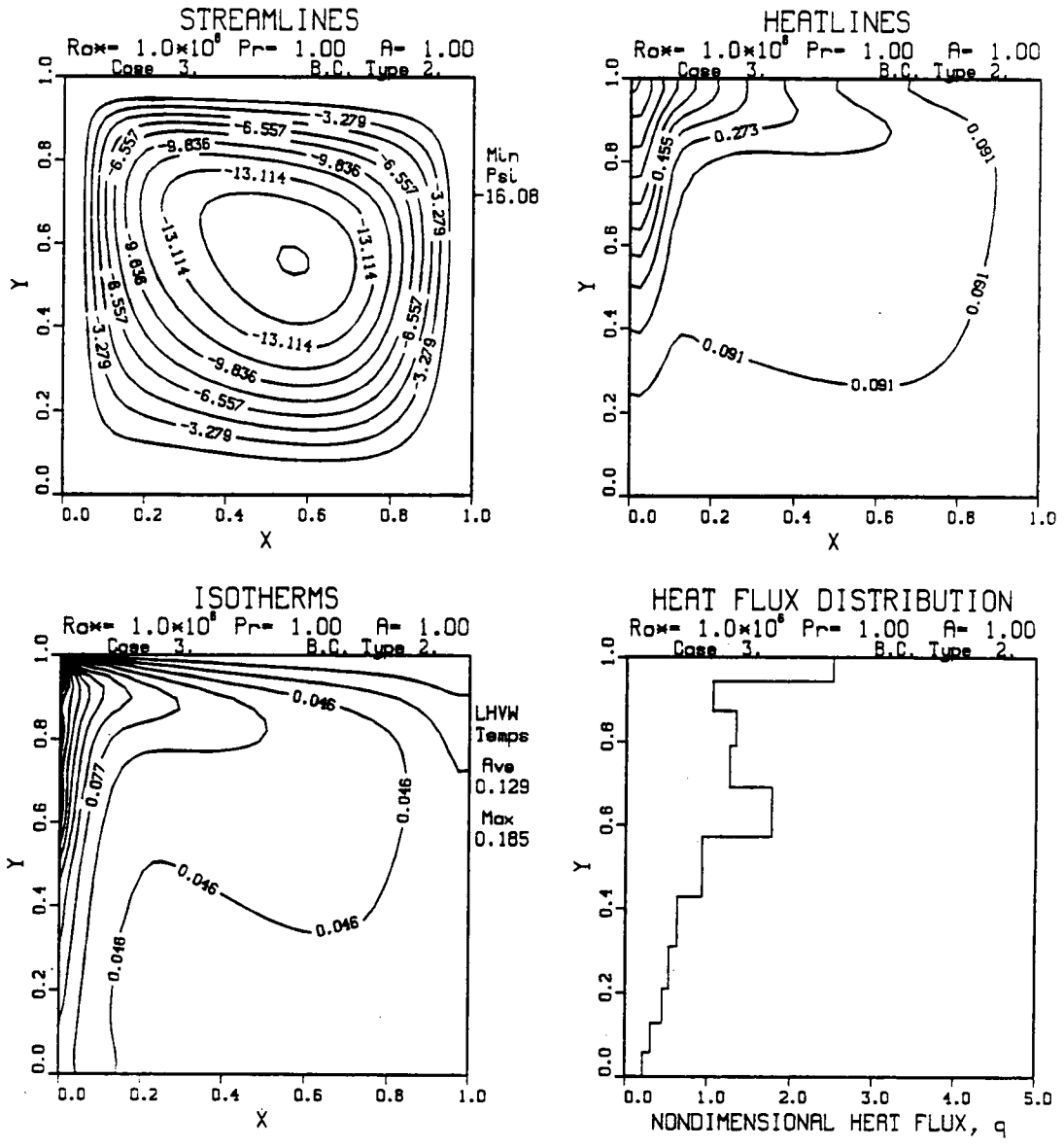


Figure C-60. Summary of results from thermal boundary condition sensitivity studies for Case 3 type optimization with thermal boundary condition Type 2 and $Ra^*=10^6$

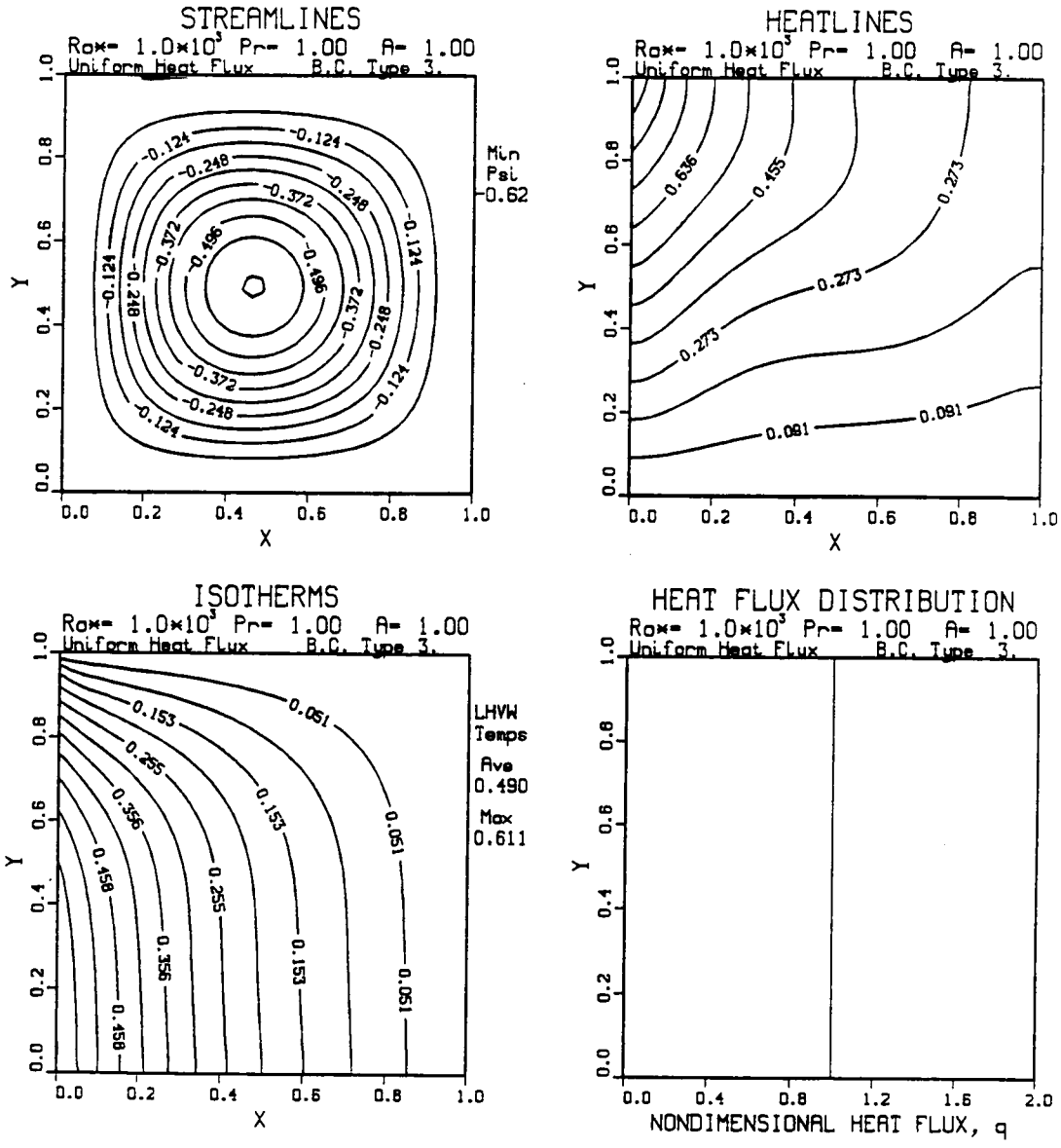


Figure C-61. Summary of results from thermal boundary condition sensitivity studies for uniform heat flux distribution with thermal boundary condition Type 3 and $Ra^* = 10^3$

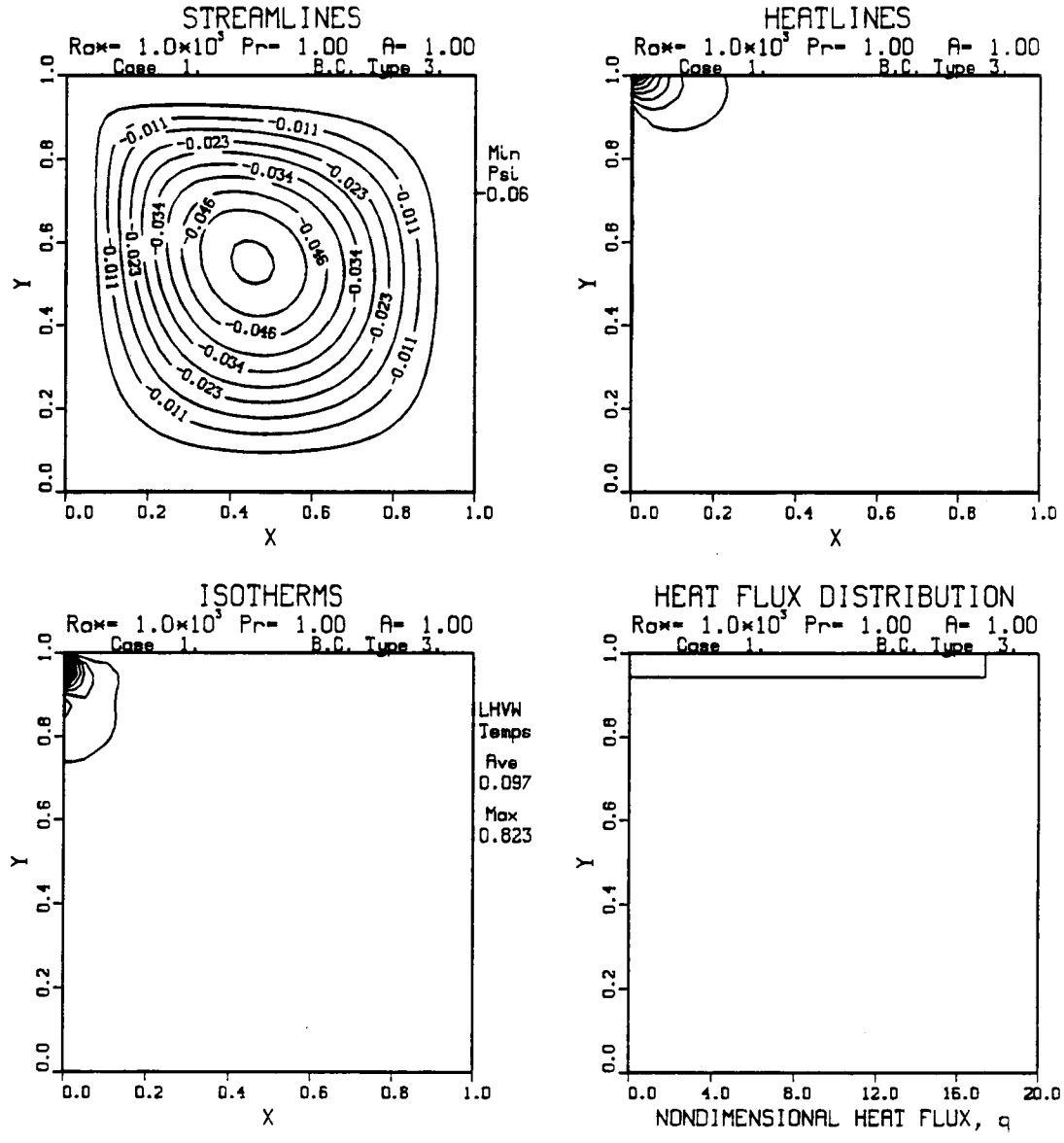


Figure C-62. Summary of results from thermal boundary condition sensitivity studies for Case 1 type optimization with thermal boundary condition Type 3 and $Ra^*=10^3$

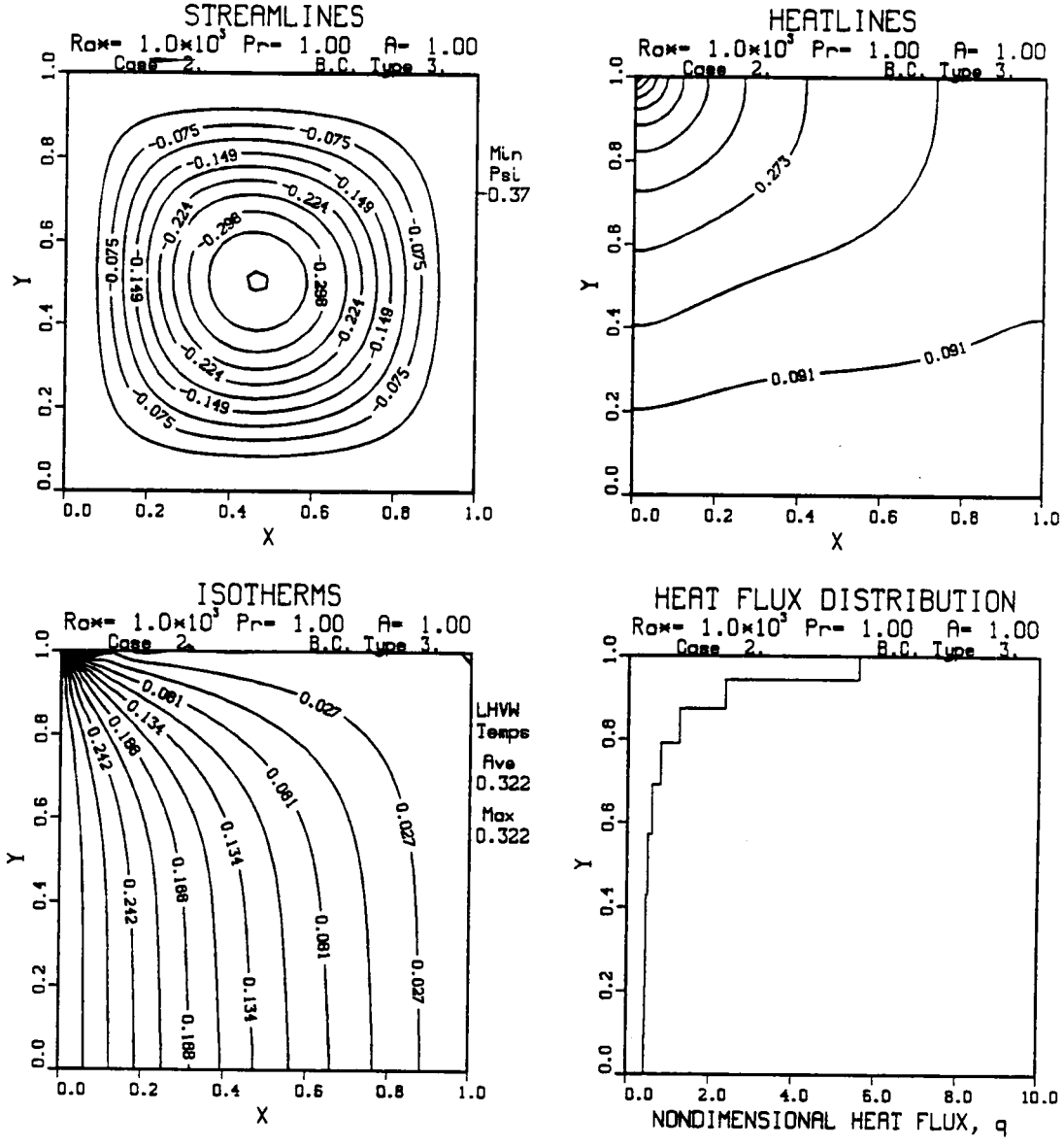


Figure C-63. Summary of results for thermal boundary condition sensitivity studies from Case 2 type optimization with thermal boundary condition Type 3 and $Ra^*=10^3$

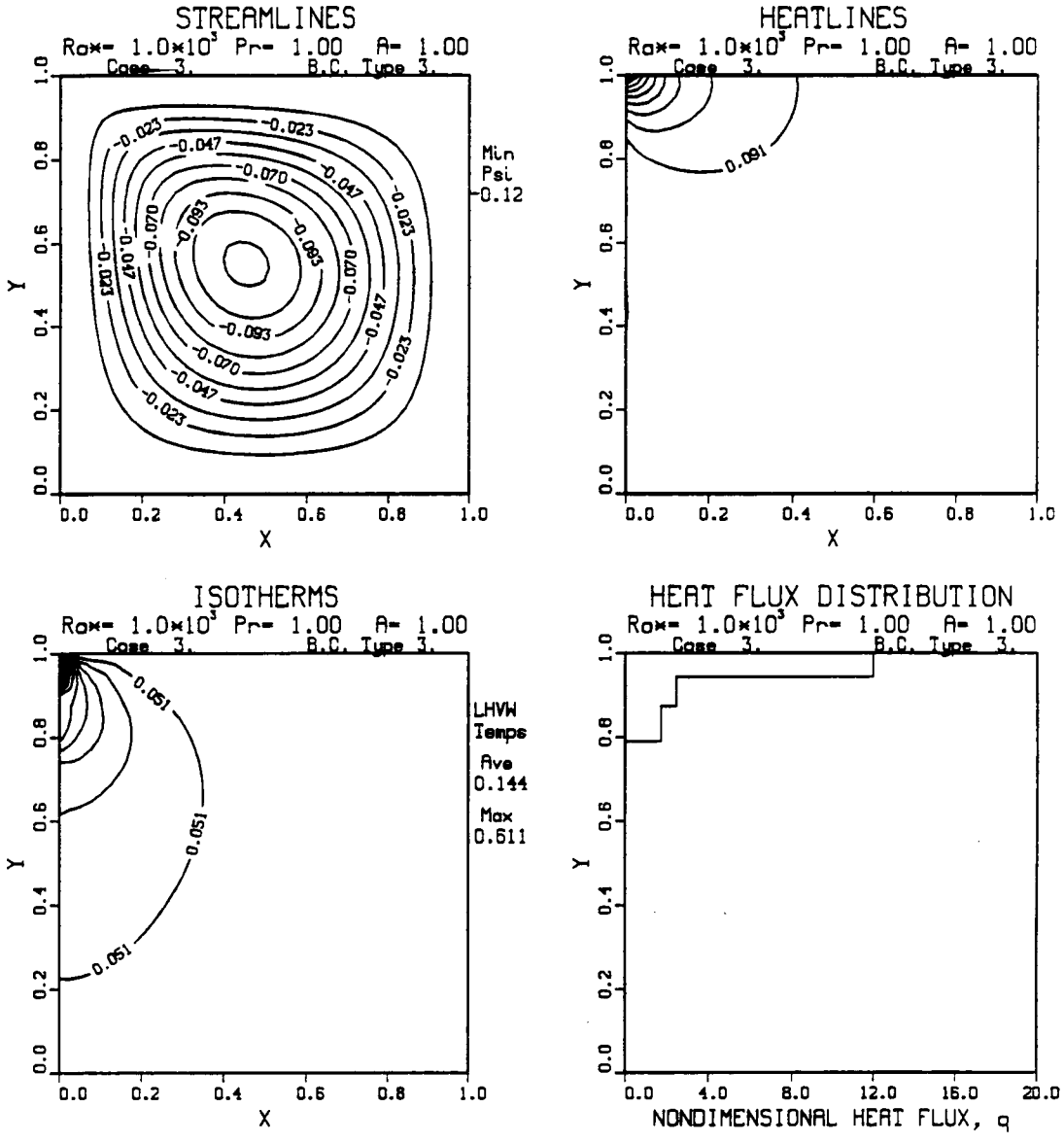


Figure C-64. Summary of results from thermal boundary condition sensitivity studies for Case 3 type optimization with thermal boundary condition Type 3 and $Ra^*=10^3$

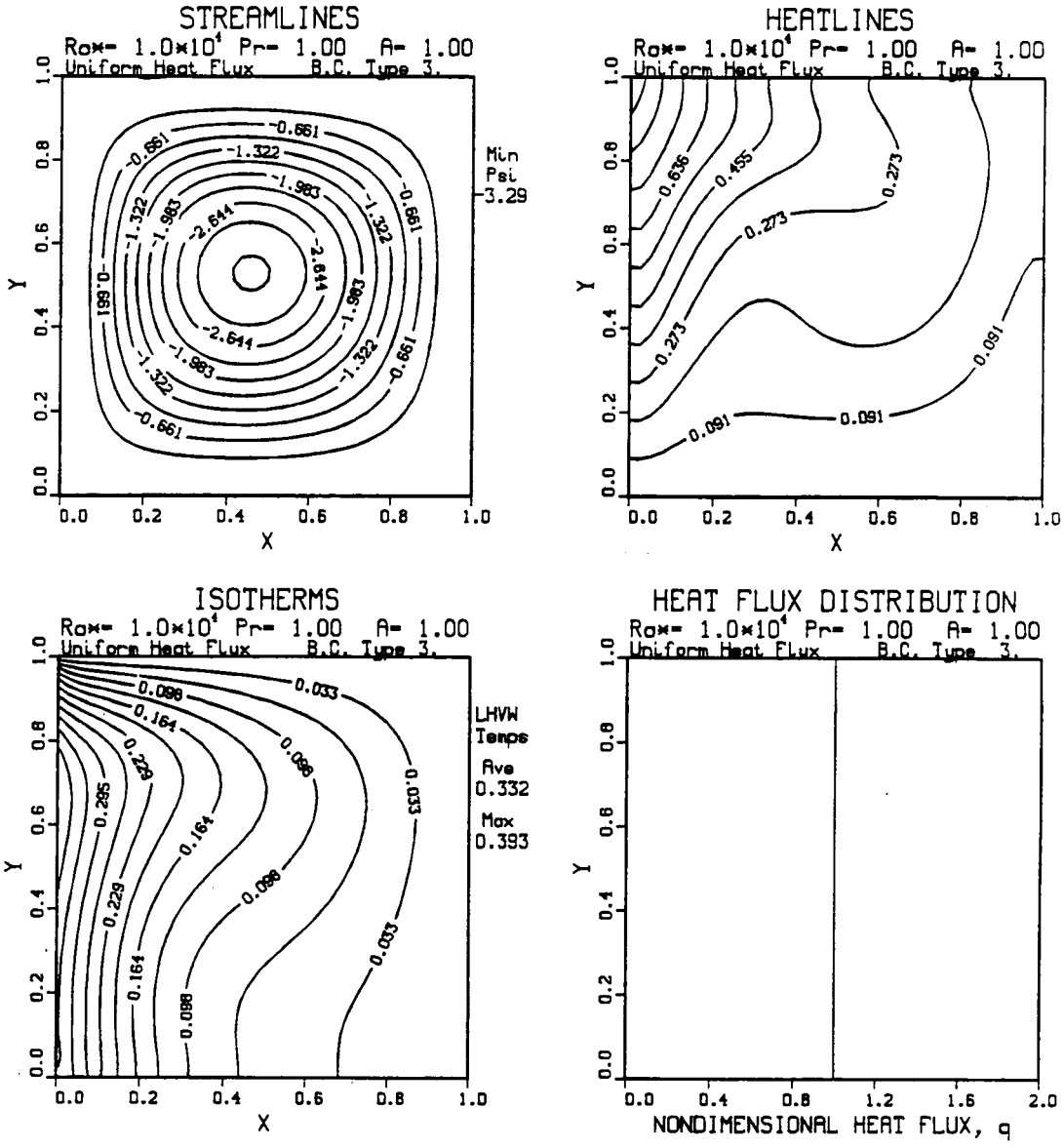


Figure C-65. Summary of results from thermal boundary condition sensitivity studies for uniform heat flux distribution with thermal boundary condition Type 3 and $Ra^* = 10^4$

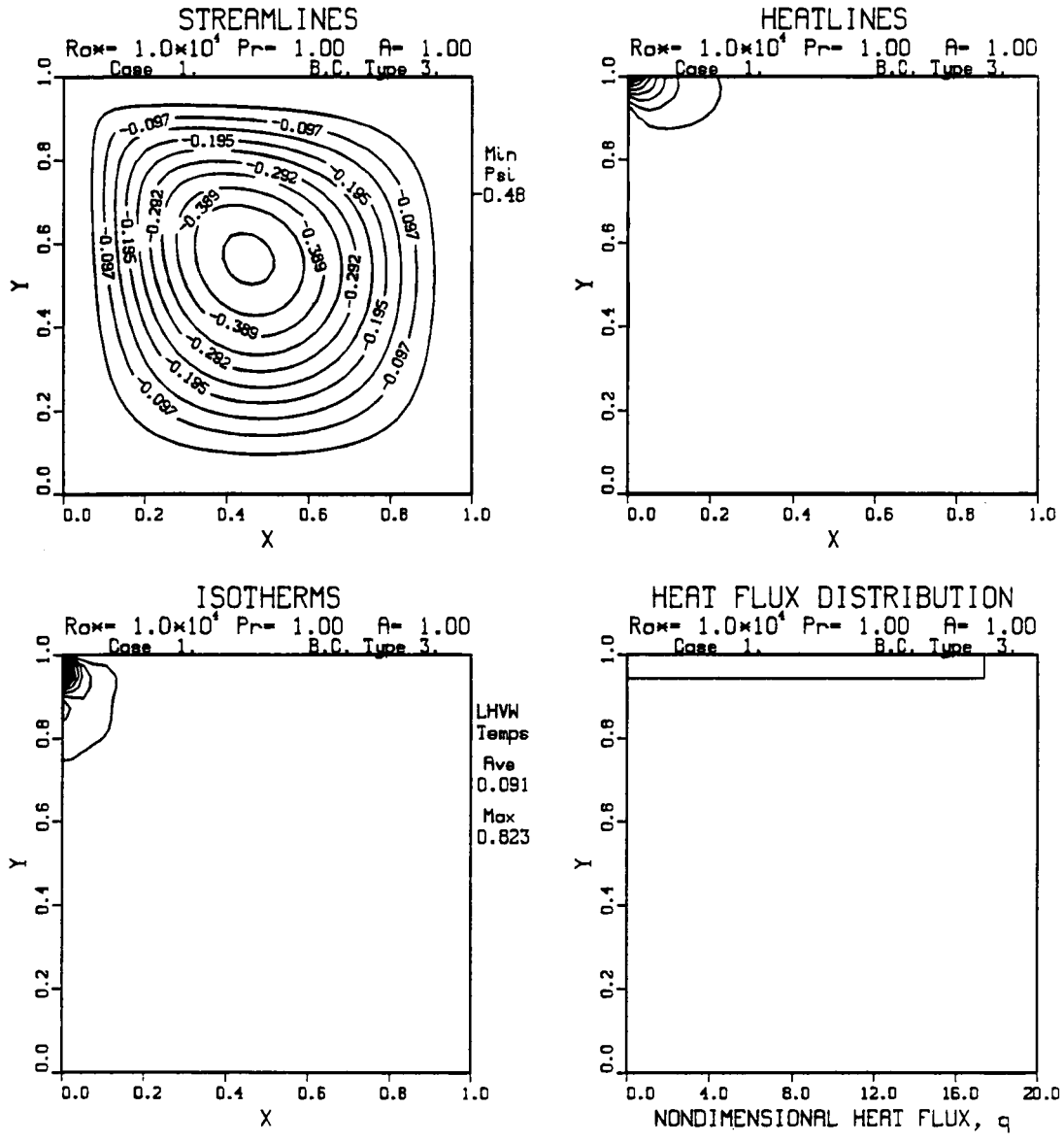


Figure C-66. Summary of results from thermal boundary condition sensitivity studies for Case 1 type optimization with thermal boundary condition Type 3 and $Ra^*=10^4$

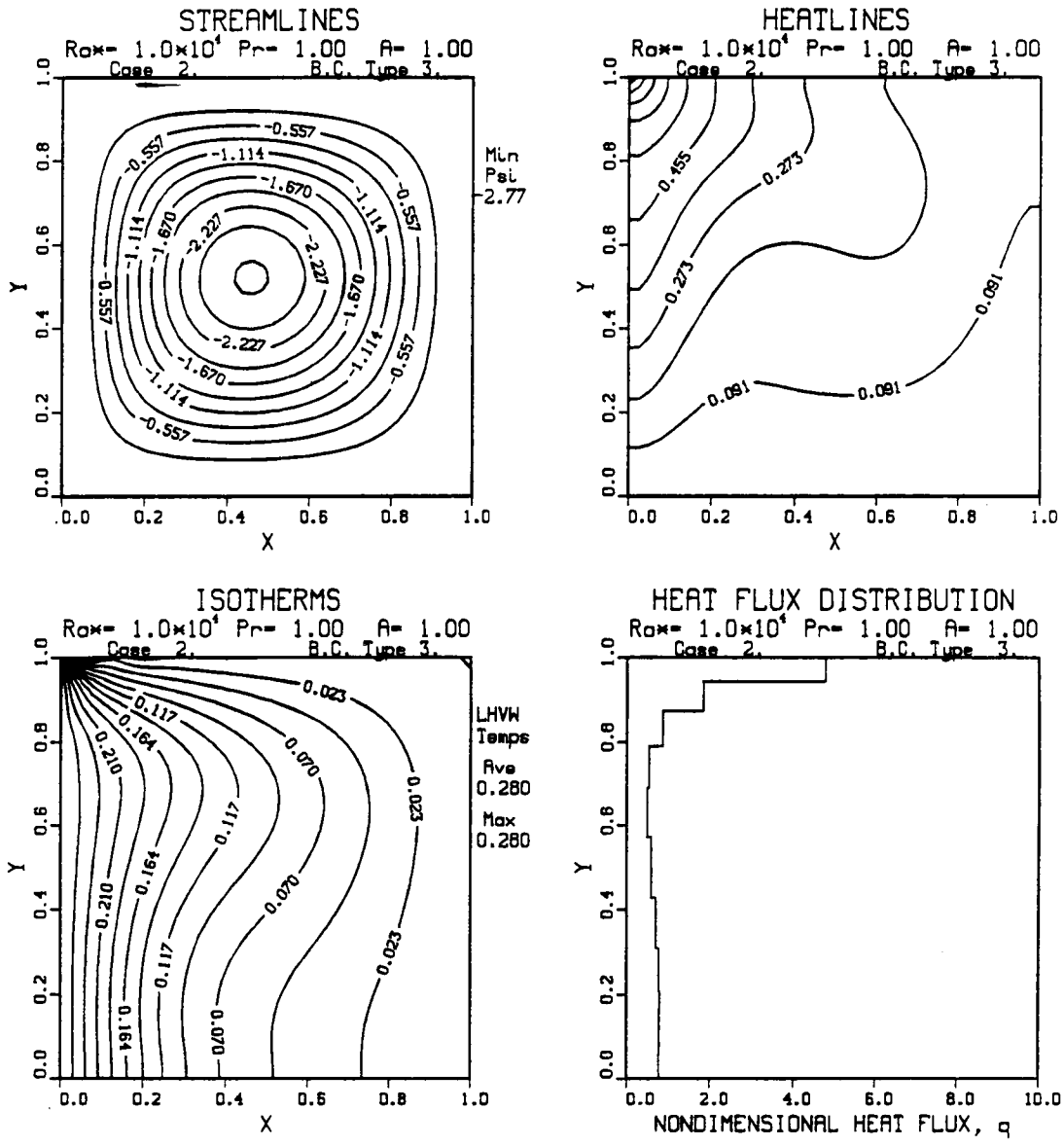


Figure C-67. Summary of results from thermal boundary condition sensitivity studies for Case 2 type optimization with thermal boundary condition Type 3 and $Ra^*=10^4$

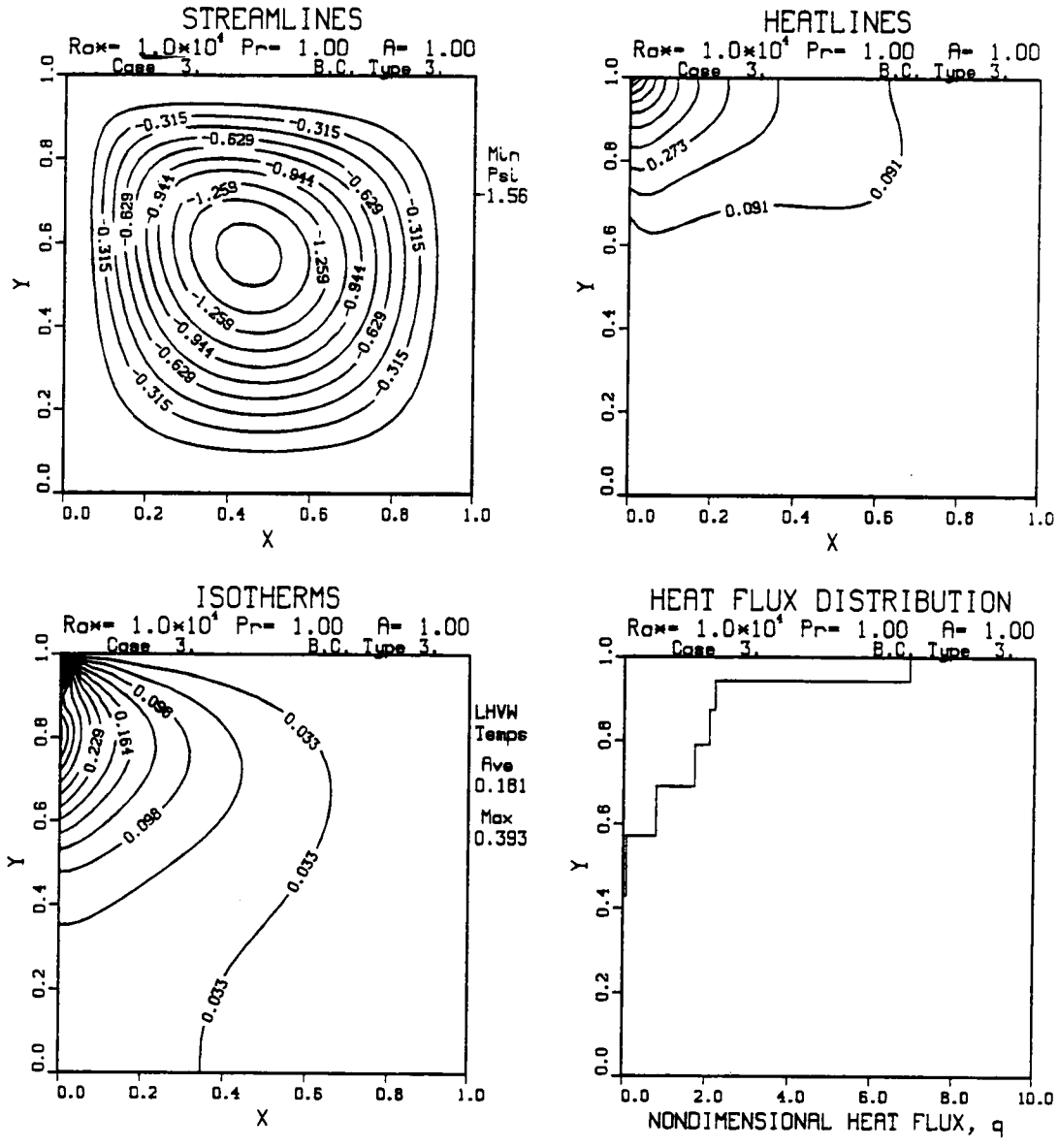


Figure C-68. Summary of results from thermal boundary condition sensitivity studies for Case 3 type optimization with thermal boundary condition Type 3 and $Ra^*=10^4$

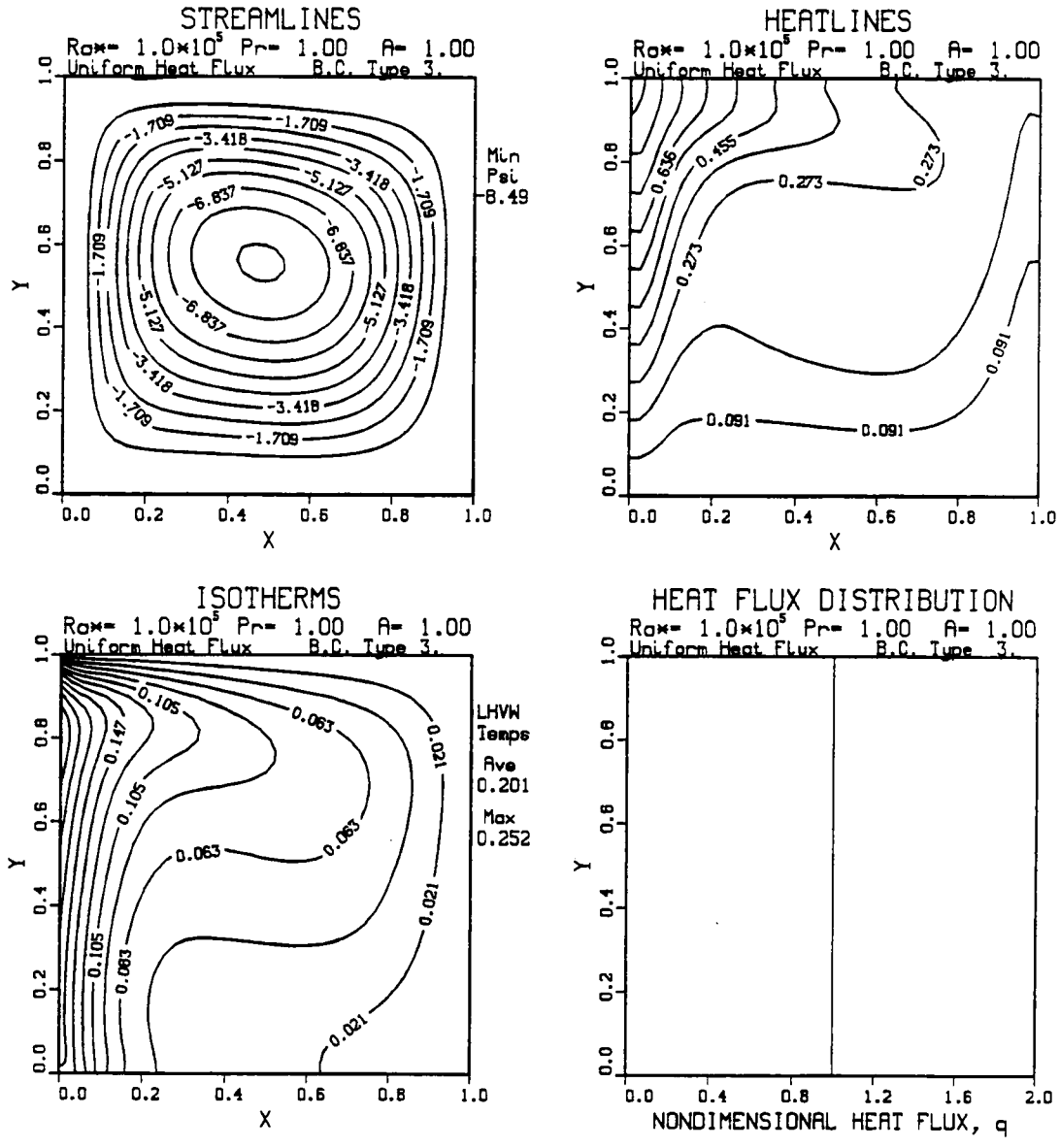


Figure C-69. Summary of results from thermal boundary condition sensitivity studies for uniform heat flux distribution with thermal boundary condition Type 3 and $Ra^* = 10^5$

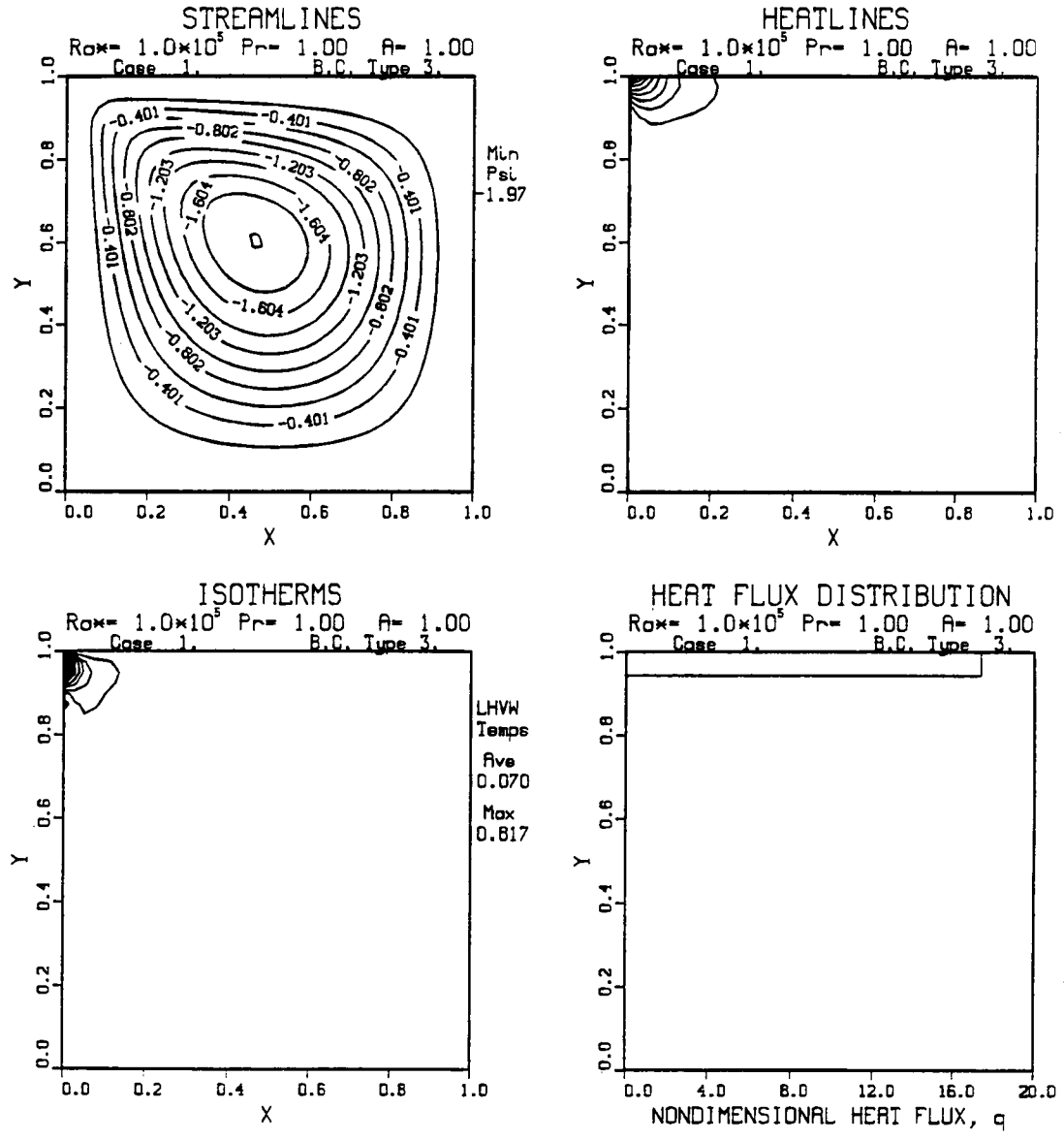


Figure C-70. Summary of results from thermal boundary condition sensitivity studies for Case 1 type optimization with thermal boundary condition Type 3 and $Ra^*=10^5$

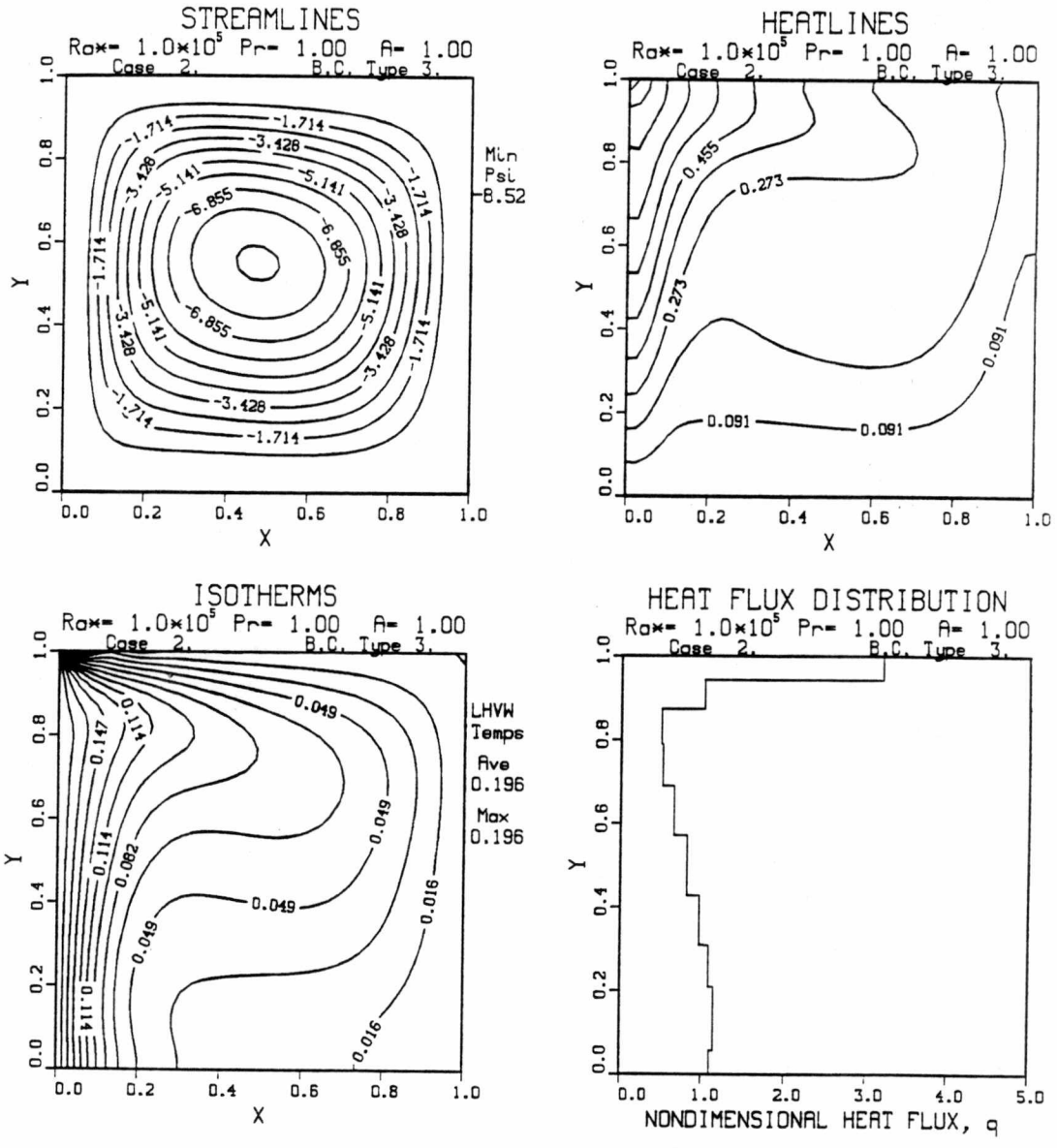


Figure C-71. Summary of results from thermal boundary condition sensitivity studies for Case 2 type optimization with thermal boundary condition Type 3 and $Ra^*=10^5$

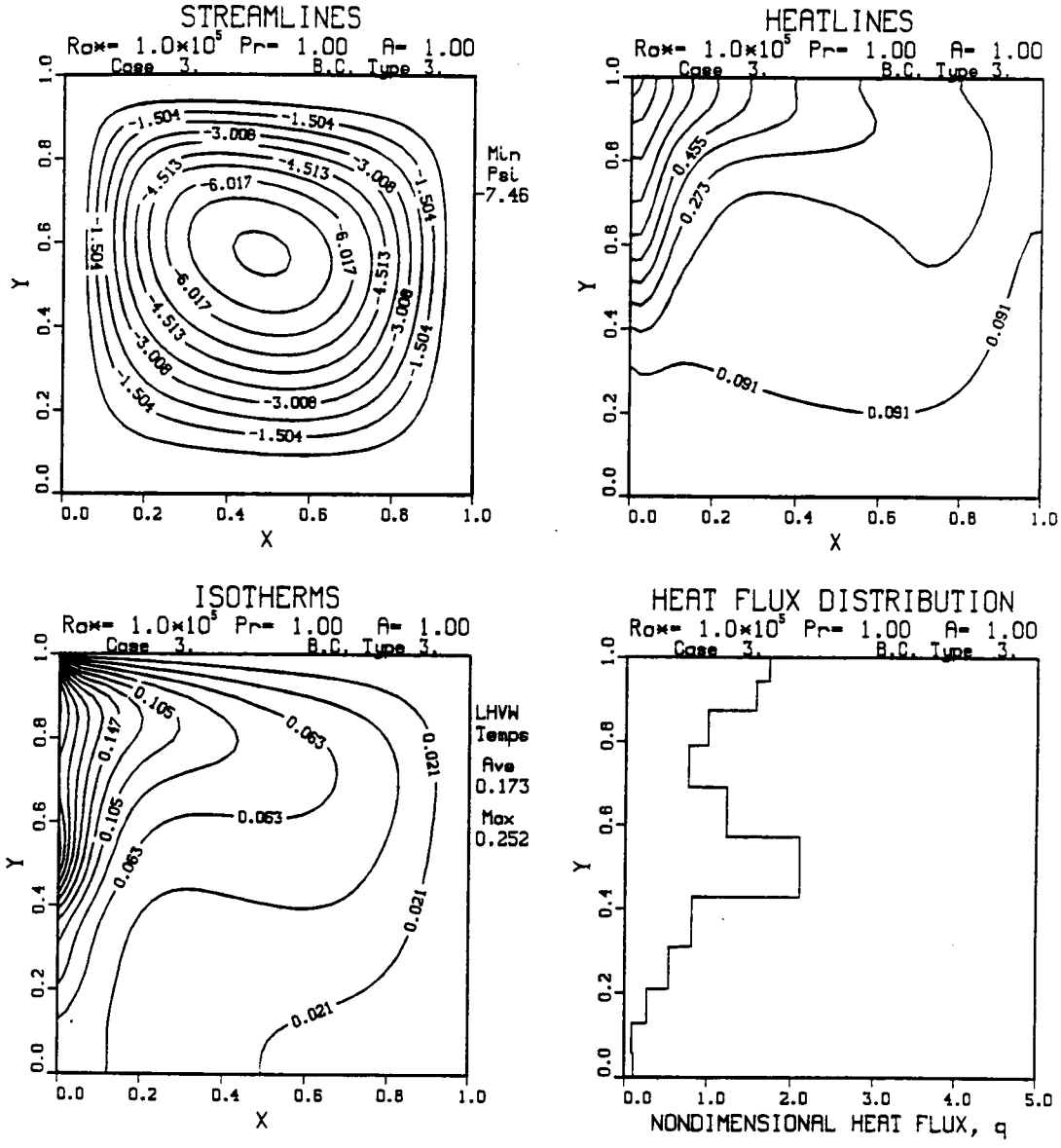


Figure C-72. Summary of results from thermal boundary condition sensitivity studies for Case 3 type optimization with thermal boundary condition Type 3 and $Ra^*=10^5$

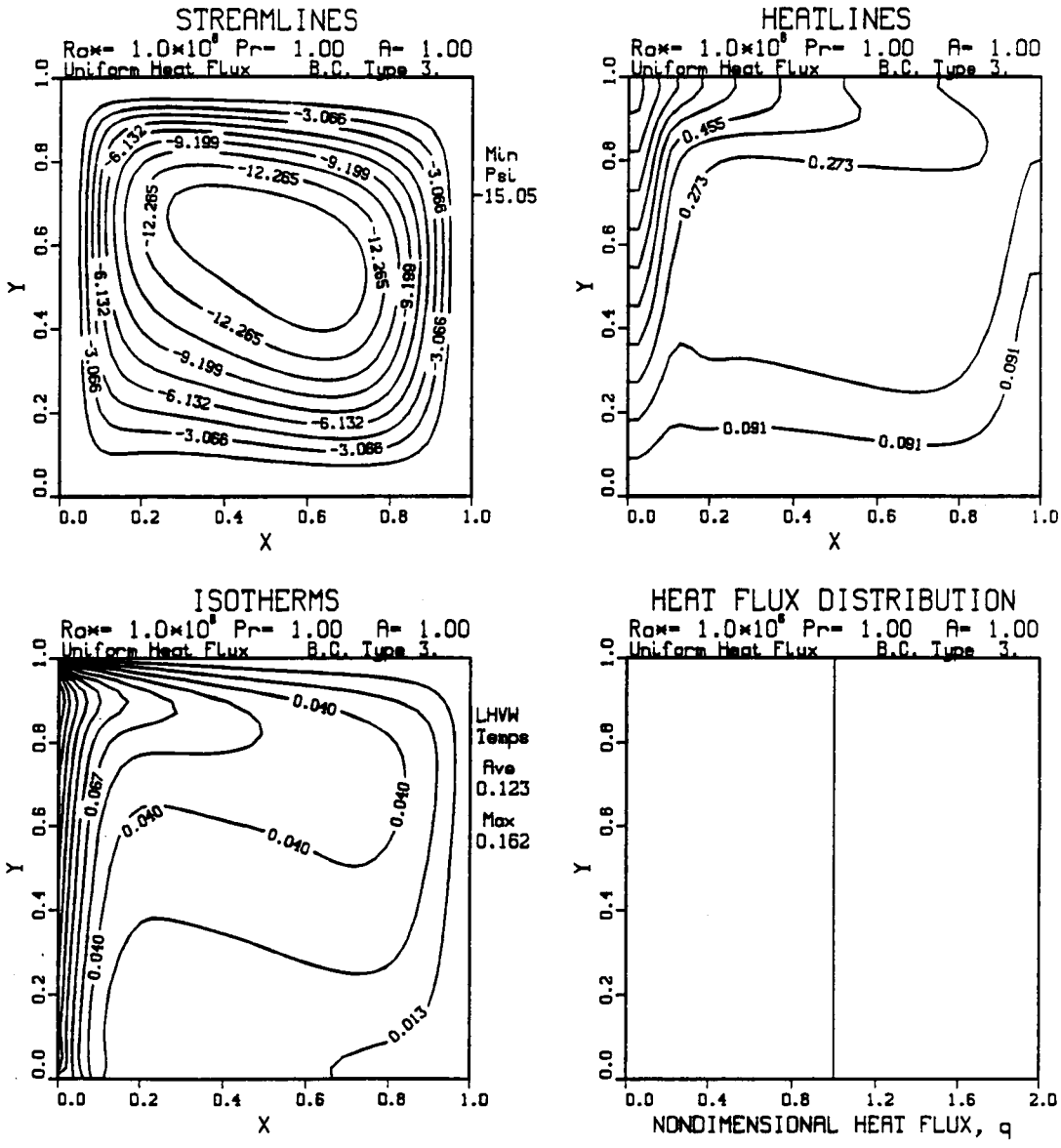


Figure C-73. Summary of results from thermal boundary condition sensitivity studies for uniform heat flux distribution with thermal boundary condition Type 3 and $Ra^* = 10^6$

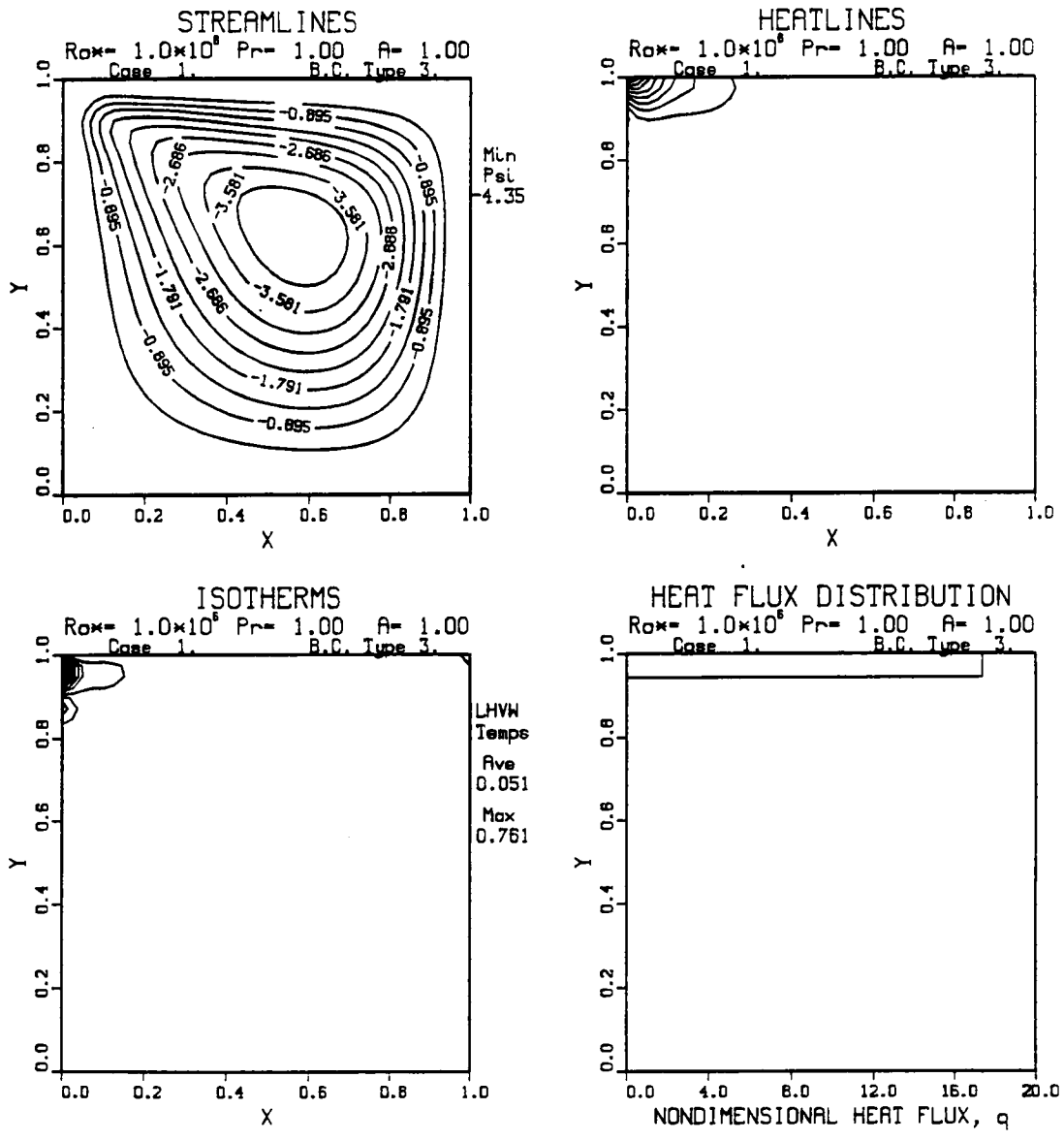


Figure C-74. Summary of results from thermal boundary condition sensitivity studies for Case 1 type optimization with thermal boundary condition Type 3 and $Ra^*=10^6$

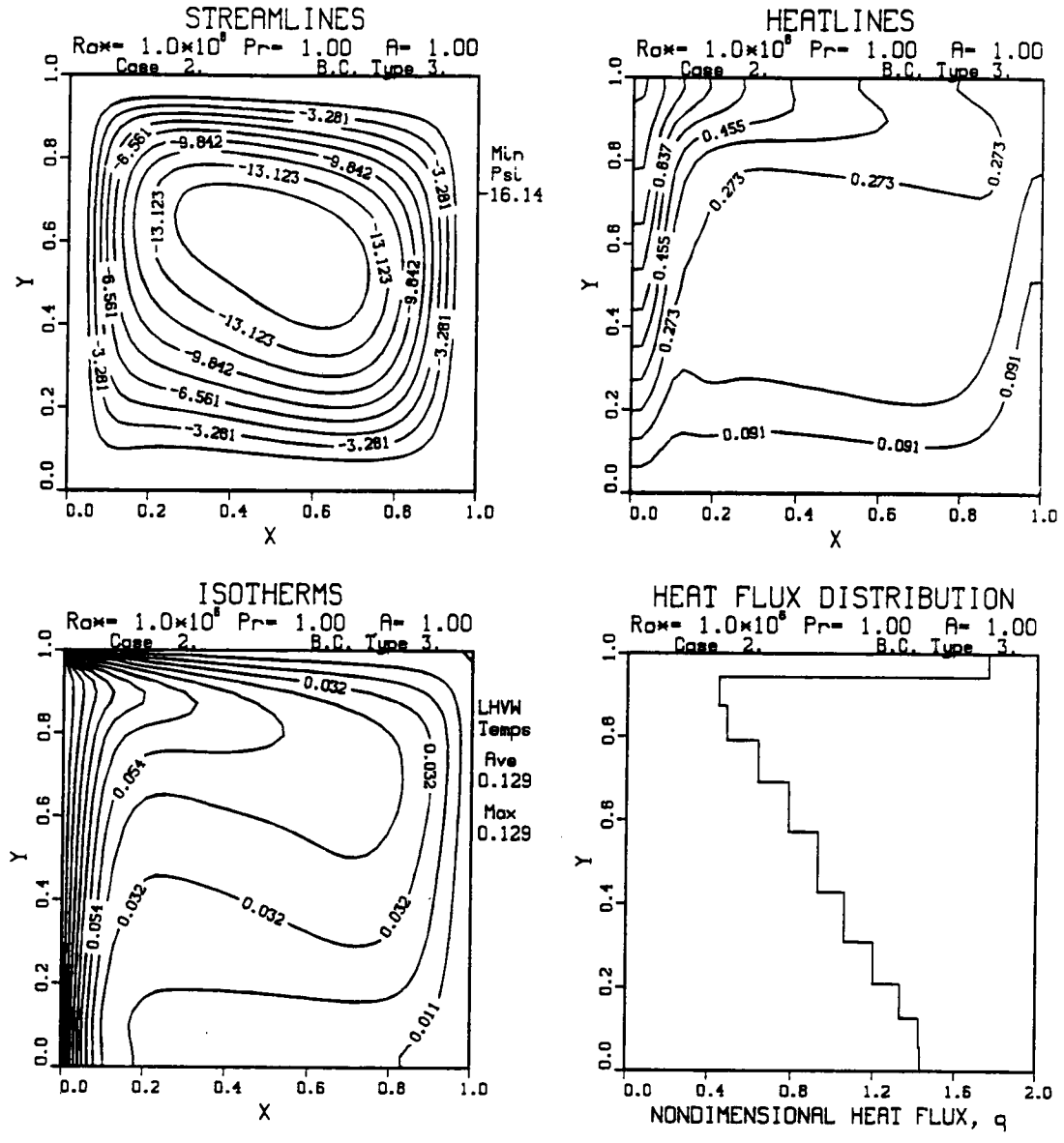


Figure C-75. Summary of results from thermal boundary condition sensitivity studies for Case 2 type optimization with thermal boundary condition Type 3 and $Ra^*=10^6$

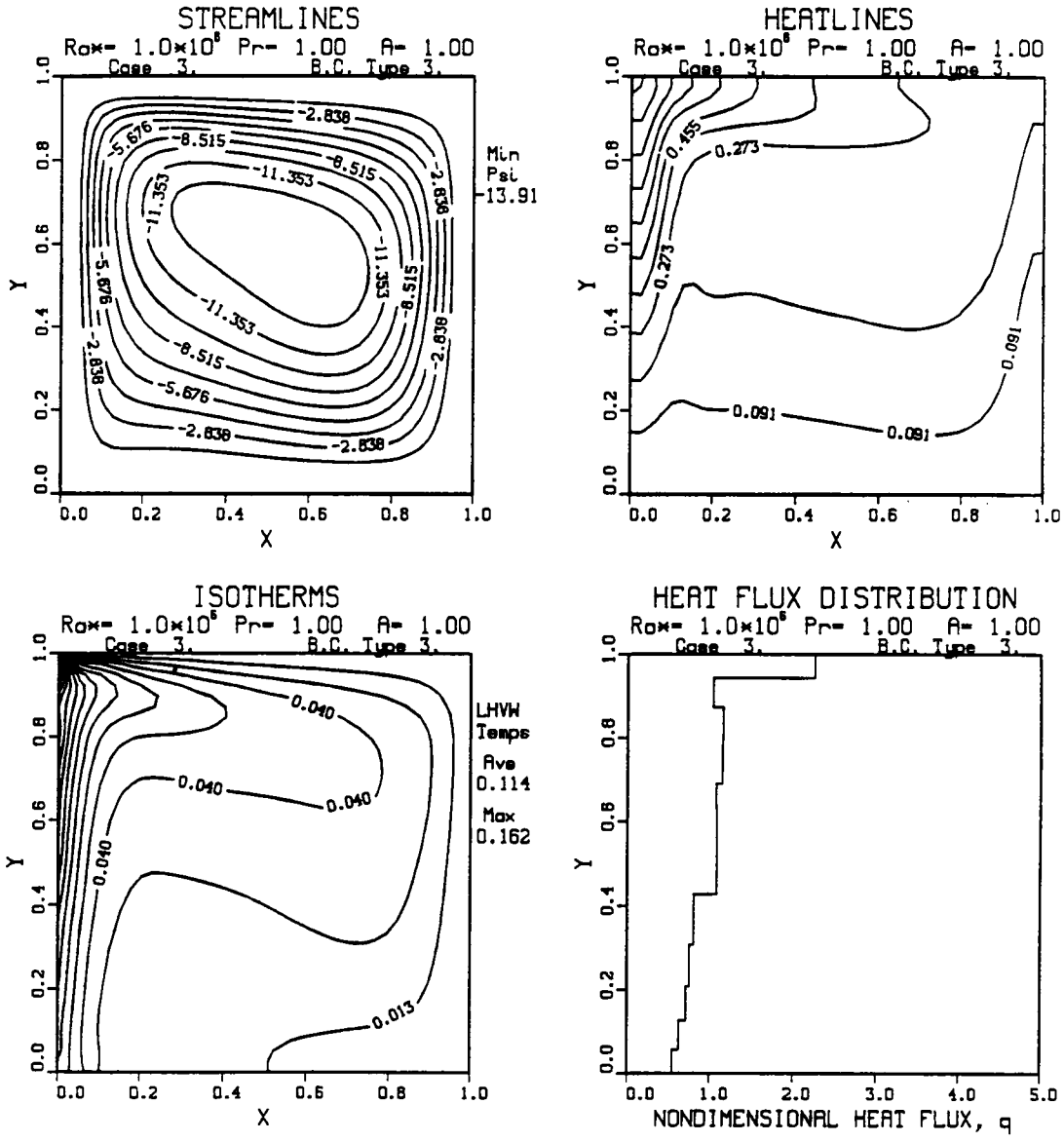


Figure C-76. Summary of results from thermal boundary condition sensitivity studies for Case 3 type optimization with thermal boundary condition Type 3 and $Ra^*=10^6$

VITA

John Raymond Haines was born in Binghamton, New York on October 10, 1953. He attended schools in that city and was graduated from Binghamton Central High School in June 1971. The following September he entered the University of Notre Dame, and in May 1975 he received a Bachelor of Science degree in Mechanical Engineering. In the Fall of 1975, he began graduate studies at Cornell University, receiving a Master of Science degree in Mechanical Engineering in December 1979.

In the summer of 1977, he began work at McDonnell Douglas Astronautics Company in St. Louis, Missouri. In 1980, he took an assignment to work at the Oak Ridge National Laboratory in Oak Ridge, Tennessee. While at Oak Ridge, he entered the Graduate School of the University of Tennessee, Knoxville in January 1981. He received the Doctor of Philosophy degree with a major in Mechanical Engineering in May 1991.

The author is a member of Pi Tau Sigma and Phi Kappa Phi honor fraternities, the American Institute of Aeronautics and Astronautics and the American Nuclear Society. He plans to remain as a member of the McDonnell Douglas engineering staff working at the Princeton Plasma Physics Laboratory after graduation.